RADIO ASTRONOMY

Journal of the Society of Amateur Radio Astronomers
March – April 2022

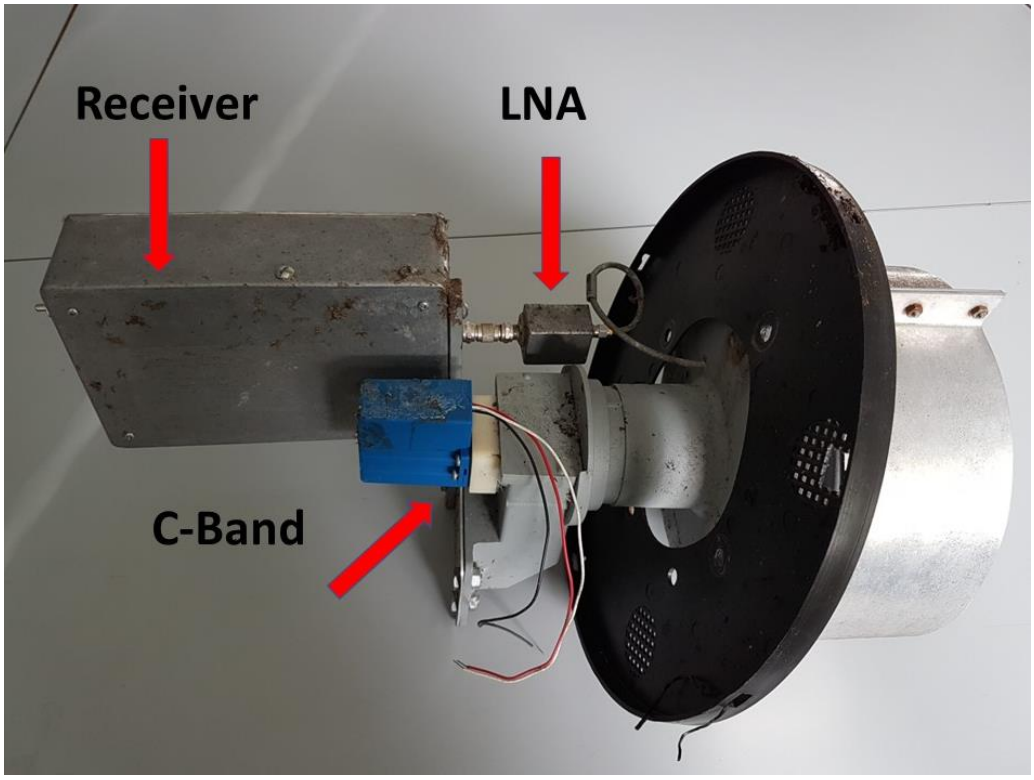

Feed Horn Assembly from an Old Small Radio Telescope

In Memoriam

SARA Past President

Bill Lord

MAY THE STARS GUIDE YOU ON YOUR NEW JOURNEY.

Dennis Farr
SARA President

Dr. Richard A. Russel
Editor

Whitham D. Reeve
Contributing Editor

Radio Astronomy is published bimonthly as the official journal of the Society of Amateur Radio Astronomers.

It is the mission of the Society of Amateur Radio Astronomers (SARA) to: Facilitate the flow of information pertinent to the field of Radio Astronomy among our members; Promote members to mentor newcomers to our hobby and share the excitement of radio astronomy with other interested persons and organizations; Promote individual and multi station observing programs; Encourage programs that enhance the technical abilities of our members to monitor cosmic radio signals, as well as to share and analyze such signals; Encourage educational programs within SARA and educational outreach initiatives. Founded in 1981, the Society of Amateur Radio Astronomers, Inc. is a membership supported, non-profit [501(c) (3)], educational and scientific corporation.

Cover Photo: Wolfgang Herrmann

Contents

Radio Waves

President's Page

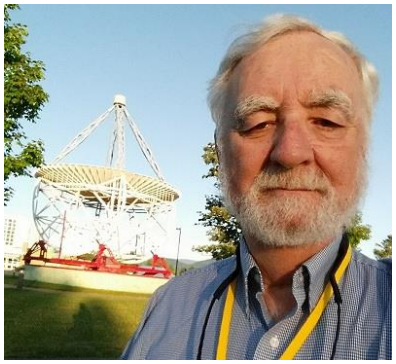

We have four main ways of sharing information.

1. The Journal which is published bimonthly.
2. Drake's lounge ZOOM meetings held monthly.
3. Western Conference held in the Spring
4. Annual Conference held in early August.

The conferences are the crown jewels for SARA members. Our stated purpose is to provide a forum for the exchange of ideas, techniques and project planning among amateur radio astronomers and other interested persons.

With over 400 members, the range of information available is truly amazing and all for the cost of only membership and a small fee for conferences. Please continue to take advantage of the resources SARA makes available to you to educate others.

Unfortunately, I must share some news. I will not be able to run for president of SARA at the elections at the next annual meeting. The reasons are personal. This is a decision I did not want to have to make.

Fortunately, there are some great people on the board that can keep SARA moving forward in the way it has. It has been a please serving SARA and I will be watching future activities with great interest.

Sincerely,

Dennis Farr
President

Editor's Notes

We are always looking for basic radio astronomy articles, radio astronomy tutorials, theoretical articles, application and construction articles, news pertinent to radio astronomy, profiles and interviews with amateur and professional radio astronomers, book reviews, puzzles (including word challenges, riddles, and crossword puzzles), anecdotes, expository on "bad astronomy," articles on radio astronomy observations, suggestions for reprint of articles from past journals, book reviews and other publications, and announcements of radio astronomy star parties, meetings, and outreach activities.

New Journal Feature – Observation Reports

We are now accepting 1-2 page observation reports. These reports should include the astronomical objects RA/DEC plus UTC of the observation. Also include the telescope configuration, process used to observe the object and results. Picture of the setup and plots of the observation are a plus to the report.

If you would like to write an article for Radio Astronomy, please follow **the newly updated Author's Guide** on the SARA web site:
http://www.radio-astronomy.org/publicat/RA-JSARA_Author's_Guide.pdf.

Let us know if you have questions; we are glad to assist authors with their articles and papers and will not hesitate to work with you. You may contact your editors any time via email here: edit@radio-astronomy.org.

The editor(s) will acknowledge that they have received your submission within two days. If they do not reply, assume they did not receive it and please try again.

Please consider submitting your radio astronomy observations for publication: any object, any wavelength. Strip charts, spectrograms, magnetograms, meteor scatter records, space radar records, photographs; examples of radio frequency interference (RFI) are also welcome.
Guidelines for submitting observations may be found here: http://www.radio-astronomy.org/publicat/RA-JSARA_Observation_Submission_Guide.pdf

Issue	Articles	Review	Distribution
2022			
May-Jun	Jun 12	Jun 22	Jun 30
Jul-Aug	Aug 12	Aug 22	Aug 31
Sept-Oct	Oct 12	Oct 22	Oct 31
Nov-Dec	Dec 12	Dec 22	Dec 31

SARA NOTES

VINTAGE SARA

If you were active in SARA's early years, 1981 – 2000, please dig into your photo archives and share some of the memories.

Most of our digital images start around 1999, but we desperately need more from the early years. If you have scanned or can scan hardcopy images or negatives we would love to share them with our new members via the SARA archives. Remember you can't create detail that isn't there, so higher resolution up to around 5MB is OK. We can always reduce resolution to create thumbnails or as needed for a given situation. On group shots even bigger is better.

Dennis has asked me to act as Historian and help dig up and orchestrate this aspect of our SARA history. Let me know what you have or show me some samples. If you have a DropBox account we can more easily share higher resolution image collections that way. If you don't have a way to scan we'll work something out.

I also have digital image collections from up on the GBT, VLBA, Arecibo, Kitt Peak, and other places where digital cameras are no longer allowed that I'll be trying to share. I have not been to the VLA or Owens Valley. We even have some video collections we are trying to share. I have video of Grote Reber visiting with the SARA members in the Drake Lounge telling stories and answering questions. Also have him giving a lecture called "The Big Bang is Bunk". So, anything similar would also be good ones to share with the rest of the membership if you have some special tour shots.

Send me an email at k4cso at twc dot com. Janis and I have pretty deep photography backgrounds. I'll give you my phone number if you have questions I can't as easily answer via email. If you don't hear back in a reasonable length of time, try me again with a short simple message to make sure it didn't autosort into a spam folder or oblivion.

Example Photos:

Jeff Lichtman, SARA Founder & Grote Reber 1996

SARA Conference Green Bank 1985 in front of 300 foot antenna (prior to the collapse), a good example of a photo that we need a higher resolution version of.

CHARLES OSBORNE,
SARA HISTORIAN

SARA Student & Teacher Grant Program

All, SARA has a grant program that is, sad to say very underutilized. We will provide kits or money to students and teachers including college students to help them with a radio telescope project. SARA can supply any of the following kits:

[1] SuperSID
[2] Scope in a Box
[3] IBT (Itty Bitty Telescope)
[4] Radio Jove kit
[5] Inspire
[6] Sky Scan

We can also provide up to five hundred dollars ($500.00 USD) for an approved radio telescope project.

We have on occasion provided more money based on the merits of the project and the SARA Grant Committee approval.

More information on the grant program can be found at the URL below.
SARA Student and Teacher Project Grants | Society of Amateur Radio Astronomers (radio-astronomy.org)

All that is required is the SARA grant request form be filled out and sent in. If it needs more work for approval, we will work with the student to help ensure their success.

Please pass the word that SARA will fund any legitimate radio telescope project anywhere in the world.

If you have a question, contact me at crowleytj at hotmail dot com.

Tom Crowley
SARA Grant Program Administrator

Drake's Lounge

Join the SARA community as we discuss the latest astronomy and radio astronomy news. The lounge also provides a forum to share and get advice on your radio astronomy projects from very experienced amateur radio astronomers.

Drake's Lounge is every month on the 3rd Sunday at 2 pm Eastern time. ZOOM email notifications will be sent to all members.

See you there!

News: (March -April 2022)

Leon Mow Radio Observatory ~ *The Dish II, a short time lapse video taken again at the Leon Mow Dark Sky site, at Victoria, Australia. The radio dish is the largest amateur radio telescope in Australia*: https://www.youtube.com/watch?v=W93TVHQWDdU

Hey, Mac, no need to get out of the sack, it's not dawn yet: Quanta magazine ~ *Four Years On, New Experiment Sees No Sign of 'Cosmic Dawn'*: https://www.quantamagazine.org/in-new-experiment-astronomers-see-no-sign-of-cosmic-dawn-20220228/

Spaceweather.com ~ *The Termination Event has Arrived*: https://spaceweather.com/archive.php?view=1&day=01&month=03&year=2022 (SARA members who attended the 2019 SARA Western Conference at UCAR/NCAR in Boulder, Colorado will remember Scott McIntosh's talk about this very subject)

ABC Australia ~ *Solar Storms: A warning from space* (This video includes some information about e-Callisto at 37-40 minutes): https://www.abc.net.au/catalyst/solar-storm-a-warning-from-space/13776860

Radio Jove ~ *Radio JOVE 2.0 Radio Telescope Kit*: https://radiojove.gsfc.nasa.gov/kits/

Nordic HF conference, HF 22, planned for 15-17 August 2022: https://www.nordichf.org/index.htm?index2.htm&2

NASA ~ *NASA Mourns Passing of Visionary Heliophysicist Eugene Parker*: https://www.nasa.gov/press-release/nasa-mourns-passing-of-visionary-heliophysicist-eugene-parker

Jet Propulsion Laboratory ~ *NASA Adds Giant New Dish to Communicate With Deep Space Missions*: https://www.jpl.nasa.gov/news/nasa-adds-giant-new-dish-to-communicate-with-deep-space-missions

Universe Today ~ *New Radio Images of Bizarre "Odd Radio Circles" Which are Vastly Bigger Than the Milky Way*: https://www.universetoday.com/155143/new-radio-images-of-bizarre-odd-radio-circles-which-are-vastly-bigger-than-the-milky-way/

University of Nevada, Las Vegas ~ *Astronomers Closer to Unlocking Origin of Mysterious Fast Radio Bursts*: https://www.unlv.edu/news/release/astronomers-closer-unlocking-origin-mysterious-fast-radio-bursts

SETI Institute ~ *CHIME to Construct Outrigger Telescope to Search for FRBs at the Hat Creek Radio Observatory*: https://www.seti.org/press-release/chime-construct-outrigger-telescope-search-frbs-hat-creek-radio-observatory

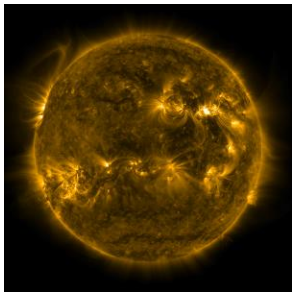

NASA ~ *Significant Solar Flare Erupts From Sun*: https://blogs.nasa.gov/solarcycle25/2022/03/30/significant-solar-flare-erupts-from-sun-2/

==========

Wanted Radio Jove Version 1 receivers.
For use in schools and Radio Jove Search for FRB's.
If you have one that you no longer need please
contact James Van Prooyen grro@sbcglobal.net

==========

Technical Knowledge & Education: (March-April 2022)

Microwaves & RF ~ *Boost In-Situ Reflection Measurement Accuracy with a Portable VNA*: https://www.mwrf.com/technologies/test-measurement/article/21216399/copper-mountain-technologies-boost-insitu-reflection-measurement-accuracy-with-a-portable-vna

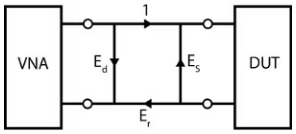

AR ~ *Antenna Far Field Distances*: https://www.arworld.us/resources/antenna-far-field-distances.asp

Community of European Solar Radio Astronomers (CESRA) ~ *Harvest of scientific results by Solar Orbiter Radio and Plasma Waves instrument*: https://www.astro.gla.ac.uk/users/eduard/cesra/?p=3215

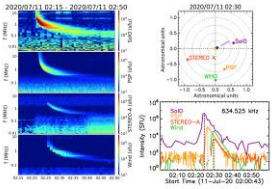

Analog Devices ~ *Radio Architecture Matters: A Review of RF Sampling vs. Zero-IF*: https://www.analog.com/en/technical-articles/radio-architecture-matters.html

Electronic Design ~ *Tektronix XYZs of Oscilloscopes Video Series*: https://www.electronicdesign.com/technologies/test-measurement/whitepaper/21163602/tektronix-xyzs-of-oscilloscopes-video-series

Electronic Design ~ *Kit Close-Up – Hands-on look at development kits and hardware platforms*: https://www.electronicdesign.com/magazine/50464

Signal Integrity Journal ~ Assembling an EMC Troubleshooting Kit: Radiated Emissions: https://www.signalintegrityjournal.com/blogs/17-practical-emc/post/2387-assembling-an-emc-troubleshooting-kit-radiated-emissions

Signal Integrity Journal 2022: https://www.signalintegrityjournal.com/articles/2447-sij-publishes-2022-issue

European Space Agency ~ *Aerial antenna for Venus mission test*: https://www.esa.int/ESA_Multimedia/Images/2022/03/Aerial_antenna_for_Venus_mission_test

Signal Integrity Journal ~ *Use a 2D Field Solver to Accurately Predict Characteristic Impedance*: https://www.signalintegrityjournal.com/articles/1726-use-a-2d-field-solver-to-accurately-predict-characteristic-impedance

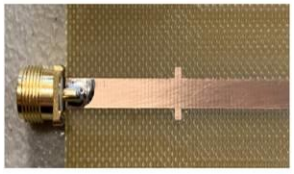

SDR makerspace ~ *Evaluation of SDR Boards and Toolchains*: https://gitlab.com/librespacefoundation/sdrmakerspace/sdreval/-/raw/master/Report/pdf/Evaluation_of_SDR_Boards-1.0.pdf

NASA Goddard Space Flight Center ~ *NASA's Heliophysics Digital Resource Library (HDRL): Data and Services for the Heliophysics System Observatory*: https://hdrl.gsfc.nasa.gov/

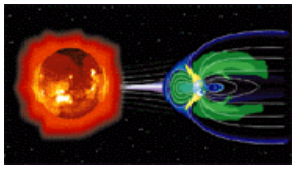

Space Weather Prediction Center ~ *Thermosphere/Ionosphere Predictions as calculated by the Coupled Thermosphere Ionosphere Plasmasphere Electrodynamics (CTIPe) model*: http://ccmc-swpc.s3-website-us-east-1.amazonaws.com/plots.html

Sierra Circuits ~ *IPC J-STD-001 Standard Soldering Requirements*: https://www.protoexpress.com/blog/ipc-j-std-001-standard-soldering-requirements/

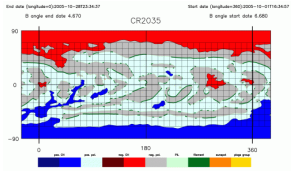

NCAR/UCAR High Altitude Observatory ~ *McIntosh Archive of synoptic maps*: https://www2.hao.ucar.edu/mcintosh-archive/four-cycles-solar-synoptic-maps

EDN ~ *Design Ideas PDF collections: 2001 – 2009*: https://www.edn.com/design-ideas-pdf-collections-2001-2009/

Youtube ~ *Planetary Ultra-Low Frequency Waves: Theory, Modelling and Observations, 11th March 2022*: https://www.youtube.com/watch?v=qrz3cYI5mDQ

Community of European Solar Radio Astronomers (CESRA) ~

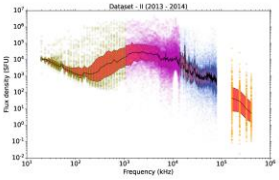

- *Spectral Analysis of Solar Radio Type III Bursts from 20 kHz to 410 MHz*: https://www.astro.gla.ac.uk/users/eduard/cesra/?p=3221
- *New results from the spectral observations of solar coronal type II radio bursts*: https://www.astro.gla.ac.uk/users/eduard/cesra/?p=3231

Signal Integrity Journal ~ *A Low-Cost Capacitor Characterization System*: https://www.signalintegrityjournal.com/articles/1976-a-low-cost-capacitor-characterization-system

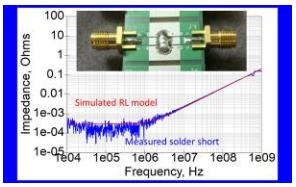

Sierra Circuits ~ *Controlled Impedance Design Guide*: https://pages.protoexpress.com/controlled-impedance-design-guide.html

Electronic Design ~ *How to Shield and Filter RF Designs from EMI*: https://www.electronicdesign.com/technologies/analog/article/21236859/electronic-design-how-to-shield-and-filter-rf-designs-from-emi

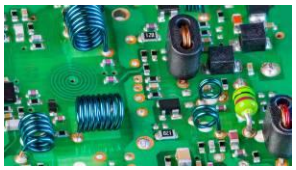

Keysight University ~ *Circuit Design, Learn from our experts how to simulate and design your next generation project with fewer revisions, in less time*: https://learn.keysight.com/circuit-design

Frontiers in Astronomy & Space Sciences ~ eBooks (select *All Stages* drop-down): https://www.frontiersin.org/journals/astronomy-and-space-sciences/sections/space-physics#research-topics

Basic Python Principles

https://colab.research.google.com/drive/1Df05mzLTyJvy-aWXO93RsYCMm6Uj5eFN

Sierra Circuits ~ *2-D Impedance Calculator*: https://www.protoexpress.com/tools/pcb-impedance-calculator/
For a short review: https://www.signalintegrityjournal.com/blogs/4-eric-bogatin-signal-integrity-journal-technical-editor/post/2436-sierra-circuits-releases-a-free-online-2d-field-solver

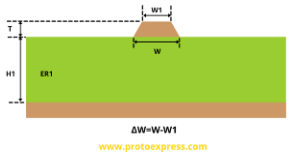

Planet Analog ~

- *A close look at active vs. passive RF converter front-ends*: https://www.planetanalog.com/a-close-look-at-active-vs-passive-rf-converter-front-ends/
- *Evaluating high-speed RF converter front-end architectures*: https://www.planetanalog.com/evaluating-high-speed-rf-converter-front-end-architectures/

KF7P ~ *Coax Stretcher: Cut your coax a few inches too short? No worries, use our new COAX STRETCHER to lengthen any coax to fit! Also performs the following vital functions:*

- *Changes RG-8 into RG-58*
- *Perfect for building tuned stubs*
- *Changes diameter of dielectric*
- *Can be used to adjust velocity factor*

https://www.kf7p.com/KF7P/Welcome.html

Announcements: March-April 2022

Release of PySPEDAS 1.3

The Space Physics Environment Data Analysis Software (SPEDAS) development team is pleased to announce the release of PySPEDAS 1.3! The latest version is available in PyPI, as well as at our GitHub repository: https://github.com/spedas/pyspedas

For those of you unaware, PySPEDAS contains tools for loading, analyzing and plotting data from a number of space- and ground-based observatories. Where to get it: The latest version can be installed using pip:

pip install pyspedas --upgrade

If you've previously installed pyspedas, the --upgrade option will be required to update to the latest version.

What's new?

- First version shipped with our experimental matplotlib backend to PyTplot
- Added wrappers for Sheng Tian?s implementation of the geopack library (T89, T96, T01, TS04)
- Large updates to the MMS plug-in, including new tools for calculating energy and angular spectrograms, as well as moments from the FPI and HPCA plasma distribution data
- Added the 0th (EXPERIMENTAL) version of the ERG plug-in from the Arase team in Japan
- Added new tools for working with various vector data stored in PyTplot variables, e.g., tkm2re, cross products, dot products, normalizing vectors
- Added routines for wave polarization calculations
- Added routines for field aligned coordinate transformations
- Added tools for Spherical Elementary Currents (SECS) and Equivalent Ionospheric Currents (EICS) from Xin Cao and Xiangning Chu at the University of Colorado Boulder
- Added initial load routine for Heliophysics Application Programmer's Interface (HAPI) data
- Added initial load routine for Kyoto Dst data
- Added initial load routine for THEMIS All Sky Imager data
- Added THEMIS FIT L1 calibration tools
- Numerous other bug fixes and updates
- Large updates to the documentation (including over 100 new copy+paste examples)

We created a notebook showing several of these new features at:
https://colab.research.google.com/drive/1_fV6Ob8rfnCkohpec5YtMY4tl7tLbuvB?usp=sharing
Where to find documentation: Please see our documentation online at: https://pyspedas.readthedocs.io/
Additional example notebooks can be found at our SPEDAS GitHub page: https://github.com/spedas
For example, more MMS notebooks can be found in the repository: https://github.com/spedas/mms-examples
Where to get help: Bug reports, help requests, and enhancement suggestions can be filed as issues directly on our repository: https://github.com/spedas/pyspedas
or can be submitted via email to: SPEDAS_Science_Support@ssl.berkeley.edu

---

MEETING: Announcement of NASA Workshop on Lightning-Related Research Beyond the Troposphere

From: Sabrina Savage (sabrina.savage at nasa.gov)

This is to announce that NASA is organizing a virtual scientific workshop to be held on May 2-3, 2022. The goal of the workshop is to identify key lightning-related research topics and science questions that fall into gaps between the NASA SMD Divisions. The workshop will cover lightning-related phenomena occurring beyond the Earth's troposphere and will include (but not limited to) Transient Luminous Events (TLEs; e.g., sprites, jets), Terrestrial Gamma-ray Flashes (TGFs), spherics, electron precipitation from Earth's radiation belts, detection of bolides by spaceborne optical lightning mappers, lightning on other planets, and more.

In addition, NASA would like to gather information to describe how lightning-related research is being carried out by the community and determine how that work could be supported through better collaboration across SMD Divisions. The community's input will then inform the agenda of the upcoming workshop. Furthermore, this community input and the results of the workshop could help formulate future NASA research opportunities. Community input on lightning-related research can be provided before 02/28/2022 @ https://TinyURL.com/NASALightning .

For more information, please reach out to Timothy Lang (timothy.j.lang at nasa.gov), Shing F. Fung (shing.f.fung at nasa.gov), Sarah Bang (sarah.d.bang at nasa.gov), Burcu Kosar (burcu.kosar at nasa.gov) and Mason Quick (mason.quick at nasa.gov)

MEETING: Parker Two - Second Annual Parker Solar Probe Conference (http://parkerseries.jhuapl.edu/), June 21-24, 2022, Johns Hopkins Applied Physics Laboratory (APL), Laurel, Maryland, USA -- First Announcement

From: Nour Raouafi, Robert Allen, Bob DeMajistre, Rob Decker (rob.decker at jhuapl.edu)

The NASA Parker Solar Probe (PSP) mission, which launched on August 12, 2018, is currently reaching perihelia as low as 13.3 solar radii. This unprecedented proximity to the solar corona has now allowed us to observe the sub-Alfv?nic solar wind and address key aspects of the mission?s main science objectives:

1) Trace the flow of energy that heats and accelerates the solar corona and solar wind;
2) Determine the structure and dynamics of the plasma and magnetic fields at the sources of the solar wind; and
3) Explore mechanisms that accelerate and transport energetic particles.

The second annual Parker Solar Probe community workshop, Parker Two, will be a hybrid meeting from June 21 - 24, 2022 with an in-person component at the Johns Hopkins Applied Physics Laboratory (APL) in Laurel, MD, and an online component using Zoom. The meeting will highlight discoveries from the first eleven encounters of the Parker Solar Probe mission. Abstracts from the solar, heliospheric, and plasma physics communities involving relevant theory, simulations, data analysis, and coordinated observations with ground and other space-based observatories are encouraged. Presentation formats will include poster, oral, and splinter sessions.

APL requires that in-person attendees be fully vaccinated and that masks be worn when indoors, for the latest information please visit https://www.jhuapl.edu/About/VisitorInformation .

Important Information: All attendees must register in order to attend the conference. Abstracts may be submitted prior to registering.

Important Dates: Registration Closes: June 3, 2022; Abstract Deadline: March 15, 2022; Talk/Poster Decisions: Announced April 30th

Conference Fees: In-Person: $250 ($150 refundable if cancelled by May 21, 2022); Virtual: $100 (Non-refundable)

For further information, visit: http://parkerseries.jhuapl.edu/

MEETING: 20th Annual International Astrophysics Conference, October 30-November 4, 2022, Santa Fe, New Mexico, USA

From: Gary P Zank (garyp.zank at gmail.com)

FIRST ANNOUNCEMENT: Anticipating that the COVID pandemic will be behind us by October 2022 (or at least endemic), we are pleased to announce that the 20th Annual International Astrophysics Conference will once again resume and be held at the La Posada Resort & Spa hotel in Santa Fe, New Mexico, from October 30 to November 4. (Welcome Reception and Evening Registration begins Sunday, October 29).

The 20th AIAC is intended to be twofold - retrospective, celebrating the solar, space, and astrophysical accomplishments of the past 20 years as expressed in the 19 prior AIAC conferences, and a future perspective, i.e., examining some of the pressing questions that taxed our community over the past 20 years from the perspective of what we think we know and understand. Accordingly, the theme of the meeting will be From the Depths of the Solar Corona to the Darkness of Interstellar Space: A 20 Year Perspective. We will follow the usual format of 25-minute presentations punctuated by selected 40-minute invited talks that will develop both the retrospective and future themes in greater detail. Since the 19 previous meetings addressed the broad themes of the interaction of the outer heliosphere and the local interstellar medium, shock waves and nonlinear processes, energetic particles, particle acceleration and transport, the heating and physics of the solar corona and solar wind, turbulence processes, and much more, these will all be themes in the 20th iteration of the AIAC. A characteristic theme of previous meetings was the universality of many of the physical processes that informed the conference, and this will be a central element of the 20th celebration.

In the spirit of keeping all attendees as safe as possible, we will be limiting the number of attendees and implementing safety protocols. In that vein, all meeting participants will be required to adhere to the following mandates:

- ☼ Provide proof of being FULLY vaccinated against COVID-19 as required by the CDC.
- ☼ N95 or KN95 masks only must be worn at all times during all conference functions.
- ☼ Provide proof of a negative COVID test taken within 24 hours of the meeting.
- ☼ Practice social distancing throughout the entire conference timeframe.

Depending on circumstances, these requirements are subject to change. Additional detail on COVID-19 safety requirements will be posted on the website soon.

The conference website will be up soon at the following address:
www.icnsmeetings.com/conference/20thannual/index.html

RSVP Required: RSVP your interest in attending to Gary Zank at garyp.zank@gmail.com .
Conference logistics and general information: Contact Adele Corona at icnsmeetings@gmail.com .

Magnetosphere Online Seminar Series (MOSS) Tutorials

Tutorials are held once every month in collaboration with the Center For Helioanalytics. You can view the tutorial material at the GitHub Repository.

Initially the tutorials will provide an introductions to Python and will expand to Heliophysics and Spacephysics packages within Python and other languages.

We will be using Jupyter Notebooks and Google Colab as much as possible. Using Google Colab means that accessing the tutorials doesn't require you to install Python; however, having Python will prove useful if you plan to transition to it for your analysis and work.

From: Dr. Donald Lubowich (donald.lubowich@hofstra.edu)

I would like to invite SARA to again participate in the FREE **Astronomy Festival on the Mall**, Saturday June 25, 2022, from 6 – 11 pm. There is no fee to participate and Hofstra University will pay for tables, chairs, tablecloths, table lamps, and a generator. The festival will be between 4th and 7th streets. We will pay parking for the amateur astronomers.

The AFNM was started in 2010 with the co-sponsorship of the OSTP. SARA has been at several AFNM events. In 2019 we were the largest annual astronomy outreach event in the US attended by 10,000 people. There were 100 educators representing 30 organizations who did hands-on science and telescope observations.

For more information: https://www.hofstra.edu/academics/colleges/hclas/physic/physic-nationalmall.html

---

MEETING: Parker Two - Second Annual Parker Solar Probe Conference (http://parkerseries.jhuapl.edu/), June 21-24, 2022, Johns Hopkins Applied Physics Laboratory (APL), Laurel, Maryland, USA -- Second Announcement

From: Nour Raouafi, Robert Allen, Bob DeMajistre, Rob Decker (rob.decker at jhuapl.edu)

The NASA Parker Solar Probe (PSP) mission, which launched on August 12, 2018, is currently reaching perihelia as low as 13.3 solar radii. This unprecedented proximity to the solar corona has now allowed us to observe the sub-Alfv?nic solar wind and address key aspects of the mission?s main science objectives:

1) Trace the flow of energy that heats and accelerates the solar corona and solar wind;
2) Determine the structure and dynamics of the plasma and magnetic fields at the sources of the solar wind; and
3) Explore mechanisms that accelerate and transport energetic particles.

The second annual Parker Solar Probe community workshop, Parker Two, will be a hybrid meeting from June 21 - 24, 2022 with an in-person component at the Johns Hopkins Applied Physics Laboratory (APL) in Laurel, MD, and an online component using Zoom. The meeting will highlight discoveries from the first eleven encounters of the Parker Solar Probe mission. Abstracts from the solar, heliospheric, and plasma physics communities involving relevant theory, simulations, data analysis, and coordinated observations with ground and other space-based observatories are encouraged. Presentation formats will include poster, oral, and splinter sessions.

Invited Speakers (Confirmed):
Marco Velli (UCLA)
Nicki Viall (NASA/GSFC)
Ronan Laker (UCL)
Anna Tenerani (UT Austin)
Jaye Verniero (NASA/GSFC)
Erika Palmerio (Predictive Science)
Christina Cohen (CalTech)
Russ Howard (APL)

APL requires that in-person attendees be fully vaccinated and that masks be worn when indoors, for the latest information please visit https://www.jhuapl.edu/About/VisitorInformation.

Important Information:
All attendees must register in order to attend the conference.
Abstracts may be submitted prior to registering.

Important Dates:
Registration Closes: June 3, 2022
Abstract Deadline: March 15, 2022
Talk/Poster Decisions: Announced April 30th

Conference Fees:
In-Person: $250 ($150 refundable if cancelled by May 21, 2022)

Virtual: $100 (Non-refundable)

For further information, visit: http://parkerseries.jhuapl.edu/

The SKA Observatory (SKAO) has signed a cooperation agreement with the CNRS . This agreement, which formalizes France's commitment to this major project, allows French laboratories and companies in particular to participate now in the construction of the two telescopes in Australia and South Africa. The signing took place yesterday, March 7, 2022, during a ceremony at the Australian Embassy in Paris. In May 2021, the SKAO Council unanimously decided to admit France as a member of the new intergovernmental organization. A few days later President Emmanuel Macron confirmed the country's decision to ratify the SKA Convention during a state visit to South Africa . While the process to complete France's membership of SKAO is underway, the agreement with CNRS is an interim step that allows the French scientific and industrial communities to continue their engagement with SKAO. The event, organized yesterday by the Australian Embassy as part of the Australia Now - France program, was also the occasion for the launch of the Australian virtual reality film " Beyond the Milky Way " and the inauguration of the " Eureka - Scientific Australia " exhibition at the Embassy, accessible all week long by registering online .

MEETING: TESS Meeting Call for Abstracts
From: Dale Gary, TESS SOC (dgary at njit.edu)

The Triennial Earth-Sun Summit (TESS, https://aas.org/meetings/tess2022) is a joint meeting of AAS/SPD and AGU/SPA, being held 8-11 August in Bellevue/Seattle, WA to encourage cross-disciplinary interaction between researchers in solar, space, and terrestrial fields of science.

The abstract submission site is open at https://submissions.mirasmart.com/TESS2022/Splash.aspx! Please submit your abstracts by Friday, 15 April to one of our special topic sessions listed at https://aas.org/meetings/tess2022/topical-sessions , or to one of the general categories: Solar, Heliosphere, Magnetosphere, Ionosphere/Thermosphere/Mesosphere, or Cross-Disciplinary.

Students, please sign up for the poster contest. Studentships (https://solarnews.nso.edu/spd-studentships-for-the-2022-tess-meeting/) for travel to the meeting are available if you apply by Friday, 18 March. Registration will be announced shortly. We look forward to seeing everyone in person at the meeting.

MEETING: Beacon Satellite Symposium - Call for Abstracts
From: Patricia Doherty (patricia.doherty at bc.edu)

We are pleased to announce that the 21st International Beacon Satellite Symposium will be held at Boston College on 1-5 August 2022.

The Beacon Satellite Symposium is a triennial event organized by the Beacon Satellite Studies Group of URSI Commission G an interdisciplinary group, servicing science, research applications and engineering aspects of satellite signals observed from the ground and in space. The Beacon Symposia provide distinctive opportunities for ionospheric scientists from all over the world to meet and collaborate on topics relevant to ionospheric effects on radio propagation.

Recent meetings of the Beacon Symposia have hosted between 125 and 200 people from over 40 countries. In our most recent meetings, we have seen an increase in the number of participants from developing countries in Africa, Asia and South America presenting the Beacon Symposia with nearly worldwide coverage.

At this time, we invite you submit your abstracts with the link provided on the website. The abstract deadline is April 15, 2022. URSI has provided a link for us to utilize their Cvent system for abstract submissions and reviews.

Please view our website for information on registration, lodging and the scientific sessions. Registration links will be open soon on the website: www.bc.edu/bss2022.

It is our intent to assist travel and lodging costs for a limited number of young scientists and participants from developing countries. Awards will be made based on the quality of the abstract and financial need of the applicant. If you wish to request consideration of financial support, please send a note describing your request to bssrequest@bc.edu.

Please check our website at www.bc.edu/bss2022 for more information as it develops over the next couple of months. Please also register your interest in this event by pre-registering with your email address on our website. We sincerely hope to see you at BSS2022 in Boston.

Best regards,
Patricia Doherty, Boston College, Chestnut Hill, MA, USA

Andrzej Krankowski, University of Warmia and Mazury, Olsztyn, Poland
Bruno Nava, Abdus Salam International Centre for Theoretical Physics, Trieste, Italy
Chairs of URSI?s Beacon Satellite Studies Group

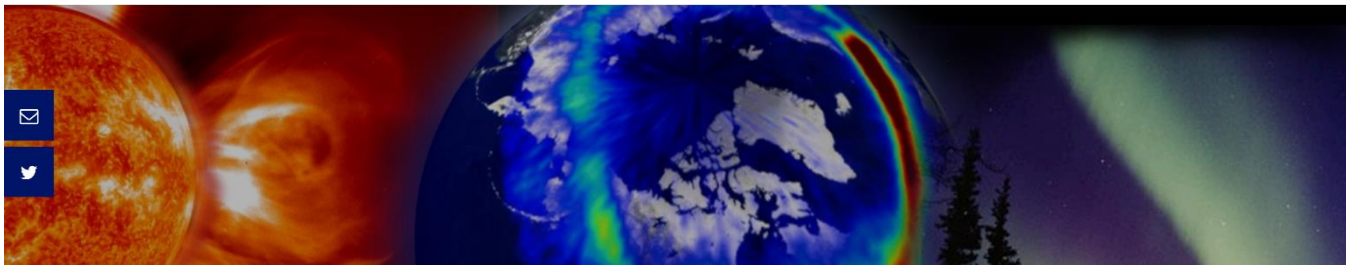

13th SCOSTEP/PRESTO Online Seminar
SCOSTEP Distinguished Scientist Award Seminar

The SCOSTEP Distinguished Scientist Award Seminar by Prof. Dr. David J. McComas will be held via online as below. To join the seminar, please register via the zoom addresses as below.

Title: First Solar Cycle of Observations of our Heliosphere's Interaction with the Very Local Interstellar Medium
Author: Prof. Dr. David J. McComas (SCOSTEP 2022 Distinguished Scientist Award Winner)
Affiliation: Department of Astrophysical Sciences, Princeton University, Princeton, New Jersey 08544, USA
Date/time: May 11 (Wed), 2022, 14:00-15:00 UT
Zoom Registration URL (pre-registration is necessary):
https://us02web.zoom.us/webinar/register/WN_h0006KUyQ_OA-9L7aUksAw

Abstract: Our heliosphere is formed by the supersonic solar wind and entrained interplanetary magnetic field (IMF) flowing outward from the sun and inflating a bubble in the very-local interstellar medium (VLISM). The global interaction of the heliosphere with the VLISM was first observed starting at the end of 2008 by the Interstellar Boundary Explorer (IBEX) mission; IBEX has now observed the 3-dimensional structure of this interaction for over a full solar cycle. IBEX observations include global Energetic Neutral Atoms (ENA) maps of ENAs produced in the heliosheath and VLISM beyond the heliopause. These maps expose a time-variable global heliosphere where solar cycle and even longer temporal variations drive a complex ever-evolving structure that surrounds us and defines our home in the galaxy. This SCOSTEP Distinguished Scientist Award Seminar will describe some of the discoveries and insights about the outer heliosphere and VLISM gleaned from the IBEX mission and link them to the much larger and even more exciting follow-on mission currently under development - the Interstellar Mapping and Acceleration Probe (IMAP).

This seminar will be recorded and opened later on the SCOSTEP Website at https://scostep.org/ .

MEETING: **NASA Virtual Science Workshop on Lightning-Related Research Beyond the Troposphere**

From: Tim Lang (MSFC), Shing Fung (GSFC), Sarah Bang (MSFC), Burcu Kosar (GSFC), and Mason Quick (MSFC) (shing.f.fung at nasa.gov)

Webex Online May 2-3, 2022, 10-2:30 Eastern US Time (9am-1:30pm Central, 7-11:30am Pacific, 14-18:30 UTC)

NASA is hosting a virtual science workshop on research regarding lightning-related phenomena beyond the Earth's troposphere. The goal of the workshop is to identify key lightning-related research topics and science questions that fall into gaps within the NASA Science Mission Directorate's current portfolio. Your input at the workshop could help formulate future NASA research opportunities.

The workshop will explore TGFs, TLEs, bolide detection by lightning mappers, effects of lightning on the ionosphere and beyond, lightning on other planets, and will explore existing and future space-borne lightning mapping capabilities. View the agenda here < https://sites.google.com/view/lightning-workshop/agenda >.

Participants are requested to register in advance for the Webex invitation. Registrants will also gain access to an online document to provide additional input on these topics (especially helpful for those who can only attend part of the meeting, or cannot attend at all).

For more information and to register, please visit https://TinyURL.com/NASALightningWorkshop

Thank you for your interest! We look forward to seeing you in May.

Workshop Organizing Committee: Timothy Lang, Shing Fung, Sarah Bang, Burcu Kosar, Mason Quick

SuperSID

Collaboration of Society of Amateur Radio Astronomers and Stanford Solar Center

- Stanford provides data hosting, database programming, and maintains the SuperSID website
- Society of Amateur Radio Astronomers (SARA) sells the SuperSID monitors for 48 USD to amateur radio astronomers and the funds are then used to support free distribution to students all over the world (image below as of Fall 2017)
-
- Jonathan Pettingale at SARA is responsible for building and shipping the SuperSID monitor kits: SuperSID@radio-astronomy.org
- SuperSID kits may be ordered through the SARA SuperSID webpage: http://radio-astronomy.org/node/210

- Questions about the SuperSID project may be directed to Steve Berl at Stanford: steveberl@gmail.com

- Jaap Akkerhuis at Stanford is responsible for the SuperSID software and SARA has provided financial support for his efforts

- SuperSID website hosted by Stanford: http://solar-center.stanford.edu/SID/sidmonitor/
- SuperSID database: http://sid.stanford.edu/database-browser/

- The data is searchable by time, station, date, and multiple plots may be placed on the same graph for comparison.

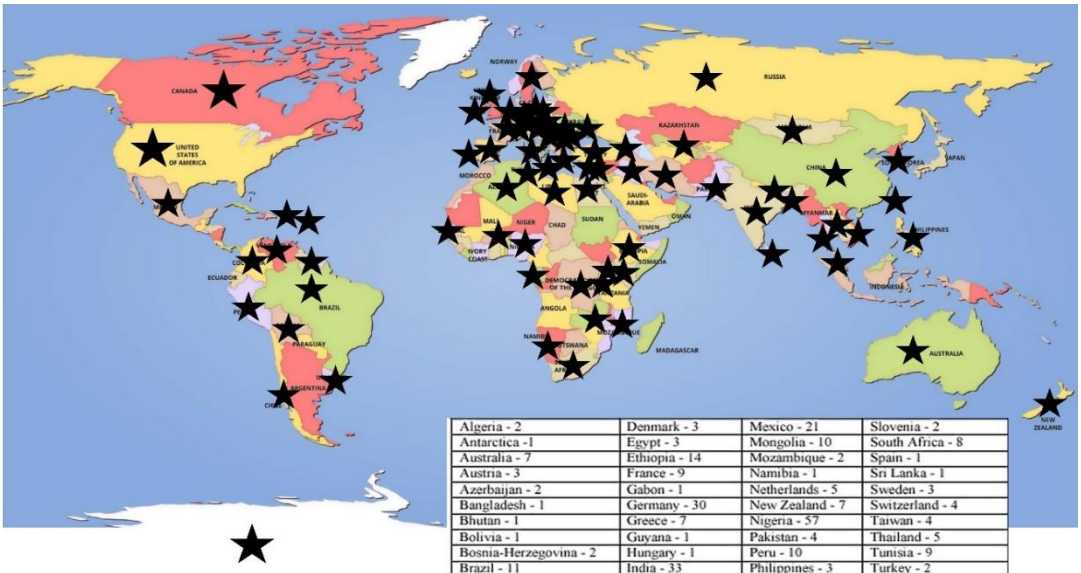

Algeria - 2	Denmark - 3	Mexico - 21	Slovenia - 2
Antarctica -1	Egypt - 3	Mongolia - 10	South Africa - 8
Australia - 7	Ethiopia - 14	Mozambique - 2	Spain - 1
Austria - 3	France - 9	Namibia - 1	Sri Lanka - 1
Azerbaijan - 2	Gabon - 1	Netherlands - 5	Sweden - 3
Bangladesh - 1	Germany - 30	New Zealand - 7	Switzerland - 4
Bhutan - 1	Greece - 7	Nigeria - 57	Taiwan - 4
Bolivia - 1	Guyana - 1	Pakistan - 4	Thailand - 5
Bosnia-Herzegovina - 2	Hungary - 1	Peru - 10	Tunisia - 9
Brazil - 11	India - 33	Philippines - 3	Turkey - 2
British Virgin Islands - 1	Indonesia - 2	Poland - 2	Uganda - 5
Bulgaria - 2	Iran - 4	Portugal - 3	UK - 32
Burkino Faso - 1	Iraq - 1	Rep of Congo - 3	Uruguay - 9
Canada - 33	Ireland - 9	Romania - 4	US Virgin Islands - 2
Chile - 1	Italy - 42	Russia - 3	USA - 491
China - 38	Kenya - 23	Rwanda - 1	Uzbekistan - 2
Columbia - 9	Korea (South) - 2	S Africa - 4	Venezuela - 2
Croatia - 7	Lebanon - 11	Senegal - 1	Vietnam - 1
Cypress - 1	Libya - 1	Serbia - 1	Zambia - 2
Czech Republic - 1	Malaysia - 19	Singapore - 3	
D Rep of Congo - 4	Malta - 1	Slovak Repub - 2	

For official use only
Monitor assigned: _____
Site name: _____
Country: _____

SuperSID Space Weather Monitor

Request Form

	Your information here
Name of site/school *(if an institution)*:	
Choose a site name: *(3-6 characters) No Spaces*	
Primary contact person:	
Email:	
Phone(s):	
Primary Address:	Name School or Business Street Street City State/Province Country Postal Code
Shipping address, if different:	Name School or Business Street Street City State/Province Country Postal Code
Shipping phone number:	
Latitude & longitude of site:	Latitude: _____ Longitude: _____

I understand that neither Stanford nor the Society of Amateur Radio Astronomers is responsible for accidents or injuries related to monitor use. I will assure that a surge protector and other lightning protection devices are installed if necessary.

Signature: _____ **Date:** _____

I will need:

What	*Cost*	*How many?*
SuperSID distribution USB Power	$48 (assembled)	
USB Sound card 96 kHz sample rate *(or provide this yourself)*	$40 *(optional)*	
Antenna wire (120 meters) *(or you can provide this yourself)*	$23 *(optional) with connectors attached and tested*	
RG 58 Coax Cable (9 meters) *(or provide this yourself)*	$14 *(optional) with connectors attached and tested*	
Shipping	US $12 Canada & Mexico $40 all other $60	

	TOTAL	$

____ I have included a $_____ check (payable to SARA)

____ I will make payment thru www.paypal.com to treas@radio-astronomy.org

or

____ If you are a Minority-serving institution, in a Developing or economically deprived nation, and/or you are using the monitor with students for educational purposes, you may qualify for obtaining a monitor at reduced or no cost. Check here if you wish to apply for this designation. Then tell us how you want to use the SuperSID monitor. Include type of site, number of students involved, whether public or private school, grade levels, etc. and describe your program. The goal of the SuperSID project is to provide as many students with systems as possible. If you are able to pay for a system, even if you qualify for a free one, please do so and help support our goal.

_____

_____

_____

For more details on the Space Weather Monitor project, see: **http://sid.stanford.edu**

To set up a SuperSID monitor you will need:

1. Access to power and an antenna location that is relatively free of electric interference (could be indoors or out)
2. A **PC**** with the following minimal specifications:
    a. A sound card that can record (sample) up to 96 kHz, or a USB port to connect such a sound card (for North and South America)
        i. All other countries can use AC97 sound card with 48 kHz record (sample) rate. Most computers made after 1997 will have AC97.
    b. Windows 2000 or more recent operating system
    c. 1 GHz Processer with 128 mb RAM
    d. Ethernet connection & internet browser (desirable, but not required)
    e. Standard keyboard, mouse, monitor, etc.
3. An inexpensive antenna that you build yourself. You'll need about 120 meters (400 feet) of **insulated** wire. Solid wire is easier to wind than stranded. Magnet wire will work but be more fragile. You can use anything from #18 to #26 size wire. The antenna frame can be made of wood, PVC pipe, or similar materials. We'll provide instructions. You can purchase the wire from us or obtain your own.
4. RG58 coax cable with a BNC connector at one end to run from the antenna to the SuperSID receiver. 9 meters is recommended, but the length will depend on where you place the antenna. You can purchase the coax from us or obtain your own.
5. Surge protector and other protection against a lightning strike

---

Return this form to: SuperSID@radio-astronomy.org

or mail to: SARA
Brian O'Rourke, SARA Treasurer
337 Meadow Ridge Rd,
Troy, VA 22974-3256

Founded in 1890

The British Astronomical Association

A company limited by guarantee
Registered Charity No. 210769

Burlington House, Piccadilly, London, W1J 0DU
Telephone: 020 7734 4145 Fax No.: 020 7439 4629
Email: office@britastro.org Website: www.britastro.org

Please send all reports and observations to jacook@jacook.plus.com

John Cook's VLF Report

BAA Radio Astronomy Section, Director: Paul Hearn

RADIO SKY NEWS **2022 JANUARY**

VLF SID OBSERVATIONS

Solar activity was lower in January compared with December, with no M-class flares recorded as SIDs. The satellite X-ray data shows three M-class flares, but they were all hidden during the European night-time. The strongest was M5.5 at 06UT on the 20th.

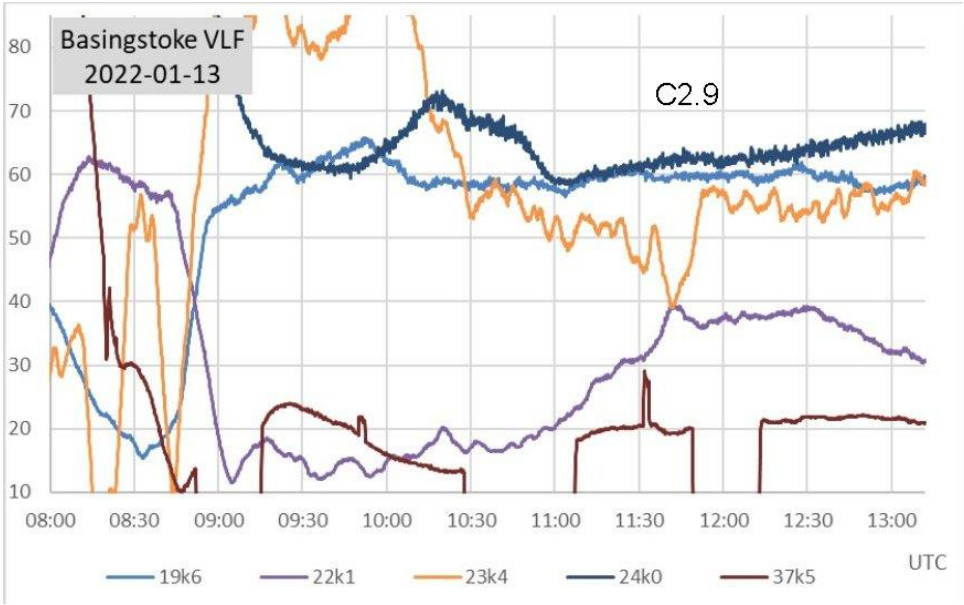

This recording by Paul Hyde shows the C2.9 flare peaking at 11:40UT on the 13th. The 22.1kHz signal from Anthorn shows a fairly clear SID, with a matching response at 23.4kHz almost hidden in the noise. Neither 19.6 or 24kHz show any response, while 37.5kHz has some drastic breaks that hide any useful data.

The C3.7 flare on the 25th was widely recorded, the chart by Mark Prescott showing the SID on some very clean signals. 22.1kHz has again given a very clear SID, with 23.4kHz smaller but very clear. Mark has also indicated the timing of an earlier C1 flare, although there are no signs of a SID on any of the three active signals.

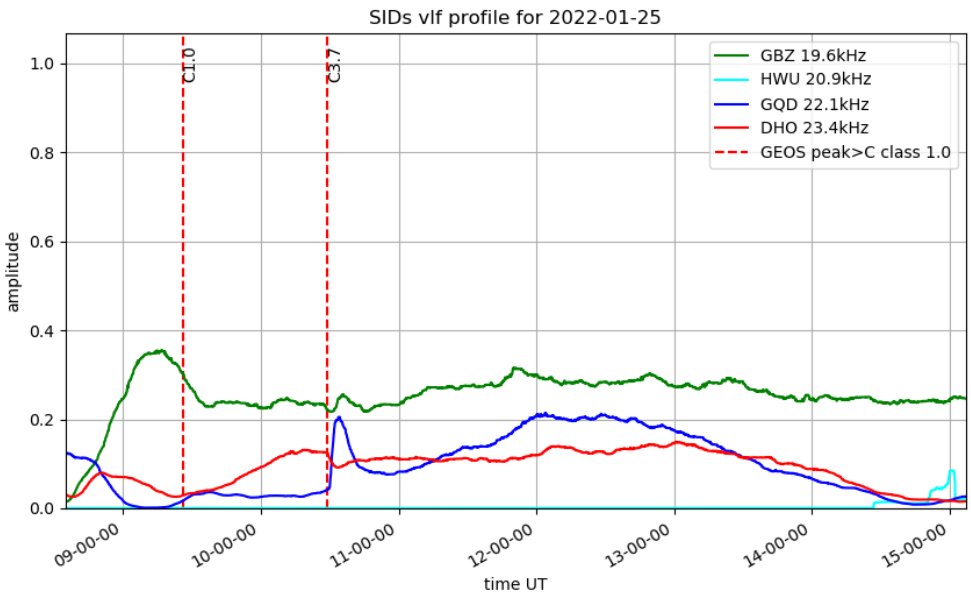

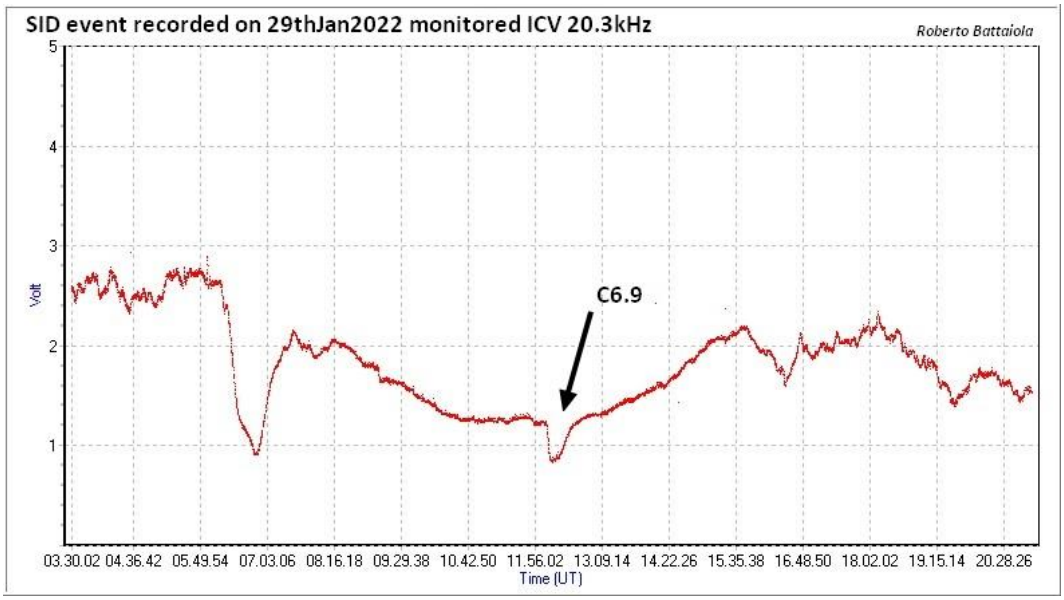

This recording by Roberto Battaiola shows the C6.9 flare on the 20.3kHz signal. This transmitter is located at Isola Di Tavolara, roughly 500km south of Roberto. It has provided a very clean day-time signal that also enabled him to catch the C7.3 flare at 07:32UT on the 16th, missed by observers here in the UK. Preceding the C6.9 in the tables is a SID marked '*'. The C6.9 flare appears to have had a fairly long rise time that included an extra peak that is not listed in the SWPC flare list. This does often happen with slower flares.

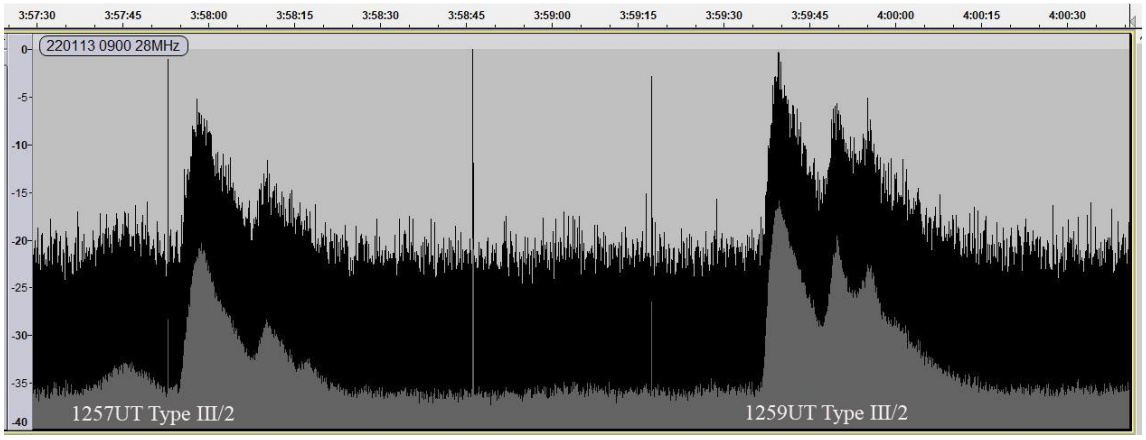

This recording by Colin Briden shows a pair of 28MHz noise bursts on the 13th. They are both of type III/2, the second being the stronger. There were no flares listed at this time, but they may possibly be related to the C2.9 flare recorded about an hour earlier.

MAGNETIC OBSERVATIONS.

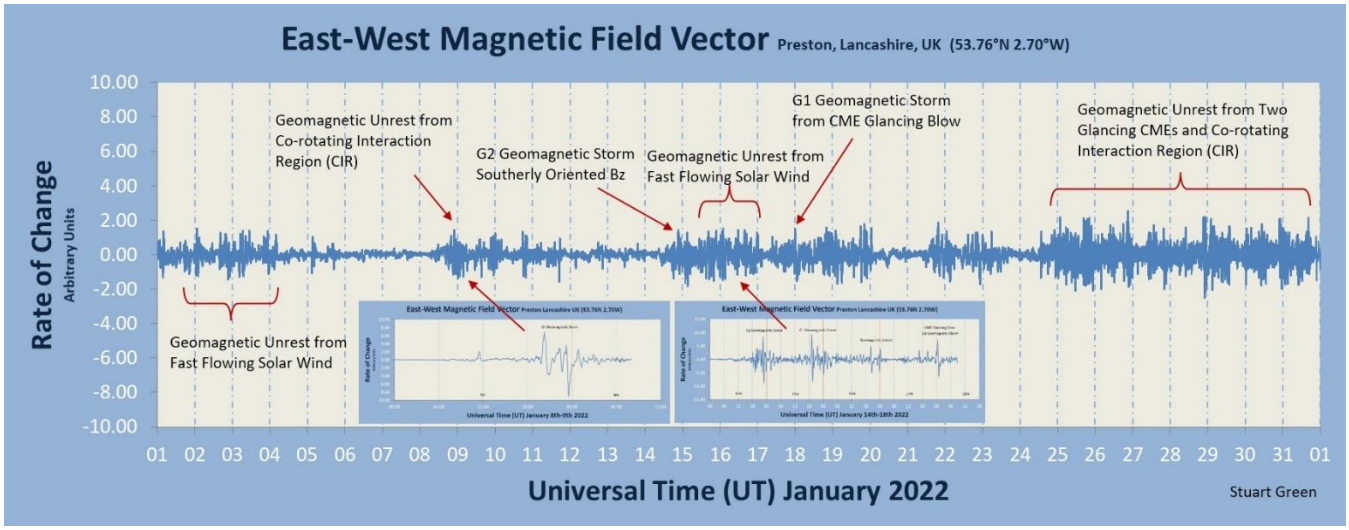

Stuart Green's summary of the month's magnetic activity shows a good mixture of high speed winds and CMEs. It seems that a number of the stronger flares during our night-time produced CMEs. An M1.5 flare listed at 17:44UT on the 18th may have produced a CME that we recorded at 13:30-13:40UT on the 21st. Its arrival was recorded by several observers, and is shown here in the chart by Callum Potter:

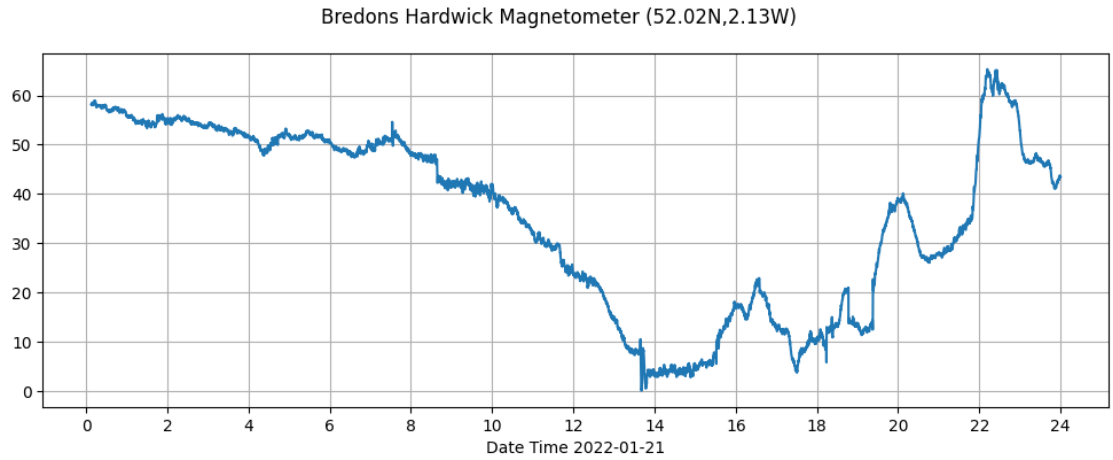

The impact shock does look like some local interference, but its appearance on a number of recordings proves that it is genuine. The following disturbance was very mild, and merged with a high speed wind as well as further weak CMEs.

An equatorial coronal hole wind stream produced a very mild disturbance to start the month, with a south polar coronal hole stream producing a short period of disturbance late in the evening of the 8th. Glancing blows from a CME added to a high speed wind to produce a disturbance on the 14th, continuing through to the 20th. This recording from Nick Quinn shows the disturbance starting around 18UT on the 14th:

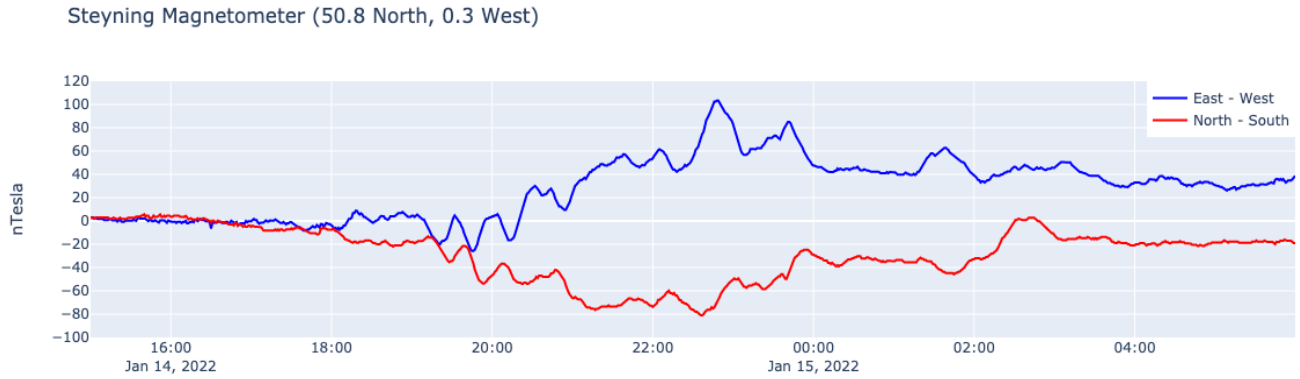

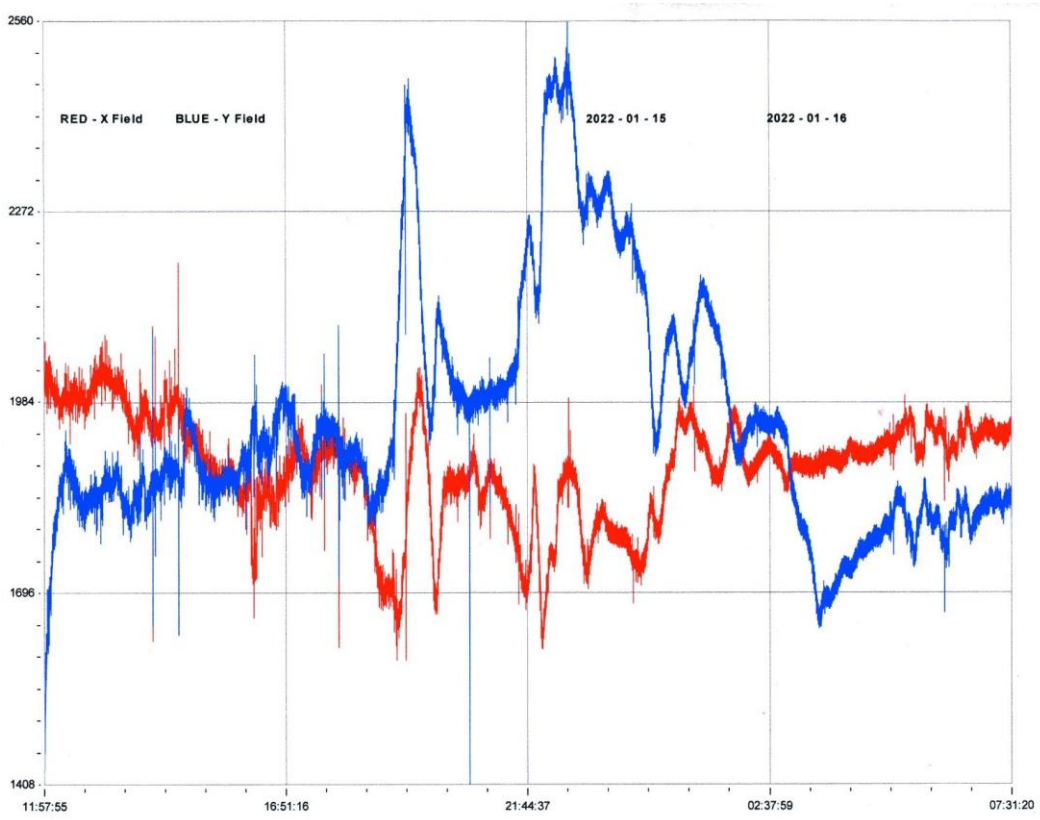

The disturbance faded out in the early morning of the 15th, but increased again later in the day, as shown above by Colin Clements. Activity remained low on the 17th, but increased again over the 18th and 19th, shown by Roger Blackwell:

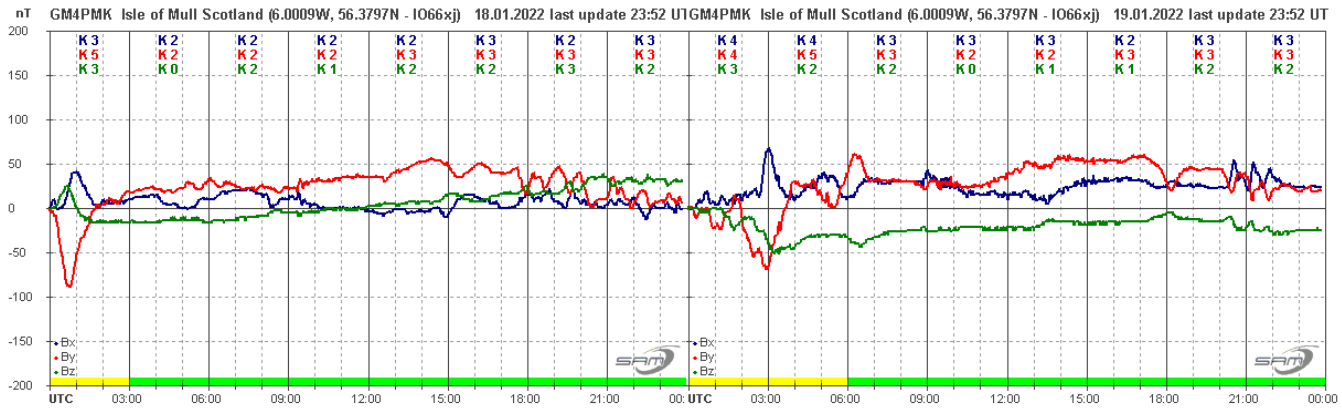

Magnetic observations received from Roger Blackwell, Colin Clements, Stuart Green, Callum Potter, Nick Quinn, Andrew Thomas and John Cook.

TONGA VOLCANO.

The volcanic eruption near the Pacific island of Tonga caused considerable damage to the nearby islands, but the effects of its rising plume of gas were felt across the globe. Mark Edwards has been analysing the recordings made here. The gas cloud rose high into the atmosphere, creating a pressure wave that radiated outwards over the Pacific ocean. The Space Weather web site showed the pressure wave being recorded moving north eastwards over America, and weather stations here in the UK also detected sudden pressure changes. These waves also affected the lower ionosphere, with Magnetic and VLF recordings showing a disturbance as well as NASA measurements showing changes in the Total Electron Content above stations close to the volcano. The eruption occurred at about 04:10UT on January 14th, and Mark noted the pressure shock at 19:19UT on the 15th. UK Met office data shows a big pressure shock between 19:00 and 19:30 recorded at Brize Norton (near Oxford). David Farn also noted a small magnetic transient at the same time.

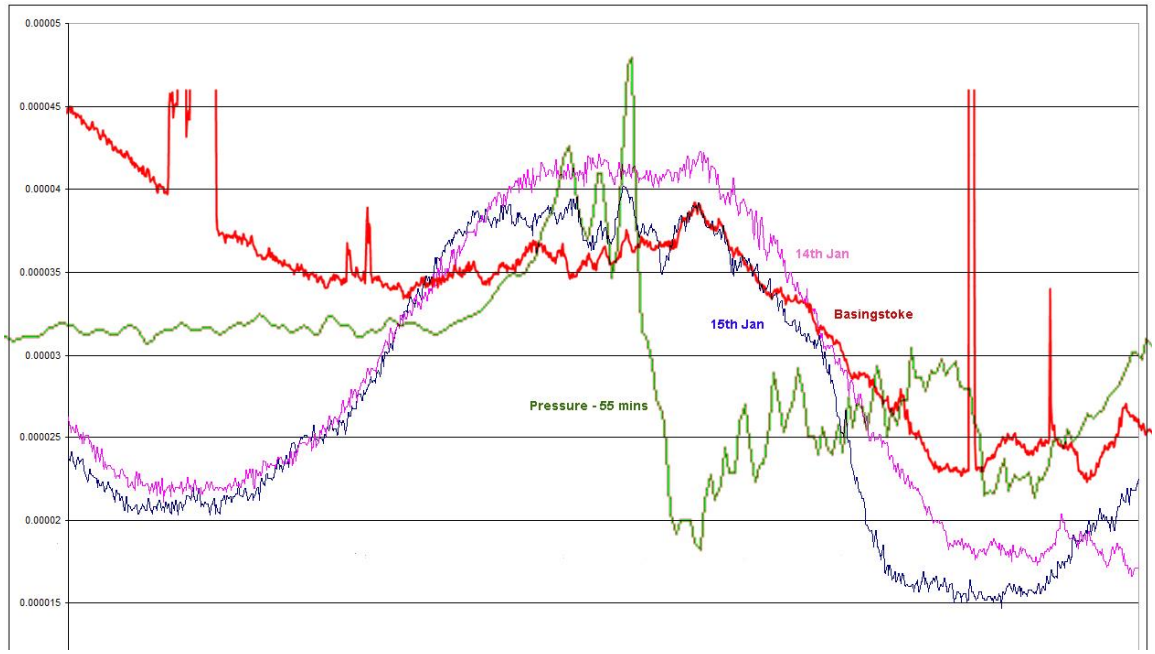

This chart is rather complicated, but shows the 24kHz trans-Atlantic signal recorded by Paul Hyde on the 15th (red) and by Mark Edwards (15th in blue, 14th in pink). There is a low level of general noise on the signals, but both traces from the 15th show some stronger waves between 18 and 19UT. The trace from the 14th does not show this activity. Using UK Met office pressure data, Mark has calculated that the pressure shock should have been about 1600km away from his location (Coventry). His path length at 24kHz is 4768km, so the shock would be about a third of the way along the path. The sunset time at this point is 17:40UT, but Mark has recorded SIDs in the past at around this time in January.

The green trace is the Met office pressure plot from Brize Norton, delayed by 55 minutes to match the VLF waves. There is a possible reason why these timings do not match: the great circle paths from Tonga to the UK and to the 24kHz signal reflection area are very different. The pressure wave would cross the 24kHz path at nearly a right angle, while the path into the UK would pass nearer to the pole, and be more nearly parallel here. Thus more of the path would be affected at the same time. The pressure wave speed to Brize Norton works out at 312m/s. This is quite a complex problem, so perhaps more work might be done in the future as other data becomes available.

METEOR OBSERVATIONS.

Colin Clements made recordings of the Quadrantid meteors using the GRAVES signal. Counts were made on the 2nd, 3rd and 4th, but significant counts were only seen late on the 3rd and into the morning of the 4th.

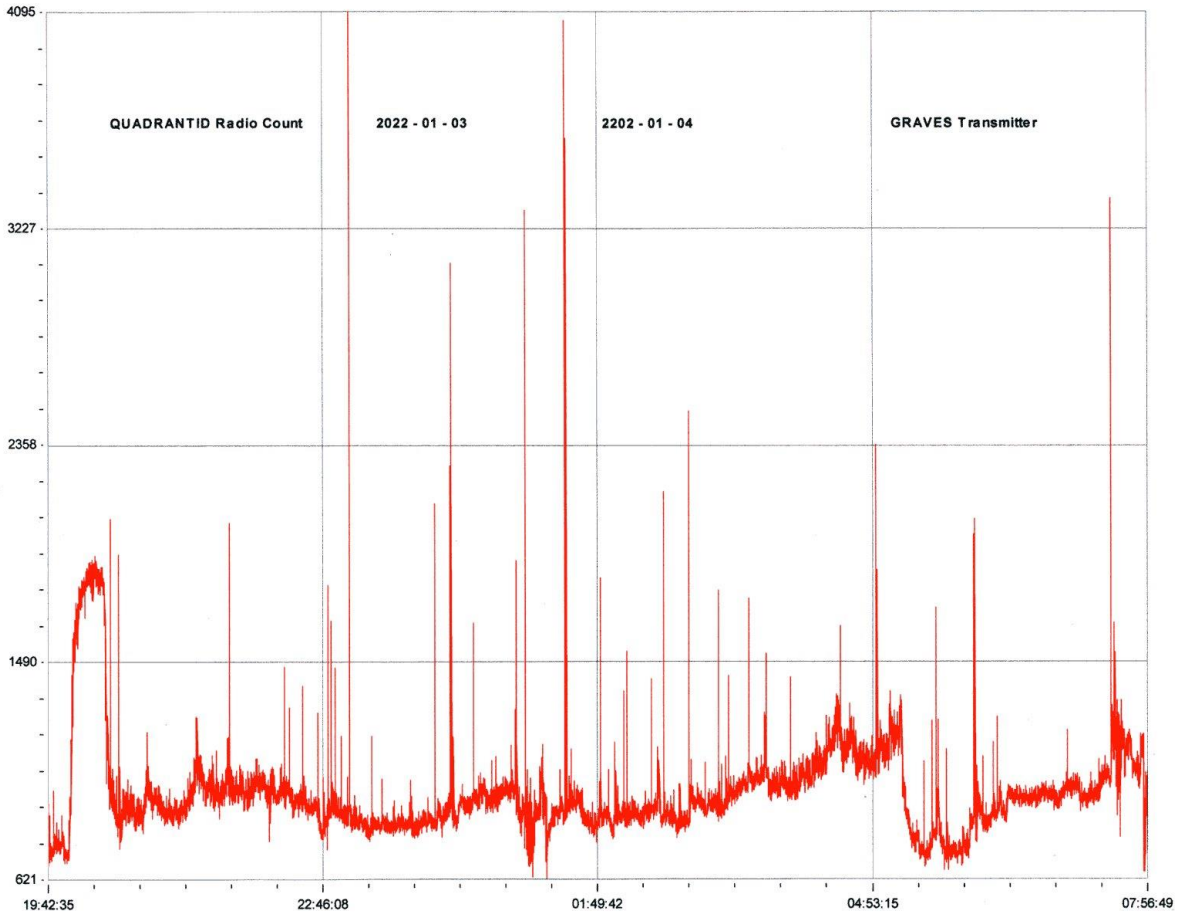

On this occasion no clear activity peak is visible, with counts fairly steady from about 21UT to 06UT.

	Xray class	Observers	John Cook (23.4kHz/*22.1kHz*)				Roberto Battaiola 20.3kHz				Paul Hyde (22.1kHz/*24kHz*)				Mark Edwards (23.4/*19.6*/***24kHz***)				Colin Clements (23.4kHz/*18.3kHz*)			
			Tuned radio frequency receiver, 0.58m frame aerial.				Modified AAVSO receiver.				Spectrum Lab / PC 1.5m frame aerial.				Spectrum Lab / PC 2m loop aerial.				Tuned Radio Frequency receivers, 0.76m screened loop aerial.			
DAY			START	PEAK	END (UT)		START	PEAK	END (UT)		START	PEAK	END (UT)		START	PEAK	END (UT)		START	PEAK	END (UT)	
13	C2.9	5	11:37	11:41	11:57	1	11:34	11:40	11:51	1-	11:35	11:42	11:52	1-	*11:37*	*11:40*	*11:45*	*1-*				
14	C2.1	1					11:42	11:51	11:59	1-												
25	C3.7	10	10:25	10:29	10:38	1-	10:23	10:29	10:53	1+	10:25	10:29	10:43	1-	10:26	10:29	10:46	1	10:28	10:32	10:45	1-
26	C7.2	1					07:29	07:32	07:37	1-												
26	C1.6	2													*10:24*	*10:26*	*10:30*	*1-*				
28	C2.6	1					08:33	08:40	08:46	1-												
29	B9.5	1													**09:01**	**09:05**	**09:09**	**1-**				
29	*	2													11:52	11:55	12:00	1-				
29	C6.9	10	12:08	12:13	12:42	2	12:04	12:13	12:40	2	12:07	12:15	12:44	2	12:07	12:13	12:28	1	12:09	12:15	12:50	2
29	C2.0	3									14:13	14:17	14:26	1-	14:16	14:17	14:22	1-				
29	C7.3	2									16:52	16:56	17:07	1-	***16:52***	***16:56***	***17:06***	***1-***				

	Xray class		Steve Parkinson (Various)				Andrew Thomas (19.6kHz)				Phil Rourke (23.4kHz)				John Wardle				Christopher Bailey			
			Tuned radio frequency receiver, frame aerials.				Tuned radio frequency receiver, 0.6m frame aerial.				Spectrum Lab, 0.6m frame aerial.				SpetrumLab/Starbase, Active mini-whip aerial.				Spectrum Lab			
DAY			START	PEAK	END (UT)		START	PEAK	END (UT)		START	PEAK	END (UT)		START	PEAK	END (UT)		START	PEAK	END (UT)	
13	C2.9						11:36	11:44	11:52	1-												
14	C2.1																					
25	C3.7		10:25	10:30	10:45	1	10:24	10:30	10:44	1									10:26	10:29	10:47	1
26	C7.2																					
26	C1.6																		10:22	10:25	10:35	1-
28	C2.6																					
29	B9.5																					
29	*						11:53	11:56	12:08	1-												
29	C6.9		12:08	12:15	12:38	1+	12:08	12:15	12:47	2									12:09	12:15	12:47	2
29	C2.0						15:30	15:34	15:45	1-												
29	C7.3																					

	Xray class		Colin Briden (22.1kHz)				Andrew Lutley (23.4kHz)				Peter Meadows (23.4kHz)				John Elliott (18.3kHz)				Mark Prescott (22.1kHz)			
			Spectrum Lab / PC, 1.2m frame aerial.				Tuned radio frequency receiver, 0.6m frame aerial.				Tuned radio frequency receiver, 0.6m frame aerial.				Tuned radio frequency receiver, 0.5m frame aerial.							
DAY			START	PEAK	END (UT)		START	PEAK	END (UT)		START	PEAK	END (UT)		START	PEAK	END (UT)		START	PEAK	END (UT)	
13	C2.9																					
14	C2.1																					
25	C3.7		10:26	10:30	10:36	1-													10:29	10:33	10:54	1
26	C7.2																					
26	C1.6																					
28	C2.6																					
29	B9.5																					
29	*																					
29	C6.9		12:08	12:16	12:28	1													12:13	12:21	12:37	1
29	C2.0																					
29	C7.3																					

VLF SID OBSERVATIONS

Solar flare activity has increased this month, with 16 SIDs recorded. The satellite data shows activity throughout February, mostly with B- and C-class flares. There were three M-class flares shown, two of which we managed to record. The M1.4 flare peaking at 08:43UT on the 12th was the strongest event of the month, and produced a clear SID on Roberto Battaiola's recording:

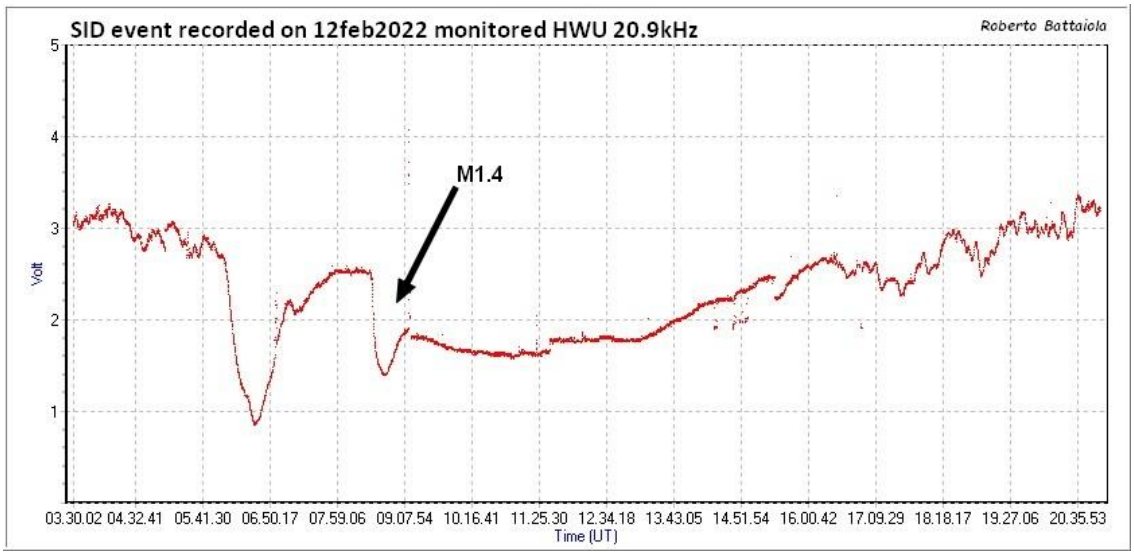

The most widely recorded event was also the most tricky to decode. My own recording shows the two SIDs well at 23.4kHz, recorded on the 14th:

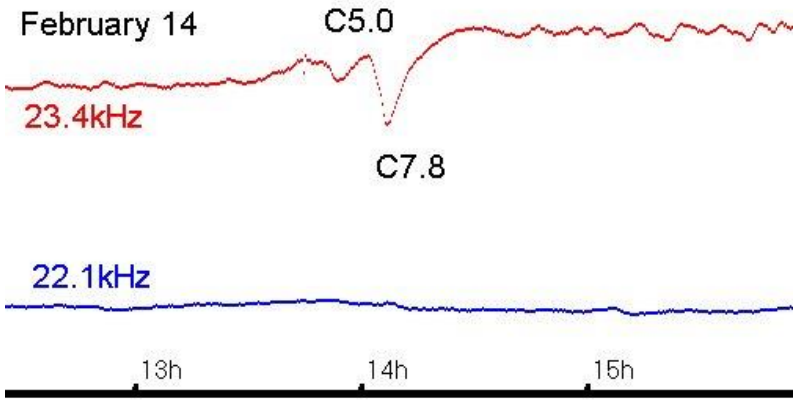

There are clearly two SIDs recorded, the second being the stronger of the pair. The SWPC bulletin lists a C5.0 flare peaking at 13:53UT, followed by an event peaking at 14:33 without a flare magnitude. By far the majority of observers recorded a peak at around 14:07, matching the second SID in my chart, above. Looking at the German GOES website www.polarlicht-vorhersage.de/goes-archive there was a double peaked flare, the second peak

reaching C7.8 and matching the timing of our observations. Another double peaked flare is shown in this recording from February 2nd by Mark Prescott:

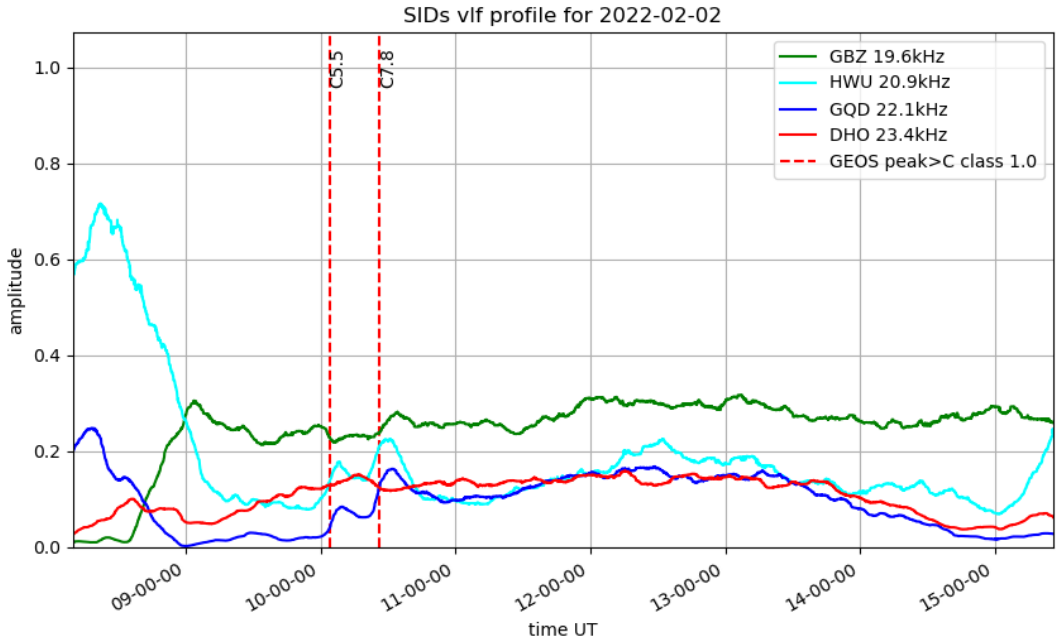

Individual SIDs show well at 22.1kHz and 20.9kHz, the second being the stronger. As with the previous pair, the second event is not listed in the SWPC bulletin.

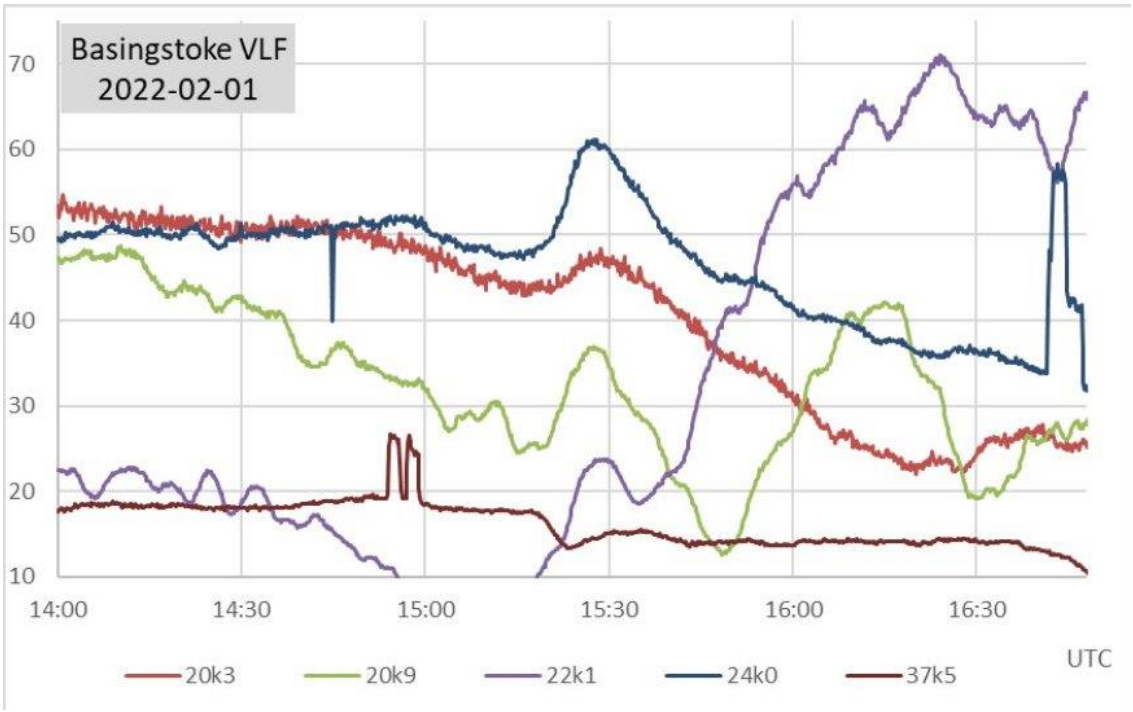

Noise on the VLF signals remains a problem in February, but this recording by Paul Hyde shows a clear SID from the C6.5 flare peaking at 15:26 on the 1st. 24kHz has a very clean signal, and matches well with the response at 20.9kHz. The more local signals are generally less stable, but the SID is clear. The Icelandic signal at 37.5kHz shows a very weak response to the flare.

MAGNETIC OBSERVATIONS.

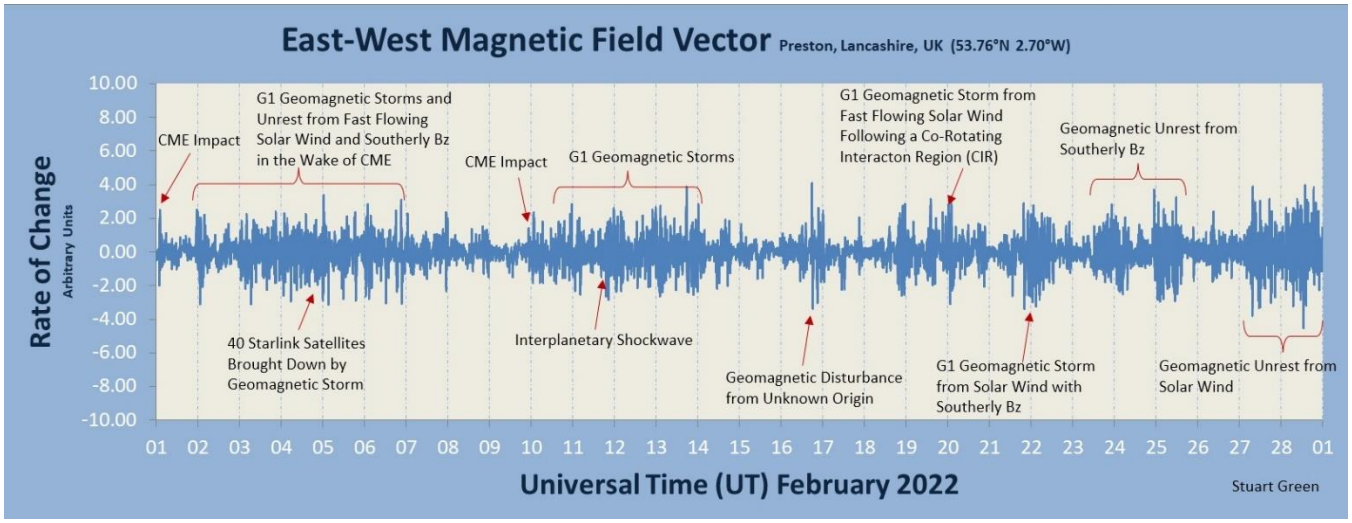

The month's summary of magnetic activity by Stuart Green shows disturbed conditions throughout the month. A CME recorded in satellite data from January 29th reached Earth late on February 1st, creating a distinct transient in our magnetometer recordings. This chart by Nick Quinn shows the impact clearly at about 22:20UT:

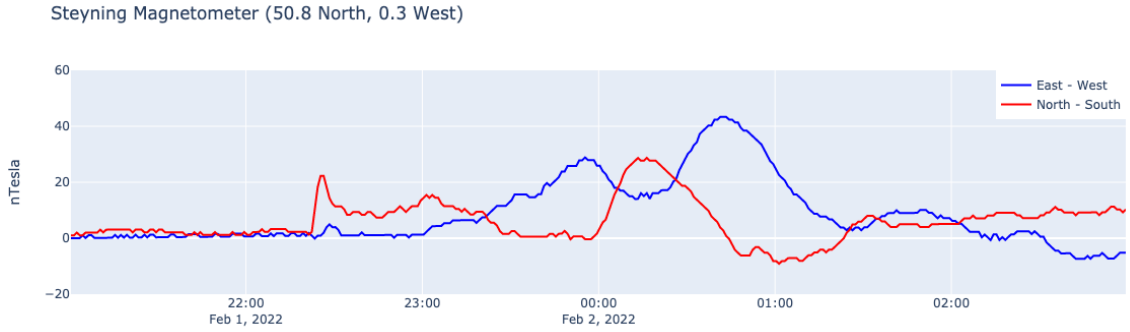

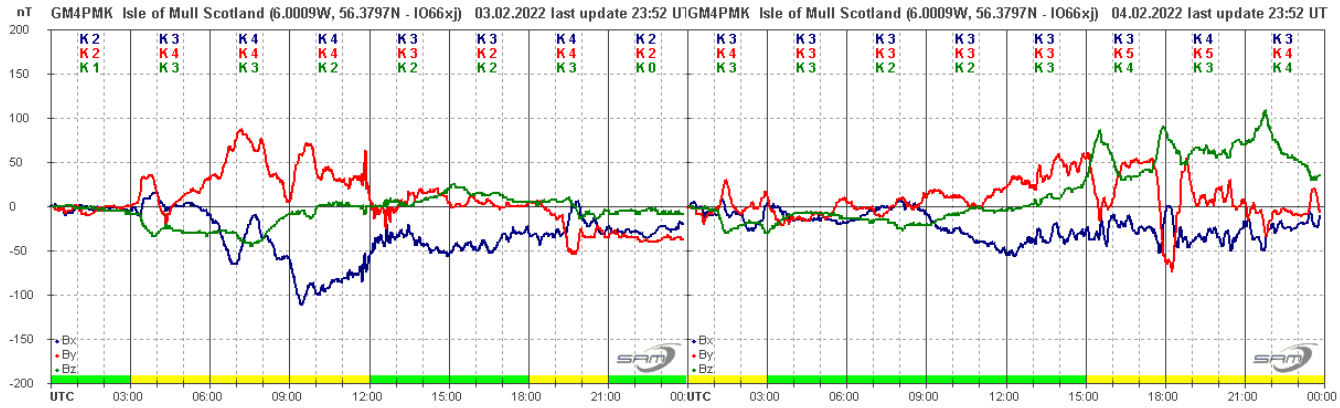

The chart by Roger Blackwell shows the strong disturbance following the impact over the 3rd and 4th. Although the CME impact was on the 1st, there was only a very mild disturbance on the 2nd. It faded out in the early hours of the 5th. This CME will no doubt be remembered for its timing during a starlink satellite launch. The initial orbit of the satellites was at a fairly low altitude, in the region severely disturbed by the magnetic disturbance. Most of the satellites were subsequently lost due to the increased atmospheric drag and loss of control.

A C3.1 flare at 12:41UT on the 6th was not recorded as a SID, but created a CME that was well recorded from the 10th. It produced some very rapid magnetic fluctuations, shown in this recording by Colin Clements:

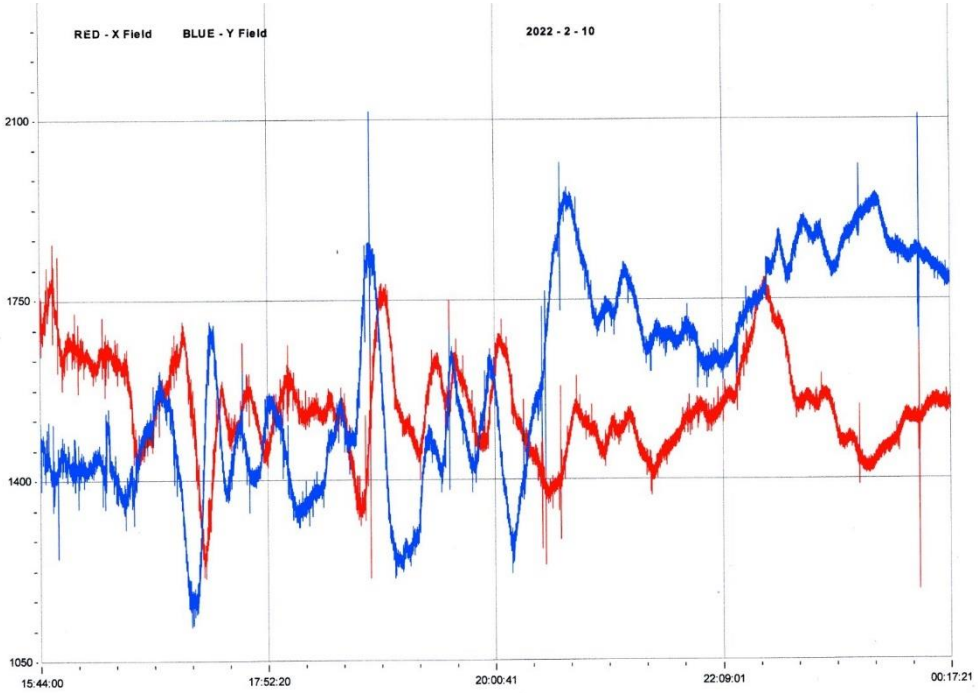

The disturbance continued on the 11th, producing some transients on the 37.5kHz signal from Grindavik, Iceland. This chart shows Mark Edwards' VLF recording (light blue) superimposed on Roger Blackwell's magnetometer:

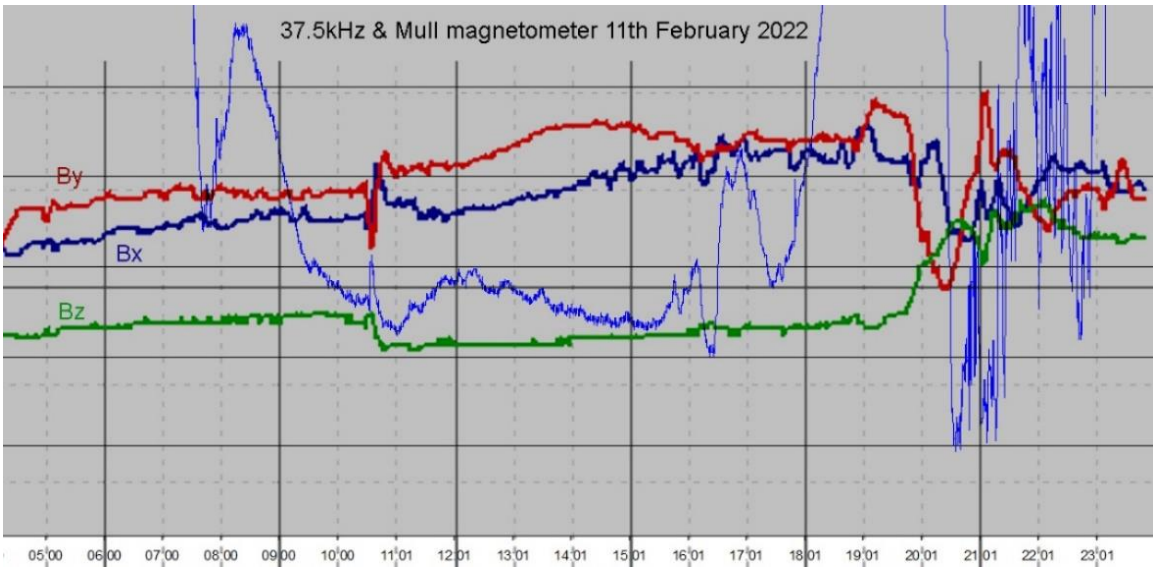

There is a good match at about 10:40 with the very rapid magnetic pulse, and again after 15:00 with a more wave-like disturbance. Paul Hyde also recorded the morning transient with a very SID-like response at 37.5kHz. 24kHz is in purple, 23.4kHz in orange, showing no sign of the magnetic pulse.

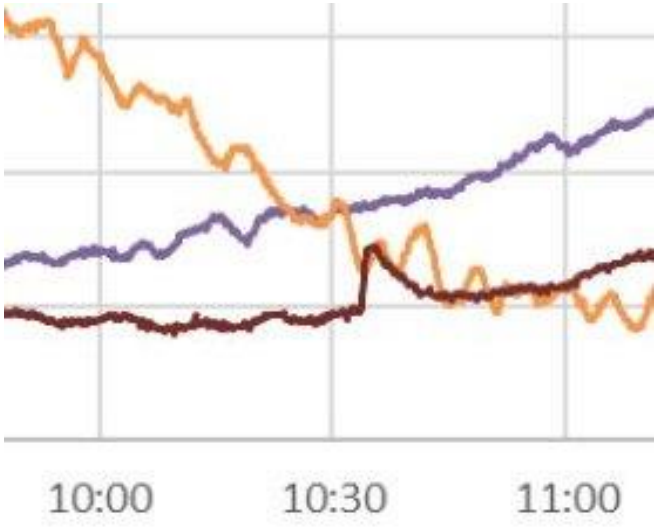

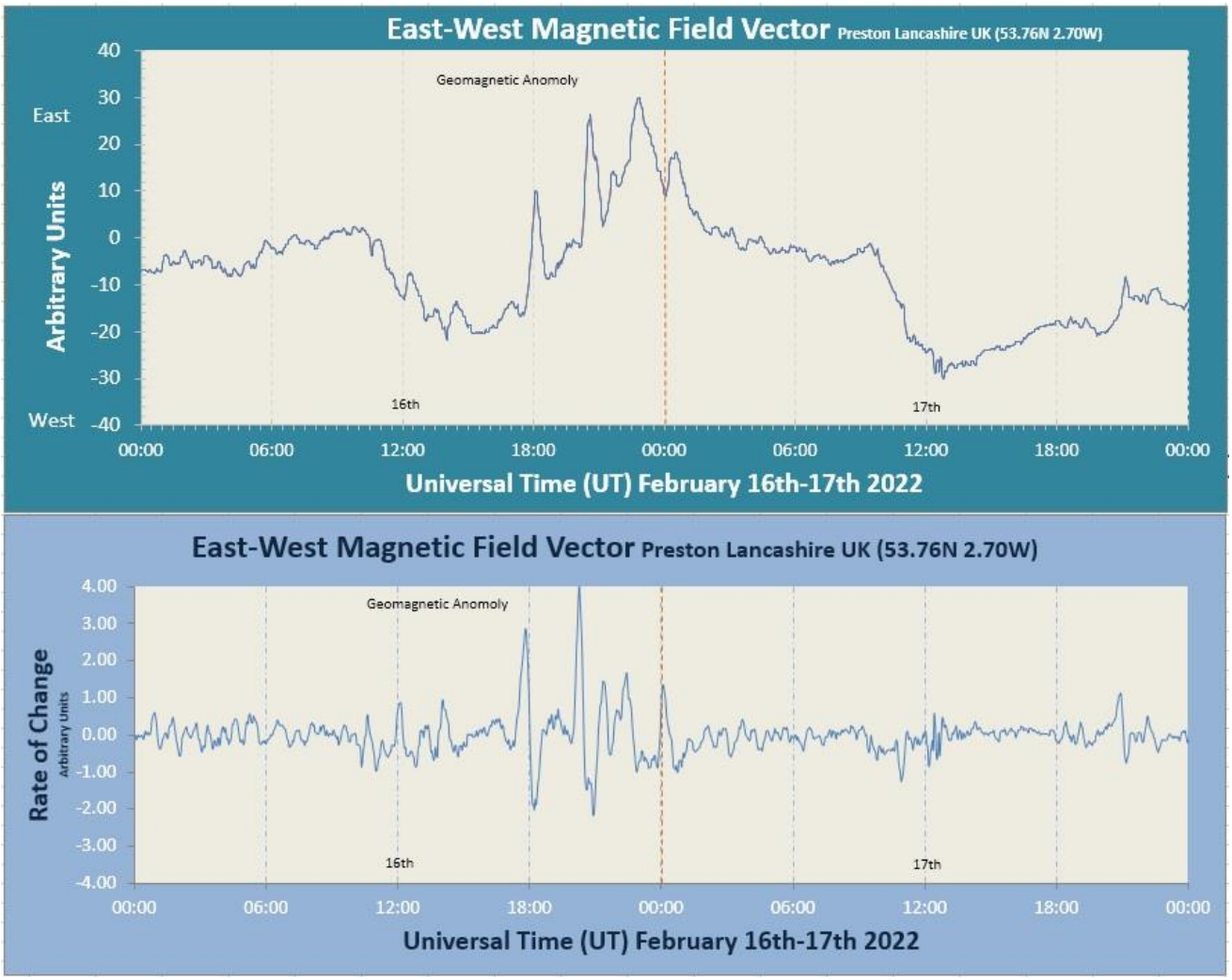

Stuart Green noticed these unusual pulses between 18UT and midnight on the 16th. The only activity at the time seems to have been a CME ejected away from Earth. He has found some similarity with an Intermagnet chart on the web, but no source is given. It does not seem to be listed in the STCE bulletin either. Roger Blackwell's recording shows a rapid disturbance around this time, along with a transient at about 10:45:

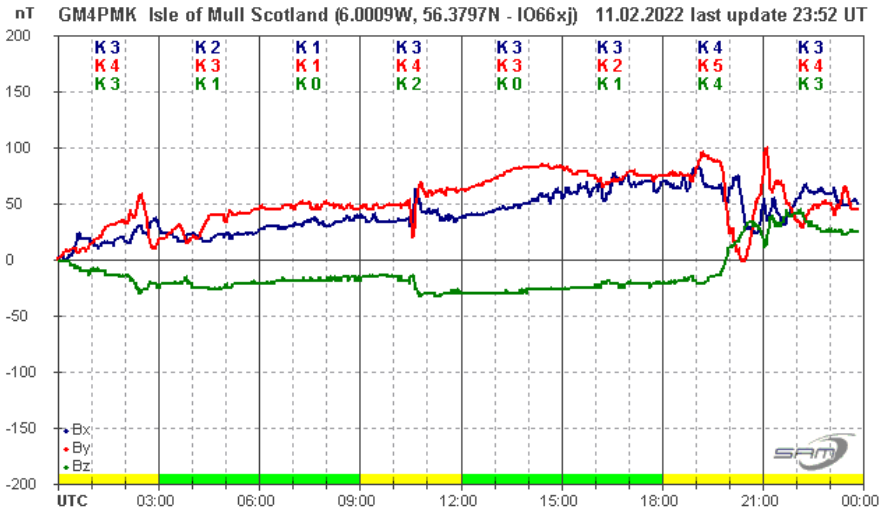

Coronal hole winds were responsible for disturbances later in February, mostly fairly gentle compared to the CME effects. This recording from the 20th by Callum Potter shows a gentle disturbance through the day:

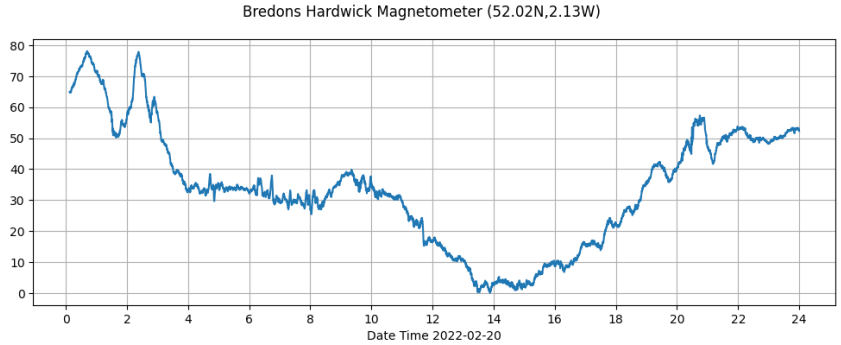

Magnetic observations received from Roger Blackwell, Colin Clements, Stuart Green, Callum Potter, Nick Quinn and John Cook.

SOLAR EMISSIONS.

Colin Briden recorded a very mild Solar Radio emission at 28MHz, rising about 5dB above the noise at 14:02 on the 2nd:

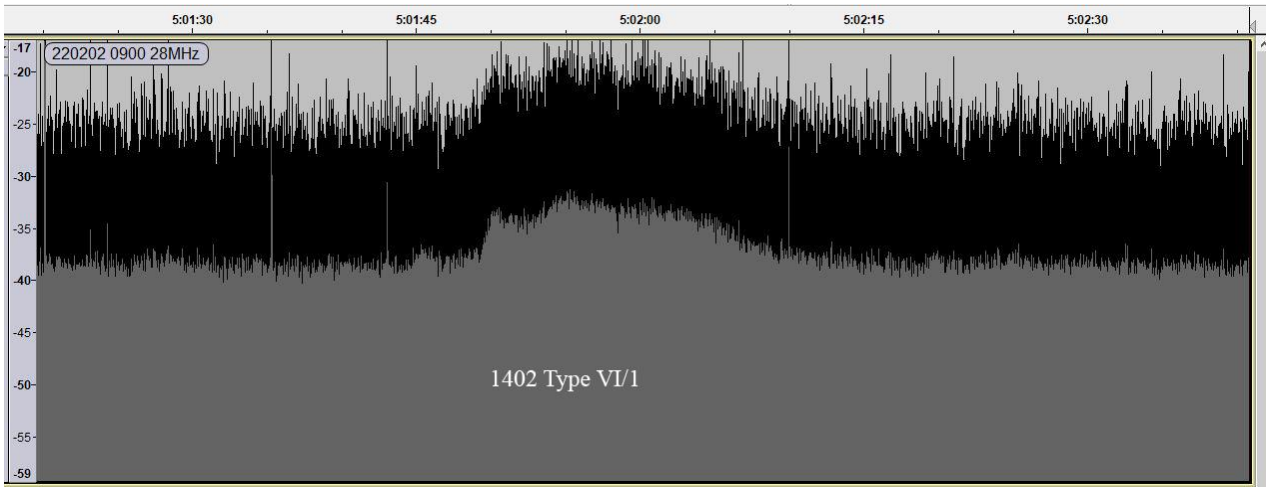

It lasted for just 30 seconds, and does not seem to be linked to any of the listed flares.

	Xray class	Observers	John Cook (23.4kHz/*22.1kHz*)				Roberto Battaiola 20.9kHz				Paul Hyde (22.1kHz/*24kHz*)				Mark Edwards (24.0kHz/*37.5kHz*)				Colin Clements (23.4kHz/*18.3kHz*)			
			Tuned radio frequency receiver, 0.58m frame aerial.				Modified AAVSO receiver.				Spectrum Lab / PC 1.5m frame aerial.				Spectrum Lab / PC 2m loop aerial.				Tuned Radio Frequency receivers, 0.76m screened loop aerial.			
DAY			START	PEAK	END (UT)		START	PEAK	END (UT)		START	PEAK	END (UT)		START	PEAK	END (UT)		START	PEAK	END (UT)	
1	C6.5	2	*15:21*	*15:25*	*15:40*	*1*					15:19	15:26	15:48	1+								
2	C5.5	6	*10:00*	*10:04*	*10:15*	*1-*	09:55	10:04	10:14	1	10:00	10:04	10:14	1-								
2	*C7.8*	5	*10:18*	*10:25*	*10:43*	*1*					10:19	10:25	10:49	1+								
4	C2.1	2									15:46	15:52	15:56	1-	15:45	15:52	?	-				
4	C2.0	1													16:00	16:11	16:50	2+				
7	C1.3	3									11:06	11:10	11:18	1-	11:07	11:10	11:14	1-				
7	C3.8	9	12:37	12:40	12:57	1	12:32	12:41	12:50	1-	12:36	12:40	13:08	1+	*12:36*	*12:42*	*13:09*	*2*				
9	C5.7	2													17:33	17:38	17:49	1-				
12	**M1.4**	3	*08:34*	*08:45*	?	-	08:26	08:43	09:08	2												
12	?	1													16:52	16:59	?	-				
12	C9.2	1													17:06	17:09	17:17	1-				
12	C8.0	1													17:22	17:25	17:29	1-				
14	C5.0	3	13:51	13:54	?	-									13:52	13:55	14:01	1-				
14	?	9	14:03	14:07	14:25	1	14:03	14:07	14:12	1-					14:03	14:08	14:20	1-				
14	**M1.0**	1													17:18	17:30	17:45	1+				
28	C3.1	2													*09:16*	*09:20*	*09:26*	*1-*				

	Xray class		Steve Parkinson (Various)				Andrew Thomas (22.1kHz)				Phil Rourke (23.4kHz)				John Wardle				Christopher Bailey			
			Tuned radio frequency receiver, frame aerials.				Tuned radio frequency receiver, 0.6m frame aerial.				Spectrum Lab, 0.6m frame aerial.				SpetrumLab/Starbase, Active mini-whip aerial.				Spectrum Lab			
DAY			START	PEAK	END (UT)		START	PEAK	END (UT)		START	PEAK	END (UT)		START	PEAK	END (UT)		START	PEAK	END (UT)	
1	C6.5																					
2	C5.5						09:56	10:15	10:36	2												
2	*C7.8*																		10:18	10:26	10:41	1
4	C2.1																					
4	C2.0																					
7	C1.3																					
7	C3.8		12:37	12:41	12:58	1	12:37	12:40	12:58	1									12:32	12:41	12:55	1
9	C5.7																		17:30	17:36	17:55	1
12	**M1.4**																		08:33	08:43	08:58	1
12	?																					
12	C9.2																					
12	C8.0																					
14	C5.0																					
14	?		14:03	14:08	14:18	1-	14:02	14:06	14:15	1-	14:03	14:08	14:18	1-					13:56	14:07	14:16	1
14	**M1.0**																					
28	C3.1																		09:07	09:10	09:40	2

	Xray class		Colin Briden (22.1kHz)				Andrew Lutley (23.4kHz)				Peter Meadows (23.4kHz)				John Elliott (18.3kHz)				Mark Prescott (20.9kHz)			
			Spectrum Lab / PC, 1.2m frame aerial.				Tuned radio frequency receiver, 0.6m frame aerial.				Tuned radio frequency receiver, 0.6m frame aerial.				Tuned radio frequency receiver, 0.5m frame aerial.							
DAY			START	PEAK	END (UT)		START	PEAK	END (UT)		START	PEAK	END (UT)		START	PEAK	END (UT)		START	PEAK	END (UT)	
1	C6.5																					
2	C5.5		10:00	10:04	?	-													09:58	10:08	10:15	1-
2	*C7.8*		10:18	10:27	10:37	1													10:20	10:30	10:45	1
4	C2.1																					
4	C2.0																					
7	C1.3		11:03	11:08	11:15	1-																
7	C3.8		12:37	12:41	12:47	1-													12:38	12:45	12:58	1
9	C5.7																					
12	**M1.4**																					
12	?																					
12	C9.2																					
12	C8.0																					
14	C5.0		13:52	13:54	13:56	1-																
14	?		14:04	14:08	14:12	1-													14:07	14:11	14:20	1-
14	**M1.0**																					
28	C3.1																					

BARTELS CHART

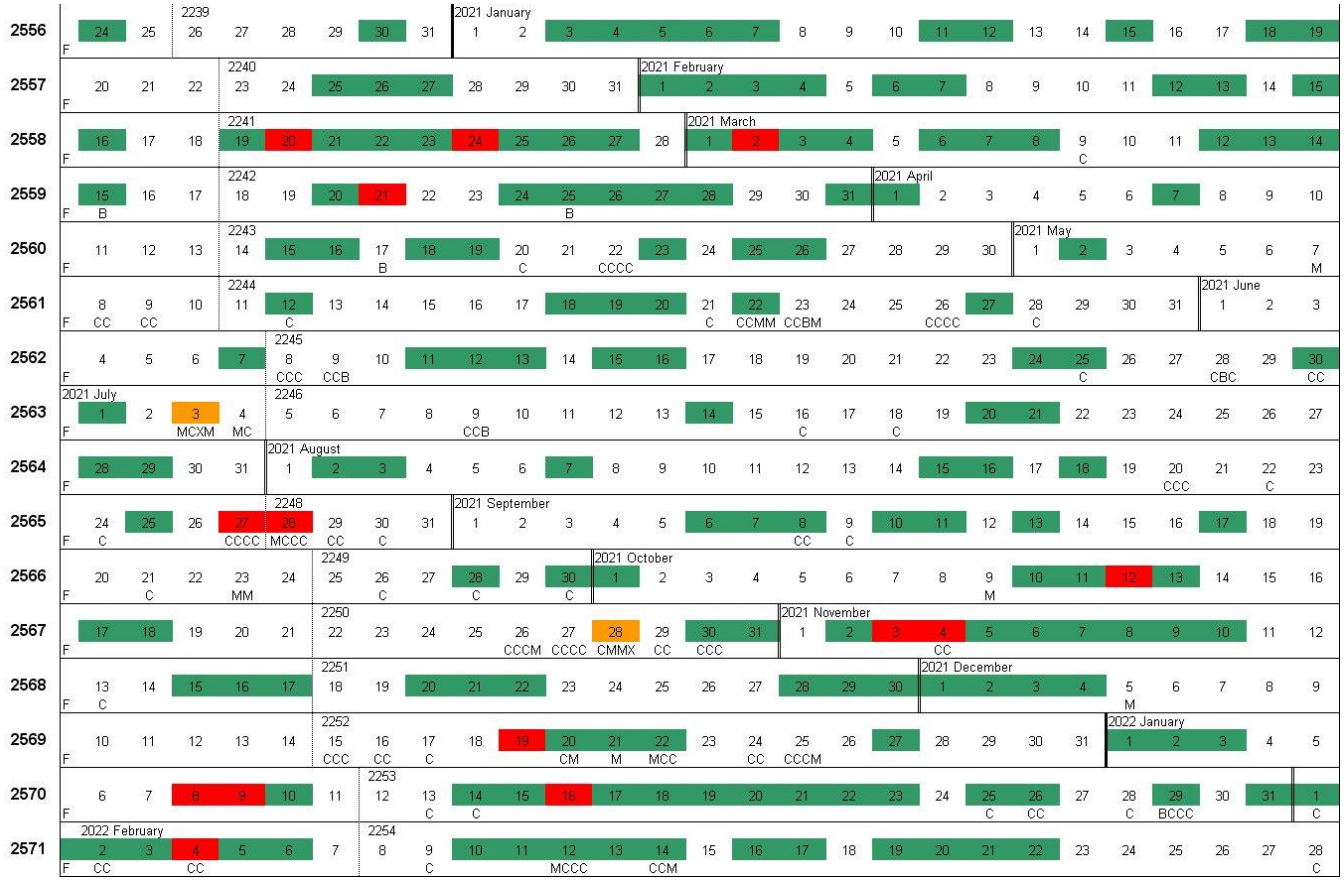

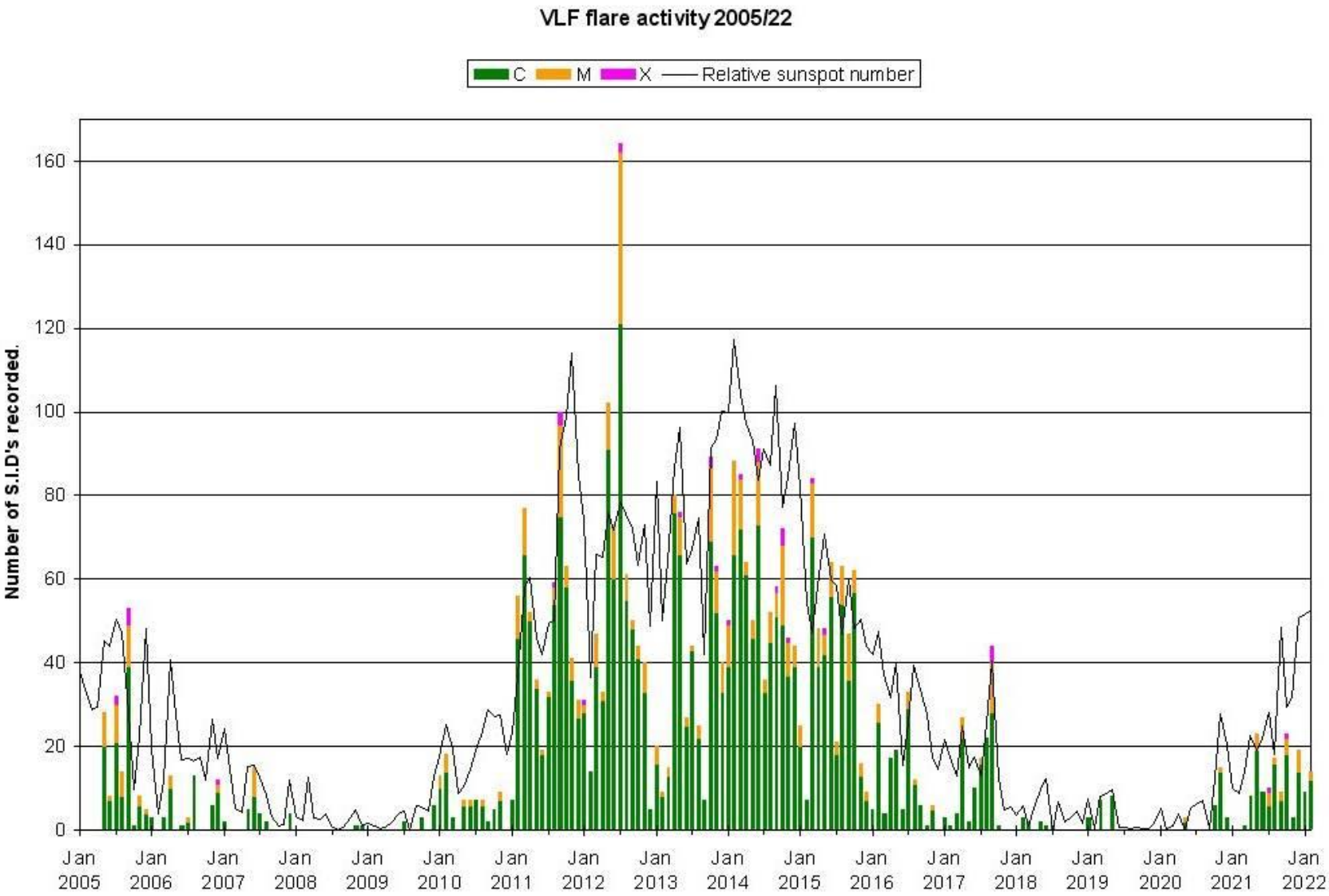
VLF flare activity 2005/22
C
M
X
Relative sunspot number
Number of S.I.D's recorded.
0
20
40
60
80
100
120
140
160
Jan 2005
Jan 2006
Jan 2007
Jan 2008
Jan 2009
Jan 2010
Jan 2011
Jan 2012
Jan 2013
Jan 2014
Jan 2015
Jan 2016
Jan 2017
Jan 2018
Jan 2019
Jan 2020
Jan 2021
Jan 2022

British Astronomical Association
Supporting amateur astronomers since 1890
Radio Astronomy Section

BAA RA Section Summer programme 2022

April 1st 19:30 BST (18:30 UTC)	**Prof. Carole Mundell** Carole Mundell is Professor of Extragalactic Astronomy at the University of Bath. She is an observational astrophysicist who researches cosmic black holes and gamma ray bursts.	***'…on Fast gamma ray bursts'*** **Gamma-ray bursts** (**GRBs**) are immensely energetic explosions that have been observed in distant galaxies. They are the most energetic and luminous electromagnetic events since the Big Bang.
May 6th. 19:30 BST (18:30 UTC)	**Professor Lea Thompson** Department of Physics and Astronomy. University of Sheffield	***'muons; Detection, Cosmology, Tomography, Navigation and Civil Engineering'.***
June 3rd. 19:30 BST (18:30 UTC)	**Dr. Leah Morabito** UKRI Future Leaders Fellow and Asst Prof. Durham University	***'LOFAR: (Low-Frequency Array)*** How high-resolution radio observations can help us understand supermassive black holes'
July 1st. 19:30 BST (18:30 UTC)	**Prof. Jim Madsen** Executive Director Wisconsin IceCube Particle Astrophysics Centre. (WIPAC)	***'Cosmic neutrinos – messengers from the cosmos arriving in Antarctica'.***

If you have any suggestions for the winter 2022 term do let me know.

Our meetings are open to all. Once you are registered on the RA Section email list the Zoom link will be sent out to you before the meeting. If you are not on the email list, please request registration from Paul Hearn RA Section Director (paul@hearn.org.uk).
All recordings will be posted on our BAA YouTube channel. https://www.youtube.com/user/britishastronomical/playlists

Refurbishing an SRT Part 1: Getting the Telescope and Inspection of the Parts

Wolfgang Herrmann

1. Introduction

We were approached with the question whether we would be interested to take over a small radio telescope which has become redundant at the "Dr. Karl Remeis-Sternwarte". This institute, located in the city of Bamberg, is the observatory of the university of Erlangen-Nürnberg [1]. We already have radio telescopes of 25, 10, and 3 meter diameter at our Astropeiler observatory. Therefore, the additional benefit of such an instrument was discussed. The idea came up that one could build an interferometer using this dish together with our existing 3-m instrument. The decision was taken to go for it. We received some photos of the dish and it became clear that it was one of the "Small Radio Telescopes (SRT)" with a 2.3-m dish. These telescopes were originally designed by MIT and sold in various versions over quite some time [2].

In this series of articles, we describe our efforts to refurbish and modernize this telescope and to bring it back to life. This part one will describe how we got the dish, inspected the bits and pieces and made design choices for the refurbishment.

Figure 1: *The SRT at its original position in Bamberg*

2. Getting the dish

The people at the observatory in Bamberg had kindly offered to dismantle the telescope so that we could come and pick it up. This had been planned for September of 2019. However, we then received a mail that it might not be a good idea to dismantle it at that time as wasps had decided to build their nest in the feed horn.

Figure 2: *Not a good idea to dismantle at that moment*

So, we had to postpone our visit to Bamberg until the wasps had given up their control of the telescope which was in November of 2019. We rented a truck and picked up things there.

Figure 3: *Securing bits and pieces in the truck*

3. Finding out about the SRT

The SRTs have been designed by MIT and had undergone various iterations over time. These telescopes can be found in quite a few places mostly for educational and outreach purposes. We could conclude from the photos that the version we would receive had a mount made by CASSI Corp. However, the other details were not known until we had the equipment at our premises and could inspect things and see what version they were.
Here is what we received:

1. The CASSI mount consisting of an azimuth drive and a linear actuator for elevation movement (SuperPowerJack QARL-3636+)
2. The dish itself, 2.3-meter diameter [3] with feedhorn support and adapter ring for the mount
3. The feed horn assembly consisting of
    a. Feed horn [4]
    b. Low Noise Amplifier (LNA) [5]
    c. Digital Receiver [6], [7], [8]
4. Ground controller [9]
5. Power supply
6. Calibration noise source [10]

With the exception of the CASSI mount itself, documentation for each component could be found on the MIT website (see the references given above).

There was also an alternate ground controller which was designed by the staff from the observatory, but while the hardware was completed, the software was not.

4. Initial design decisions

We enjoyed looking through the documentation from MIT learning how the receiver was done. We found it was well designed at the time. However, for today's standards it is using outdated technology. Today's approach is to use software defined radios which make things much easier. Also, we wanted to re-use the receiving tool chain designed for our 3-m dish. This is based on SDRs and we decided that this was the way to go.

We also looked at the documentation how the telescope control was done. Here we also concluded that it would be better for us to build a new control system, duplicating major hardware and software components from our existing 3-m dish design.

As a consequence, we did not make an attempt to put things back together in their original form and use the software from the MIT website to put it into operation. We rather looked at the individual components which we wanted to continue to use to assess their condition and modify and refurbish where needed.

5. Inspection of the different parts

5. 1 Dish

The dish itself was in good condition. There were no dents or similar defects which could affect the aperture efficiency. No work was needed other than some cleaning and re-assembly. According to the documentation the f/D ratio of the dish is 0.375.

5.2 Azimuth drive

The azimuth drive consists of a Valeo 404 854 gear motor to which a cog wheel has been attached. A chain is used to drive another cog wheel (see fig. 4).

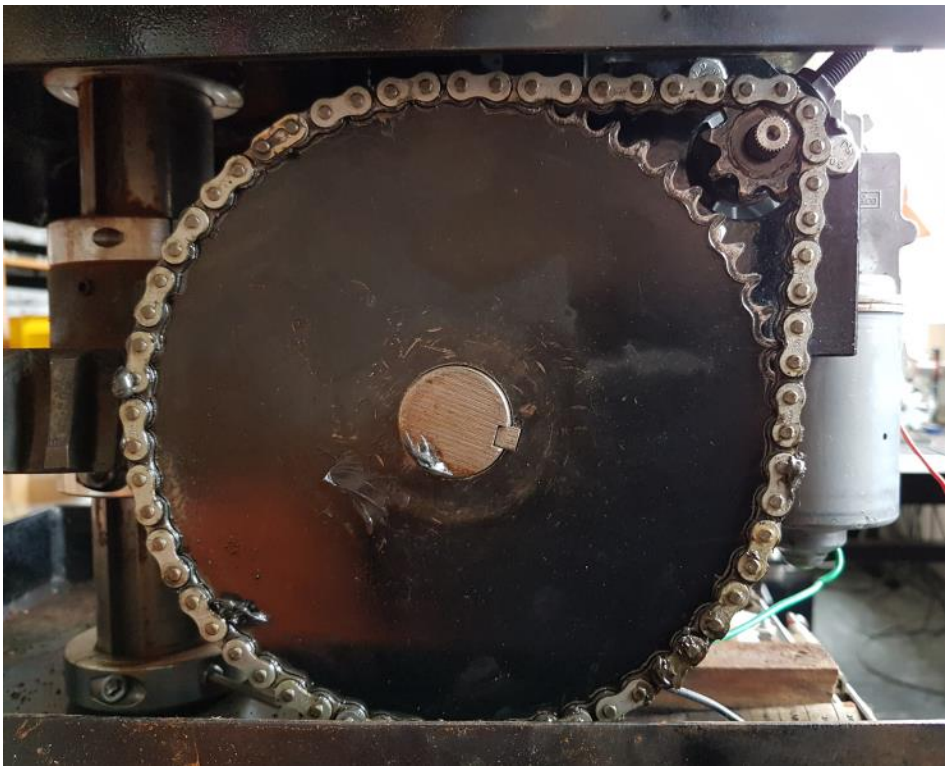

Figure 4: *Cog wheel assembly*

This cog wheel is attached to the axis of a worm gear as shown in fig. 5.

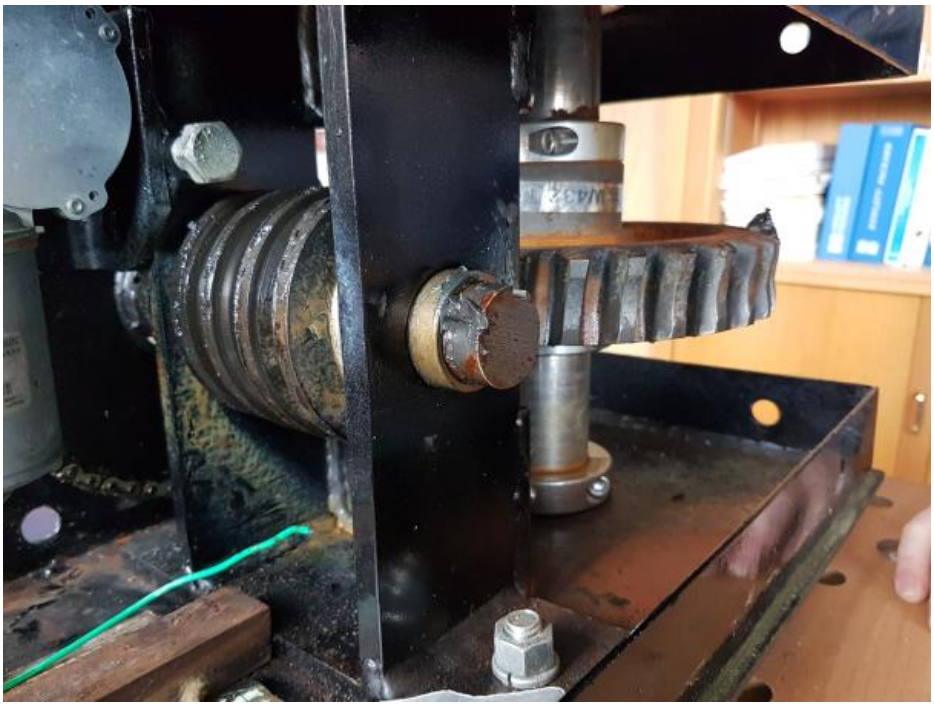

Figure 5: *Worm gear assembly*

The drive assembly makes a very sturdy impression and is very heavy.

A bit of cleaning and removing of corrosion was necessary. Other than that, we noticed that the overall gear assembly has some backlash of about 0.6°. This will limit the pointing accuracy but is still fully adequate for a 2.3-meter dish at 21cm.

The drive is equipped with end switches which interrupt the motor current after one full turn. Diodes are provided across these switches so that the drive can still be moved in the opposite direction and release the end switch, see fig. 6.

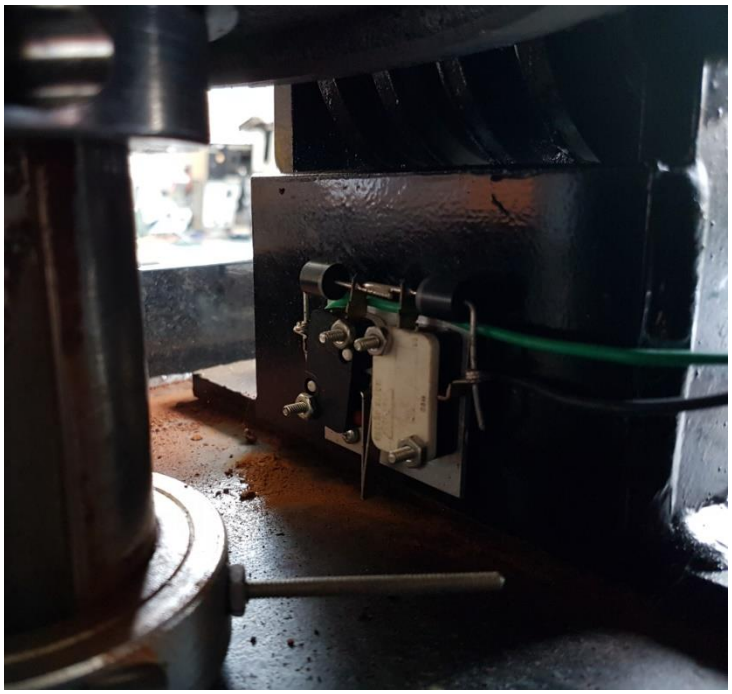

Figure 6: *End switches*

A Hall sensor at the motor delivers 8 impulses per turn. This can be used to determine the position in azimuth if one uses the end switch to determine a starting point see fig. 7.

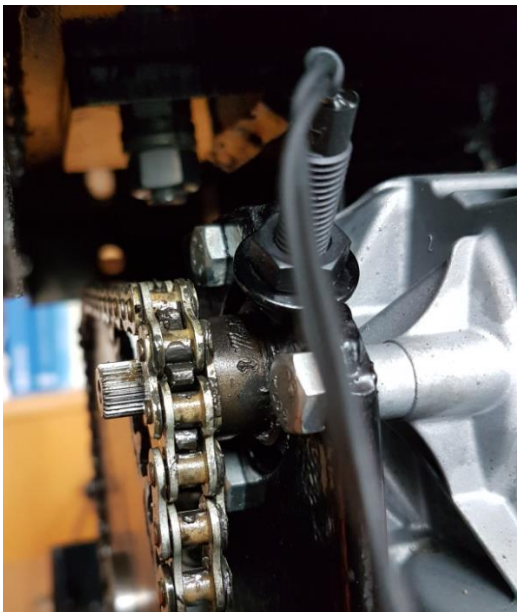

Figure 7: *Hall Sensor*

5.3 Elevation drive

The elevation of the telescope is controlled by a linear actuator. A SuperPowerJack Type QARL-3636+ is used for this purpose. The unit we received required some maintenance. It was taken apart, corrosion was removed and the parts were cleaned and greased (fig.8). After that it was fully functional again.

This unit is also equipped with a hall sensor which detects motor revolutions which can serve to monitor the position.

Figure 8: *Giving the actuator the final touch after cleaning*

5.4 Feed horn assembly

The feed horn assembly combines feed horn, LNA and receiver in one unit as shown in fig. 9.:

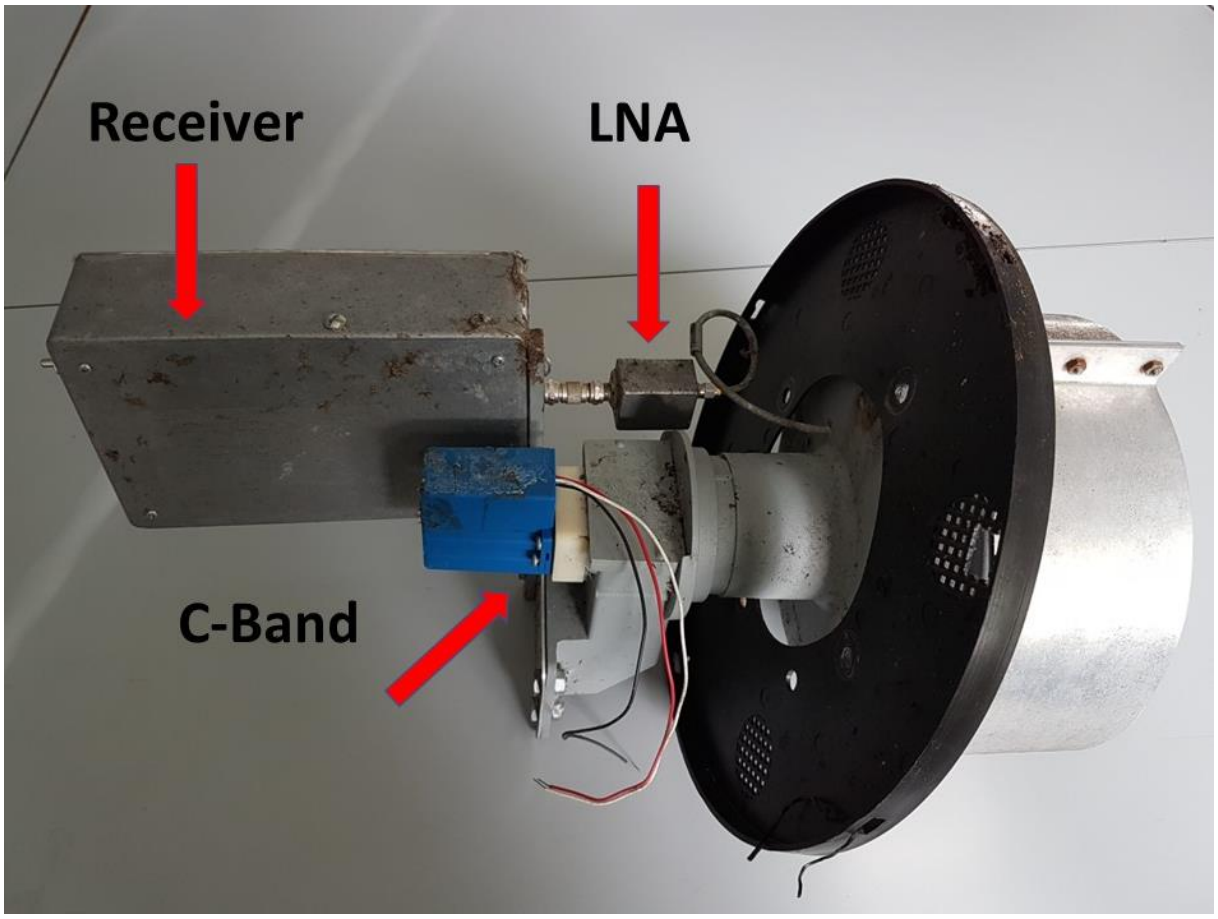

Figure 9: *Feed horn assembly*

Since wasps had inhabited this assembly, the nest had to be removed. In the figure 9 above one can see some leftovers from that.

The horn is basically a horn for C-Band which has been modified. The C-band part has a waveguide which has been closed and used as fixture for the receiver. The blue box controls the polarization of the C-Band by rotating a probe. All C-Band stuff is unused. There is a second probe (see below) which is connected to an LNA, and the LNA is connected to the receiver.

5.4.1 Feed horn

It is amazing that a C-Band feed horn can be modified to work at L-Band. The modification which has been done is shown in a drawing which can be found at [4]. There is an extension of the outer ring, so that it becomes deeper. Then there is an additional probe which can be seen in figures 10 and 11 below.

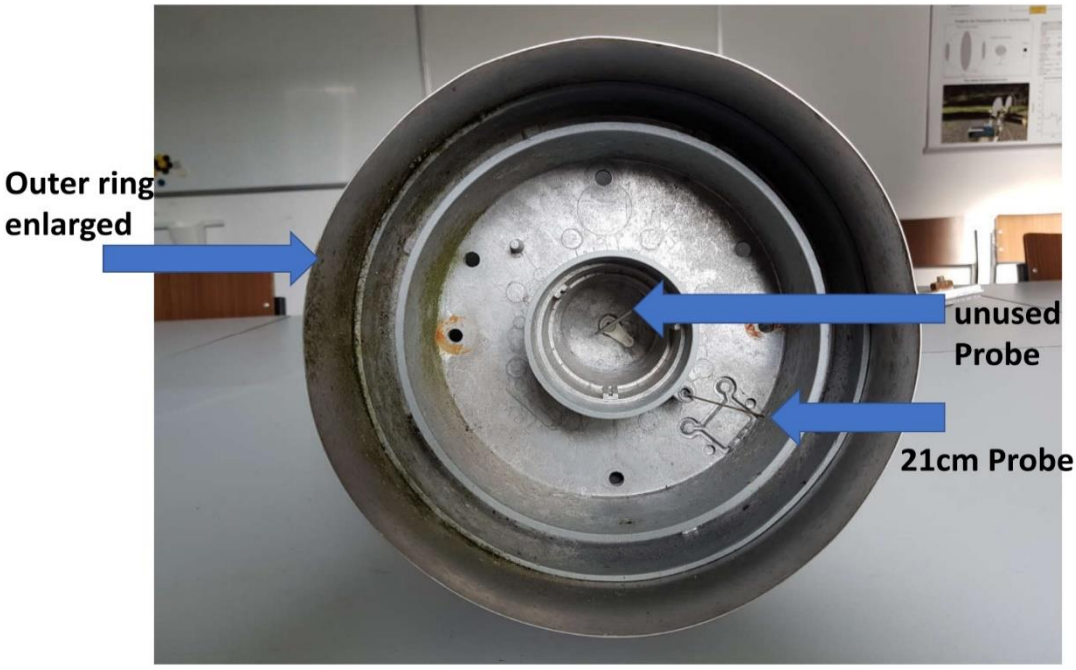

Figure 10: *Feed horn*

Figure 11: *Detail view of the probes in the feed horn*

The probe for 21 cm can be adjusted by sliding the semirigid cable a bit in and out. By this method, a good match can be achieved for 1420 MHz as shown in the network analyzer plots in fig. 12.

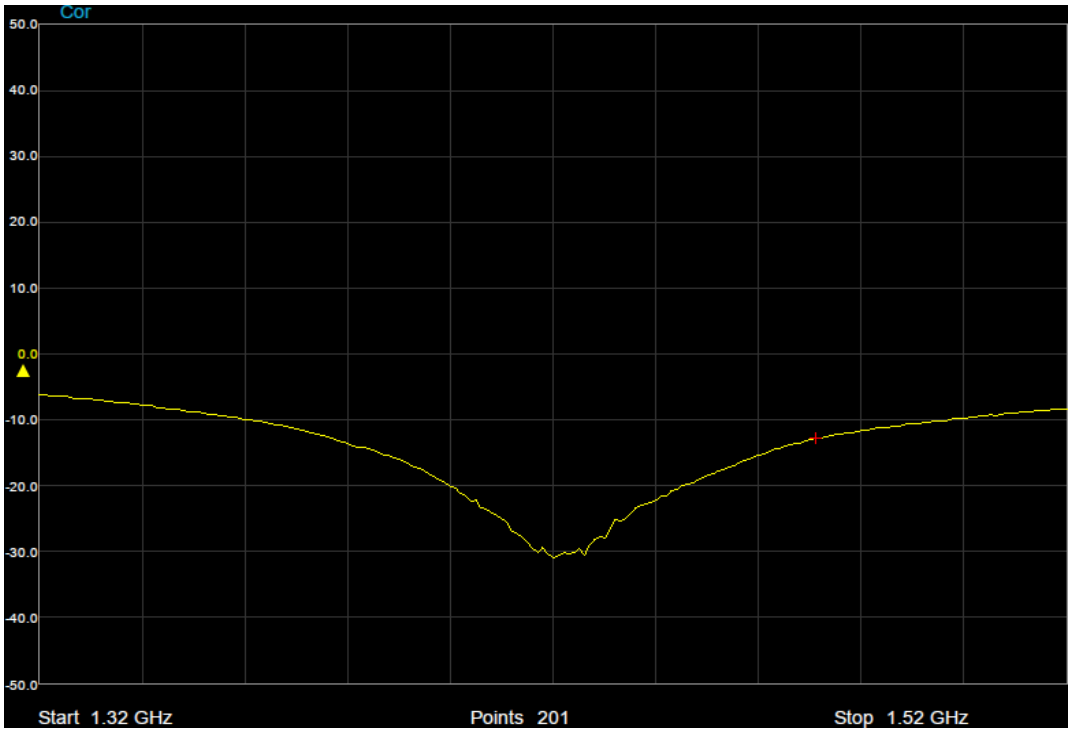

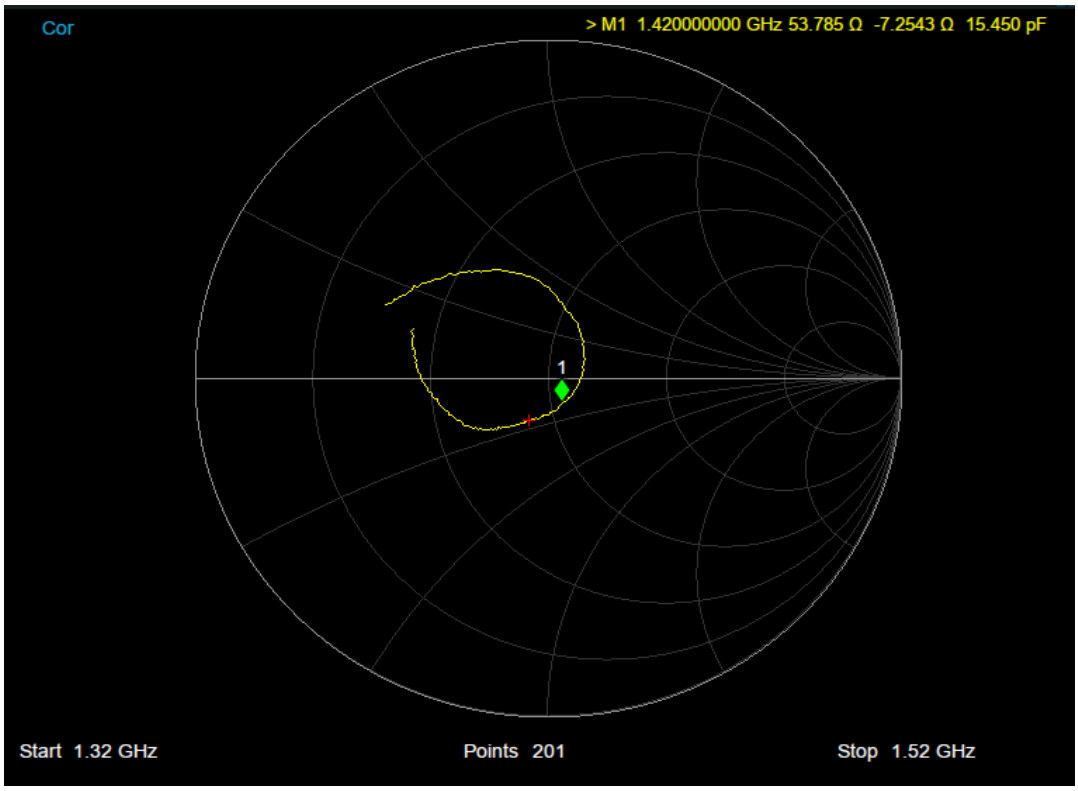

Figure 12: *S11 vector analyzer plots of feed horn*
Return loss and Smith chart

5.4.2 Beam profile

The beam profile of the horn was measured at 1420 MHz to check whether it is suited for the dish with a f/D ratio of 0.376. In particular, the unusual design of the horn did not allow any prediction what might be expected. Fig. 13 below show the measured profile in the E- and H-plane. The blue arrows denote the direction to the rim of the dish, which is 67° to either side.

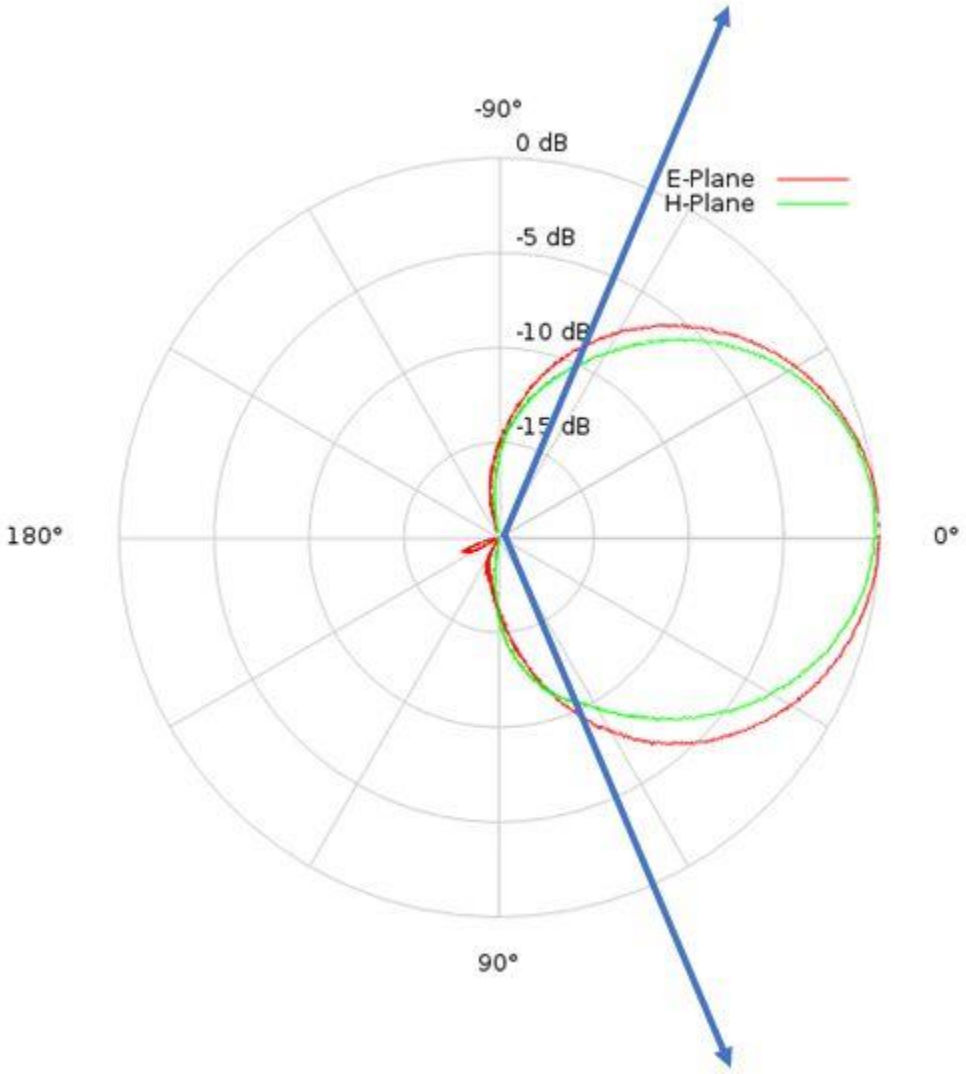

Figure 13: *Profile of the feedhorn*

Attenuation at the rim is 10 dB as common for parabolic dishes. Both this and the low gain at larger angles are expected to allow for low spillover and a good system temperature. In contrast to this, the illumination of the dish may not be optimal as the profile drops of already at smaller angles. This is due to the compromise one needs to make if one re-purposes a commercial feed horn for C-band for L-band.

5.4.3 LNA

The LNA is enclosed in a small aluminum box, see fig. 14. The input connector is SMA, the output connector is F. The power is supplied through the coax cable connecting the LNA to the receiver.

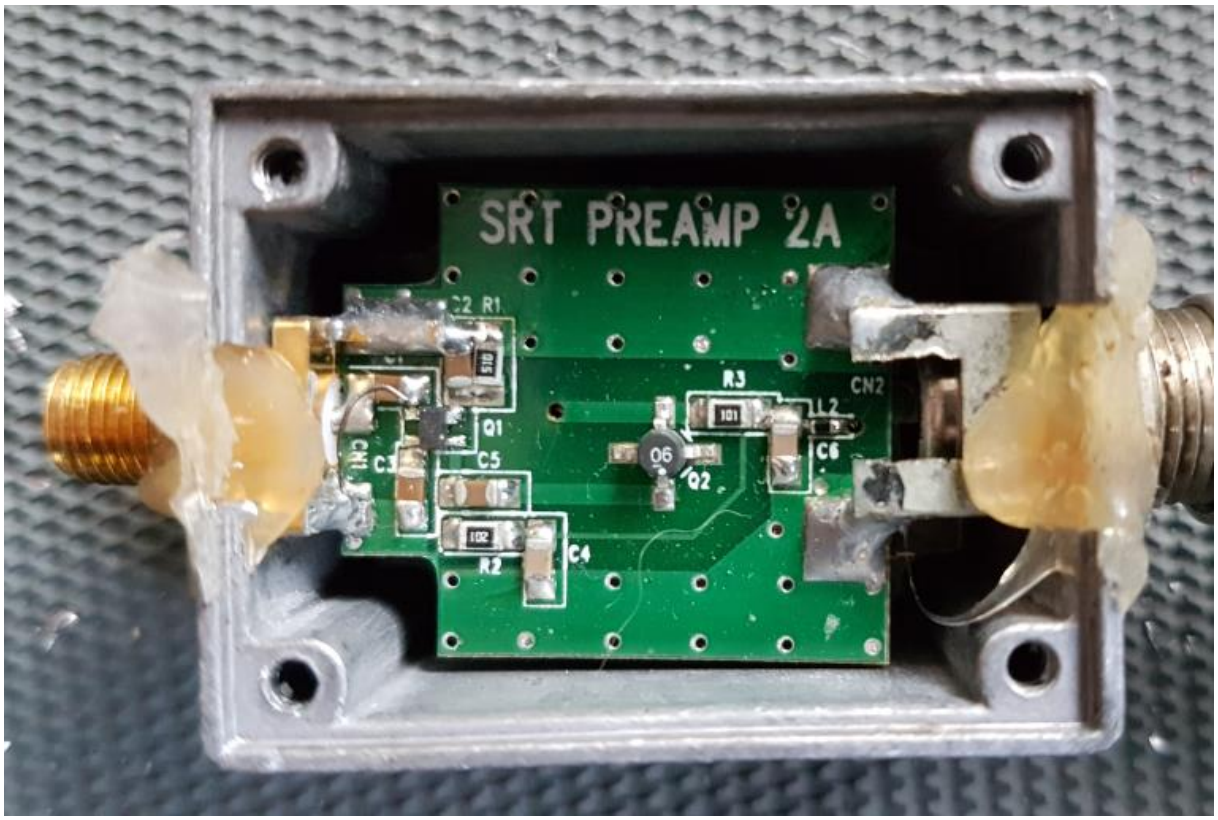

Figure 14: *LNA*

We have measured a gain of 29 dB and a noise figure of 0.46 dB at 1420 MHz for this LNA which is quite satisfactory.

The LNA is equipped with an internal filter with a bandwidth about 55 MHz around 1420 MHz. The gain curve of the LNA/Filter assembly is show in fig. 15 below.

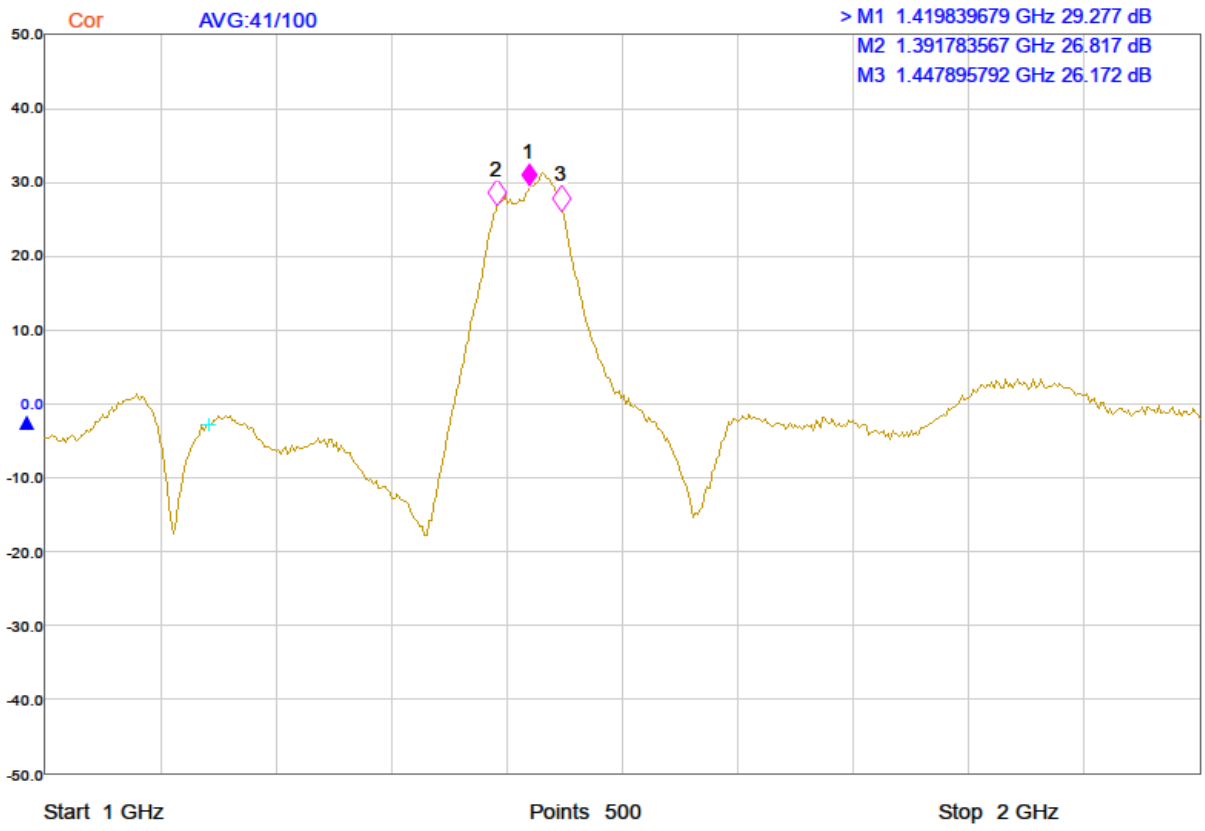

Figure 15: *Gain and filter curve of the LNA*

5.4.4 Noise Source

The noise source for calibration purposes consists of a small board with a Noise/Com noise diode inside some PVC tubing and two brass rods as dipole antenna, see fig. 16 and 17. A further description of this design is available at [10]. We verified the proper operation by monitoring the radiation emitted from the noise source with a Log/Per antenna and a spectrum analyzer.

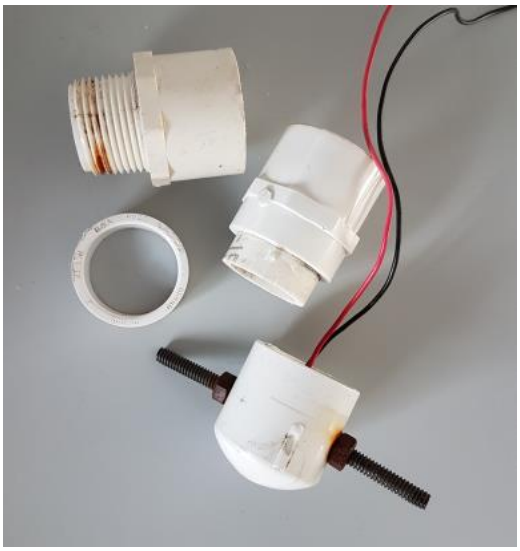

Figure 16: *Noise source assembly*

We found, however, that our version differed from the documentation in [10] as a 51 Ohm/20 pF circuitry between the antenna rods was not present. As per this documentation the purpose of this was to reduce the radiated noise power to a convenient level.

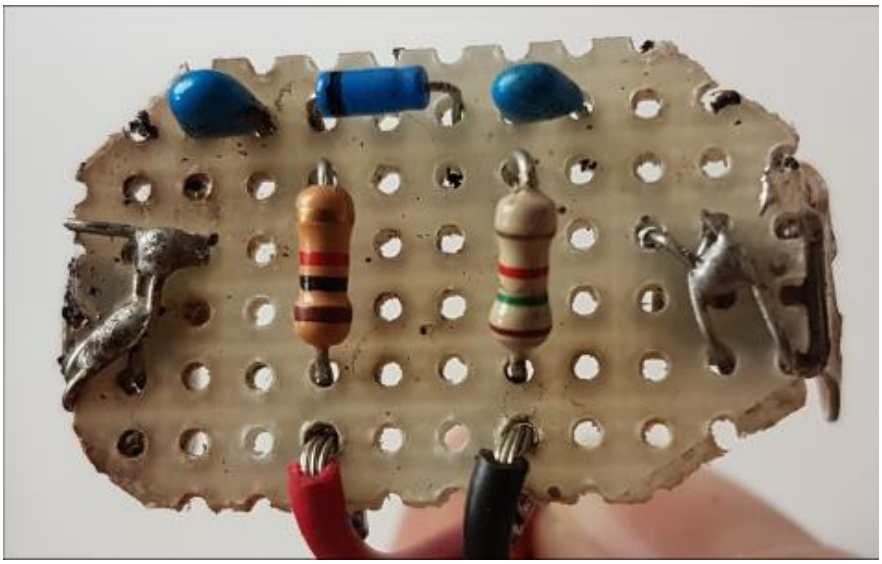

Figure 17: *Noise source board*

6. Conclusions and decision for next steps

All the parts which we inspected were in a useful condition. Only some maintenance such as corrosion removal, cleaning and lubrication was necessary. There were no defects which would have required any extended repair work. Based on the findings, the following way forward was decided:

1. The azimuth drive will be complemented with a quadrature encoder instead of the existing hall sensor for feedback of the position. This ensures that the direction of motion can be recognized and that the setup is compatible with the motor controllers we use for our other small telescopes.
2. The end switches of the azimuth drives will be modified so that the software can recognize the activation of end switches.
3. The elevation drive remains unchanged. However, the hall sensor for the counting of revolution of the motor will no longer be used. Instead, an independent inclination sensor will be used to measure elevation.
4. The RF-chain will be tested for basic functionality. In order to perform the test, the dish will be set up on the ground just looking straight up. The feed and LNA will be installed. Looking for the hydrogen line, the chain will be checked for stability and noise. Also, the dish will be directed manually towards the sun to see the increase in total power.
5. Based on this test, a decision will be taken whether to use the existing LNA or to replace it. Furthermore, it will be decided whether to continue using the feed horn.
6. Provided that the trial with the feed horn is successful, it will be equipped with a second probe. This will be interchangeable to either have the second linear polarization or to be optimized for 1612 MHz (OH-Maser).

The next steps will be described in the second part of this series of articles.

14 Acknowledgement

We gratefully acknowledge the donation of this telescope by the Dr. Karl Remeis-Sternwarte and the support of their staff for getting it ready for transportation.

References:

[1] https://www.sternwarte.uni-erlangen.de/
[2] https://www.haystack.mit.edu/edu/undergrad/srt/index.html
[3] https://www.haystack.mit.edu/edu/undergrad/srt/antenna/antenna_info.html
[4] https://www.haystack.mit.edu/edu/undergrad/srt/receiver/schem9.pdf
[5] https://www.haystack.mit.edu/edu/undergrad/srt/receiver/schempre.pdf
[6] https://www.haystack.mit.edu/edu/undergrad/srt/receiver/srtdig2.pdf
[7] https://www.haystack.mit.edu/edu/undergrad/srt/receiver/receiver_circuit.html
[8] https://www.haystack.mit.edu/edu/undergrad/srt/receiver/schemrecdig.pdf
[9] https://www.haystack.mit.edu/edu/undergrad/srt/receiver/schemgndctl2.pdf
[10] https://www.haystack.mit.edu/edu/undergrad/srt/receiver/calibrator_report.PDF

About the Author: Dr. Wolfgang Herrmann is the president of the "Astropeiler Stockert e.V.", the organization which operates the observatory.

He received his PhD in Physics from the University of Bonn. He has spent most of his professional career in the telecommunication industry. At retirement age, he now enjoys learning as much as possible about radio astronomy, doing observations and improving the instruments at Astropeiler.

Contact the author at messbetrieb@astropeiler.de

Development of a Telescope Tracking System Part 2

Jack H. Lobingier

Introduction

This article is the second in a series of articles describing the development of a tracking motor and speed control system for my three meter antenna. This design does not use available rotators, but is more generalized to use almost any dc motor and gear train along with incremental digital encoders. In this second article in the series, the design of the altitude and azimuth motor and speed control system will be detailed. Figure 1 shows the mounted hardware as it is currently installed.

Figure 1: Motor and Speed Control Hardware Mounting

Figure 1 shows the 24VDC power supply[1], mounted at the bottom, the motor and speed controllers in the mid area and the azimuth rotation safety switch at the top. In the first version of the motor and speed controller design there were local switches to allow for manual position control at the mount, however these proved to be problematic, so they were removed in this second design. The linear actuator[2] for altitude positioning has its own limit safety switches, so one only needed to be added to the azimuth gear to safely limit rotation. The motor and speed controller NEMA3R box contains two small computers[3][4], relay[5] and Digital-to-Analog Converter (DAC)[6] hardware, along Pulse Width Modulation (PWM) motor controllers[7] and a network switch[8] for communication to the control software. Figure 2 is a block diagram of the hardware organization. All of this is connected to the Python control software over fiber optics.

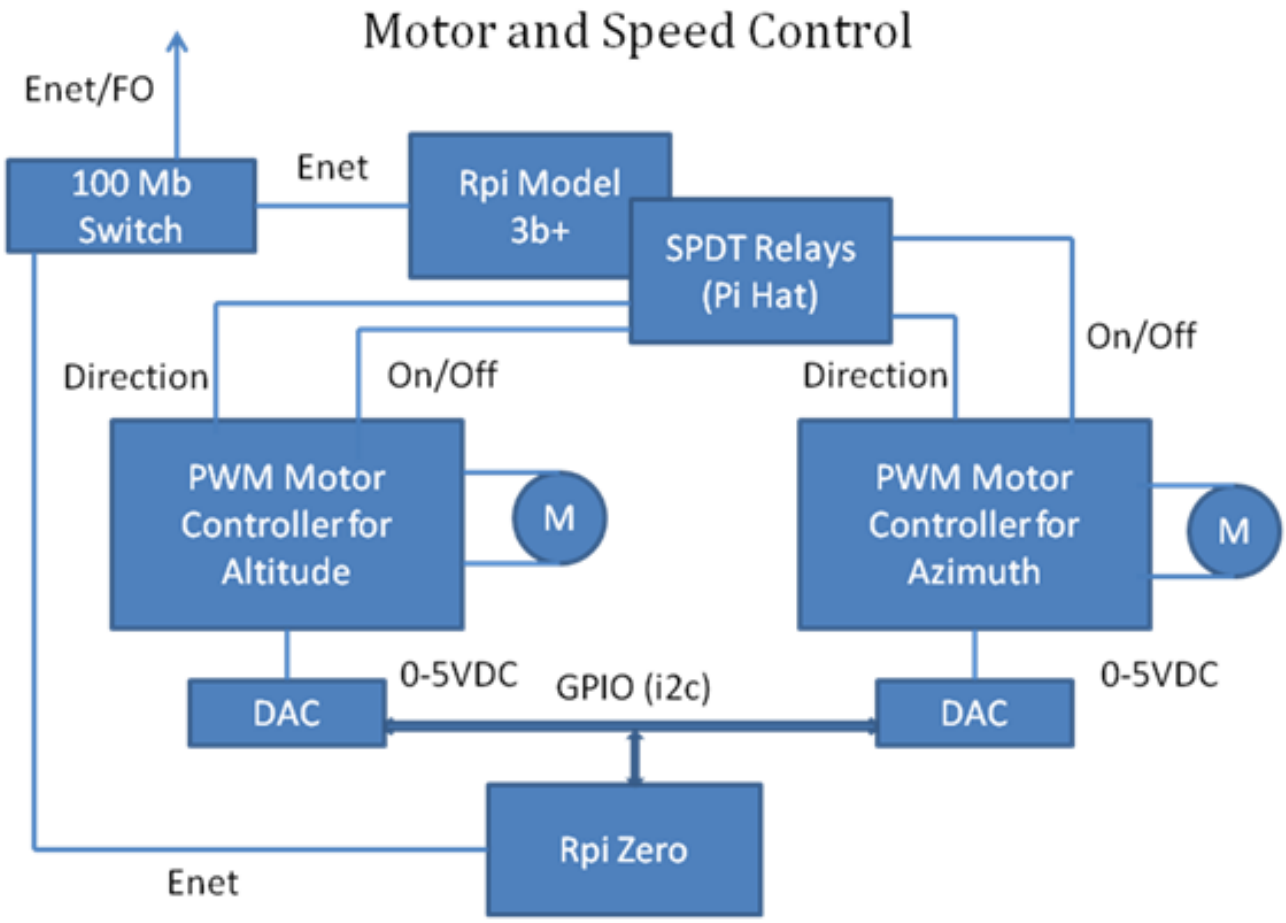

Figure 2: Motor and Speed Control Block Diagram

Part 1 of this series talked about the position encoders for both altitude and azimuth. That position information is sent back to the Python motor and speed control software, and provides the positions for closed loop control of the motor and speed control software.

Power Supply for Motor Control

The supply power for this system is provided by a 24VDC, 15A bulk supply[1]. In Figure 1 it is locate at the bottom of the picture. As with all the electronics that have potential RFI, it is enclosed in a grounded steel box. The altitude positioner[2] uses 12VDC, so a 24 to 12VDC regulator supplies the altitude motor control. All other voltages for the RPi, DAC units and the Ethernet Switch are provided by regulators as well.

PWM Motor Control Units

The PWM units[7] are from eBay, and are capable of driving motors of up to 40A and 40VDC. They are bi-directional, which is normally set by a SPDT center off switch. In this application the switch has been replaced by a SPDT relay controlled by the RPi3b+. As supplied, these units also have a 100K potentiometer with an intergal SPST switch. This varies the PWM and hence the speed of the motors. This really supplies 0-5VDC, so in this application a Digital to Analog Converter[6], driven by a RPi Zero[4] is used to set the speed. The SPST switch function is controlled by part of SPDT relay controlled by the RPi3b+[3]. The reason for having speed control on this application is to allow for finer tracking with less overshoot as well as higher speed slewing to position, as required. All of these functions are part of

the graphical interface of the Python motor and speed control program, which will be discussed in the next, and final part of this series.

Azimuth Motor Drive and Gearing

Figure 3 is a close-up of the azimuth motor drive. The most custom mechanical part of this setup is the large diameter 152 tooth spur gear that drives the four inch diameter azimuth axis. I cut this gear, over several weeks, on a small mill. The gear is welded to the upper part of the mount, and slips over a slightly smaller O.D. pipe, that is embedded in the ground and in a four foot cube of concrete. That upper part of the mount rests on a large thrust bearing. The large spur gear is driven by a smaller 19 tooth gear resulting in an 8:1 drive ratio. Also, visible in Figure 3 are the 300 ppr encoder, which when driven by the 8:1 gear ratio results in a 2400 ppr, or 0.15 degree per pulse resolution. 1000 ppr encoders are readily available as a potential upgrade. Below the base plate in Figure 3 is a 30:1 right angle speed reducer and the right angle 24VDC, 50 RPM gear motor. At full speed, this results in a 75 degree per minute rotation rate.

Figure 3: Azimuth Motor Drive

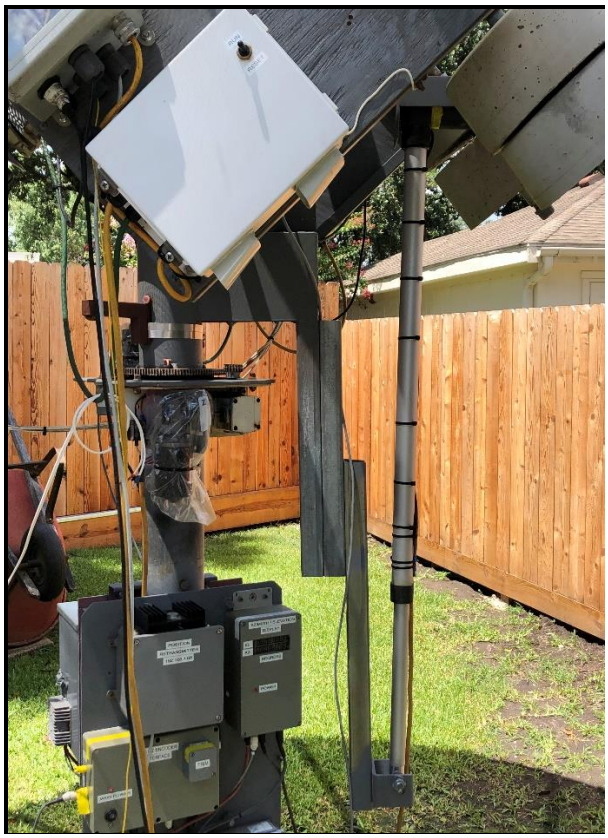

Figure 4: Altitude Motor Drive

Altitude Motor Drive and Gearing

Figure 4 is a close-up of the linear actuator[2] that provides altitude movement. This is a 30 inch, 400 pound force, 12VDC actuator. It has integral limit switches and is IP66 rated. The standard unit is a 0.98 inches per second unit. This results in a horizon to zenith time of about 31 seconds. Part of the reason for having speed control on both axes is the need to slow down this movement. This is especially true for tracking. I have since learned that the manufacturer has a lower speed option, and I would encourage anyone using this device to investigate that for their project. Also visible in Figure 4 are the concrete counterweights used to offset the weight of the dish and feed. In determining the weight

to use I purchased an inexpensive Micro Crane Scale with a 500kg range to measure the force that would be seen by the actuator. Figure 5 shows that device.

Figure 5: Micro Crane Scale

Networking

As is the case with all the other electronic subsystems at the antenna, the motor and speed control units are server applications that are in communication with their client counterparts installed in computers inside my house. All these units are connected by Ethernet and use TCP/IP over a one gigabit fiber optic link. For example, the motor and speed control RPi3b+ server in Figure 2, is networked over that fiber optic link to communicate with its client counterpart, which is part of the Python real time tracking motor and speed control program. In addition, to that normal graphical interface, all computing units have VNC servers as part of their software. This allows me to connect with a VNC Client to do programming and maintenance on those individual units.

Conclusion

This project has evolved over a period of years, and represents my attempt at having a networked, remote -controlled and maintainable RA setup. With this in place I can, most of the time, position, track, and collect data from my 3 meter dish. Next in this series of articles will be the details of the real time tracking motor and speed control program, written in Python3, and hosted on Ubuntu Linux. I will be glad to discuss any of the details relative to this project, hardware choices, etc.

References:

[1] https://www.ebay.com/itm/SHNITPWR-24V-DC-Power-Supply-15A-360W-AC-DC-Adapter-24-Volt-15-Amp-/313893323945?mkcid=16&mkevt=1&_trksid=p2349624.m46890.l49286&mkrid=711-127632-2357-0
[2] https://www.ebay.com/itm/12V-Electric-Linear-Actuator-2-40-stroke-100-400-lbs-force-PA-04-model-/274495676018?mkcid=16&mkevt=1&_trksid=p2349624.m46890.l49286&mkrid=711-127632-2357-0
[3] Raspberry Pi Model 3b+

[4] Raspberry Pi Model Zero Ver 1.3
[5] RPi 4 channel relay shield with 4 SPDT relays, controlled by the Pi GPIO. http://www.keyestudio.com model ks0212
[6] MCP4725 Breakout Board - 12-Bit DAC with I2C Interface [STEMMA QT / qwiic] : ID 935 : $4.95 : Adafruit Industries, Unique & fun DIY electronics and kits. https://www.adafruit.com/product/935
[7] https://www.ebay.com/itm/10-50V-40A-PWM-Motor-Speed-Control-Controller-CW-CCW-Reversible-Pulse-DC-Driver-/264565476536?mkcid=16&mkevt=1&_trksid=p2349624.m46890.l49286&mkrid=706-127636-26712-0
[8] https://www.ebay.com/itm/TP-Link-TL-SG105-5-Port-Gigabit-Ethernet-Unmanaged-Network-Switch-/114988917575?mkcid=16&mkevt=1&_trksid=p2349624.m46890.l49286&mkrid=711-127632-2357-0

About the author: The author has been interested in radio astronomy since about 1983. He worked as a Systems Consultant for Honeywell, and is now retired. His main interests are in the areas of hardware and software improvement moving towards lower system temperature along with Hydrogen line and Pulsar hunting. You can contact the author at 49jhanl@gmail.com.

Symbol quantization in interstellar communications: methods and observations

William J. Crilly Jr

Green Bank Observatory

West Virginia, USA

Abstract— Interstellar communication transmitters, intended to be discovered and decoded to information bits, are expected to transmit signals that contain message symbols quantized in at least one of the degrees of freedom of the transmitted signal. A hypothesis is proposed that signal quantization, in the form of multiplicative values of one or more signal measurements, may be observable during the reception of hypothetical discoverable interstellar communication signals. In previous work, using single and multiple synchronized radio telescopes, candidate hypothetical interstellar communication signals comprising Δt Δf opposite circular polarized pulse pairs have been reported and analyzed. (ref. arXiv:2105.03727, arXiv:2106.10168, arXiv:2202.12791). In the latter report, an apparent quantization of Δf at multiples of 58.575 Hz was observed. In the current work, a machine process has been implemented to further examine anomalous Δf and Δt quantization, with results reported in this paper. As in some past work, a 26 foot diameter radio telescope with fixed azimuth and elevation pointing is used to enable a Right Ascension filter to measure signals associated with a celestial direction of interest, relative to other directions, over a 6.3 hour range of Right Ascension. The 5.25 ± 0.15 hr Right Ascension, -7.6° ± 1° Declination celestial direction presents repetition and quantization anomalies, during an experiment lasting 157 days, with the first 143 days overlapping the previous experiment.

***Index terms*— Interstellar communication, Search for Extraterrestrial Intelligence, SETI, technosignatures**

Introduction

Communication signals may be classified by the ease with which transmitted signals may be discovered, received and decoded to information bits. At opposite extremes of classification, transmitted signals may be designed to be almost indistinguishable from random noise, or, may continuously present a single orthonormal function, or single measurement value, in each degree of freedom [1][2]. Examples of extremes include spread spectrum modulated signals, and unmodulated carriers. The former provides high information rate at the expense of discovery, while the latter provides discovery at the expense of information rate. Interstellar communication systems are hypothesized to present receiver measurements between these extremes.

An additional expectation of interstellar signals is that signal measurements should themselves provide a logical path to at least some signal message decoding. A single isolated anomaly should not require an increase in receiver sensitivity, to further examine the signal. For example, a signal's carrier may be used to measure the center frequency and arrival direction of a signal. However, its transmitted power is wasted if the highest sensitivity receiver on a planet discerns no other signal anomaly. The discovery of an anomalous signal measurement should preferably present at least one additional measurement that leads the same receiver to glean a process to decode the signal to information bits, or to an analog representation of information. A signal comprising opposite circular polarized pulse pairs is an example of such discoverable signals.

In the current work, hypothetical quantization of the difference in measured frequency of opposite circular polarized pulses is examined, while assuming that an Additive White Gaussian Noise (AWGN) model, augmented with Radio Frequency Interference (RFI) amelioration methods, is expected to explain measurements.

The remainder of this paper contains a hypothesis, method of measurement, observations during a 157 day experiment, discussion and conclusions.

Hypothesis

***Hypothesis*:** Hypothetical energy-efficient

William J. (Skip) Crilly Jr. is a Volunteer Science Ambassador in Education & Public Outreach
of the Green Bank Observatory. email: wcrilly@nrao.edu

discoverable interstellar communication signals [3][4], comprising Δt Δf opposite circular polarized pulse pairs, are expected to present quantization and repetition of one or more of the degrees of freedom of the signal. The hypothesis may be conditionally falsified [5] by finding an absence of such radio telescope receiver measurements, assuming an RFI-augmented AWGN signal explanatory model. Measurements are to be diurnally performed across a range of Right Ascension (*RA*) values, including a prior celestial direction of interest at 5.25 ± 0.15 hr *RA*, -7.6° ± 1° Declination (*DEC*).

Method of Measurement

Traceability, repeatability and testability are primary objectives of the measurement protocol in this work. Consequently, the method of measurement is entirely machine implemented, from radio telescope signal capture to presentation of results image production. A few anecdotal insights were used in the establishment of hyperparameters in the quantization filters in the present work, and are described in the paragraph below. Further anecdotal insight is often most useful after a methodical procedure has been implemented. Then, a collection of anecdotal insights may guide and prioritize further work.

The methods described in previous reports [6][7][8] are retained in the current work, with an additional process to build and test two Δf multiplicative quantization filters, processing previously captured files, and new radio telescope files, comprising 153 days of 100% duty-cycle dual circular polarized radio telescope data. The Δf quantization filters added in the current work quantize $|\Delta f|$ to 58.575 Hz multiples with ± 10.5 Hz span, and half these values, using $|\Delta f|$ quantized to 29.288 Hz multiples spanning ± 5.5 Hz. In other words, in the 58.575 Hz quantizing filter, the quantized filtered $|\Delta f|$ range of 80 to 400 Hz, is reduced to output pulse pairs' data that have $|\Delta f|$ values that measure within 10.5 Hz of multiples of 58.575 Hz. The 58.575 Hz and ± 10.5 Hz range were set from the 3.7 Hz FFT bin width, equipment metrology estimates, and the observation of high SNR_{METRIC} anomalous Δt = -3.75 s polarized pulse pairs. The 29.288 Hz ± 5.5 Hz quantization filter values are chosen to be close to half of the 58.575 Hz and ± 10.5 Hz values.

During exploratory investigation of quantization hyperparameters, an extended range Δf filter is implemented, with results reported in **Figure 11**. The use of various quantization filters is a topic of ongoing and future work.

Observations

Figures 1 through 11 present image files produced by machine processes of radio telescope data files, in a multi-step signal processing system. The machine processes, measured parameters, and machine hyperparameters are described in previous reports [6][7][8], in METHOD OF MEASUREMENT above, and in this section.

The experiment conducted in recent work spanned 157 days, with 153 days of telescope data included in the presentation of results. Days not included were the result of power outages and equipment issues. Due to the 143 day overlap of measurement days in the quantized filter results presented in the current report, and unquantized filter output reports in [8], there will be similarities seen between the sets of plots in this work and in [8].

Figure 1 plots Δt = -6.25 s, 29.288 Hz quantized polarized pulse pairs, against *RA* bins from 0 to 6.3 hours in 0.3 hour intervals. The 29.288 Hz filter was chosen after the twice valued 58.575 Hz quantized filter was gleaned from post-processed measurement results reported in [8] Figure 6.

Figure 2 plots the Modified Julian Date (MJD) of the polarized pulse pair events observed in **Figure 1**, i.e. of a Δt = -6.25 s Δf quantized measurement set.

Figure 3 plots the RF Frequency measurement of the polarized pulse pair events of the Δt = -6.25 s Δf quantized measurements. Widely spaced RF frequencies are expected from a transmitter intending the receiver to conduct Angle of Arrival (AOA) measurements, described in TRANSMITTER DESIGN, and FURTHER WORK in [6]. In addition, communication information rate and RFI amelioration are improved. Ideas about the possible presence of relatively narrow bandwidth energy bursts, spread across a wider bandwidth, are detailed in DISCUSSION in [8].

Figure 4 plots the Δf of the polarized pulse pair events, of the Δt = -6.25 s Δf quantized measurement set.

Figure 5 plots the log likelihood of the Δt = -3.75 s events observed during the 157 day duration

experiment, after quantizing the | Δ*f* | to be within 10.5 Hz of a multiple of 58.575 Hz and within a range of 80 to 400 Hz.

Figure 6 plots the MJD of the Δ*t* = -3.75 s quantized Δ*f* events plotted in **Figure 5**.

Figure 7 plots RF Frequency measurement of the Δ*t* = -3.75 s quantized Δ*f* events plotted in **Figure 5**. RF Frequency is spread, for possible reasons described above in **Figure 3**.

Figure 8 plots the Δ*f* measurement of the Δ*t* = -3.75 s quantized Δ*f* events plotted in **Figure 5**.

Figure 9 plots log likelihood of polarized pulse pairs in the 5.1 – 5.4 hr *RA* range, over |Δ*t* | ≤ 10 s using the described 58.575 Hz quantizing filter. Multiple anomalous polarized pulse pairs are presented, given that one polarized pulse pair is expected below a log likelihood of -2.0, per experiment.

Figure 10 plots log likelihood of polarized pulse pairs in the 5.1 – 5.4 hr *RA* range, over |Δ*t* | ≤ 10 s using the 29.288 quantizing filter. As observed in **Figure 9**, multiple anomalous polarized pulse pairs are presented below a log likelihood of -2.0. Certain | Δ*t* | values matching in **Figure 9** and **Figure 10** are described in text below the two figures.

Figure 11 shows results of a high SNR_{METRIC} polarized pulse pair exploratory search above the 400 Hz previous upper limit of |Δ*f* |. An unusual set of five pulse pairs were observed at Δ*t* = +7.25 s, in the 5.1 to 5.4 hr *RA* direction. The five pulse pairs were observed on MJD 59588, 59517, 59575, 59515, and 59592. The Δ*f* quantized value range threshold, set to ±3.5 Hz, is lower than the value used in other observations. One possible explanation for the reduced range entails the possibility that all of the five pulse pairs computed no difference in post-multiplied FFT bin index, relative to quantizer multiplier predicted bin indexes, and receiver equipment metrology did not increase this value above one FFT bin width, i.e. 3.725 Hz. Intentionally discoverable transmitters sometimes provide a means for the receiving entity to verify that receiver processing is working as intended. The receiver test then occurs as a natural result of transmitting a combination of repetitive and quantized transmitter settings, within discoverable symbols. There is a possibility that a transmitter is designed with this intended purpose.

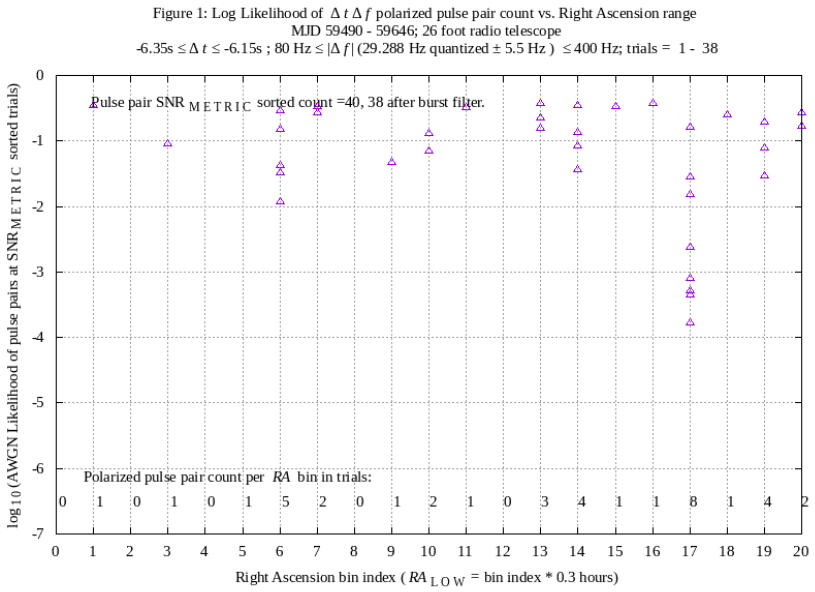

Figure 1: 29.288 Hz Δ*f* quantized polarized pulse pairs having Δ*t* = -6.25 s, observed in the 5.1 to 5.4 hour *RA* range, during 157 days, present likelihood approximately a thousand times less than expected from an RFI-augmented AWGN noise model. The binomial distribution of eight events seen in 38 tries, given an event probability of 1/21, equals 3 x 10^{-4}. The highest five SNR_{METRIC} *RA* bin 17 Δ*f* quantized polarized pulse pairs are ranked 4 ,6, 13, 14 and 16.

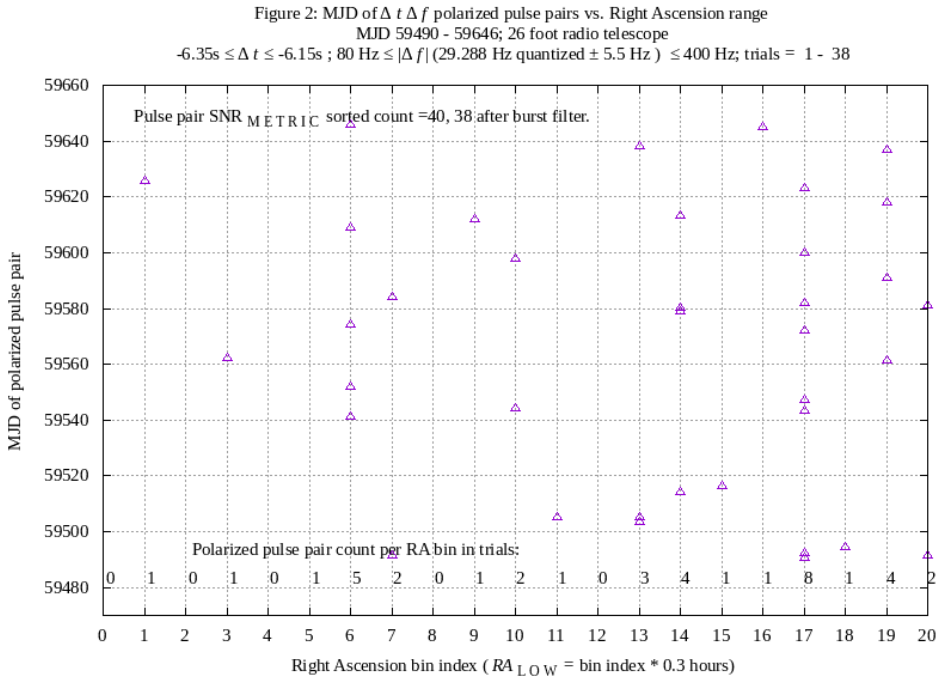

Figure 2: The MJDs of the eight quantized polarized pairs observed in **Figure 1** appear distributed, potentially refuting a hypothesis of some diurnal RFI models explaining the events. Events do not appear to be repeatedly replicated on the same MJD, expected from intra-day persistent RFI. Robust RFI filters, quantization filters and *RA* binning reduce the number of observed events to less than or equal to one, in thirteen of the twenty-one *RA* bins, implying that RFI may have been largely removed using machine processes.

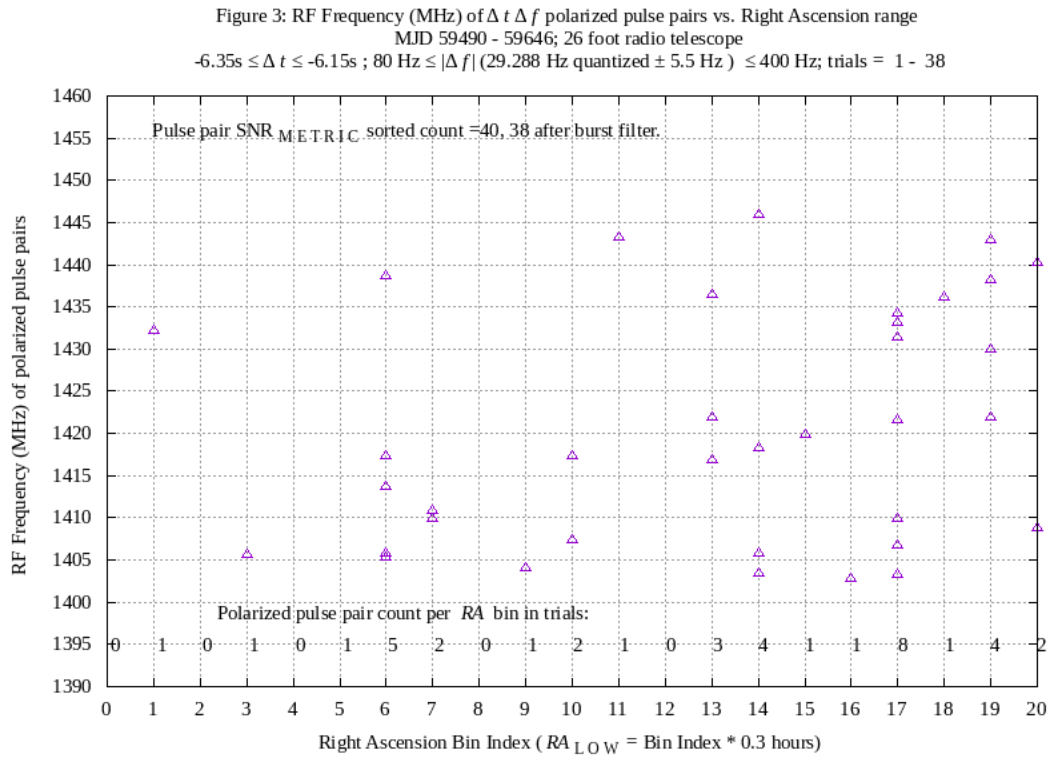

Figure 3: A high concentration of RF frequency of filtered quantized polarized pulse pairs does not appear evident. There might be significance to a higher number of pulse pairs observed at lower RF frequency.

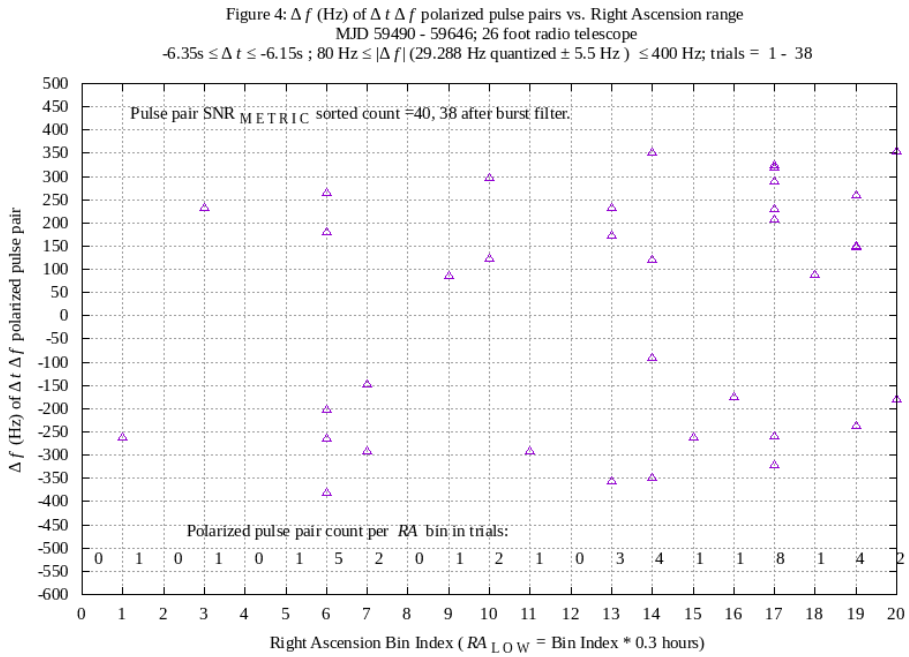

Figure 4: | Δ*f* | of apparently significant bin 17 pulse pairs may be concentrated to a region less than the 80 to 400 Hz range, particularly at the low range. The low range of | Δ*f* | rejection is useful in the receiver to ameliorate narrowband RFI that may mimic pulse pairs, due to Doppler spread of an RFI source-to-radio telescope propagation path.

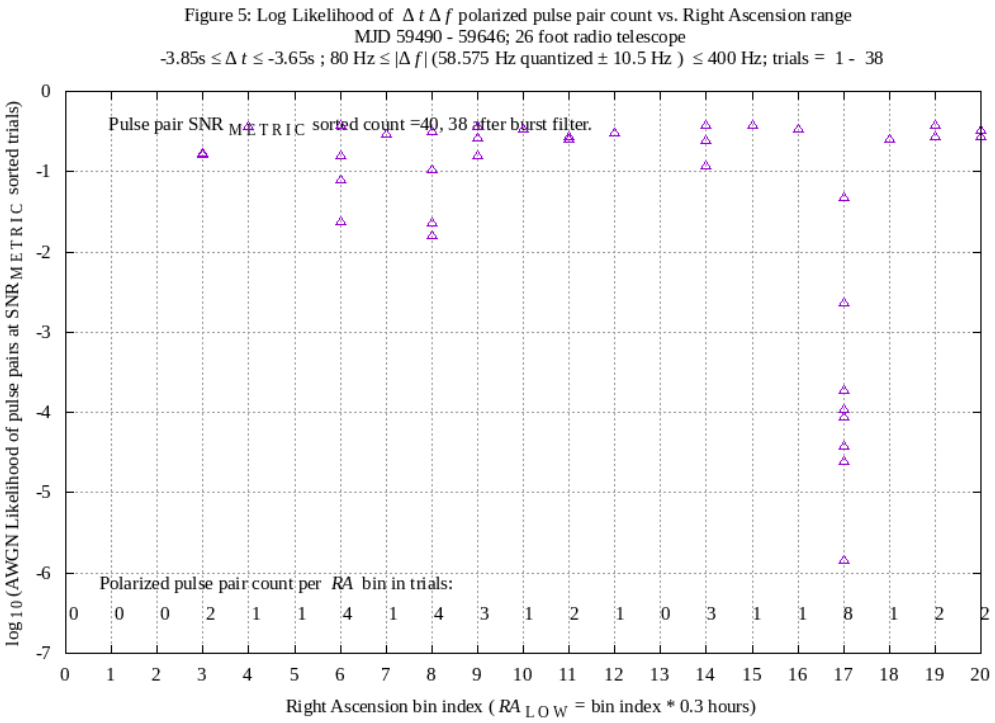

Figure 5: 58.575 Hz | Δ*f* | quantized polarized pulse pairs having Δ*t* = -3.75 s, observed in the 5.1 to 5.4 hour *RA* range, during a 157 day experiment, present likelihood approximately a hundred thousand times less than expected from an RFI-augmented AWGN noise model.

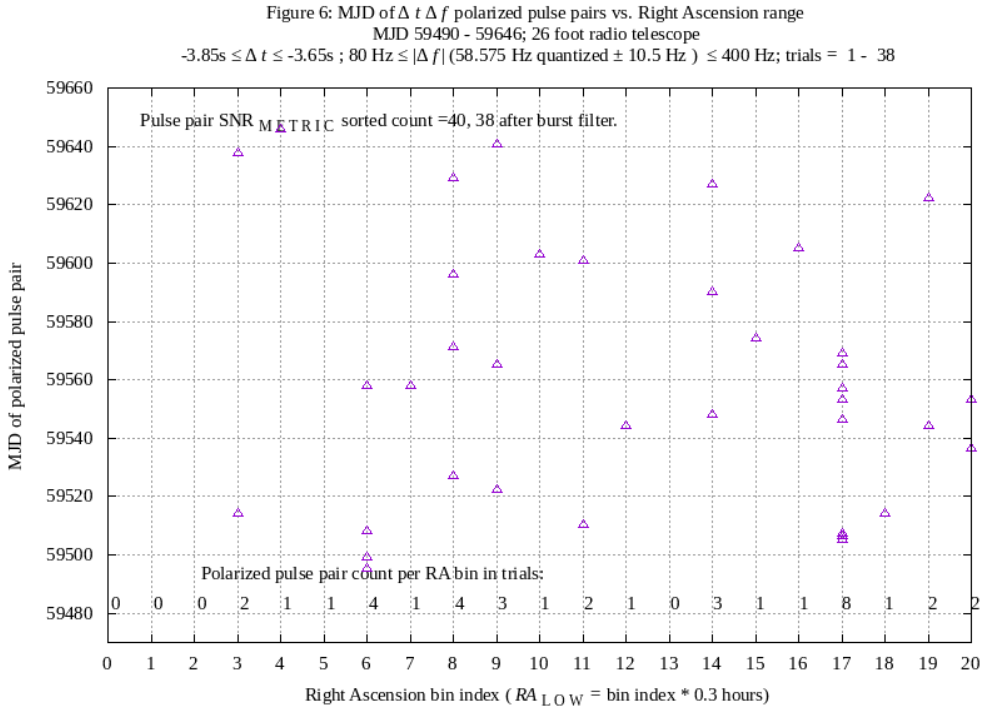

Figure 6: Δ*f* quantized polarized pulse pairs observed in the 5.1 to 5.4 hour *RA* range appear to present an MJD concentration greater than concentrations presented in other *RA* ranges. An intentionally discoverable transmitter might be designed to concentrate highest power transmissions during a group of days.

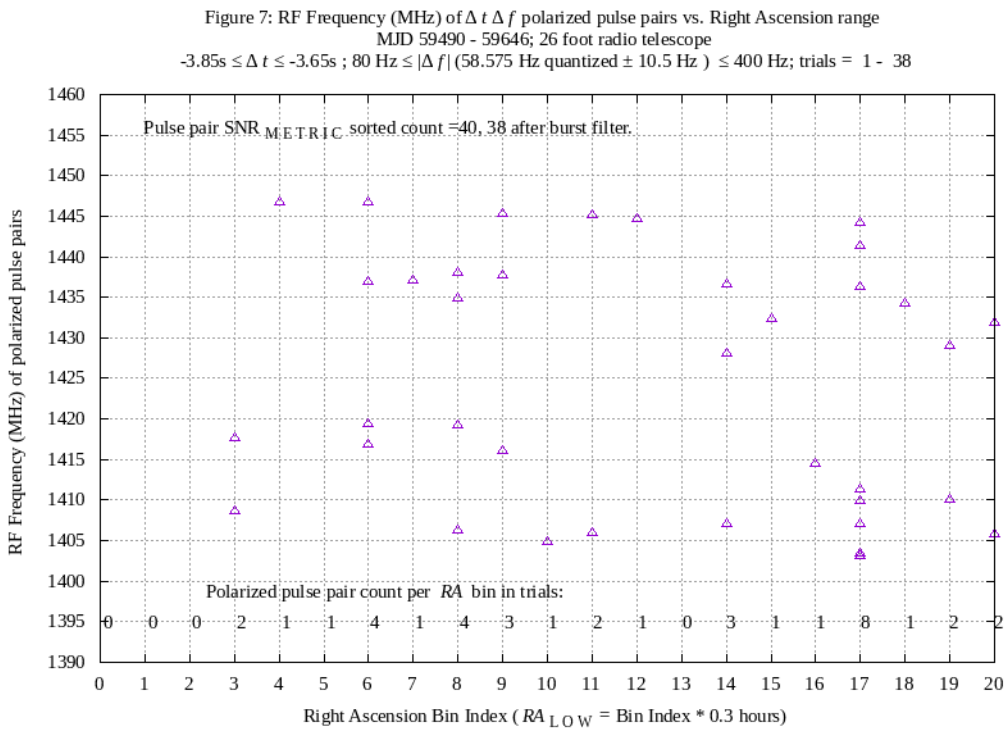

Figure 7: RF frequency of quantized polarized pulse pairs in the direction of interest appear distributed, with an exception near 1403 MHz.

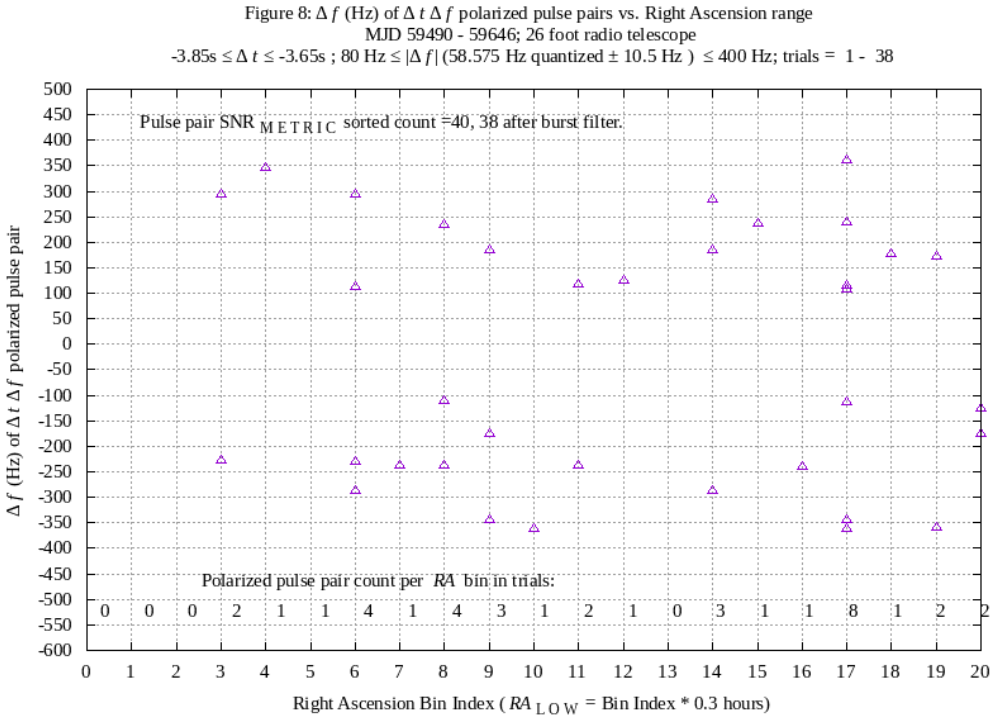

Figure 8: Δ*f* measurements of polarized pulse pairs is plotted for the Δ*t* = -3.75 s apparently repetitive and quantized measurements, described in prior work, e.g. Figure 6 of [8]. Comparison of the bin 17 indications implies that the quantization filter significantly reduces the filter output response in other *RA* bins, relative to bin 17, 5.1 – 5.4 hr RA.

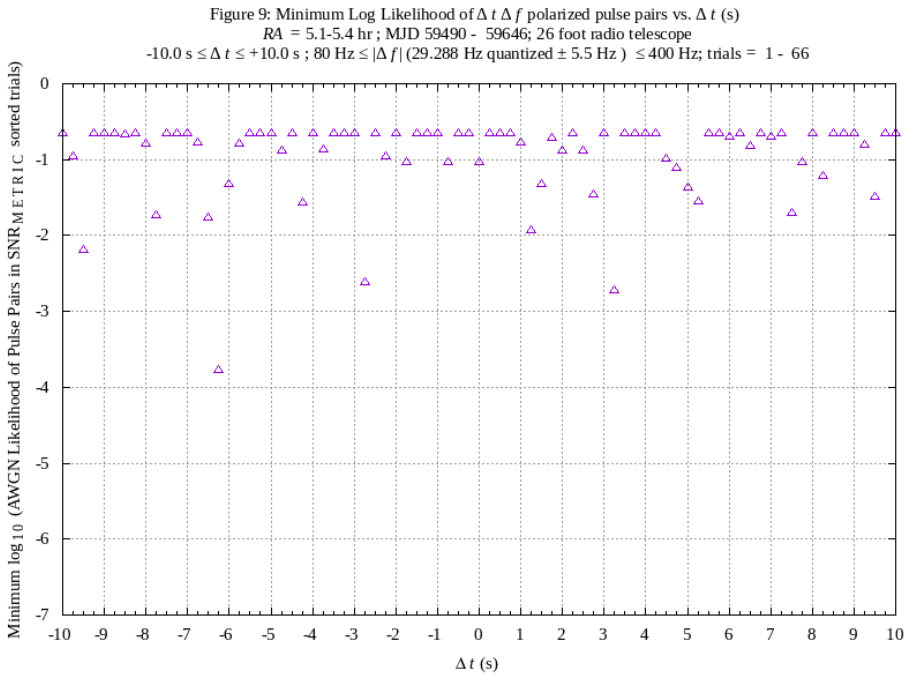

Figure 9: The process used to measure log likelihood of quantized repetitive Δ*t* symbol count in *RA* ranges, yielding **Figure 1** and **Figure 5**, was modified to measure minimum log likelihood in the 5.1 to 5.4 hr *RA* range, at 81 Δ*t* values, -10.0 ≤ Δ*t* ≤ 10.0 s. Several settings of Δ*t* indicate anomalous log likelihood, i.e. at Δ*t* values of -9.5 s, -6.25 s, -2.75 s, +1.25 s and +3.25 s. Log likelihood, due to an RFI-augmented AWGN model, is estimated to occur with one log likelihood event having a value less than -2.0, per 157 day duration experiment. Four such events are observed.

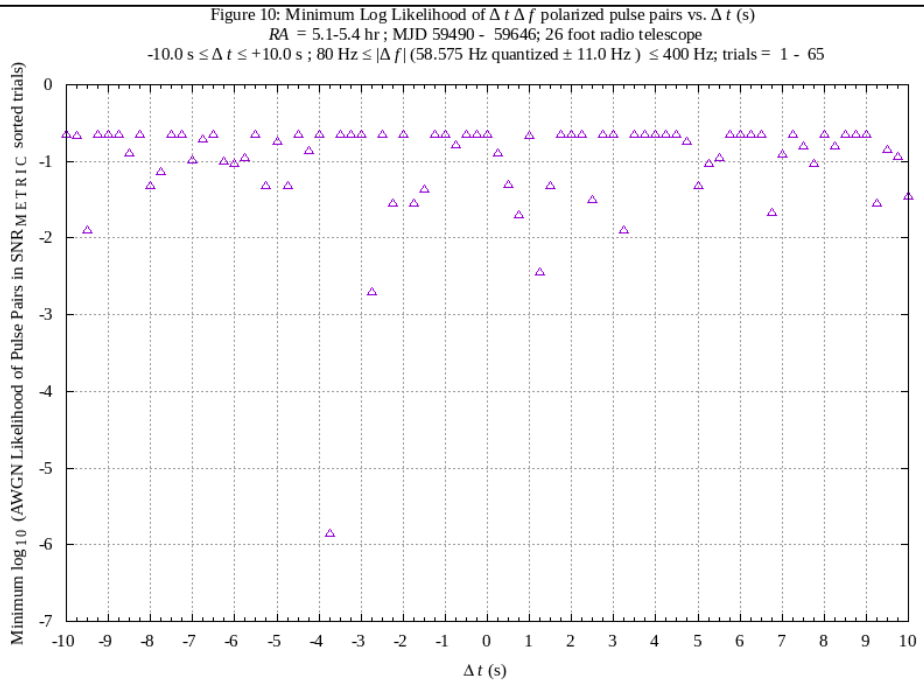

Figure 10: In addition to 58.575 Hz quantized anomalies observed at Δ*t* = -3.75 s, four Δ*t* values -9.5s, -2.75 s, +1.25 s and +3.25 s, observed in **Figure 9,** appear significant at 58.575 Hz quantization. Each of the four Δ*t* events is present, using an RFI-augmented AWGN model probability, at **≤** -1.9 log likelihood. The binomial distribution of five events seen in 81 trials, at event pr. = $10^{-1.9}$, equals 0.003. The presence of four of the same Δ*t* values observed in **Figure 9** data, supports a thought that Δ*t* and Δ*f* in polarized pulse pairs are each quantized and repetitive.

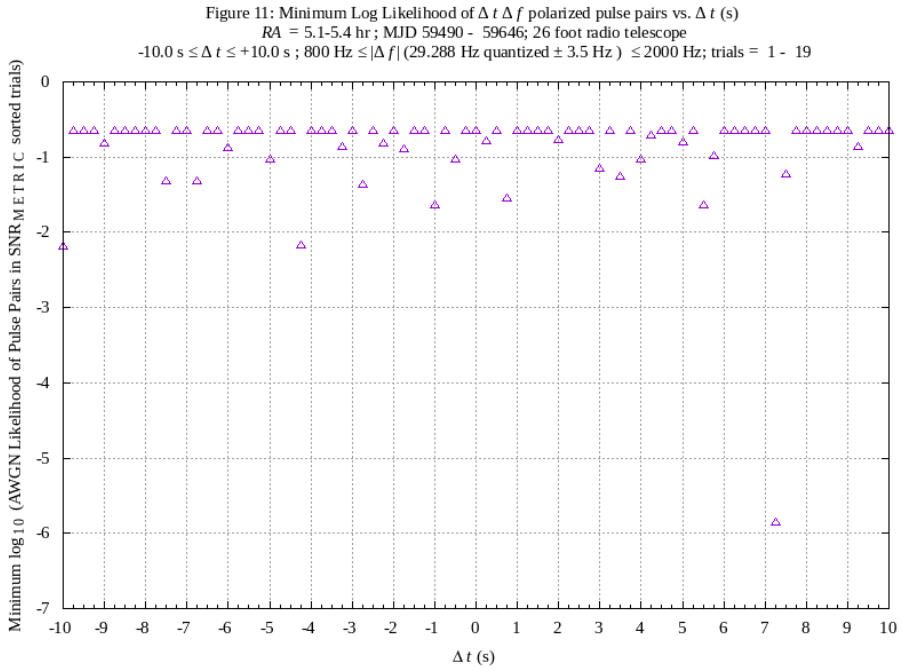

Figure 11: A Δ*t* = +7.25 s anomalous high SNR_{METRIC} set of polarized pulse pairs was found in a search of 157 day duration polarized pulse pairs at an extended |Δ*f* | range. Filters were quantized to multiples of 29.288 Hz, each within ±3.5 Hz, and having 800 Hz ≤ |Δ*f* | ≤ 2000 Hz. *RA* = 5.1 - 5.4 hr polarized pulse pairs measured SNR_{METRIC} ranked 1, 2, 3, 4, and 6, among 21 *RA* bins. This measurement compels further work to build and test symbol repetition and quantization machines that eventually might facilitate hypothetical transmitter message decoding.

Discussion

Many explanations may help one understand the cause of observed anomalies. Ideas and examples of explanations are described below.

Potential population selection bias

The observed 58.575 Hz, and half of 58.575 Hz apparent quantization of Δf in polarized pulse pairs, may perhaps be explained using an auxiliary hypothesis that predicts the choice of these value to be statistical noise induced by population selection bias. The 58.575 Hz value was chosen due to investigation of Δt = -3.75 s repetitive pulse pairs reported in [8] Figure 6. The 29.288 Hz half value was chosen during examination of the RFI-augmented AWGN model's log likelihood of the apparently repeating Δt = - 6.25 s polarized pulse pairs. When a quantization base value is chosen from the results of an experiment, one requires models and statistical analysis to test significance of the chosen value, e.g. using the *pr*. = 0.05 composite value calculated from observations described in [8] OBSERVATIONS, related to [8] Figure 6. On the other hand, observation of twice harmonic quantization base values, i.e. at 29.288 Hz and 58.575 Hz, on almost alternate sets of days, implies a more complex auxiliary hypothesis, describing selection bias, that is yet to be developed.

Equipment issues

Anomalies may be caused by equipment issues. Some possibilities are described.

1. The use of numerous RFI rejection filters [6][7][8], each having chosen hyperparameters, e.g. filters, rejection thresholds, risks a leakage of RFI into measurement results. RFI algorithm output files need to be examined.

2. Telescope data capture processes may lead to RFI leakage into measurement results. Simulations and further long term artificial noise source tests are required to understand this possibility.

3. Natural objects, together with equipment algorithms, may produce results that mimic communication signals.

4. The physical temperature of the low noise amplifiers at the telescope feed are expected to induce receiver sensitivity changes over time, affecting measurements.

5. Software errors may be present.

Absence of corroboration increases uncertainty

At present, independent observation and analysis of polarized pulse pairs in the hypothetical direction of interest are not known to have been performed. Sporadic presence and pointing uncertainties of the reported highest SNR pulse pairs make follow-up with larger single pixel radio telescopes potentially time consuming. Prediction of pulse pair events and direction-finding seems important to ameliorate the follow-up issue.

Limited, or changing, matched filter range

Apparent repetition and quantization of signal measurements compels a search for potentially associated anomalies to help explain measurement results. An exploratory search for pulse pairs having $|\Delta f|$ greater than 400 Hz has been conducted, with some preliminary indication of anomalous results above 400 Hz, plotted in **Figure 11**. There is a possibility that a transmitter is switching its parameters over time, to allow greater likelihood of discovery, a lower risk of mimicking RFI, and/or given thoughts that a receiver might be set to a relatively confined and fixed set of filters for a long duration, for reasons unknown to the transmitter. Switching transmitter parameters from one set to another may be an inherent aspect of discoverable interstellar communications transmitters. Electromagnetic propagation systems that are designed to be difficult to detect are expected to not repeat quantization base values during relatively short time periods. RADAR systems, and secure communications systems often develop a variety of methods to prevent discovery. These concealment methods do not appear to be present in observations in this and previous work. Polarized pulse pairs are observed using wide beamwidth, wide bandwidth radio telescopes without difficult searches.

Correlations may be difficult to explain

The apparent correlation of high SNR_{METRIC} levels, having multiples of a base Δf value, at one Δt value, and also at multiples of half the base Δf value, at a different Δt value, and having *RA* correlation during long periods, seems difficult to explain, without introducing various intentional transmitter models and unusual RFI models. On the other hand, there may be an ultimately simple explanation currently unknown.

Conclusions

The RFI-augmented AWGN model continues to not explain experimental results. Observations indicate that repetition and quantization of polarized pulse pair

measurements seem to exist, associated with the hypothetical celestial direction of interest. However, a definitive conclusion is not presently possible, due to many other possible explanations. The mechanisms that produce the anomalies observed in this work are therefore concluded to be not understood, compelling further work.

Further Work

Items of further work have been proposed in past reports [6][7][8]. Prioritization should focus on better understanding the anomalies that are being currently observed. Given this idea, a search for additional repetition, quantization, and hyperquantization [9] seems important, together with the development of polarized pulse pair prediction, squelch and direction-finding equipment algorithms.

Acknowledgements

Many contributions of workers of many organizations have made this work highly enjoyable, including the Green Bank Observatory, Deep Space Exploration Society, Society of Amateur Radio Astronomers, SETI Institute, Berkeley SETI Research Center, Breakthrough Listen, product vendors, and open source software community. Guidance from family and friends is greatly appreciated.

References

[1] J. M. Wozencraft, I. M. Jacobs, *Principles of Communication Engineering*, New York, NY: John Wiley & Sons, p. 376, 1965

[2] J. G. Proakis, *Digital Communications*, 4th Ed., New York, NY: McGraw-Hill, pp. 176-181, 743-753, 2001

[3] C. E. Shannon, W. Weaver, *The Mathematical Theory of Communication*, Urbana and Chicago, IL: University of Illinois Press, pp. 97–103, 1949

[4] D. G. Messerschmitt, *End-to-end interstellar communication system design for power efficiency*, arXiv 1305.4684v2, pp. 26–27, 70–74, 86–106, 201–223, 2018

[5] K. P. Popper, *The Logic of Scientific Discovery*, New York, NY: Basic Books, Inc., pp. 40–42, 1934

[6] W. J. Crilly Jr, *An interstellar communication method: system design and observations*, arXiv: 2105.03727v2, v1 May 8, 2021

[7] W. J. Crilly Jr, *Radio interference reduction in interstellar communications: methods and observations* , arXiv: 2106.10168v1, June 18, 2021

[8] W. J. Crilly Jr, *Symbol repetition in interstellar communications: methods and observations*, , arXiv:2202.12791v1, Feb 25, 2022

[9] J. R. Pierce, *An Introduction to Information Theory, Symbols, Signals and Noise*, 2nd Ed., New York, NY: Dover Publications, Inc., p. 132, 1961, 1980

Symbol repetition in interstellar communications: methods and observations

William J. Crilly Jr.

Green Bank Observatory, West Virginia, USA

Abstract— Discoverable interstellar communication signals are expected to exhibit al least one signal characteristic clearly distinct from random noise. A hypothesis is proposed that radio telescope received signals may contain transmitted Δ*t* Δ*f* opposite circular polarized pulse pairs, conveying a combination of information content and discovery methods, including symbol repetition. Hypothetical signals are experimentally measured using a 26 foot diameter radio telescope, a chosen matched filter receiver, and machine post processing system. Measurements are expected to present likelihoods explained by an Additive White Gaussian Noise model, augmented to reduce radio frequency interference. In addition, measurements are expected to present no significant differences across a population of Right Ascension ranges, during long duration experiments. The hypothesis and experimental methods described in this paper are based on multiple radio telescope Δ*t* Δ*f* polarized pulse pair experiments previously reported. (ref. arXiv:2105.03727, arXiv:2106.10168). In the current work, a Right Ascension filter spans twenty-one 0.3 hour Right Ascension bins over a 0 to 6.3 hr range, during a 143 day experiment. Apparent symbol repetition is measured and analyzed. The 5.25 ± 0.15 hr Right Ascension, -7.6° ± 1° Declination celestial direction has been associated with anomalous observations in previous work, and continues to present anomalies, having unknown cause.

***Index terms*— Interstellar communication, Search for Extraterrestrial Intelligence, SETI, technosignatures**

William J. (Skip) Crilly Jr. is a Volunteer Science Ambassador in Education & Public Outreach
of the Green Bank Observatory. email: wcrilly@nrao.edu

I: Introduction

Hypothetical discoverable interstellar communication signals may be guessed to exhibit certain characteristics. The signals may utilize energy-efficient information transfer methods, produce relatively low interference to other communication systems, and contain at least one signal design element that aids discovery. The signal discovery mechanism is expected to provide unique transmitter identification, and to contain one or more seeds for a receiver to learn the information in the signal. The design space of such signals is large, yet may be reduced by studying communication systems based on principles of mathematics and physics [1][2], assumed to be similarly understood at the transmitter and receiver. The analyzed existence of an interstellar coherence hole (ICH) communication method is an example of such similar shared principles.[2] The characteristics of signals and systems proposed in this paper are based on these principles.

In previous work, Δ*t* Δ*f* opposite-polarized pulse pairs were examined as possible interstellar communication signals. [3][4] The arrival time and RF frequency differences between the polarized pulses in each pulse pair, i.e. Δ*t* Δ*f* measured values, of decreasingly-sorted Signal to Noise Ratios (SNR) of the pulses were used to measure the pulse pairs' likelihood due to an Additive White Gaussian Noise (AWGN) model, augmented with robust RFI amelioration.

The augmented AWGN model was apparently refuted as a likely cause of the anomalies observed, in past work. Similar anomalies appear in the current work, and new anomalies that indicate a symbol repetition scenario have been observed. Experimental results of recent work are reported here in **IV. Observations**. Anomalous hypothetical symbol-based matched filter responses have been observed while a 26 foot diameter radio telescope beam transits the celestial direction of interest, 5.25 ± 0.15 hr Right Ascension (*RA*) and -7.6° ± 1° Declination (*DEC*), during 143 days of observations.

An important objective of this investigation is to automate the receiver's signal processing processes as much as reasonable. In past work, manual activities involved spreadsheet examination, sorting, and results plotting. In the current system, receiver signal file examination, filtering, sorting, statistical analysis and plotting of results are performed within the software system. Results reported here are the output of the multi-step signal processing machine, without human intervention, other than steps believed to be traceable to the machines' source code files, output files and lab notebooks.

A related objective of this investigation is to design machines that permit testing of various hyperparameters of the receiver system, for enhanced Bayesian data analysis, non-ergodic analysis, and Markov Chain model development, topics of intended further work.

Hypotheses and models, other than the RFI-augmented AWGN model, have not been introduced to an extent needed to try to explain the Δt Δf anomalies. A lack of experimental evidence to support the RFI-augmented AWGN model leads to a belief that the cause of the repeated Δt Δf anomalies are unexplained. Equipment, RFI, experimental methods, various types of bias and other explanations are being examined to attempt to explain the cause of the anomalies.

Past and present work emphasizes that many alternate and auxiliary hypotheses have not been modeled, tested and examined, to try to explain observed anomalies. Independent corroboration of these experimental results is absent. Therefore, no conclusions can be made regarding the presence of an interstellar communication signal in these experimental results.

The following sections of this paper describe the hypothesis, experimental methods, observations, discussion, conclusions and further work.

II: Hypothesis

The hypotheses in previous work, [3][4], have been modified, as follows, to include an augmented AWGN explanation of anomalies in hypothetical discovery elements, including transmitter symbol repetition.

***Hypothesis*:** An RFI-augmented AWGN model is expected to explain observations of one or more signal discovery elements contained within Δt Δf opposite circular-polarized pulse pairs, while a radio telescope beam diurnally scans the 0 to 6.3 hr Right Ascension range, including a direction of interest at celestial coordinates *RA* 5.25 ± 0.15 hr and *DEC* -7.6° ± 1°.

The current hypothesis implicitly contains a choice of matched filter to be used at the receiver. The matched filter is defined to be the bandwidth and time duration of the energy detection system of the receiver, resulting from the FFT-based signal processing system, together with a filter that limits the range of polarized pulse pair Δt and Δf values, applied to statistical analysis, to seek symbol repetition in a population of quantized *RA* directions. A symbol is defined in the context of this work to be a unique element among a set of possible pulse pair signals, indexed by quantized values of composite signal dimensions, including amplitude, RF frequency, pulse pair Δt and Δf values, pulse energy detection bandwidth and integration time, the latter two having fixed values in this work. Symbol repetition is defined to be the observed presence of one value of at least one hypothetically quantized dimension, repeated over time.

In past work, the matched filter used a 3.7 Hz binned FFT, 0.27 s integration, $|\Delta t| \leq 3$ s and $|\Delta f| \leq 400$ Hz, with a $|\Delta f| < 80$ Hz rejection region, the latter to ameliorate potential Doppler-spread RFI.[4] In the current work, the same matched filter is used to report follow-up measurements. In addition, two Δt values, Δt = -3.75 s and -6.25 s, are used in the matched filter, together with other filter parameters set as above.

The stated uncertainty range of the *DEC* of the hypothetical direction of interest, ± 1°, is the value of the estimated uncertainty range in previous presentations, [3][4]. The radio telescope used in the

current work has a measured power Full Width Half Maximum (FWHM) beamwidth, in the *RA* plane, of approximately 2°, based on telescope continuum measurements made during Sun transits in the Fall of 2021. These calibrations had azimuth and elevation of the telescope set to values used during the beam transit tests described in this work. Circular beam symmetry is assumed. Therefore, the ± 1° *DEC* uncertainty only applies when examining the prior experimental results, or current results analyzed under assumptions of significant prior results. The *RA* uncertainty is based on the observation of anomalies in prior experiments.

Discovery processes in interstellar wideband communication are hypothesized to produce statistically anomalous changes in signal measurements, over time, i.e. differing from noise model and highly coded transmitter predictions. This changing signal concept is rationalized by considering an alternative argument, i.e. that the intended discoverable transmitter does not change its wideband signal properties. A continuously transmitting set of identical modulation properties, appearing to continuously have the properties of random noise, might communicate much information, yet does not lead a receiver designer to glean a method of decoding the signals to transmitted information. Therefore, it is expected that some discovery mechanisms, e.g. symbol repetition and matched filter changes, will be present in interstellar discoverable transmitter signals. In general, highly ergodic, low duty cycle signals present discovery difficulties. Some changes in signal properties, over time, are required, within the ensemble of transmission events, to aid in signal discovery and information recovery.

Changes in receiver settings during a multi-stage experiment tend to confound statistical analysis and Bayesian data analysis, because priors are potentially invalid during Bayesian posterior analysis. In addition, near-zero valued priors are problematic as they result in near-zero valued posteriors.[5] Hypothesis testing might yield no new information to guide further investigation, other than continued refutation of a prior explanatory model.

Standalone new observations, using new receiver settings, might yield highly unlikely noise-cause results, even when many possible changed receiver filters are factored in. For example, if a receiver's pulse pair Δf search range is doubled from its prior experimental setting, and new anomalies are found, an RFI-augmented AWGN model likelihood may be assumed to increase by a factor of $N = 2$, to account for the two Δf search range filter possibilities. In another example, if a single value of seemingly arbitrary pulse pair Δt presents anomalies, and an N quantity of Δt values could have been chosen to seek anomalies, the factor N may be used to increase the RFI-augmented AWGN model likelihood.

If a single Δt value is found to have anomalous presence, and has other measured significance, e.g. anomalous repetition at highest values of SNR, within a single *RA* range, then the single Δt value may be examined for additional repetition, at lower SNR values. The use of one value of N, or another, depends on how arbitrary is the choice of one value of Δt in a symbol repetition detection receiver.

In addition to a speculated discovery intent, interstellar communication signals are expected to contain some change in transmitted signal properties, to help the receiver further analyze the signal. An example of such hypothesized changes is a change in the matched filter required for reception. For example, a receiver might observe a disappearance of received signals, speculated to be due to a transmitter filter having changed. The receiver will presumably expect some significance to this event, and attempt to learn more about the transmitter signals, while attempting to understand why, and in what way, the transmitter filter appeared to change. The observed change might lead to understanding the information in the signal and the transmitter characteristics. In addition, changes in transmission properties might lead to unique identification of transmitters, when multiple transmitters may be present.

III: Method Of Measurement

The receiver processes used in the current work adhere to the processes described in prior work, [3][4], with several changes, described in this section.

Central IF rejection region increased

Sporadic apparent spurious signals were observed in the region surrounding the 1425 MHz local oscillator. Leakage of low RF frequency signals into the IQ digitizers' inputs is suspected. The excised region surrounding the local oscillator is set to 1422 to 1428 MHz to prevent sporadic signals from affecting pulse pair AWGN likelihood calculations. The possible presence of associated spurious signals outside the excised range is an important aspect of equipment-cause hypotheses, requiring further study.

RFI burst rejection filter IIR filter threshold increased

The IIR narrowband RFI burst rejection filter, RFI amelioration method 3, in [3][4], was observed in the current work to reject single pulse pairs at high levels of SNR. The purpose of the filter is to reject rarely occurring repeated pulses, confined to a narrow range of RF bandwidth. The loop gain of the first-order IIR filter is therefore set to a high value, 0.99**.** A shortcoming of the filter is that a single pulse having a high SNR value can result in the filter output exceeding the SNR_{IIR} threshold, without time integration, and a rejection of the pulse pair. Rejecting single pulses in pulse pairs is not desirable, because spectral outliers, rarely occurring Δt Δf polarized pulse pairs, are sought by the receiver. SNR_{IIR} threshold was increased from 11.84 to 11.88 dB to ameliorate this effect.

An energy burst filter is added

In this work, wideband, short-time energy bursts have been observed in apparently random directions, MJD days, RF frequency and, in some Δt , Δf measured values. The observed bursts appear similar to a group of pulse pairs observed on MJD 59332, described in Figures 9 and 10 in [4]. The hypothetical random energy burst observed pulse pairs in this work do not appear similar to observed standalone Δt Δf polarized pulse pairs. Rather, the observed energy bursts present multiple values of Δt and Δf in the polarized pulse pairs, and confined to a duration of several to multiple tens of seconds, without repeating in *RA* direction, and not appearing on subsequent days in the same *RA* direction. The energy burst pulse pairs appear to present Δt values concentrated approximately within ± 1 s. Approximately ten discrete energy bursts were observed during the 143 days of the current experiment, at 6.3 hours of observation per MJD day. The cause of these receiver responses is unknown. The SNR measurement and thresholding method in the pulse detection system of the receiver uses different integration times and RF bandwidth for signal and noise measurements, [3][4] and is therefore sensitive to the high energy spectral outliers of energy bursts, resulting in associated observed Δt Δf pulse pairs in the receiver output.

A decision was made to design and implement a filter to separately measure high counts of Δt Δf responses observed on one day, occurring within a short time, to differentiate sporadic bursts of pulse pairs from apparent anomalous standalone Δt Δf polarized pulse pairs. The reasoning behind this decision is: 1) short duration wideband transient energy bursts are common phenomena in radio astronomy, and may be included in filters that augment the AWGN model, 2) transient receiver gain fluctuation, RFI and other mechanisms might cause the response, 3) the absence of observed repetition in the same *RA* direction, during multiple days, leads to an apparent absence of persistent interstellar communication signals, and 4) if an interstellar communication signal has properties that are similar to natural object signals, interstellar communication signal discovery is speculated to be difficult.

An SNR burst metric was developed to measure the concentration of burst-caused pulse pairs, binned by MJD, and by *RA* sub bins, each spanning 0.03 hr *RA*, resulting in 210 *RA* sub bins per MJD day, as follows,

$$\mathrm{SNR}_{\mathrm{BURST\ METRIC}}[MJD, RA_{subbin}] \triangleq \sum \frac{(SNR_{\mathrm{LHC}} + SNR_{\mathrm{RHC}})}{2}, \qquad (1)$$

where the summation includes Δt Δf pulse pairs present with less than 30 seconds of time to a subsequent pulse pair time, within an MJD and RA sub bin. SNR_{LHC} and SNR_{RHC} have decibel units, and have a minimum of 11.8 dB. LHC and RHC indicate left and right hand circular polarizations.

The energy burst rejection filter is set by performing a single set of measurements of the SNR burst metric on all MJD days, at pulse pair $|\Delta t| \leq 3$ s and $80\ \mathrm{Hz} \leq |\Delta f| \leq 400$ Hz. Subsequent pulse pair counts, using different Δt Δf filters, and/or trial count number, use the single set of SNR burst metric measurements, and a burst SNR

metric threshold, set to 150, to reject pulse pairs observed within the indexed MJD and *RA* sub bin..

Polarized pulse pair symbol repetition

Signal processing methods filter candidate polarized pulse pairs into one of several possible repetition classes, given the number of degrees of freedom in the polarized pulse pair signals. The primary repetition class implemented in this work utilizes two Δt values, and a range of Δf values specified at $|\Delta f| \leq 400$ Hz, with a $|\Delta f| < 80$ Hz rejection region. The Δf range is chosen to equal the Δf range used in the 164 day and 40 day beam transit tests, and the 44 day artificial sky noise test previously reported [3][4]. Δt values are indexed at 0.25 second quantization increments. Δf values are generally quantized to the 3.725 Hz FFT bin width, with measured residuals less than one bin width. The residuals are due to quantization, metrology and calibration. RF frequency Doppler correction is referenced to 180 degree pointing azimuth at the Green Bank Observatory.

The values Δt = -3.75 s and Δt = -6.25 s are chosen for the repetitive symbol parameter. These two values were determined after observing an anomalously high number of high SNR repetitions in the hypothetical direction of interest at *RA* 5.1 to 5.4 hr, *DEC* -7.6°. The Δt value is negative due to a chosen convention that Δt measures the left-hand circular polarized pulse arrival time minus the right-hand circular polarized pulse arrival time, quantized to 0.25 s increments.

In the presentation of results, signal repetition measurements are plotted over a range of *RA* values from 0 to 6.3 hr, in 21 *RA* bins, or across a range of Δt values in the *RA* direction of interest, observed during the 143 days.

Energy burst repetition ameliorates transmitter-receiver filter mismatch

Measured repetition of nearly equal values of Δt is a method that differing receivers may use to discover repetitive signals in noise, without prior transmitter-receiver coordination. Identical repetitively transmitted signals result in identical repetitive observed spectral properties, at the output of an unchanging filter receiver, given a constant observation time that spans at least the duration of the energy burst, a fixed instantaneous bandwidth receiver, and the absence of noise and propagation channel fluctuations. When repetitive signals are present, two receivers, having different filtering processes, will each observe a repetition of outlying spectral properties, albeit different across receivers. In other words, a repetition receiver does not need to have a filter matched to a transmit filter, in order to detect a repetitive energy burst, transmitted in the ICH.

When noise is included in the repetitive received signal, and transmitter duty cycle considered, spectral outliers are expected to be observed using each of two differing receivers, with randomness estimated by Ricean statistics. Transmitted signals may have energy confined to narrow RF bandwidths to increase the number of pulses having low values of Δf , with bursts transmitted at time spacing Δt.

Using a repetitive transmit method, the issue of transmit and receive filter mismatch can be largely avoided, at the cost of energy required to repeat identical energy bursts. The cost may be justified if the repetitive signals are designed to contain information, using degrees of freedom in the signal properties.

***SNR*$_{HIGH}$ vs. *SNR*$_{LOW}$ sorting has been replaced with SNR sorting using a new metric**

In current and past work, a question has arisen as to the choice of which polarization's SNR to sort, for the computation of likelihood functions. Sorting by SNR_{HIGH}, the higher of the two polarizations, has been used to measure likelihood values when searching for Δt = 0 s polarized pulse pairs, while SNR_{LOW} sorting has been used when searching within a range of $\Delta t \neq 0$ s values. The rationale for the two methods is explained in past work [4]. The two choices appear to not exhibit a potential sorting that optimizes a search for combined polarization high SNR outliers, given an AWGN model. In each method, SNR information about the pulses in pulse pairs is being discarded.

In the current work, a sorting metric has been produced that combines the left hand and right hand polarized SNRs into a single value, derived from the AWGN model likelihood of Rayleigh-distributed joint polarization signal amplitudes.

The sorting metric is designed while considering that the cumulative probability of power in Rayleigh distributed amplitude signals, above a given power value, is exponentially distributed as a function of the given power value. Polarization independence is assumed, creating a circularly symmetric joint distribution. A base ten logarithm function is added for

convenience in relating the metric to orders of magnitude of decreasing likelihood,

$$\mathrm{SNR}_{\mathrm{METRIC}} \triangleq -\sum \log_{10} e^{-SNR_p} \ , \qquad (2)$$

where the summation is over *p*, the left-hand and right-hand circular polarization indexes. SNR_p uses linear signal power to linear noise power ratio, after conversion from $(S_p+N_p)/N_p$ decibel measured values.

The SNR metric in (2) is based on the joint polarized pulses' cumulative likelihood of polarized pulse pairs observed at values equal to or higher than $\mathrm{SNR}_{\mathrm{METRIC}}$, given an AWGN model, Rayleigh amplitude distributed, and exponential cumulative power distributed. The use of the metric in sorting ameliorates the issue of potentially significant signal information lost when SNR_{HIGH} and SNR_{LOW} are separately used when sorting polarized pulse pairs during statistical analysis.

Rationale for the new metric considers the joint probability distribution of polarized RF tones combined with noise. **Figure 1** plots a calculated log likelihood function, based on the joint probability distribution function of the opposite polarized pair SNR levels, expected in an AWGN plus tone model, at three tone levels, 0, 1.5σ and 3.0σ, while σ is the standard deviation of the noise, normalized to one. The underlying mathematics is explained in Appendix B of [3]. The rightmost section of the plot favors the discovery of tone-carrying polarized pulse pairs.

The metric defined in (2) is expected to prioritize tone-carrying candidate pulse pairs observed most often at the highest sorted values of the metric, given the polarized signals' tone amplitudes. The pulse pair transmitted duty cycle is an implicit factor.

A binomial probability distribution function is used to measure *RA* density likelihood

Binomial probability calculations are used to estimate the likelihood that one *RA* range will contain a number of polarized pulse pairs, within a number of highest to lowest $\mathrm{SNR}_{\mathrm{METRIC}}$ sorted trials, including all measured *RA* ranges. The number of trials is equal to the rank, after the sort, of the measured $\mathrm{SNR}_{\mathrm{METRIC}}$ in the one *RA* range. The count of events seen is the number of filtered pulse pairs observed in an *RA* range, up to the trial number. The event probability used is one divided by the number of *RA* bins, equal to 1 / 21. Binomial density values that indicate a lower number of counts seen, in the trials, than expected due to noise, are set to equal the probability density value expected due to noise. Presentation of results plots therefore indicate anomalous presence of polarized pulse pairs, not their absence.

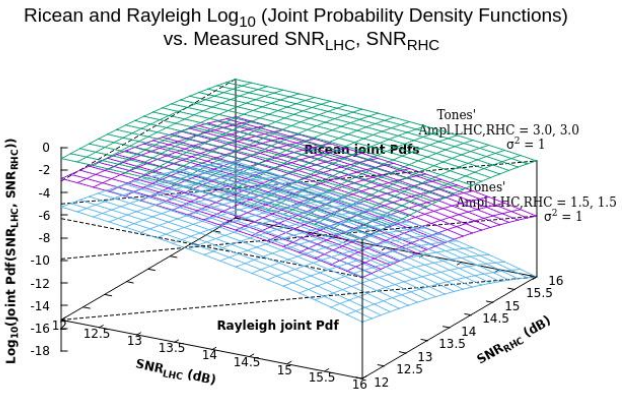

Figure 1: Calculated theoretical log joint probability density function values vs. SNR_{LHC}, SNR_{RHC}, where $SNR_{(\cdot)}$ is signal and noise power divided by noise power**,** measured at the output of each polarization receiver, at three levels of tone amplitudes, 0, 1.5 and 3.0, and where noise variance σ^2 is normalized to a value of one. Highest joint SNR values result in orders of magnitude decreased likelihood of an AWGN cause explaining polarized pulse pair events measured at highest SNR values. A Ricean amplitude probability distribution, Equation (7) in [3], Appendix B , was used to develop the probability density functions in the figure, together with a conversion of the measured SNR_{LHC} and SNR_{RHC} decibel values into amplitudes, and a $\log_{10}$ function applied to each density function calculated results.

Signal processing data flow

Three software steps are implemented, described as follows. 1. and 2. are described in [3][4].

7. FFT-based receivers, RFI amelioration

Radio telescope signals are digitized, and high SNR pulse characteristics are stored in four hour duration files per polarization, and per one second of a three second

time interval. GPS clocks trigger six two-channel baseband IQ digitizers at the start of three time phases during a three second interval. RFI amelioration is described in past work. [3][4]

8. Δ*t* and Δ*f* search algorithm, RFI amelioration

Software searches of the output files of 1. are performed, logging polarized pulse pairs' properties having | Δ*t* | less than 10 seconds and | Δ*f* | less than 2 kHz, producing an output file for each MJD. The primary purpose of this step is to reduce the overall signal processing time, e.g. when different Δ*t* and Δ*f* filter hyperparameters are set in the next step.

9. Application of Δ*t* and Δ*f* filters, RFI amelioration

The output files of 2. are processed to produce a presentation of results for a set of hyperparameters. This process includes SNR_{METRIC} sorting, hyperparameter filters, Right Ascension binning, RFI burst rejection, statistical analysis, and presentation of results development. The image files of the plots presented in **IV. OBSERVATIONS** are produced in the latter machine processing step.

IV: Observations

Figure 2 presents a follow-up of the experiments performed in prior work, [3][4], using new radio telescope data from the recent 143 day experiment. The modified augmented AWGN model is used, with the same Δ*t* and Δ*f* filter ranges used in the prior work. The *RA* range 5.1 - 5.4 hr does not indicate an anomalous presence of polarized pulse pairs, compelling a search for anomalies using larger values of |Δ*t* |.

Figure 3 presents an unlikely apparent repetition of a single value of Δ*t* = -3.75 s in the *RA* direction of interest.. The absence of points above a value of -1 log likelihood is due to the presence of five of the ten highest SNR_{METRIC} values, having Δ*t* = -3.75 s, among all 21 *RA* ranges, presented in the 5.1 to 5.4 hr *RA* direction.

Figure 4 indicates an anomalous presence of filtered Δ*t* = -3.75 s pulse pairs during MJD days 59505 – 59569. An expected average AWGN-caused pulse pair flux of 1.5 pulse pairs per *RA* bin occurs in 65 days of observation, assuming that the non-bin 17 points in **Figure 4** are explained by noise events. The presence of eight pulse pairs in the *RA* bin 17 direction in 65 days seems anomalous, having binomial likelihood 0.004. On the other hand, the eight pulse pairs might be explained as random population selection effects.

When the log likelihood of the sorted SNR_{METRIC} pulse pairs is re-calculated for a sample population of MJD 59500 - 59569, the *RA* bin 17 log likelihood value decreases from the minimum value indicated in **Figure 3** to -5.29. The five highest SNR_{METRIC} pulse pairs appear in the *RA* direction of interest, i.e. 5.1-5.4 hr *RA*.

Figure 5 indicates that polarized pulse pairs are distributed somewhat uniformly across RF frequency. This behavior is expected due to an AWGN model, and due to a model of a high information capacity communication signal.

Figure 6 presents Δ*f* measurements of polarized pulse pairs having the highest 70 values of SNR_{METRIC} at **Δ*t*** = -3.75 s during the 143 day experiment, binned to 21 *RA* ranges. The highest eight SNR_{METRIC} polarized pulse pairs in *RA* bin 17 (5.1-5.4 hr *RA*) appear to present a repetition of **Δ*f*** values at quantized multiples of ±58.575 Hz.

Monte Carlo simulations of uniform distributed Δ*f* values, within the Δ*f* filtered range, estimate a 58.575 Hz multiplier event probability of 0.259, and a standard deviation of residuals, $\sigma_{RESIDUALS}$, measured at 8.43 Hz. In other words, the probability of a single pulse pair having a multiplier event residual less than or equal to 8.43 Hz, given a 58.575 Hz multiplier, simulated to 0.259. A binomial likelihood function was used to estimate the event probability in the Monte Carlo method, using 1000 trials. The Monte Carlo derived event probability, 0.259, may be compared to an intuitive probability estimate of twice the $\sigma_{RESIDUALS}$ divided by 58.575 Hz. The 0.259 value calculates to 1.8 $\sigma_{RESIDUALS}$ / 58.575. The event probability

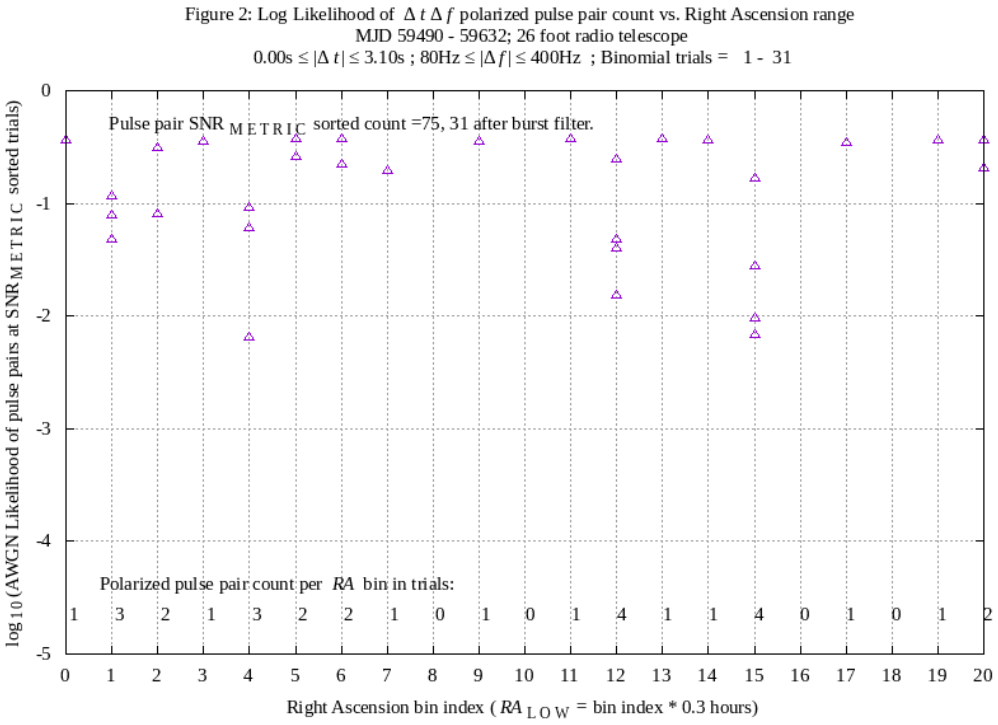

Figure 2 : The Δ*t* Δ*f* matched filter used in previous observations [3][4] does not present anomalies in *RA* bin 17 (5.1-5.4 hr *RA*). The single observed pulse pair in bin 17 compelled a search of Δ*t* values outside the previous Δ*t* range.

estimated in this process is used, as follows, in a likelihood function estimating multiple event probabilities that each appear to fit a multiplier pattern.

The Δ*f* residuals of the eight highest SNR_{METRIC} Δ*t* = -3.75 s pulse pair events in the 5.1-5.4 hr *RA* direction measure within ± 10.25 Hz, using a ±58.575 Hz Δ*f* base multiple. Using the Monte Carlo above-derived estimate of event probability, at 1.8 $\sigma_{RESIDUALS}$ / 58.575, computed at $\sigma_{RESIDUALS}$ = 10.25 Hz, yields a pulse pair multiplier event probability of 0.315.

The binomial distribution of eight events seen in eight trials, at a probability of 0.315, calculates to 9.7 x 10^{-5}. Various factors significantly increase this value. For example, the freedom in the choice of base multiplier Δ*f* values may be estimated to be the ratio of 58.575 to the FFT bin width in the signal processing system, resulting in a factor of 58.575 Hz / 3.725 Hz = 16. The use of this factor in calculating likelihood increases the augmented AWGN model likelihood of the eight polarized pulse pairs presented in the experiment, to 0.0015. Another consideration is that some of the eight values are expected to be noise-caused, because one noise-caused pulse pair is expected on average, in a number of trials equal to the number of *RA* bins, 21. In this case, perhaps only five pulse pair events, ranked 2, 3, 6, 7 and 11 in SNR_{METRIC}, should be used when calculating likelihood. Five events seen in five trials at the event probability of 0.315 estimates the 58.575 quantized pulse pairs' likelihood present in the experiment at 0.0031, and 0.05 using sixteen base multiplier values.

The number of trials used for binomial calculations is the number of pulse pairs output from the energy burst filter. The numbers of these are posted near the top of each plot. Relative differences from plot to plot occur due to different Δ*t* filters used in plots.

Figures 7 - 10 plot log likelihood, MJD, RF frequency and Δ*f* measurements of the apparent repeated Δ*t* = -6.25 s polarized pulse pairs, observed in *RA* bin 17.

Figure 11 plots values of | Δ*t* | ≤ 1.1 s, speculated to be present if a natural object produces bursts of energy into the radio telescope receiver. The direction of interest does not indicate anomalies. Models of natural objects and associated receiver response are preliminary.

Figure 12 plots the MJD of a range of Δ*t* values from -8 to –3 s, containing the two anomalous Δ*t* values at -

3.75 s and -6.25 s. A search of other Δ*t* values, to ± 10 s, did not result in an indication of anomalous pulse pairs in the *RA* direction of interest. The elements of two sets of pulse pairs, each set having either Δ*t* values of -3.75 s and -6.25 s, do not overlap with the same MJD, except for two pulse pairs at 59546.2542303 and 59546.2540972, respectively, occurring 11.25 s apart. In **Figure 5**, two Δ*t* = -3.75 s pulse pairs are observed relatively close in RF frequency, 1403.3933225 MHz on MJD 59546 and 1403.1295031 MHz on MJD 59565. The former pulse pair is the pulse pair that indicates Δ*t* = -3.75 s and Δ*t* = -6.25 s overlap on 59546 MJD. The presence of the MJD overlap, close RF frequency spacing, close time spacing, leads to a conjecture that pulse pairs might be transmitted in bursts spanning a few hundred kHz, and having durations of a few tens of seconds.

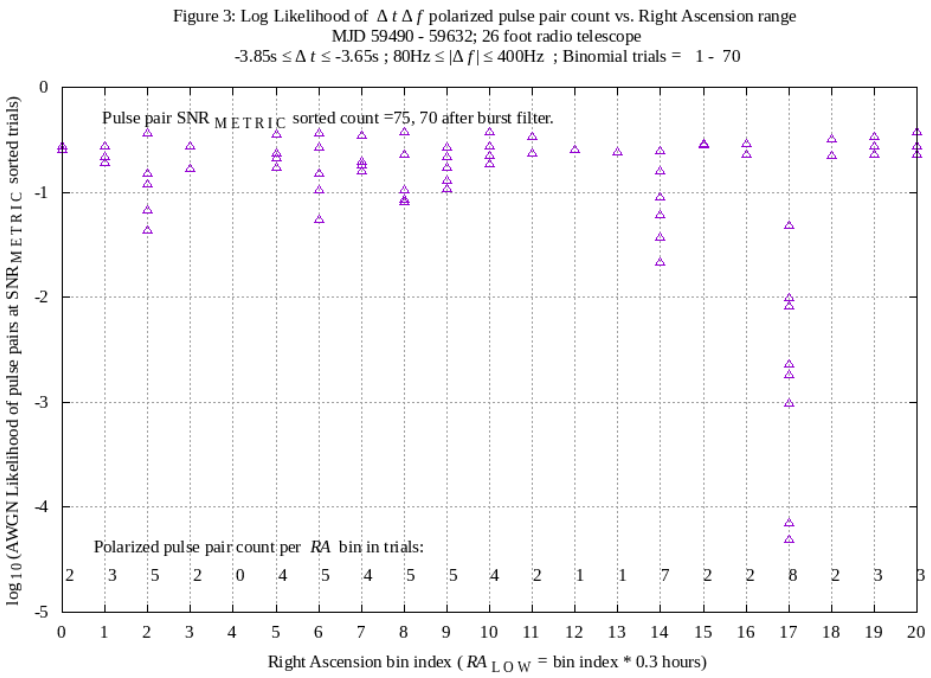

Figure 3: A Δ*t* = -3.75 s matched filter presents an anomalous number of highest SNR_{METRIC} polarized pulse pairs. The *RA* 5.1 to 5.4 hr polarized pulse pairs ranked 1, 2, 5, 6, 10 in the SNR_{METRIC} highest 10 values across all *RA*s. The AWGN likelihood of the direction of interest observations calculate approximately 1000 times less than expected.

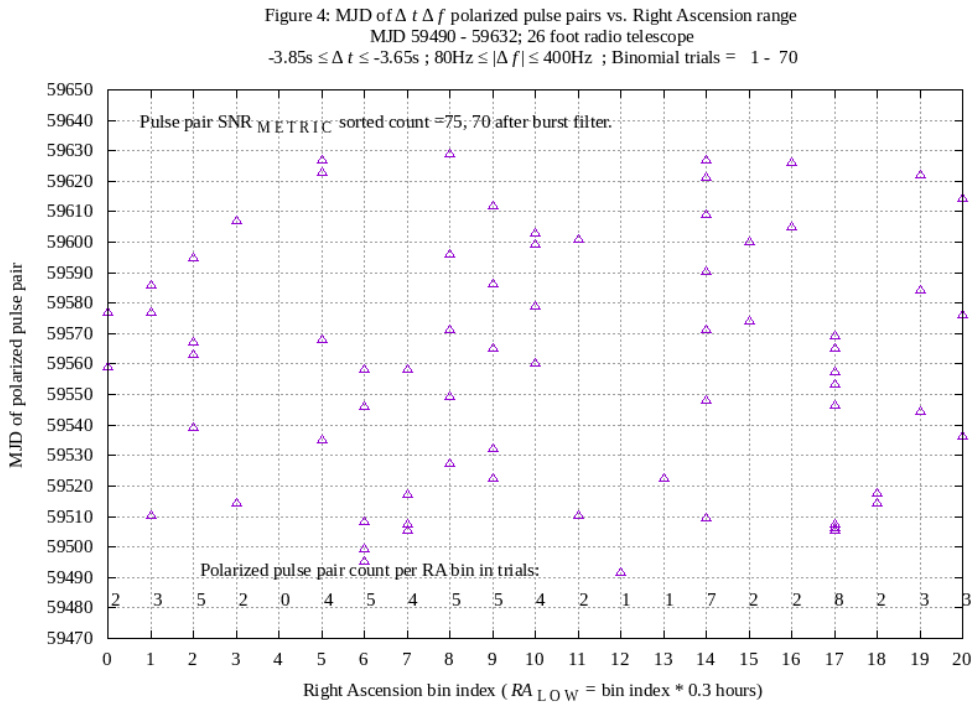

Figure 4: The 5.1 to 5.4 hr *RA* anomalous Δ*t* = -3.75 s polarized pulse pairs were observed on MJD days 59505, 59506, 59507, 59546, 59553, 59557, 59565, and 59569. The bin 17 MJD concentration appears unusual and non-ergodic**.**

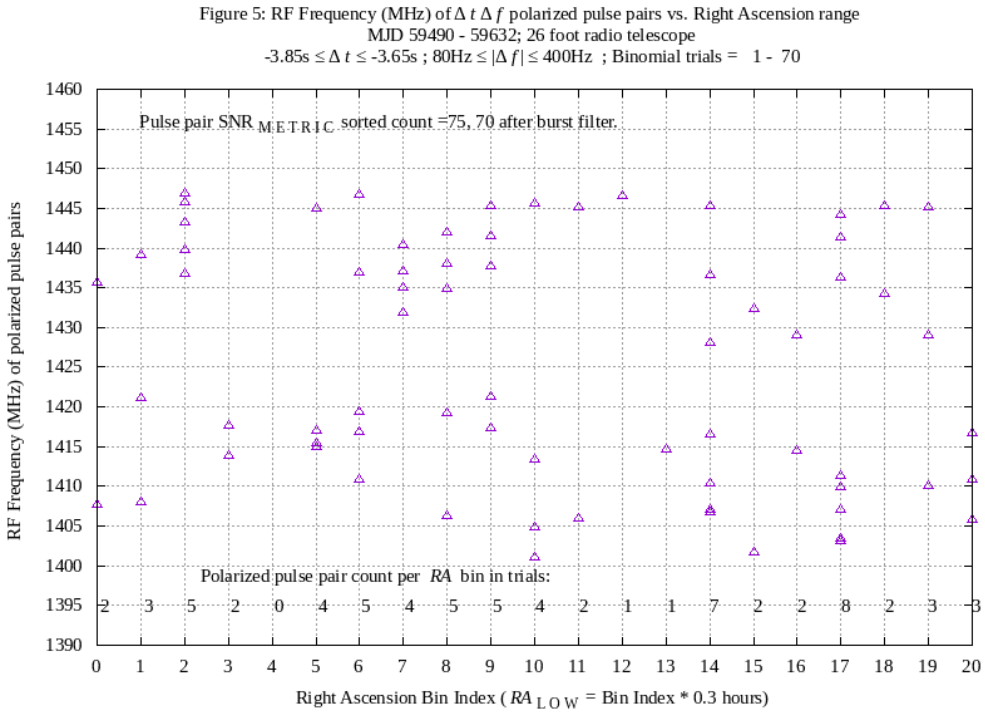

Figure 5: Measured RF frequency of the polarized pulse pairs appear distributed across the receiver range. A central region of 1422 to 1428 MHz was excised due to suspected RFI at low intermediate frequencies, surrounding the local oscillator. Two *RA* bin 17 points measured 1403.3933225 MHz on MJD 59546 and 1403.1295031 MHz on MJD 59565.

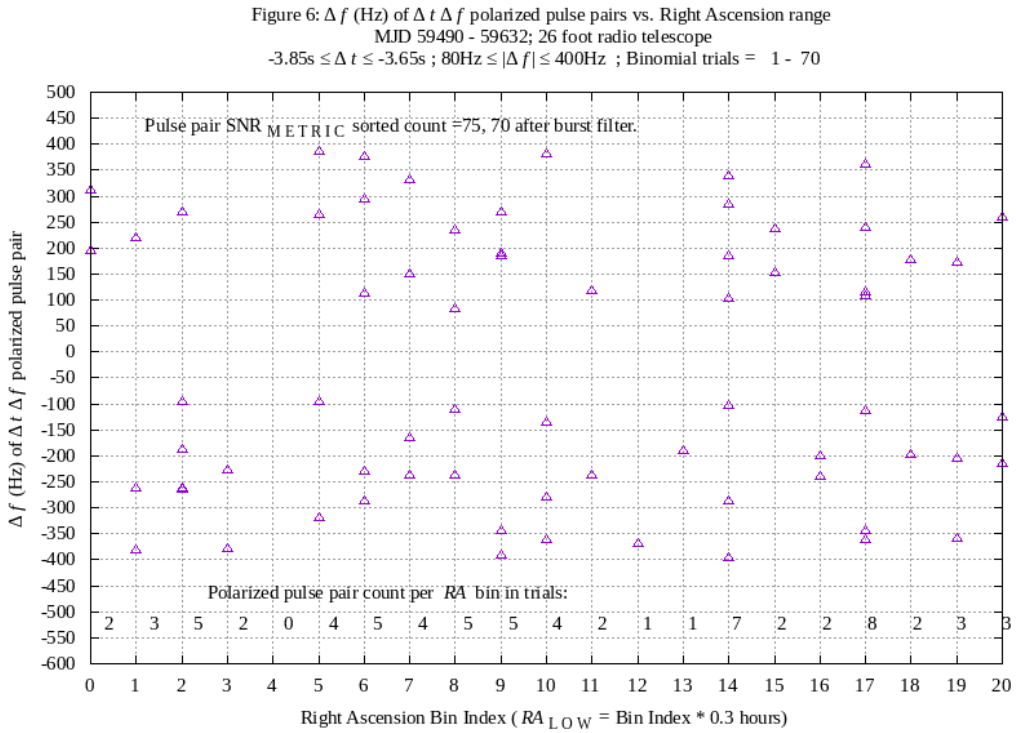

Figure 6: The eight anomalous Δ*t* = - 3.75 s pulse pair events appear concentrated near multiples of Δ*f* = 58.575 Hz, and measure maximum absolute residuals ≤ 10.25 Hz. The binomial distribution of 8 events seen in 8 tries, at event pr.0.315, calculates to 9.7 x 10^{-5}. Sixteen possible multiplier values increase this AWGN model likelihood to 0.0019.

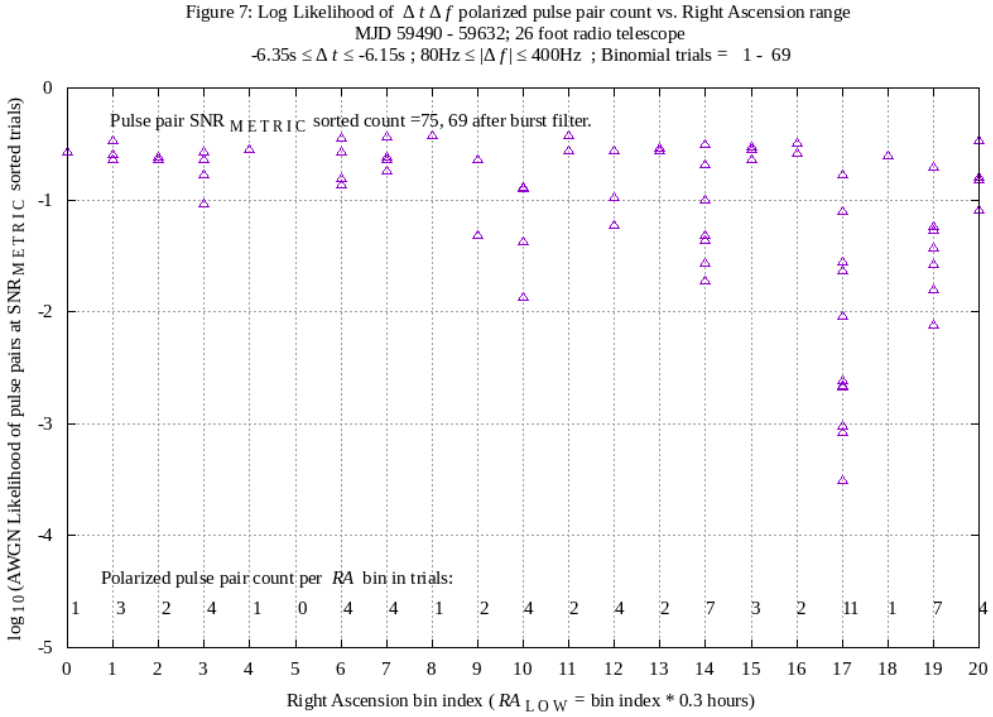

Figure 7: A Δ*t* = -6.25 s matched filter presents anomalous log likelihood measurements in *RA* bin 17.

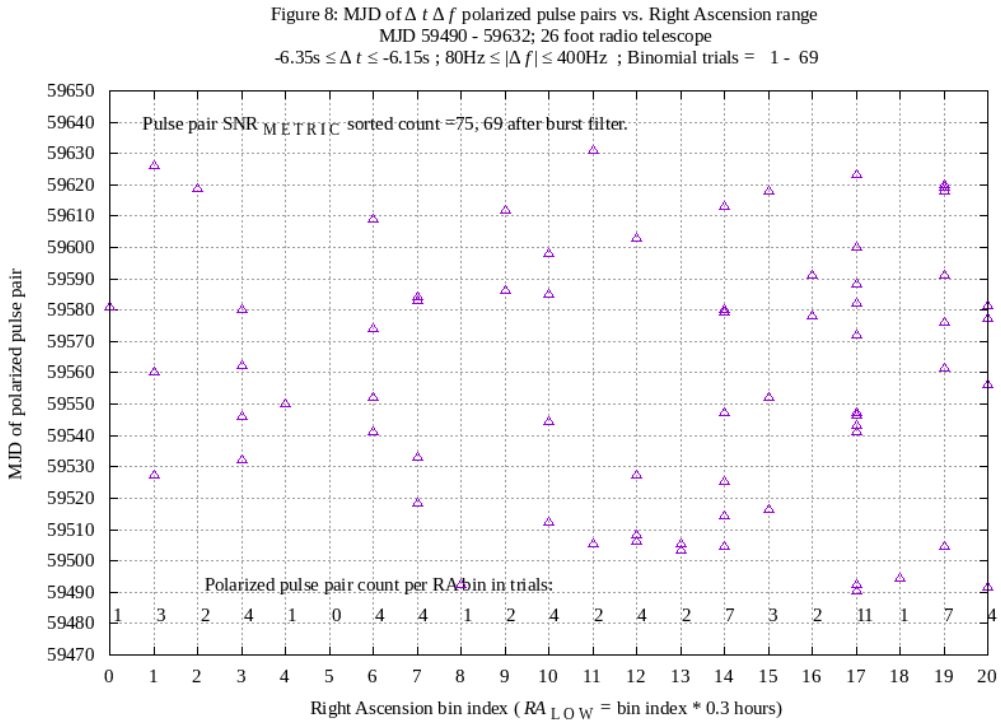

Figure 8: Polarized pulse pairs in *RA* bin 17 and Δ*t* = -6.25 s, appear concentrated in MJD ranges having almost no overlap of the MJD ranges observed with Δ*t* = -3.75 s polarized pulse pairs. **Figure 12** describes these relative MJD concentrations.

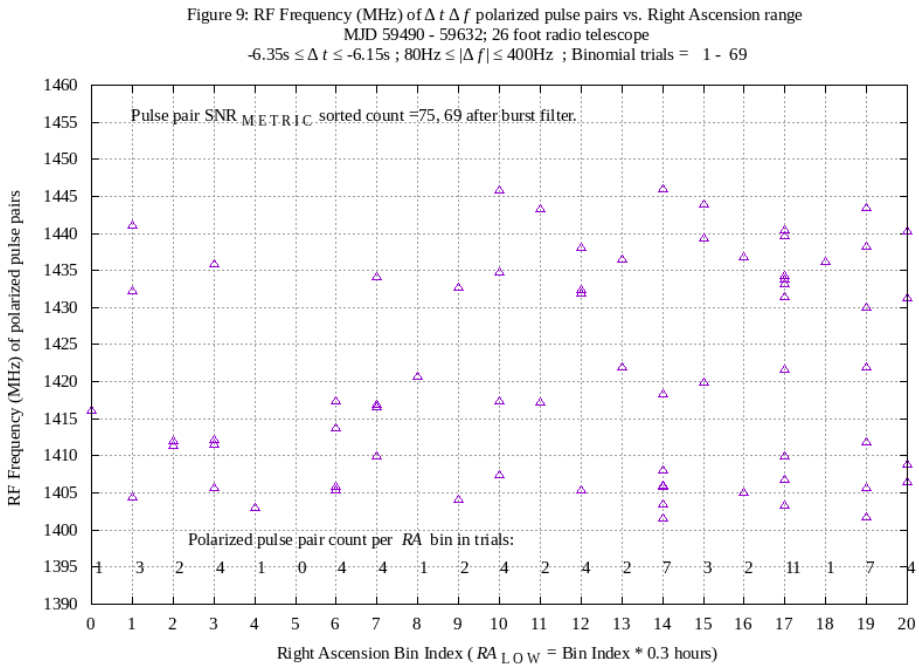

Figure 9: Δ*t* = -6.25 s polarized pulse pairs appear to be largely distributed across RF frequencies, while in the direction of interest, three pulse pairs were observed at 1433.1568978, 1433.8466790, and 1434.2319196 MHz.

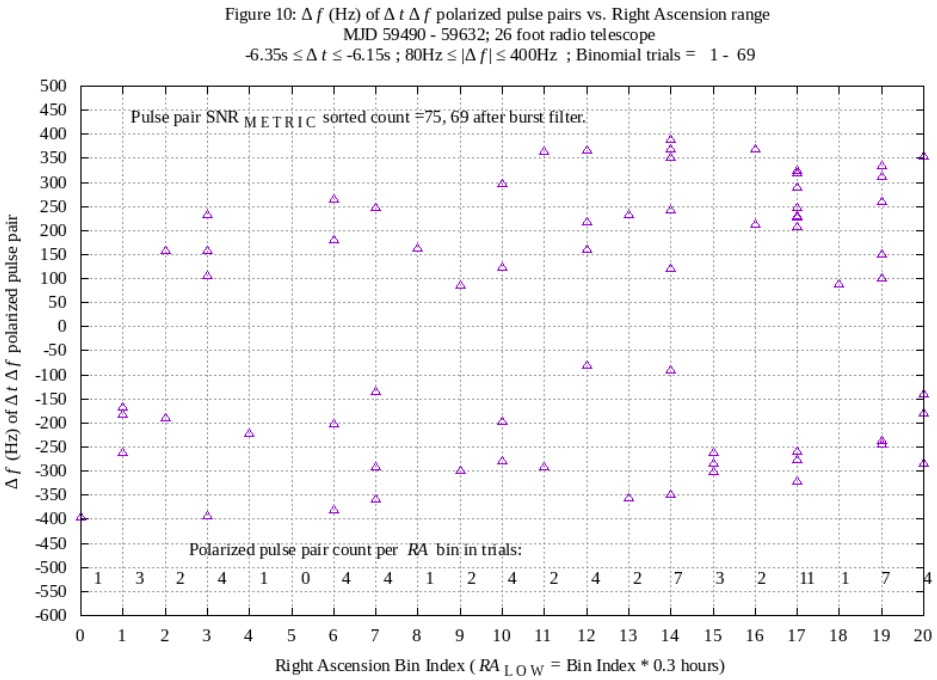

Figure 10: Eleven Δ*t* = - 6.25 s polarized pulse pairs observed in the 5.1 – 5.4 hr *RA* region appear to have | Δ*f* | concentrated between 200 - 350 Hz, approximately half the hyperparameter filter range. This | Δ*f* | concentration may be estimated to occur with a probability of one in 2^{11} tries, multiplied by two, to account for two possible hyperparameter ranges. Three of the eleven Δ*f* values appear to repeat close in value.

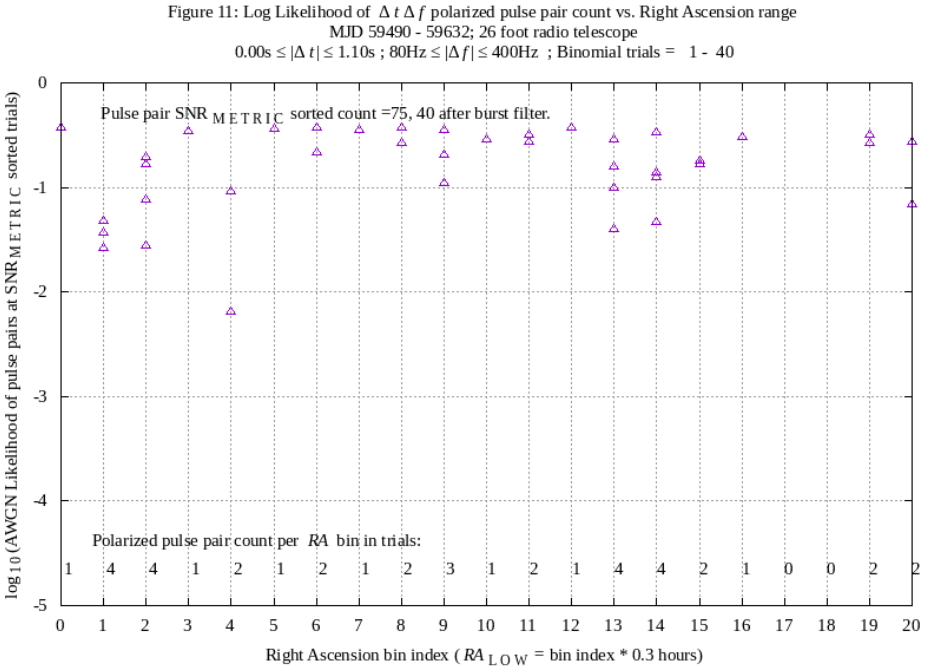

Figure 11: Assuming the Δ*t* = -3.75 s and Δ*t* = -6.25 s repetitions are explained by one or more unpolarized repetitive natural objects, pulse pairs would be expected to be observed in at least a few of the nine 0.25 s quantized Δ*t* values having | Δ*t* | ≤ 1.1 s, in *RA* bin 17. Such responses are absent in the measurement of the direction of interest, indicating that spectral power outliers, due to a natural source, are not near-simultaneously present in opposite circular polarizations.

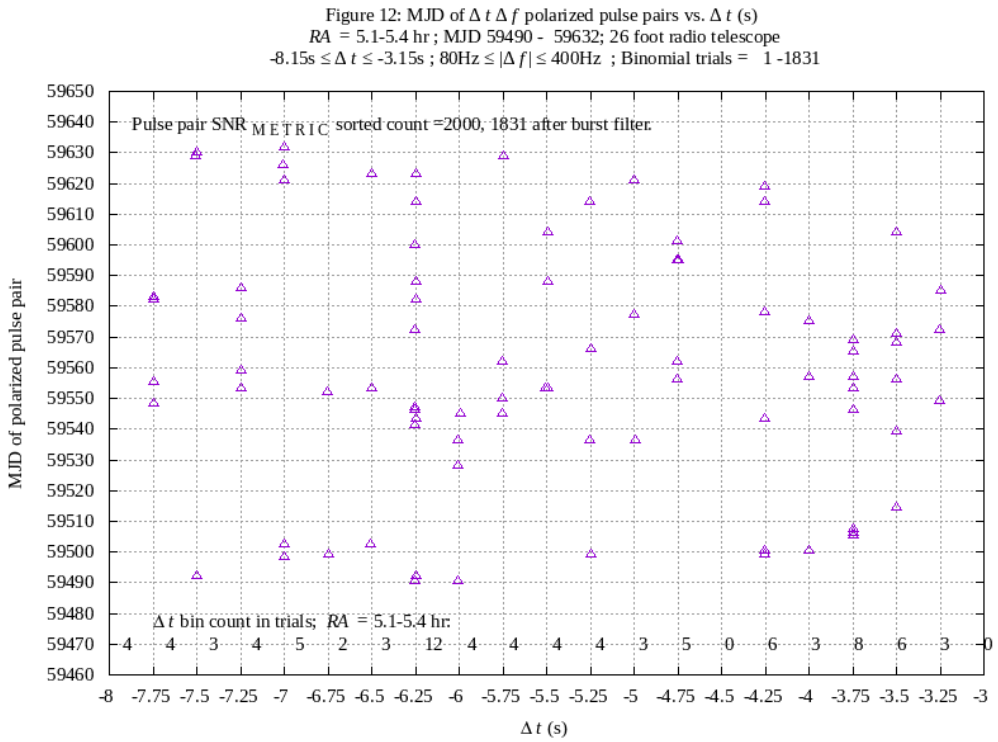

Figure 12: The Δ*t* = -3.75 s and Δ*t* = -6.25 s apparent symbol repetitions are concentrated in non-overlapping MJD groups, with one exception, at MJD 59546.2542303 and 59546.2540972, respectively, 11.25 s apart. The Δ*t* = -3.75 s pulse pair is one of the two pulse pairs having close RF frequencies, described in text in **Figure 5**.

V: Discussion

There are a number of issues that potentially confound the analysis of signals and anomalies identified in this work.

Anomaly identification potentially has observer bias

Some of the anomalies mentioned in this work have associated stochastic calculations, while others do not. Confirming the true nature of an anomaly requires one to consider many possible explanations, and combinations of explanations.

Population selection bias

The selection of Δ*t* candidate values, based on concentration of Δ*t* data, leads to a concern of sample collection bias. For example, Δ*t* is quantized to 0.25 second steps, and the Δ*t* = - 3.75 s value is three quantized values outside the Δ*t* range used in the prior experiment [4]. Considering positive and negative possible values, a factor of six needs to be applied to measured likelihood values, calculated using a noise-cause model.

Leakage of RFI and burst filters

The RFI and natural object burst filters may be allowing anomalous responses to indicate. Measurement data and output files produced by these filters need to be examined in a systematic way to develop metrics that seek to refute this auxiliary hypothesis that might explain anomalies.

Natural objects require models

Repeating indications at values of Right Ascension implies a celestial source. A celestial hypothesis may be tested using simulations and measurements. This work is required before natural object likelihood can be quantified.

Geostationary satellite RFI

The radio telescope pointing direction is near the geostationary Clarke Belt. A satellite-common RFI cause seems unlikely to show *RA* concentration during 143 days, but might be present.

Human error and human-made machine errors

The benefit of all-machine processing raises the countervailing issue of human error made when writing source code, albeit the latter generally having better traceability and testability.

There are anomalies in this work that suggest a conjecture that the *RA* 5.1 - 5.4 hr pulse pairs might be caused by an intentional low duty cycle transmitter having up to a few hundred kHz of RF bandwidth, and a few tens of seconds of transmit duration, indicated by MJD, time and frequency range overlap of pulse pairs in observations shown in **Figures 5, 8 and 12,** and Green Bank and Haswell associated pulses reported in [3] Figures 7, 12 and 13. The anomalous Δt = -6.25 s , $| \Delta f |$ concentration of pulse pairs shown in **Figure 10** is difficult to explain, due to noise or natural objects, and further leads to conjectures about hypothetical transmitter signal characteristics and receiver equipment causes.

VI: Conclusions

The AWGN model, augmented with extensive RFI amelioration, does not adequately explain the observed results. A large number of alternate and auxiliary hypotheses may be considered to potentially explain the anomalies seen in this experiment. Further work is required.

VII: Further Work

1. Further work described previously. [3][4]
2. Markov Chain analysis, using Monte Carlo methods [5].
3. The apparent non-ergodic properties of signals compels a need to create signal source models and processes that may be used to test various transmitter and natural object scenarios against observed results.
4. Continue radio telescope receiver captures at -7.6° DEC, and continue signal analysis.
5. Search additional signal dimensions for symbol repetition. Check various hyperparameter ranges.
6. Perform tests to verify equipment and software operation.
7. Help others seeking replication and corroboration.

VIII: Acknowledgements

Many people helped make this and previous work possible, and highly enjoyable. The author is grateful for the many contributions of workers of the Green Bank Observatory, Deep Space Exploration Society, Society of Amateur Radio Astronomers, SETI Institute, Berkeley SETI Research Center, Breakthrough Listen, product vendors, and open source software community. The author is grateful for guidance and encouragement from family and friends.

IX: References

[1] C. E. Shannon, W. Weaver, *The Mathematical Theory of Communication*, Urbana and Chicago, IL: University of Illinois Press, pp. 97–103, 1949

[2] D. G. Messerschmitt, *End-to-end interstellar communication system design for power efficiency*, arXiv 1305.4684v2, pp. 26–27, 70–74, 86–106, 201–223, 2018

[3] W. J. Crilly Jr, *An interstellar communication method: system design and observations*, arXiv: 2105.03727v1, May 8, 2021

[4] W. J. Crilly Jr, *Radio interference reduction in interstellar communications: methods and observations* 2106.10168v1, June 18, 2021

[5] A. Gelman, J. B. Carlin, H. S. Stern, D. B. Dunson, A. Vehtari, D. B. Rubin, *Bayesian Data Analysis*, Boca Raton, FL: CRC Press, p. 95, pp. 275-310, 201

Low Cost Radio Meteor Forward Scatter

Mike Otte

Radio Meteor detection is 1 of the 5 radio astronomy projects that amateur radio astronomers can explore and participate in. Meteors traditionally have been recorded in counts per hour. This comes from the visual observers who sit out in the cold and feed the mosquitoes. Radio meteor observers by contrast get to sit in their armchairs at their leisure and observe. They can contribute to the community by submitting their observations online. Examples of world wide observations can be seen at https://www.rmob.org/index.php and http://www.astrofiliabologna.it/graficocarmelo .

Forward scatter radio meteors occur when meteoroids burn up in the thermosphere and mesosphere about 60 to 100 km above the Earth. They create ionized clouds that reflect radio signals. This is passive radar where you use somebody else strong transmitter (TV carrier, FM station) and pick up the reflected wave with your receiving station. The strongest have been the TV video carrier at 55.250 Mhz but the US went to digital TV and even now the Canadians just shutdown my favorite on 55.240. I see a few people are using 54.309 mhz which is the digital pilot frequency but is is much weaker, < 2000 w EIP.

For many years I have been using 5 element yagi, Alinco DX70, and a Desktop PC for receiving radio meteors. In the PC I ran SpectrumLab for both detection and automatic counting. I ran Colorgramme software for submission to the www.rmob.org group. Last couple years, I have replaced the Alinco with a SDR receiver:

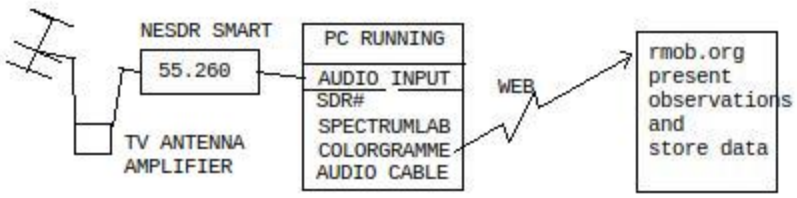

What do you hear and see? When a meteor creates a trail it causes the TV station to be temporarily heard as a "ping". Some pings are short. Some go up or down in frequency because of doppler shift. Some are long and wavy. On the screen you see the colored "blip" on the fft waterfall with the trail of colors. Sometimes you see meteor trails explode into making a paintbrush 'blip' that looks like many trails in many directions and intensities.

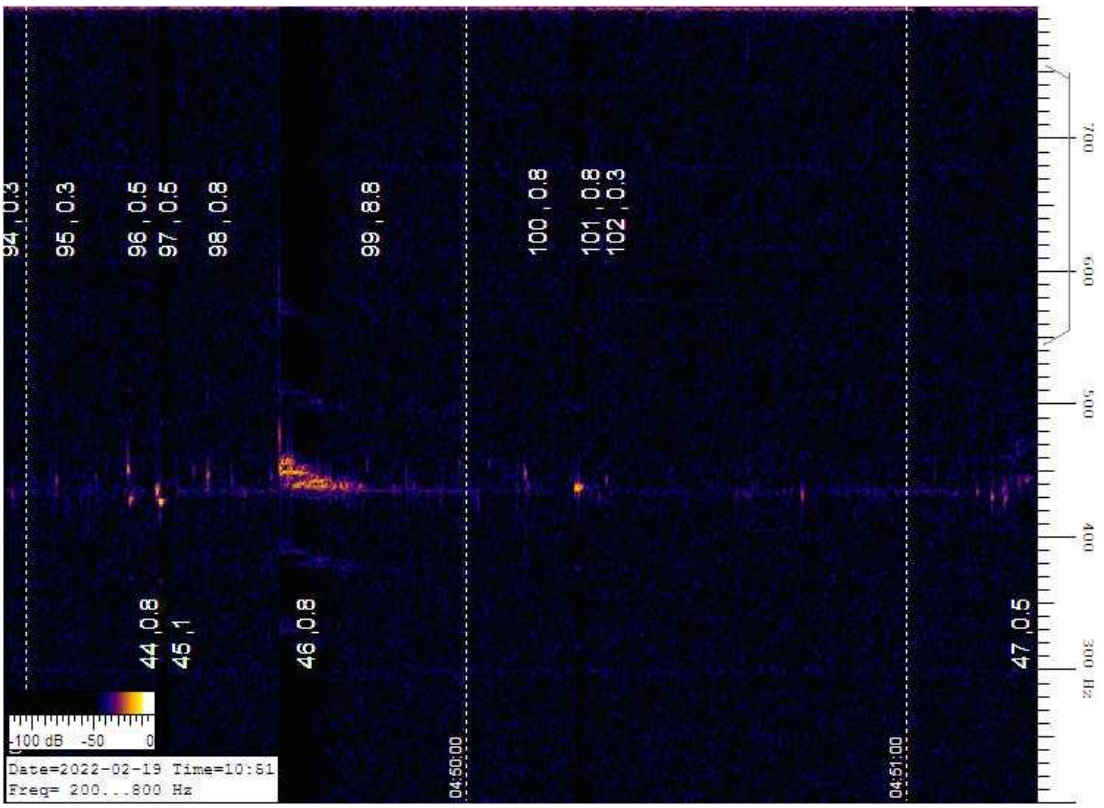

This setup runs 24/7/365 so it has electrical costs for running the receiver and PC. Power outage was always a problem. Getting the receiver to stabilize and keeping the programs running also was a problem. Also the Spectrum Lab took some "tuning" by adding the scripts and adjusting the triggers/ limits for automatic counting.

Now came along CARMELO (Cheap Amatorial Radio Meteor Echoes Logger) . This network is a recent startup using inexpensive equipment to record meteor echoes. Instead of detecting the signal and converting it to sound for examination by SpectrumLab or Argo, CARMELO measures the power and frequency of the echo and records that into a text file for examination and display later. It automatically sends the data to a server every 5 minutes.

The equipment list includes a NESDR Smart, Raspberry PI (3 or 4), an antenna, a LNA preamp, and a pre-programmed micro sd card that automatically runs the whole thing. No local displays but there is a LED card for "I am alive" . I am used to receivers having knobs and meters. But the displays are on a website. **http://www.astrofiliabologna.it/graficocarmelo** and **http://www.astrofiliabologna.it/graficocarmelohr** . This all runs on <15 watts instead of the >100 watts
of my original system.

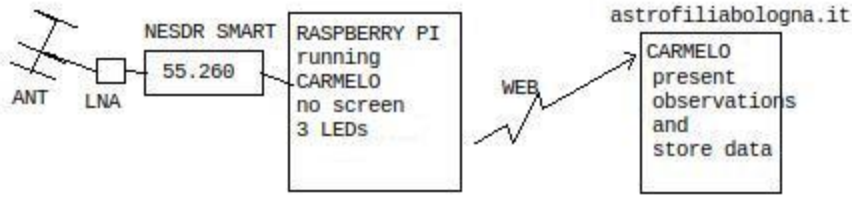

So each meteor is recorded with time and measurement data then displayed as a different symbol. The diurnal increase and decrease as the Earth rotates is easily seen. Groups, like what were were caused by strands of meteors and simultaneous detections between observers are apparent . Also the hourly counts are displayed as in traditional meteor counting.

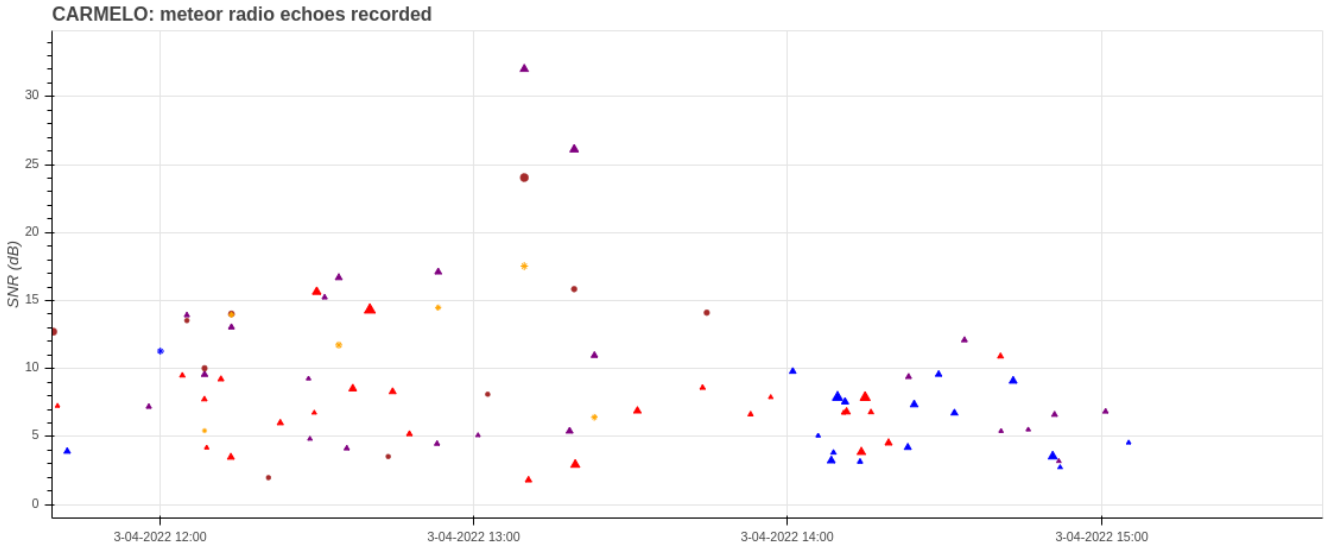

These are dynamic displays that can be “zoomed”. The symbols represent a meteor event and can be “hovered” over for more info or “clicked” to open this trend screen.

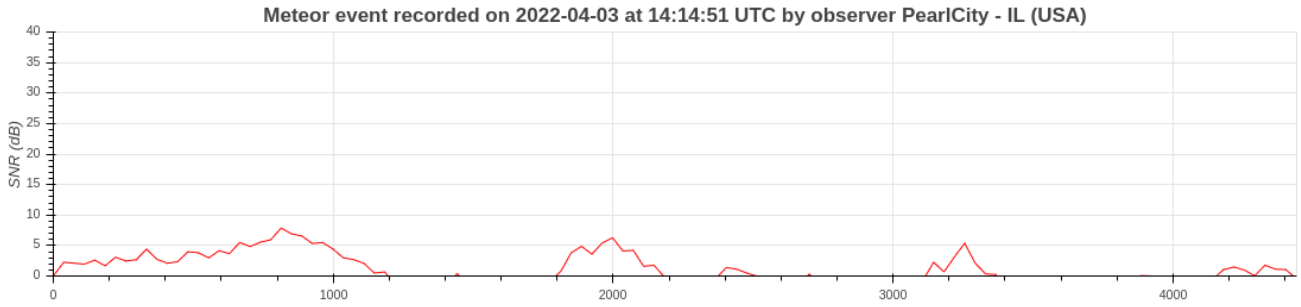

Ultimately the time and power data might permit one to compare simultaneous observations in order to calculate velocity or trajectory.

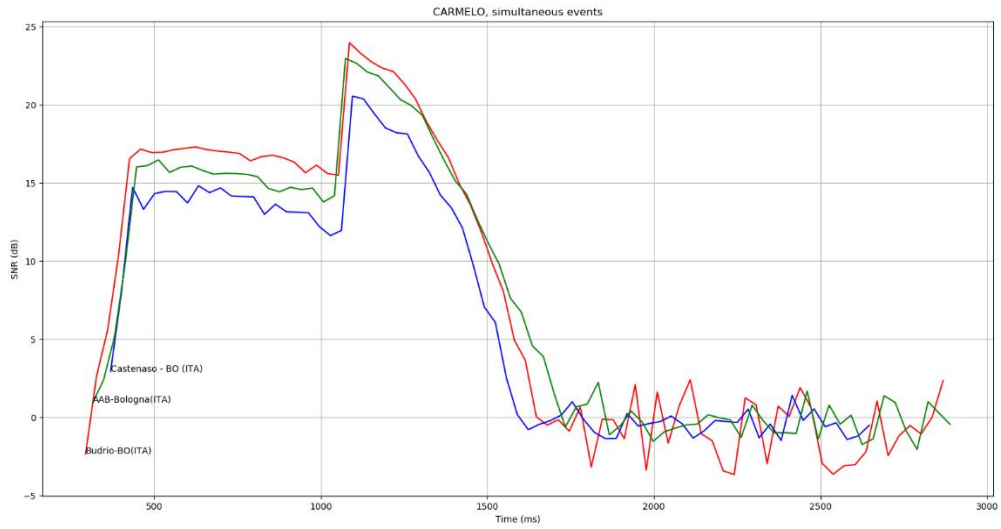

Some ground work has to be done first. Of course the antenna has to be built. A frequency has to be selected. Frequency selection is critical. Lower frequencies give better reflections. Stronger signals are generally better but you do not want direct path signals. Maybe a ham friend with a receiver or using the sdr to monitor some frequencies to see what is available to you, before incorporating it into this system. Finally, you'll need read the article on the CARMELO site on how to build your node.

Evaluating the Fast Folding Algorithm for Pulsar Detection

Dan Layne

Abstract

The Fast Folding Algorithm (FFA) is a phase-coherent search method to detect periodic signals from pulsars. It is not often used primarily because it is more computationally expensive than Fast Fourier Transform (FFT) methods, such as PRESTO. However, a recent FFA implementation called RIPTIDE makes efficient use of modern CPU cache architectures so that FFT methods no longer have a great speed advantage. In theory, the FFA method is more sensitive than FFT methods, including for longer period pulsars and lower Signal-to-Noise Ratio (SNR). This empirical study compares PRESTO with RIPTIDE on a small set of data to see if RIPTIDE can be an alternative to PRESTO for detecting known pulsars, especially at low SNR. The results show that PRESTO and RIPTIDE both give reliable results when SNR > 10. When SNR is between 4 and 10, both methods can produce acceptable results. PRESTO is inconclusive when SNR is below 4. However, RIPTIDE can produce acceptable results when SNR is 2.7. With more familiarity RIPTIDE could be an alternative method for detecting pulsars.

Introduction

Pulsars are rapidly rotating neutron stars that are identified by their emission of a periodic sequence of pulses. Pulsars have very stable periods, and can be used as celestial clocks. Periods for known pulsars range from a few milliseconds to a few seconds. Pulse intensities vary widely, due to scintillation from scattering in the ionized interstellar medium. Some pulse profiles are complex with several identifiable components, yet observations show that each pulsar's pulse profile is unique. The most common general shape for a pulse profile is the single Gaussian peak [1], while more complex pulse shapes can be modeled with multiple Gaussian components. A typical pulse sequence is shown in Figure 1.

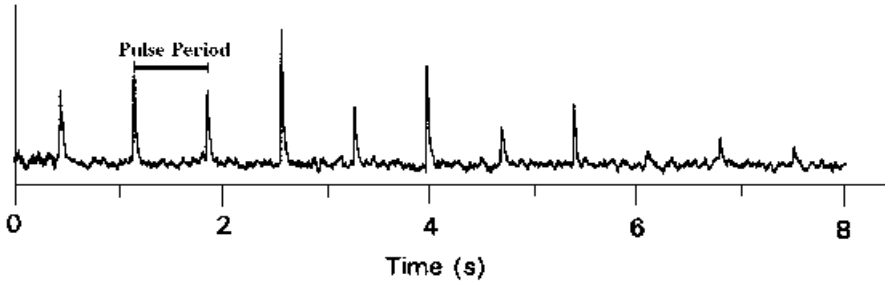

Figure 1: Pulse sequence from PSR B0329+54. Image credit: Manchester, R.N. and Taylor, J.H., Pulsars, Freeman, 1977

To confirm if a pulsar is detected, amateurs often make use of professional software packages. While professional tools are designed to search for unknown pulsars, amateurs can use the same tools to detect known pulsars by constraining the search parameters. Frequency domain methods, using the Fast Fourier Transform (FFT), are based on incoherent harmonic summing to integrate the pulse. The FFT method PRESTO [2], with TEMPO for timing, is used by some amateurs. However, the PRESTO statistical search methods were not designed to be optimal at low Signal-to-Noise Ratio (SNR) where amateurs tend to operate. Peter East [3] described modifications to PRESTO to improve detection at low SNR by using SNR measures instead of the reduced chi-square statistic for peak sensing.

In contrast, the Fast Folding Algorithm (FFA) [4] directly folds data in the time domain at a range of narrowly spaced trial periods. This is a phase-coherent search technique using a matched filter to find the best SNR, with a divide-and-conquer search scheme to reduce redundant calculations. Theoretically the FFA method is more sensitive than the FFT method, including at lower SNR. Although the FFA was proposed five decades ago it has not been widely

used, mainly because of its high computational cost. However, a recent implementation of the FFA, called RIPTIDE [5], makes efficient use of modern CPU cache architectures so FFT methods no longer have a great speed advantage. RIPTIDE potentially offers a simpler method for searching for unknown pulsars and for detecting known pulsars. At least when searching for new pulsars, the FFA offers better sensitivity than FFT spectral methods [6], especially for long-period (P > 2 s) pulsars [7].

The purpose of this paper is to evaluate the FFA method RIPTIDE by comparing it with the standard FFT method PRESTO when detecting known pulsars. Rather than a theoretical analysis, this evaluation is based on a small set of observational data. The motivation for this study is to see if RIPTIDE is a viable alternative to PRESTO for detecting and reporting known pulsars, especially at low SNR. This paper is organized as follows: the next section briefly reviews pulsar detection methods and SNR. Then the data collection and system configuration is described. The approach for the evaluation is then presented followed by results and conclusions.

Pulsar Detection and Signal-to-Noise Ratio

A fundamental procedure for detecting known pulsars is the synchronous averaging (folding) of the data at the pulse period. Since most pulsars are very weak radio sources, folding many (hundreds or thousands) of pulses enables the signal to become visible above the background noise. Prior to folding, the data must be dedispersed. Pulse dispersion in the interstellar medium causes higher frequencies to be detected slightly earlier than lower frequencies, thus smearing the pulse across the phase. Dedispersion corrects this smearing. The Dispersion Measure (DM) is proportional to the density of electrons along the line of sight, and DM is an indicator of the distance to the pulsar. After dedispersion and folding, the resulting integrated pulse profile represents the average emission from the neutron star as a function of its rotational phase. RIPTIDE performs folding (and matched filtering for peak detection) in the time domain.

The signal-to-noise ratio is an estimate of the signal amplitude relative to the standard deviation of the background noise. For reliable results, a general rule-of-thumb is SNR > 10. However, depending on pulsar scintillation, collection sampling rate and other factors, acceptable results can be obtained with SNR around 4:1, or sometimes lower. Note that SNR is estimated differently in the frequency domain than in the time domain, and their values will not be directly compared here (although they both follow the same trends). The PRESTO SNR is based on the frequency spectrum. This is the usual pulsar signal-to-noise ratio as defined by equation 7.1 in Lorimer and Kramer [7]. Here we use the PRESTO SNR linear measure as the primary SNR. On the other hand, the RIPTIDE SNR is based on the profile, and it will be denoted SNR_{TIME}. During RIPTIDE searches, the highest SNR_{TIME} is a function of both the trial period and the width. The majority of pulse shapes are approximately Gaussian [5], and RIPTIDE uses boxcar (top-hat) filters to search for peaks. Boxcar matched filters are computationally efficient techniques for finding Gaussian shapes.

Data Collection and System Configuration

The pulsar data used in this study was collected between August, 2020 and March, 2022 using the 60 ft (18.3 m) parabolic dish at the Plishner Radio Astronomy facility near Haswell, CO (Figure 2). This facility is maintained by the Deep Space Exploration Society (DSES). Three different feed horns were installed during this time: 408 MHz, 1296 MHz, and 1420 MHz. Data collected in 2020 used the USRP N210 receiver, while data from 2021-2022 used the USRP B210 receiver. GnuRadio 3.8 was used to record the data in filterbank file format, using a derivative of Marcus Leech's pulsar filterbank software [8]. PRESTO 4.0 running on Ubuntu 20.04 was used for pulsar detection. Stellarium and Murmur (I0NAA) are used to plan observations.

Figure 2: Deep Space Exploration Society 60 ft dish

RIPTIDE is a Python and C++ package. Version 0.2.4 [9] was installed on an 8-core laptop and a 16-core desktop, both running Ubuntu 20.04. While PRESTO is a large suite of mature tools, RIPTIDE is a smaller package under current development. PRESTO performs both dedispersion and folding, while RIPTIDE only performs folding. That is, RIPTIDE requires input time series data to be dedispersed, in either PRESTO format or SIGPROC format. This is because RIPTIDE is designed for professional labs where dedispersed time series files are readily available in the processing pipeline. Here both dedispersion methods were used in the folding evaluation. The SIGPROC dedispersion utility does not require TEMPO. For Windows 10/11 users, RIPTIDE installs via "pip install." However, compiling SIGPROC requires Gnu Autotools, which may require Windows Subsystem for Linux. Both PRESTO and SIGPROC are freely available and well tested.

Evaluation Methodology

The approach is illustrated in Figure 3. The first step records the data using the system configuration described above. The second step performs dedispersion on the filterbank file, using the published value for DM. The SIGPROC dedisperse utility generates the dedispersed time series data for RIPTIDE on the left path. In the middle path, PRESTO prepdata generates dedispersed time series for RIPTIDE. Folding occurs in the third step, using the rffa script for RIPTIDE. The DM search is disabled by using a single time series, with a narrow search range for the known period. PRESTO prepfold combines steps 2 and 3, performing both dedispersion and folding on the raw filterbank file. All times are reported in topocentric coordinates. In the last step the results are evaluated by comparing phase plots, pulse profiles and numerical results, including SNR.

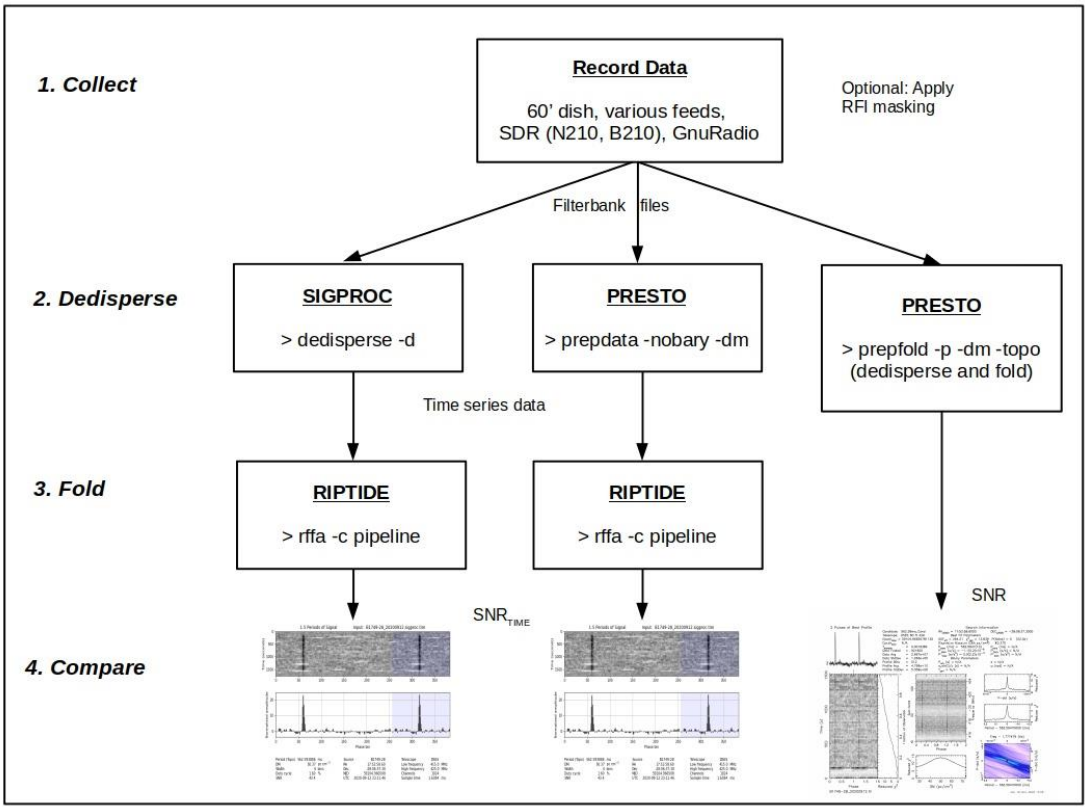

Figure 3: Evaluation Methodology

The radio telescope is in a remote location, so masking for Radio Frequency Interference (RFI) is generally not needed. However, even with masking, low-level harmonic RFI can be present, which can appear as false peaks in the time series data. RIPTIDE subtracts a running median filter from the input data to reduce low-frequency noise.

Results

A total of fifteen experiments were run on 10 different pulsars. Each experiment included three tests: RIPTIDE folding with SIGPROC dedispersion, RIPTIDE folding with PRESTO dedispersion, and PRESTO folding. One goal was to evaluate the algorithms at low SNR, so four B0329+54 experiments are based on the same baseline filterbank file (collected at 10 MHz bandwidth). Three of these B0329+54 files were successively shortened in time to effectively reduce SNR. The results for the first 5 tests are summarized in Table 1 and shown in this section. The remaining 10 tests are summarized in Table 2 in the Appendix. Both tables have the same structure, listing the source pulsar and UTC value (file identifier). The values for DM, period, W50, and flux are from ATNF. The duty cycle (DUCY) is W50/Period. The frequency and time columns are collection parameters, followed by RIPTIDE SNR_{TIME} from PRESTO, RIPTIDE SNR_{TIME} from SIGPROC, and the basic PRESTO SNR, which is used as the comparison SNR. The last column references the figure number below.

A	B	C	D	E	F	G	H	I	J	K	L	M	N
	Data Sheet for B2020+28 and 4 Samples of B0329+54												
#	Source	UTC / File ID	DM	Period sec	W50 ms	DUCY %	S1400 mJy	Frequency MHz	Time mins	SNR-TIME PRESTO	SNR-TIME SIGPROC	SNR PRESTO	Figure #
1	B2020+28	20220304_191940	24.63	0.343402	12.00	3.49	38.0	1285 – 1315	180	16.7	16.3	4.8	4
2	B0329+54	20220304_181641_tr1	26.76	0.71452	6.60	0.92	203.0	1286 – 1296	10	36.6	35.4	10.8	5
3	B0329+54	20220304_181641_tr2	26.76	0.71452	6.60	0.92	203.0	1286 – 1296	3.6	19.9	20.0	4.5	6
4	B0329+54	20220304_181641_tr3	26.76	0.71452	6.60	0.92	203.0	1286 – 1296	2.5	18.4	18.2	2.7	7
5	B0329+54	20220304_181641_tr4	26.76	0.71452	6.60	0.92	203.0	1286 – 1296	1	11.4	11.2	2.5	8

Table 1: Pulsar Data Sheet

B2020+28

The results for B2020+28 are shown below in Figure 4 from data collected on March 4, 2022. The RIPTIDE plot is on the left, with the standard PRESTO prepfold plot on the right. Although RIPTIDE generates separate output plots for the two dedispersion methods, only one is shown in each case below because the two RIPTIDE outputs are nearly identical in appearance for the phase plot and pulse profile. The SNR_{TIME} values differ slightly, as seen in columns K and L of Table 1, due to differences in how dedispersion is implemented in SIGPROC and PRESTO.

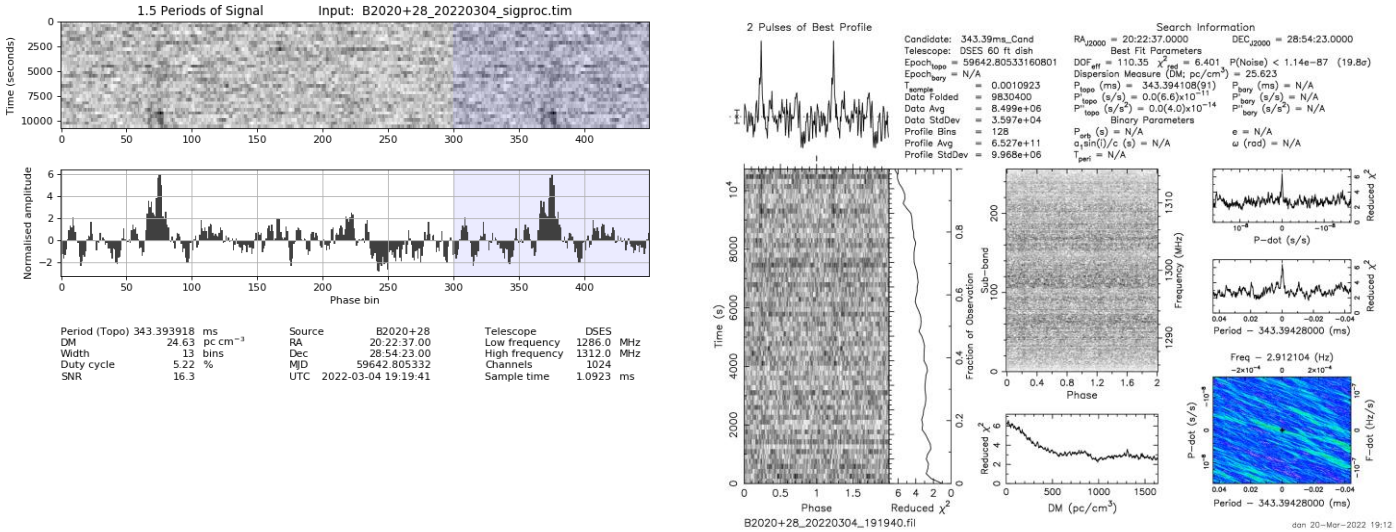

Figure 4: B2020+28 20220304_191940 SNR = 4.8

On the right in Figure 4, the PRESTO plot, at SNR = 4.8, appears acceptable. The pulse trace is discernible in both the phase-time plot and the phase-frequency plot. The pulse profile is reasonable for this SNR level, and the p and p-dot plots look good. The values for DM and topocentric period appear correct.

On the left in Figure 4, the RIPTIDE plot for SIGPROC dedispersion also appears acceptable. RIPTIDE plots 1.5 periods of signal for both the phase and profile for peaks with the highest SNR_{TIME} (PRESTO plots 2 phase periods on a shorter scale). Time goes down on the RIPTIDE phase plot, while time goes up on the PRESTO phase-time

plot. Notice that the phase plot signal appears strong only towards the end of the the 3 hour data collection (at the top of PRESTO phase plot and at the bottom of RIPTIDE phase plot). RIPTIDE reports approximately the same (to 5 digits) topocentric period as PRESTO, and the pulse width is in bins. At first glance it appears the RIPTIDE pulse profile is too wide, with two peaks. But B2020+28 is mode-changing with a double peak, which can barely be discerned in the PRESTO profile. This illustrates that the RIPTIDE boxcar (top-hat) matched filter discerned the double peak.

Timing performance is reported for B2020+28, since it was the longest test (180 minutes at 30 MHz bandwidth). Running on a 4.9 GHz CPU, dedispersion (which is not being evaluated here) took 31 seconds for PRESTO and 80 seconds for SIGPROC. The raw filterbank file is 20.25 GB, with the dedispersed time series files ~40 MB each. Folding required 6 seconds for PRESTO and 12 seconds for RIPTIDE. So time series folding is comparable in performance, and certainly adequate for amateurs.

B0329+54 Sequence

The next series of 4 figures shows the SNR sequence on B0329+54. Figure 5 shows results for B0329+54 20220304_181641. This baseline is 600 seconds at 10 MHz bandwidth, with SNR = 10.8. Again, PRESTO on the right, RIPTIDE on the left. The plots are acceptable in both cases. Some harmonic noise appears near the folding period.

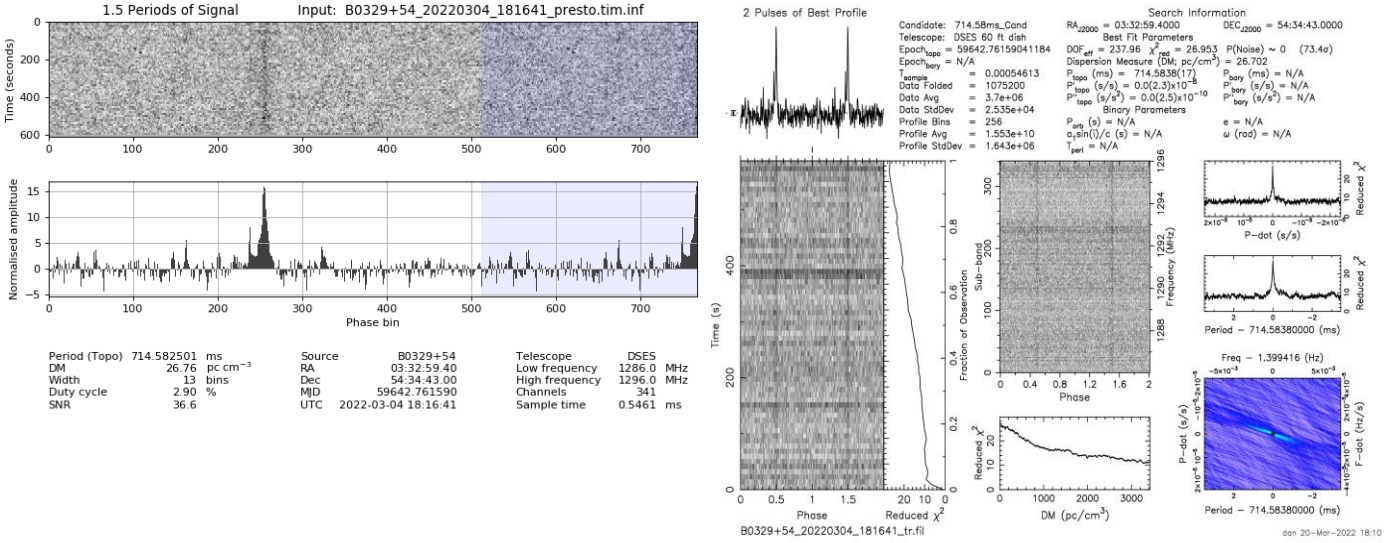

Figure 5: B0329+54 20220304_181641_tr1 SNR = 10.8

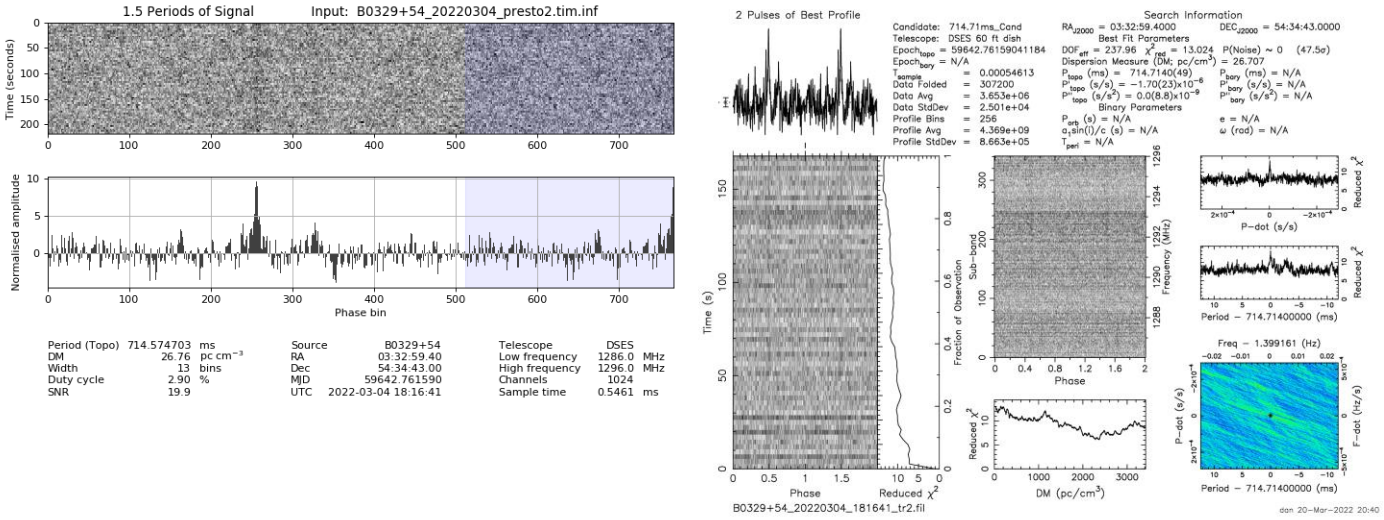

Figure 6: B0329+54 20220304_181641_tr2 SNR = 4.5

Continuing the B0329+54 sequence, Figure 6 above shows the same file reduced to 220 seconds, resulting in SNR = 4.5. In this case the PRESTO plot is marginal, but still acceptable, while the RIPTIDE still shows discernible phase and good profile, albeit with a smaller SNR_{TIME}.

Figure 7 below shows the baseline file trimmed to 150 seconds (PRESTO doesn't always plot the whole collection time in the phase-time plot). Here SNR = 2.7. The PRESTO plot is inconclusive, while the RIPTIDE plot still indicates a pulse at the correct period, again at smaller SNR_{TIME}. In this case, RIPTIDE provides evidence of a pulsar while PRESTO does not.

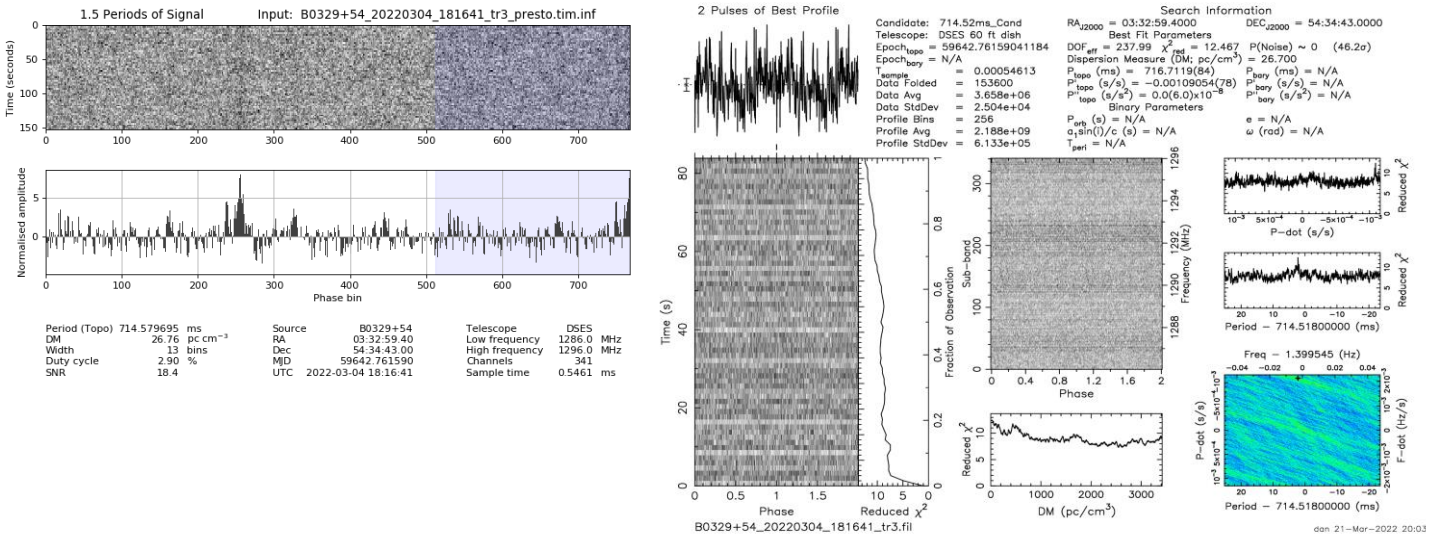

Figure 7: B0329+54 20220304_181641_tr3 SNR = 2.7

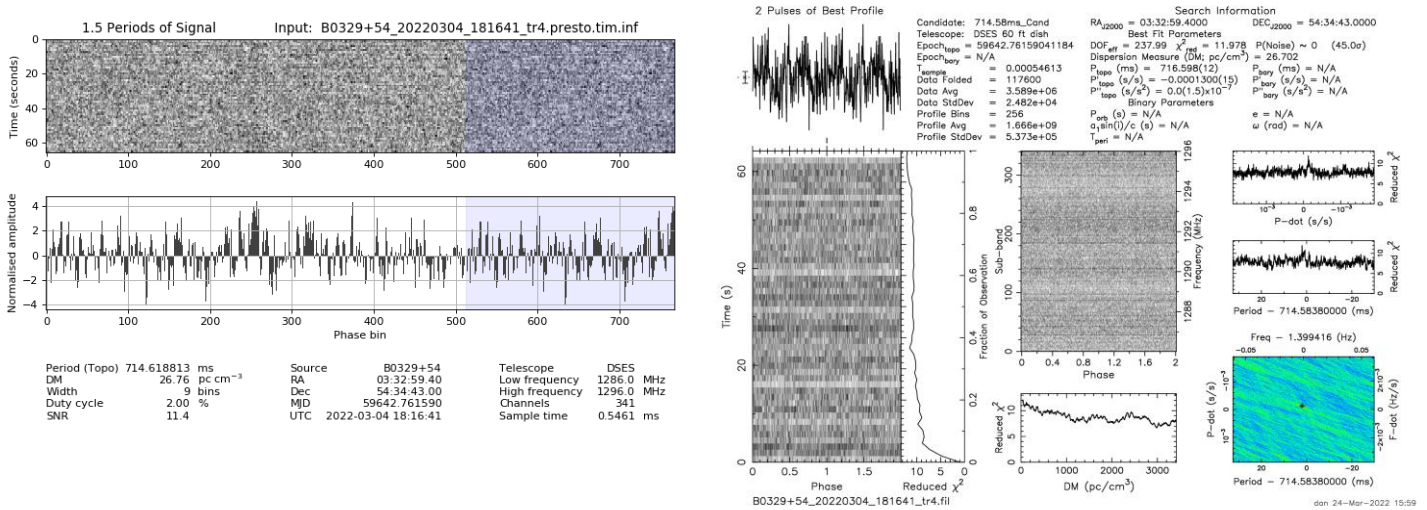

Figure 8: B0329+54 20220304_181641_tr4 SNR = 2.5

Figure 8 above shows the final test in this B0329+54 sequence, with the baseline trimmed to 60 seconds for SNR = 2.5. In this case neither PRESTO nor RIPTIDE provide sufficient evidence of the presence of a pulsar.

The results in the Appendix show the same pattern at low SNR where RIPTIDE can sometimes produce conclusive results when PRESTO fails. This is not criticizing PRESTO, as it was not designed for the low SNR pulsar detection that amateurs often deal with. In all cases when PRESTO failed, several iterations were attempted to achieve results.

Conclusions

The goal of this study was to use observational data to evaluate the time domain folding method RIPTIDE by comparing it with the FFT method PRESTO. Of particular interest is how both methods perform when SNR < 10. RIPTIDE is a modern implementation of the Fast Folding Algorithm and is easier to install, learn and modify than PRESTO. With its python interface RIPTIDE may be executed interactively in a notebook environment, or via scripts that enable a pipeline process. RIPTIDE was recently developed, and enhanced versions may be released in the future. This version of RIPTIDE may miss a few pulsars that have complicated pulse shapes that are not readily modeled by Gaussian curves, which is assumed by the matched filter (boxcar). RIPTIDE distinguished the double-peaked B2020+28 in this study. A potential drawback for Windows users is that RIPTIDE requires an external dedispersion tool, such as PRESTO or SIGPROC, which are easier to build on linux.

For the small data set in this study, RIPTIDE performed better at lower SNR, indicating the presence of pulsars when PRESTO was inconclusive.

PRESTO results:

- Reliable for SNR > 10
- Generally acceptable for 4 < SNR < 10
- Inconclusive for SNR < 4

RIPTIDE results:

- Reliable for SNR > 10
- Generally acceptable for 4 < SNR < 10
- Sometimes acceptable for 2.7 < SNR < 4
- Inconclusive for SNR < 2.7

For consistency, the same PRESTO SNR measure is used when comparing the two algorithms. For RIPTIDE the user specifies the number of search candidates within the defined period range. The highest SNR_{TIME} peak is not always the correct period, depending on noise. So all candidates should be examined for the best peak at the correct folding period. Execution times on a modern CPU for either method are adequate for amateur use, with the longest RIPTIDE run-time of 12 seconds (B2020+28) in this study. The results from this study indicate that RIPTIDE at least compliments PRESTO for detecting and reporting pulsars. With more familiarity, RIPTIDE could be an acceptable method, especially at low SNR. We plan tests with a 3.8 m dish later this year.

Acknowledgments

The author appreciates the assistance of Dr. Richard Russel and Ray Uberecken, who collected the 2020 data. The author also appreciates the whole DSES team, who make observations with the 60’ dish possible.

References

[1] ATNF. https://www.atnf.csiro.au/outreach/education/pulseatparkes/pulsar_properties.html
[2] PRESTO Home. https://github.com/scottransom/presto
[3] PW East. Getting the Best out of PRESTO - Part 3: Waterfalls and Conclusions., Journal of the Society of Amateur Radio Astronomers. July-August 2021.
[4] DH Staelin. Fast Folding Algorithm for Detection of Periodic Pulse Trains, Proceedings of the IEEE, P 724, April 1969.
[5] V Morello, et al. Optimal periodicity searching: Revisiting the Fast Folding Algorithm for large-scale pulsar surveys. arXiv:2004.03701v2 [astro-ph.IM], 3 Aug 2020.
[6] PW East. Speeding Up Search Folding for Amateur Pulsar Hunters., Journal of the Society of Amateur Radio Astronomers. September-October 2021.

[7] D Lorimer and M Kramer. Handbook of Pulsar Astronomy. Cambridge University Press. 2005.
[8] CCERA filterbank software. https://github.com/ccera-astro/pulsar_filterbank
[9] RIPTIDE home. https://github.com/v-morello/riptide
[10] SIGPROC home. https://github.com/SixByNine/sigproc

Appendix

Table 2 below, following the same format as Table 1, summarizes 10 additional experiments. The first 5 produced acceptable results for RIPTIDE, with 4 of the 5 acceptable for PRESTO. The case of inconclusive PRESTO results had SNR = 2.8. The plots are shown below. The final five pulsars all failed for both algorithms, so no plots are shown. When RIPTIDE fails it either generates bad plots with noise peaks at incorrect periods, or it generates no peaks at all. These failed tests had SNR between 1.9 and 3.5.

A	B	C	D	E	F	G	H	I	J	K	L	M	N	O
	Appendix SNR Data Sheet													
#	**Source**	**UTC / File ID**	**DM**	**Period sec**	**W50 ms**	**DUCY %**	**S400 mJy**	**S1400 mJy**	**Bandwidth MHz**	**Time mins**	**SNR-TIME PRESTO**	**SNR-TIME SIGPROC**	**SNR PRESTO**	**Figure #**
1	B0329+54	20200905_212432	26.76	0.71452	6.60	0.92	1500.0	203.0	415 – 425	5	25.1	24.2	11.0	9
2	B0329+54	20220304_230507	26.76	0.71452	6.60	0.92	1500.0	203.0	1286 -1296	10	11.3	11.0	2.8	10
3	B1641-45	20210808_015721	478.66	0.455078	8.00	1.76	375.0	300.0	1400 – 1440	30	62.2	57.0	41.5	11
4	B1749-28	20200912_231146	50.37	0.562558	6.10	1.08	1100.0	47.8	415 – 425	30	49.4	43.4	27.4	12
5	B2021+51	20210918_212315	22.55	0.529197	7.40	1.40	77.0	27.0	1392 – 1448	15	35.3	33.6	18.6	13
	Both algorithms fail													
1	B0355+54	20210807_232515	57.14	0.156384	3.90	2.49	46.0	23.0	1400 – 1440	60	no peaks	no peaks	2.0	
2	B0531+21	20200704_163202	56.77	0.033392	3.00	8.98	550.0	14.0	412 – 422	60	no peaks	no peaks	1.9	
3	B0736-40	20210808_145301	160.90	0.374921	22.70	6.05	190.0	112.6	1400 – 1440	30	bad plots	bad plots	2.1	
4	B2154+40	20220227_210642	71.12	1.525266	38.60	2.53	105.0	17.0	1285 – 1315	90	no peaks	no peaks	3.5	
5	J0437-4715	20210808_140611	2.64	0.005757	0.14	2.45	550.0	150.2	1400 – 1440	30	bad plots	bad plots	2.8	

Table 2: Appendix Pulsar Data Sheet

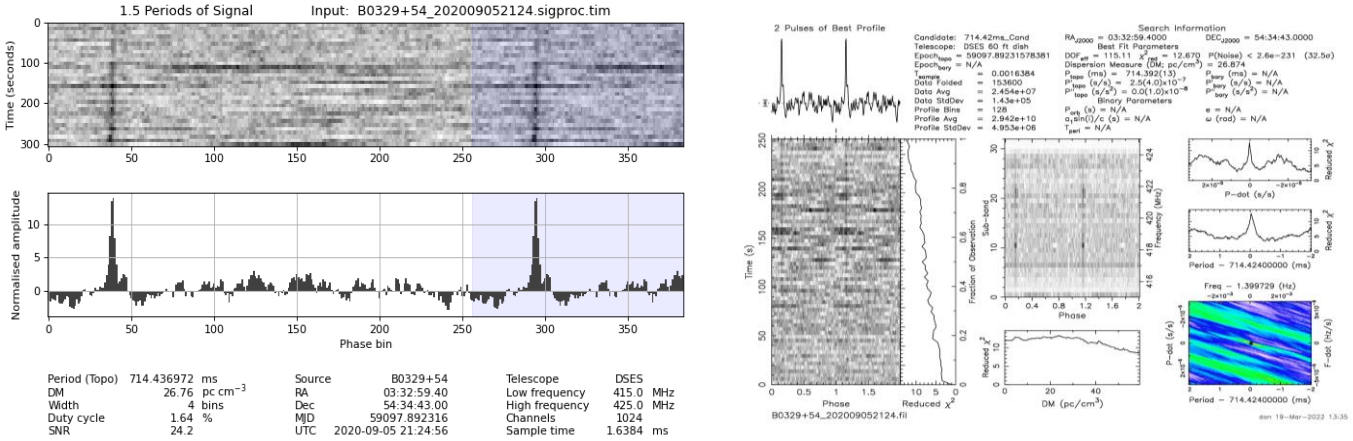

Figure 9: B0329+54 20200905_212432 SNR = 11.0

Figure **Error! Reference source not found.** above shows results for B0329+54 20200905_212432, a 5 minute c ollection at 420 MHz with SNR of 11.0. RIPTIDE plots are on the left, and PRESTO on the right. Both show good phase plots and profiles. In this case, noise visible in the PRESTO phase-time plot is also visible in the RIPTIDE phase-time plot.

Figure 10 below shows results for B0329+54 220304_230507, a 600 second, 10 MHz at 1296 MHz with SNR = 2.8. PRESTO offered hints of a detection, but nothing conclusive. In this case RIPTIDE generated a good peak in the profile above the surrounding noise at the correct period. Although it is faint, the corresponding trace can be seen in the phase plot. Although marginal, the RIPTIDE results do indicate a pulsar was detected.

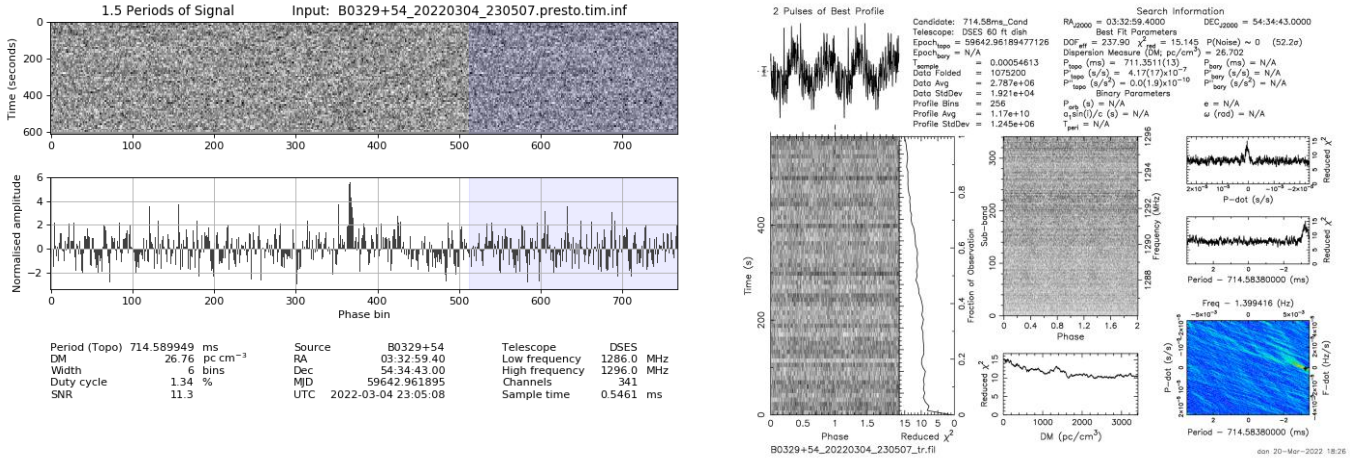

Figure 10: B0329+54 20220304_230507 SNR = 2.8

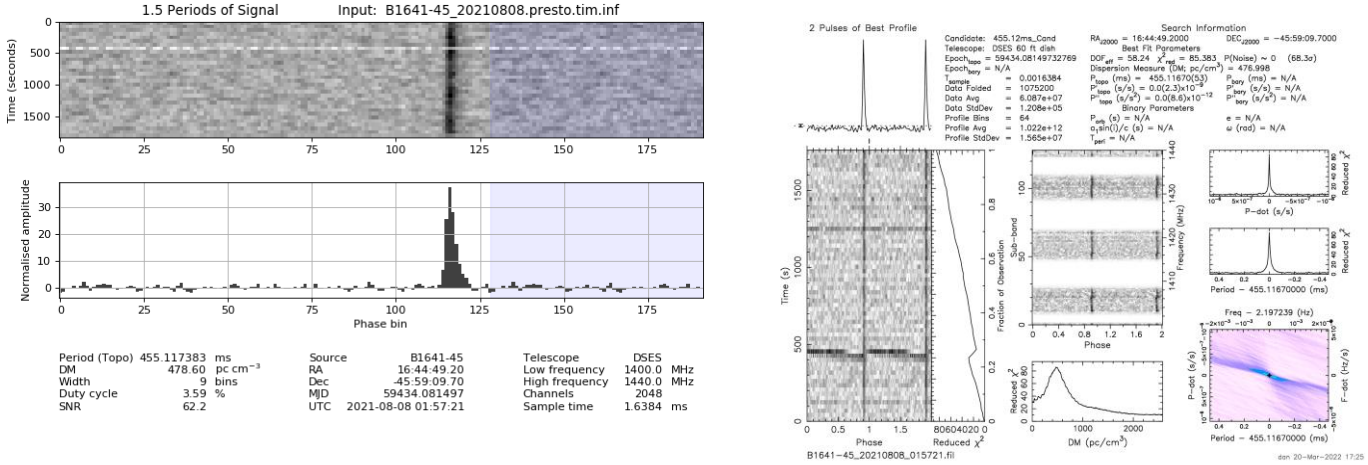

Figure 11: B1641-45 20210808_015721 SNR = 41.5

Figure *11* above shows results for B1641-45, the brightest and furtherest pulsar in this study. It was a 30 minute collection of 40 MHz bandwidth at 1420 MHz, with SNR = 41.5. Both algorithms did quite well. The noise at ~450 seconds is visible on both phase plots.

Figure *12* shows results for B1749-28 20200912_231146, a 30 minute, 10 MHz collection centered at 420 MHz, with SNR = 27.4. As in the previous case, both algorithm did well. Also, due to noise, both phase plots show missing phase data at the beginning and end of the collection.

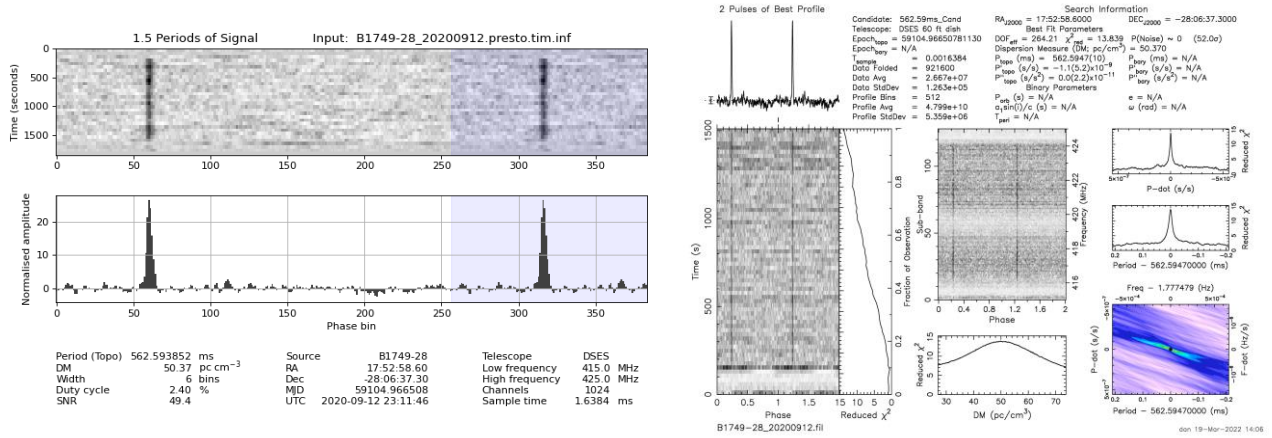

Figure 12: B1749-28 00912_231146 SNR = 27.4

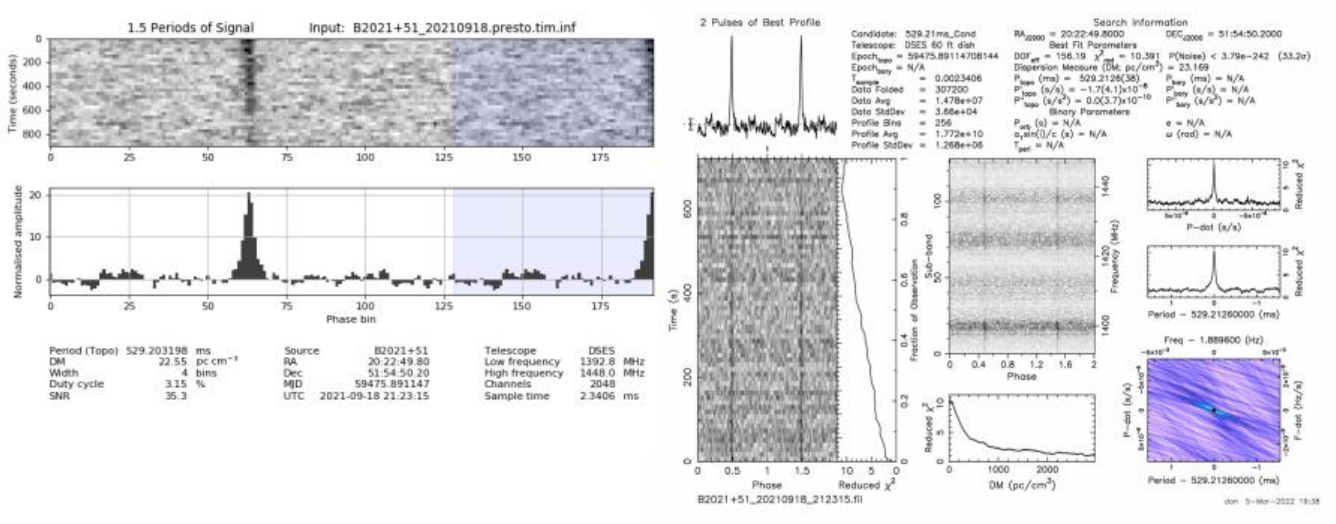

Figure 13 B2021+51 20210918_212315 SNR = 18.6

Figure 13 shows results for B2021+51 20210918_212315. a 15 minute, 56 MHz collection centered at 1420 MHz, with SNR = 18.6. Both algorithms performed well.

Biography

Dan Layne, AD0CY@arrl.net, is retired from the aerospace industry, having worked in software engineering, systems engineering and data sciences. He has an M.S. degree in Mathematics from Colorado State University. As a ham radio operator (AD0CY) Dan studies weak signal propagation. He has had a lifelong interest in exploring celestial mysteries and is active in amateur detection of pulsars and hydrogen. Dan joined DSES and SARA in 2020.

Detailed Evaluation of Low SNR Pulsar Data Records

Peter East

Abstract

Amateur detection of weak, low signal-to-noise ratio (SNR) pulsars with small aperture systems demands long observation times, implying extremely large data files. As a consequence, the processes necessary to prove pulsar recognition working on these large files can take a considerable time. This article offers some data processing techniques that significantly reduce the operating file sizes without losing valuable information. The result is much faster processing, tens of seconds rather than hours, allowing extraction of more and improved pulsar recognition detail than required by the usual professional validation measures [1,2]. In this paper, the methods of analyzing pulsar properties to complete validation will be described from real data collected on pulsar B0329 by a small aperture system, through to the software working on full data analysis.

Introduction

Of the various approaches to pulsar detection and recognition, a number of amateur pulsar enthusiasts are using Andrea and Giorgio Dell'Immagine's Linux software for data collection by the RTL, Airspy or Hack-RF SDRs and subsequent processing with PRESTO professional pulsar software [3].

Marcus Leech has produced his 'Stupid Simple Pulsar' software running in the GNU Radio environment for data acquisition by a wide range of SDRs; again outputting data in filterbank file format for analysis by PRESTO [4].

For the RTL SDR, Michiel Klassen has developed his 3pt tools which together with his Python GUI allows the data to be examined and presents a nice plot from which pulsar B0329 can be recognized [5].

This article describes another alternative to PRESTO, enabling improved examination of weak low SNR pulsar acquisitions. The technique involves a cut-down version of Marcus Leech's GNU Radio software for data collection followed by bespoke software for compressing and analyzing very long data recordings without losing any pulsar information. This is so that many post-processing folding algorithms can be applied to rapidly explore in detail, various pulsar recognition aspects.

The software initially implements the data compression process to speed post processing together with pulse bandwidth matched-filtering to improve the data time resolution. All pulsar validation processing is based on the standard folding algorithm. Two adaptations of conventional folding are implemented to add credence to pulsar detection by tracking pulsar pulse scintillation along the data record and these involve the techniques of cumulative and rolling-average folding. The output is 21 text files in under half a minute containing folded results that can quickly be plotted to demonstrate data conformance to known pulsar signal properties.

The article leads by describing the observation hardware for pulsar B0329+54 used to collect the data later used for software testing. The data compression and matched-filtering processes are then justified before explaining how this data is conditioned and used to produce the validation results.

The Appendix contains a summary of the pulsar analysis files plotted in MathCad.

The Hardware

The receiver system uses a pair of 2.5m Yagis (Figure 1a), tuned to the 611 MHz radio astronomy band, directly feeding a matched pair of 0.4 dB Mini-Circuits amplifiers and combined in a 3 dB in-phase splitter plus a 608 MHz to 614 MHz in-line filter box from JJ Antenna Components.

A 6 m low-loss cable feeds a receiver panel (Figure 1b) with two more low-noise amplifiers split by a second in-line filter driving a 10 MHz RF bandwidth Airspy SDR, frequency locked by a GPS disciplined oscillator (www.sdr-kits.net). The system housing comprises a large aluminium box containing a transformer fed analog power supply stabilized by a 12 volt sealed rechargeable battery, the receiver panel and a laptop PC controlling data acquisition. The box lid is closed during data recording for RFI screening .

Figure 1. a) Antenna LNAs and Combiner. **b)** Receiver Panel. **c)** System Housing and Data Collection PC.

Data Collection and Pre-Processing

Data collection is by a laptop PC using a cut-down version of Marcus Leech's 'stupid_simple_pulsar' GNU Radio software [4]. A distinct advantage of choosing GNU Radio for radio astronomy is its support for most modern SDRs - in this case the Airspy R2.

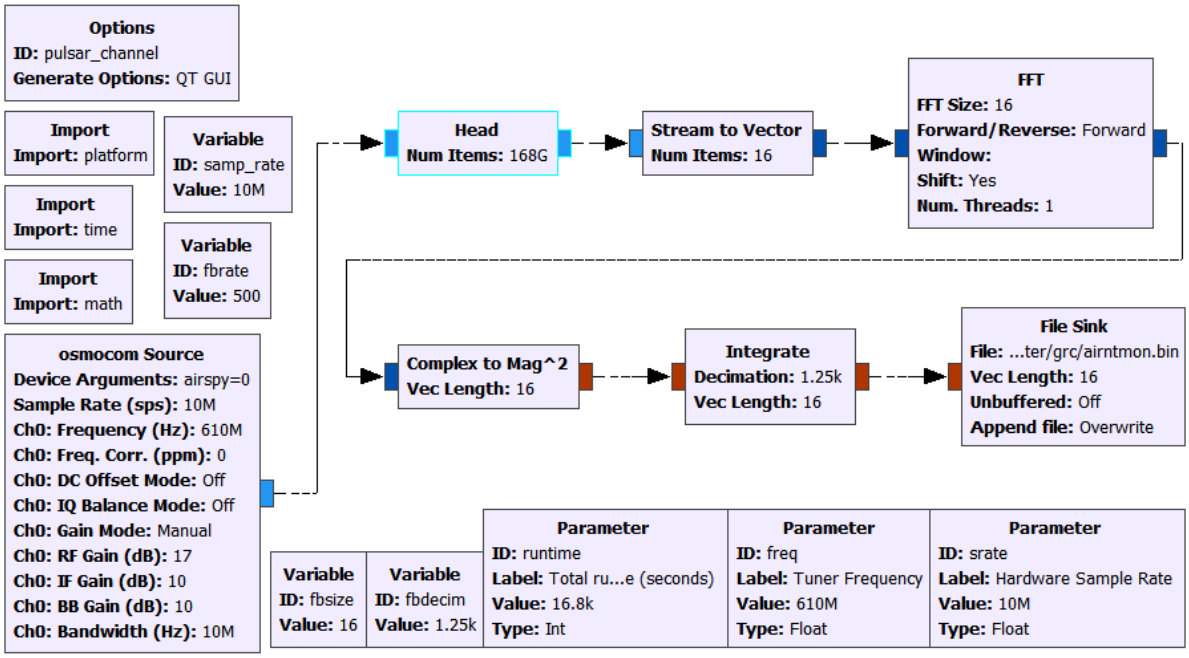

Figure 2. GNU Radio Flowchart

The 'Head' (highlighted) block in Figure 2 defines the number of complex data samples processed in the observation, determined by the observation duration in seconds specified by the 'runtime' parameter. The 'Stream to Vector' block splits the data into 16 complex streams ready for the 16-bit 'FFT block 'Size'. The FFT 16 complex outputs are then converted to 32-bit floating point magnitudes proportional to the input power in the 16 RF bands before being averaged over 1250 integration periods in the 'Integrate' block to downsize the data to 16 x 500 samples per second (S/s) rate for recording in the 'File Sink' block. The output file format is standard 32-bit binary.

To minimize amplifier effects of amplifier drift, the data recording was started an hour before the designated start time and quickly restarted at the designated start time.

With this system, even for 4+ hours intercepting pulsar B0329+54 scintillations, integrated (folded) data is only expected to produce final signal-to noise ratios of between 3:1 and 7:1.

Data was collected in the early hours of the morning of 25 October 2021; it was relatively free from RF interference and is analyzed as the example in the following sections.

Using the Airspy SDR, running at 10 MS/s and tuned to 611 MHz for 4 hr 40 mins, 168 Gs of I/Q data was sampled by the SDR and after 16-band channelization in the FFT and downsampled by running integration over 1250 samples, in this instance, the output file contained 134.4 Ms based on a 2 ms output data clock.

Pulsar Recognition Features - Weak signals

The key identifying properties of a pulsar are,

1. Regular pulse train
2. Stable averaged pulse width
3. Accurate predictable topocentric period
4. Highly stable source - known spin-down rate
5. Wide band noise source
6. Dispersed in frequency - lower frequencies follow higher frequencies
7. Predictable dispersion measure (DM), period and period change rate (P-dot) search properties
8. Random scintillating pulse amplitude with time and frequency
9. In drift-scan mode, received pulse amplitude generally follows the beam pattern

The analysis reported in this article seeks to investigate various aspects of the recorded data by using only the basic folding algorithm to check conformance with the unique properties listed above. The pulse matched-bandwidth folding algorithm has been shown to be the most efficient tool for extracting pulsar signals from noise [6].

Data Compression - Partial Folding [7]

Data compression and improving the data time resolution of the GNU Radio data with minimum information loss is attractive as it can seriously reduce the total computation time when analyzing the detailed pulsar validation characteristics to prove pulsar presence. The validation standard set by the professional pulsar detection software PRESTO is assumed the target to match. Loss-less data compression is particularly important for long observation times and weak signals as is apparent here. This can be achieved by using a synchronous, partial folding algorithm. A C-program, *syn_compress.exe* has been written to accomplish the data reduction with negligible loss of timing information and accepts the GNU Radio output files directly .

The partial folding principle of operation can be described with reference to Figure 3. The input data file can be regarded as a sequence of pulsar periods (period value as given by TEMPO). A simple method of data compression is to divide the data record into say, *S* equal sections and synchronously fold each section into a single period of *B* bins as depicted in Figure 3.

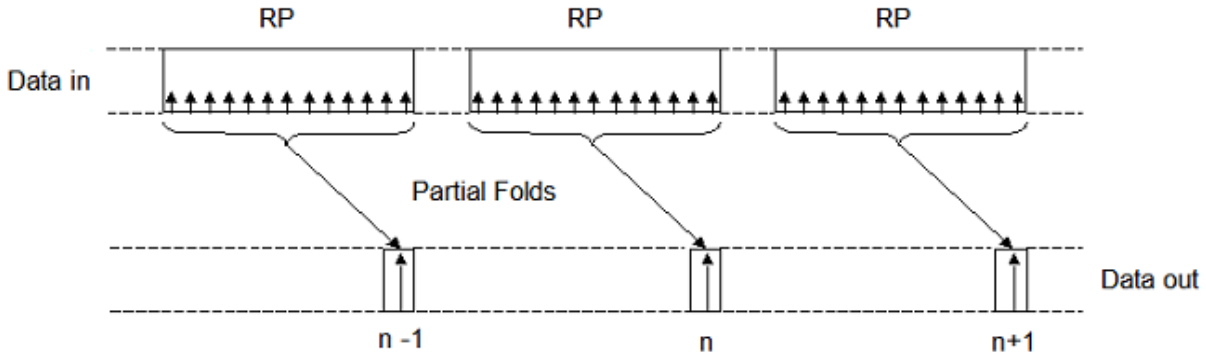

Figure 3. Partial Folding Operation

where,
P = Pulsar Topocentric period
R = Number of periods folded per Section
S = Number of Sections
n = Section Number
B = Number of fold bins = New effective compressed data period

Stacking or adding the section folds in parallel is the same as folding the whole file into one period as the standard method. On the other hand, adding the section folds in series creates another file with all the information held in the original file but now shortened by a factor, *R,* equal to number of pulsar periods in the input data file divided by the number of sections, *S*. The sensitivity to period and P-dot search parameters consequently change by the factor 1/*R*. For further folding the fold period is adjusted to equal the number of bins chosen for the compressed data.

In this example, the compressed file, locked to the TEMPO derived value of the pulsar topocentric period, comprised 16-channels of 131072 samples (*S* = 128, *B* = 1024, *R* ~ 183) folded to approximately 0.7 ms resolution (pulsar B0329 period is approximately 714.5 ms) .

Matched-Filter Folding [8]
In standard folding, the pulsar pulse is recovered by stacking periods so the pulsar pulse adds linearly and the noise as the square root so increasing the signal-to noise ratio by the square root of the number of periods added. The summing effectively reduces the data noise bandwidth which is eventually limited in the standard algorithm by the number of fold bins. The optimum bin number, in this case, is equal to the pulsar *P*/*W*, period/pulse width ratio. But we can do better than this since we do not need to rely on averaging process to reduce the noise bandwidth, we can do this by filtering the noise to control its bandwidth to be matched to the bandwidth required to just pass the pulsar pulse shape.

Another problem with low bin numbers, apart from limited resolution, is that the pulse phase may straddle two bins affecting the perceived SNR.

The FFT can be used to band limit the data spectrum in two easy ways,
1) FFT data x modulus (FFT pulse shape) –> Inverse FFT
2) FFT data –> zero high frequencies –> Inverse FFT

This process can be carried out at any stage on the detected data, the compressed data or also on the folded data.

Figure 4 compares the standard and matched-filter bandwidth limiting methods. The green and magenta curves describe the theoretical performances for Gaussian shaped pulses of the two methods. The red and blue dots are the results on real data of modifying the fold bin number over the range 10 to 800 in 1- bin increments.

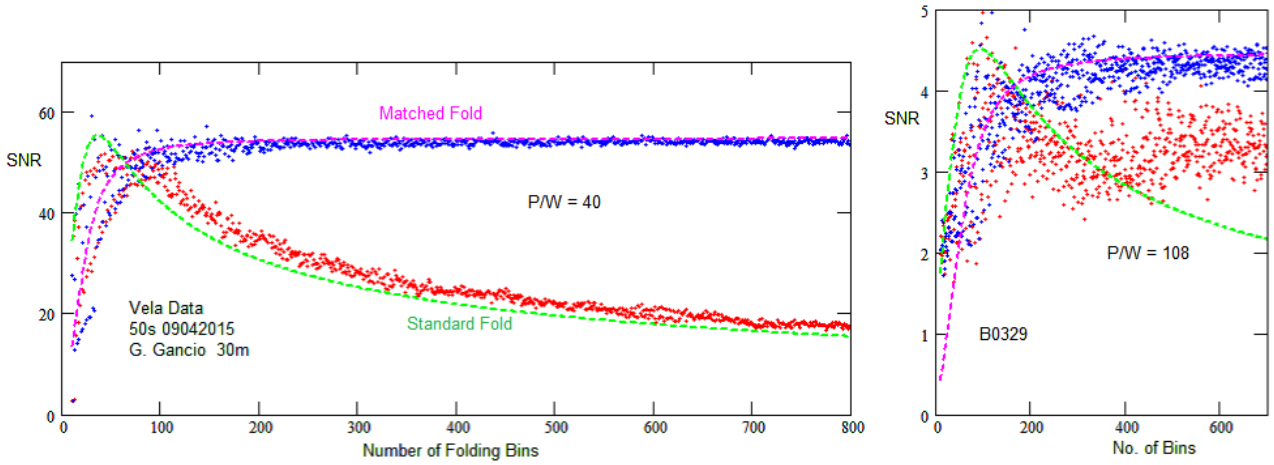

Figure 4. Comparison of Matched-filter and standard Fold Algorithms

The left hand plot uses Vela pulsar data collected by Guillermo Gancio on the Argentine 30 m radio telescope. The large antenna aperture provides a strong signal with a large SNR and the data tracks the theoretical data very well. The right-hand plot displays the performance with the weaker, much lower SNR, B0329 signal (~4.5:1 SNR) typical of small aperture amateur systems as described here. The consequences of the low SNR is a much wider measurement uncertainty. The matched filter system providing a much more confident measure whilst the standard method plateaus out on typical Gaussian noise peaks around SNR of 3:1.

The wider variation at low bin numbers is caused by the pulsar pulse straddling bins.

Data Conditioning

The Figure 5 processing chart summarizes the data processing operation sequence for extracting pulsar characteristics generally used to validate true pulsar detection. The chart shows the recommended data reduction paths to usefully speed up the computation times, particularly for the more computationally intensive 2-D period/P-dot search plot.

Data Compression and Matched Filtering

In this example, the GNU Radio detected data file comprised 16 frequency channels each of 8.4MS of video data at 2ms clock rate. The compression and matched filtering functions reduced this to 16 channels of 128 sections, each synchronously partially folded into 1024 bins. This process loses no timing information as it can be shown that folding/summing the 128 sections produces an identical result as if the whole data were folded prior to the compression process. There is no observable difference if the GNU Radio data were produced at a 1 ms or lower clock rate, even though the final folded result now indicate, sampling at approximately 0.7 ms intervals.

In the data compression process, DC removal of each section prior to re-composition was essential to ensure that any low frequency drift over the observation period did not corrupt the resulting data with DC steps between sections.

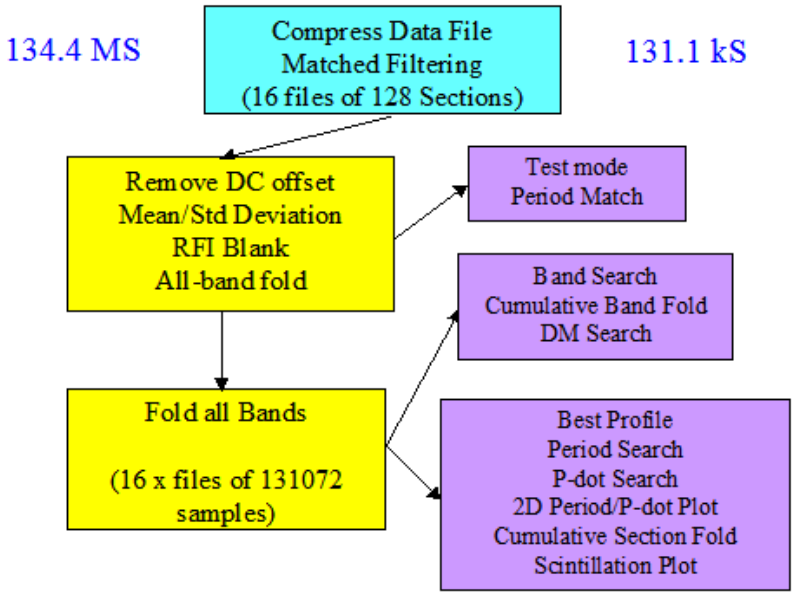

Figure 5. Validation Processing Chart

RFI Blanking

The 16 frequency band files each comprise 131072 samples. In this example 16-bands was chosen so that if a narrow band interfering signal was present in the data, that channel could be blanked without losing too much overall bandwidth. Similarly if one or more sections were obviously corrupt, these can also be blanked. The blanking method employed uses two text files identifying the channel band and/or sections to be blanked.

The number of folding bins was set at 1024 to define the final timing resolution (for B0329) to be close to 0.7 ms. Similarly 128 sections was chosen so that if one or more of these were affected by severe RFI then blanking a few of these may be an acceptable data loss.

In this case, night time data collection ensured that locally generated RFI was minimized.

Extracting Pulsar Characteristics

The final stage, once the data has been suitably conditioned is to extract the target pulsar's detailed characteristics by various folding arrangements. Initially, all the compressed band data are folded both individually, then all together with the bands combined.

The software has a quick reaction test mode that just carries out period and P-dot searches with data presented in the command terminal so that minor adjustments can be made to the TEMPO defined topocentric period.

Once period adjustment has been set, the full analysis, producing 21 specific space-separated text files that can be examined using Excel, Notepad, MathCad MatLab or Python to investigate pulsar parameters in detail. These are demonstrated in the following sections.

Software Tool

The post processing software, *syn_compress.exe* runs in a 64-bit WINDOWS command terminal (*cmd.exe*) .

The command calling terms are of the form;-

syn_compress <infile> <No. FFT bins><data clock (ms))><period (ms)> <No. sections><No. bins><pulse width><DM><ppm adjust><Test T><RF bandwidth (Mhz)><RF Center (MHz)><Roll average No.>

Example:

syn_compress.exe data.bin 16 2 714.492092 128 1024 6.5 26.7 0.1 04 10 611 32

where,

data.bin is the input data file generated by GNU Radio as a 32-bit binary file of detected data samples

16 is the number of FFT channels/bands.

2 is the Gnu Radio set data clock in ms.

714.492092 is the TEMPO topocentric period for the observation site and recording UTC

128 and *1024* are the numbers of compressed file sections and fold bins - both binary numbers.

6.5 is the target pulsar pulse width.

26.7 is the target pulsar dispersion measure

0.1 is the period correction offset in ppm.

04/T4, *0* or *T* , the first character, specifies normal or test mode. *4* is the period range divisor.

10 is the SDR RF bandwidth in MHz

611 is the RF center frequency

32 is the rolling average section range.

The Command Terminal Response reports the key parameter data:-

P:\grc>syn_compress.exe airntmon.bin 16 2 714.492092 128 1024 6.5 26.7 0 04 10 611 32

Mode = 0 Period Range Divisor = 2
Pulsar Period = 714.492092 ms
Data clock= 2.00 ms
Pulsar Pulse Width = 6.50 ms
Pulsar Dispersion Measure = 26.70
Rolling Average Number = 8
Input file bytes =537600000
RF Centre = 611.0 MHz, RF Bandwidth = 10.0 MHz
DM Band Delay = 9.716ms, No. Delay bins = 13.924
Blanked Bands: 0
Blanked Sections: 0
No. Data Samples = 134400000
No: FFTs = 16
Input Data per FFT channel = 8400000
No. of Output fold blocks 128 ; bins = 1024
No. of Output samples = 131072
Working file duration = 16800 secs
Number of pulsar periods = 23513
ppm adjustment = 0.00
Max Pulse ppm drift = 0.00 ms
Compression Ratio = 183.70
Period Search Range = -12.50 ppm to 12.50 ppm
P-dot Search Range = -10.63 pp10e10 to 10.63 pp10e10

Blank data files:

The software expects two blanking files to be available. These are, *Blanks.txt* and *Blankf.txt*

These are standard space separated number files, identifying section and band numbers to be blanked for RFI or bad data reasons. They can be empty files where all data is to be processed. Data to occupy the files can be obtained from the output file plot analysis.

Processed Output Data Files and content description:-

1. Raw compressed channelized data file: rawdat.txt
2. Compressed filtered channelized data file: outdat.txt
3. Compressed filtered combined bands data file: allbands.txt
4. Pulse profile: profile.txt
5. Period search: periodS.txt
6. P-dot search: pdotS.txt
7. 2-D Period/P-dot peak SNR: ppd2d.txt
8. DM search: dmSearch.txt
9. DM search target blanked: dmSrchns.txt
10. DM peak best fold data: dmprf.txt
11. Band Peak SNR: bandS.txt
12. Folded bands: bandat.txt
13. Cumulative band Peak SNR: cumbands.txt
14. Cumulative folded bands: bndcum.txt
15. Section peak SNR: secsnr.txt
16. Section folded data: puldat.txt
17. Cumulative section peak SNR: cumsec.txt
18. Cumulative folded section data: foldat.txt.
19. Rolling average section peak SNR: secavsnr.tx
20. Rolling average section folds: secavfol.txt
21. Rolling section block peak SNR: secavrol.txt

These files are used to construct the plots in the following Results and Appendix sections. Running the software tool on a modern 64-bit computer, the run time for the test mode is about 10 seconds and for the full analysis mode is about 25 seconds. Output data files used for the analysis figures following are identified in numbered brackets at the end of the figure titles.

Test Mode - Period Correction

Mode = T Period Range Divisor = 4

With any amateur potential pulsar data collection, the pulsar identity and position is known and the data collection set up accordingly. Knowing the time, one can use TEMPO to predict the likely observed topocentric period and this is the usual fold period used in the subsequent data search. Due to receiver clock limitations, the measured period may be slightly different to the predicted figure requiring a search sequence.

ppm = -0.75	SNR = 3.22	bin = 401	pdot = -0.64	SNR = 3.76	bin = 61
ppm = -0.50	SNR = 3.51	bin = 643	pdot = -0.43	SNR = 3.34	bin = 60
ppm = -0.25	SNR = 4.43	bin = 640	pdot = -0.21	SNR = 4.40	bin = 639
ppm = 0.00	**SNR = 4.85**	**bin = 637**	**pdot = 0.00**	**SNR = 4.85**	**bin = 637**
ppm = 0.25	SNR = 4.74	bin = 634	pdot = 0.21	SNR = 4.69	bin = 635
ppm = 0.50	SNR = 4.38	bin = 632	pdot = 0.43	SNR = 4.21	bin = 634

Table 1 Period Adjust Error Indicator

The software designed here, therefore has a fast testing mode that lists a period search range in the command terminal that may be inspected to determine any possible error which can then be added in the software command line to correct the deviation and revert to full analysis mode. In Table 1, the maximum SNR is indicated

at zero period ppm error so needs no adjustment. Note that the P-dot error is also zero, implying negligible period rate drift over the observation time confirming a very stable source.

Results

Full Data Folding

Figure 6 plots the best folded result (red) and the peak DM search folded result (blue). The unexpected difference is because the best result is obtained by a simple method of better utilizing the group of sections folded and is discussed later.

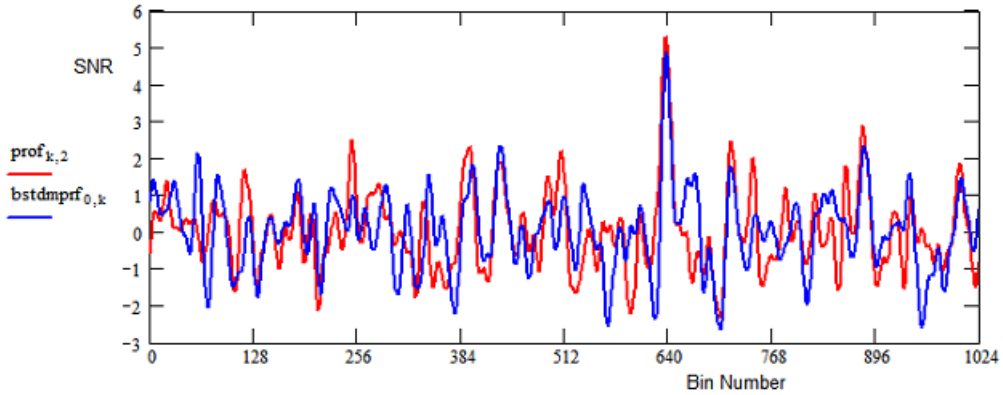

Figure 6. Matched Topocentric Period Folded Data (4,10)

Period/P-dot Search

Period and period rate variations about the expected values confirm both pulsar period accuracy and negligible period variation over the observation time.

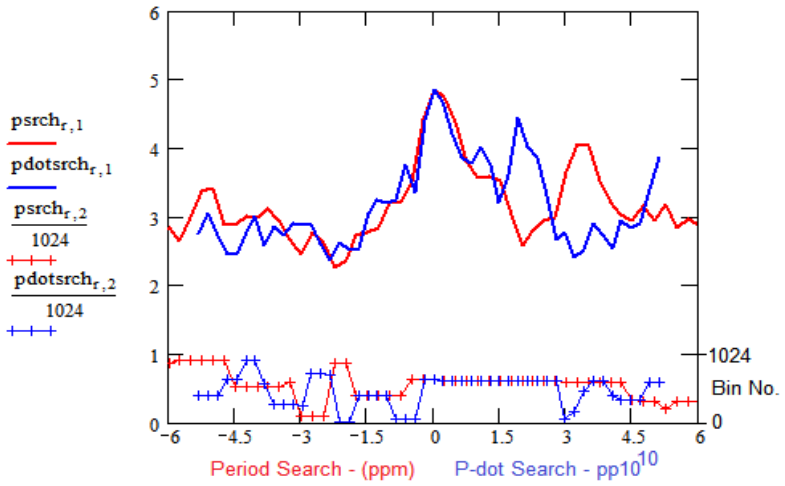

Figure 7. Period/P-dot Search (5,6)

The period/P-dot plot above also includes the bin number at which the moving peaks occur. With both these changes, the target pulsar peak varies at a predictable rate, determined by the extent in the record that it is observed. With low SNR values as recorded here, local noise peaks tend to take over affecting the data quality.

With both parameters peaking at zero offsets, this test proves exact match to the pulsar expected topocentric period and confirms the stability with no period drift within the 4+ hour observation time.

2D Period/P-dot Plot

Figure 9 aims to explain the operation and characteristics expected from the typical 2-D period/P-dot search plot of Figure 8. The test examines the peak response of data folded over a range of period values around the period topocentric value and over a positive and negative range of P-dot values to explain the 'ridge' observed. The theoretical ridge slope is given by $pd/p = -2/N$, where pd and p represent the P-dot and period offset values and N is the total number of pulsar periods in the observation record. For Figure 8, the scales have been adjusted to make the correct ridge slope occur at -45 degrees.

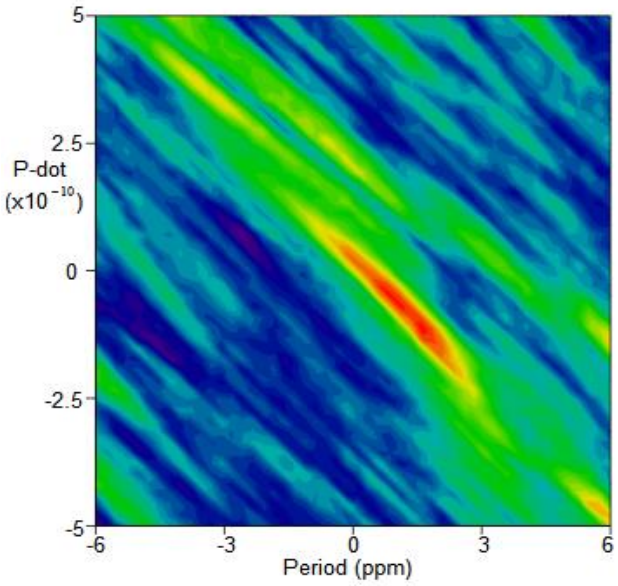

Figure 8. 2-D Period/P-dot Search (7)

A clear central peak at coordinates 0,0 and sloping extended ridge is evident confirming period match and nominally zero spin-down.

An explanation for the ridge effect follows. Addressing Figure 9, the central green horizontal line with notional period intervals indicated corresponds to the test period value matching the pulsar topocentric period together with a zero P-dot value. The result is the horizontal green maximum fold response to the right.

The magenta line represents a period positive offset, still with zero P-dot, which tends to spread the (magenta) folded result to the right and lowering its amplitude as shown.

The red P-dot line starts with a test period matching topocentric figure together with a P-dot value which progressively reduces the folding test period resulting in the red folded response to the right. Whereas the period offset response is symmetrical, the P-dot starting at zero and working negative, shortens the folding test period, moving it from a matched condition to unmatched exhibiting an asymmetrical (red) response peaking closer to the matched position.

Finally, the blue P-dot line on the left starts with a positive period offset coupled with a P-dot value which progressively shortens the period over the observed periods such that the final period matches the original topocentric period resulting in the much increased blue folded response the right.

The black ellipse indicates the range within which combined opposite polarity period and P-dot offset values can give rise to the stronger fold (blue) peak.

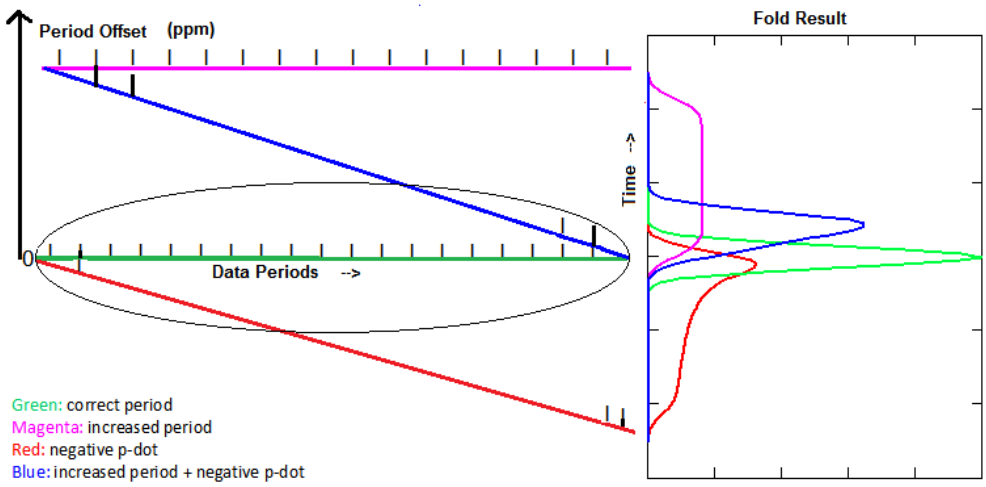

Figure 9. 2-D Period/P-dot Operating Characteristics

This compensating property of opposite polarity period and P-dot offsets is responsible for the extended diagonal ridge observed through the center of the 2-D period/P-dot search plot. Figure 9 can explain the extended ridge observed in the 2-D plot by noting that for a any given positive period offset (magenta) a very wide range of negative P-dot slope values (blue) can produce a period range closely matching the data period (within the black ellipse). The closer the initial period offset, the larger the fold amplitude contributing to the ridge.

Efficient and timely computation of the 2-D Period/P-dot search plot is the main reason for wanting to compress the data. The separate period search and P-dot search plots are relatively easy to produce, typically requiring less than a hundred iterations to plot the relevant sub-plots in Figure 7. To calculate the 2-D plot requires some 2500 iterations. With multi-mega-sample files the computation time can be very long but by compressing the data to 131072 samples or so the computation time becomes more acceptable.

Dispersion Search

Data de-dispersion involves separating the received signal bandwidth into a number of sub-bands and delaying the higher sub-bands before video or digital summing to compensate for the interstellar delays.
For dispersion measure search, the band delays are varied linearly over a range about the band center to accomplish both positive and negative dispersions; the combined data SNR is then calculated to produce a plot similar to the red crossed plot in Figure 10.

A simple check that it is indeed the candidate pulse that is responsible for the dispersion search peak around DM = 26.7 is to blank the pulse response around the candidate (in this case, bin 637) and repeat the search routine (magenta curve). It is seen that subtracting the two measurements now produces the blue curve which is identified as the DM contribution of the nulled candidate peak. This gives a much clearer indication that pulse at bin 637 peaking around DM = 26.7 and confirms the dispersion measure expected for pulsar B0329.

The horizontal crossed red plot reports the bin number of the peak response (scale to the right), noting that it is indeed constant and correctly reporting the target bin number. The figure remains constant as the band positive and negative band delays are maintained relative to the total band center.

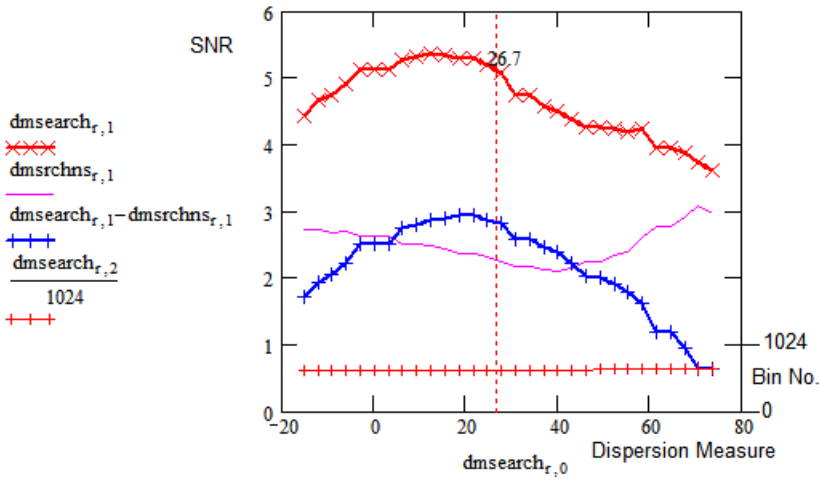

Figure 10. Improving Dispersion Search Discrimination for low SNRs (8,9)

Once the band delays that produce the maximum pulsar amplitude has been identified, the sub-band files are delayed as required and the files added to produce a single file to support the remaining validation processes.

Cumulative Frequency Waterfall

Waterfall plots are usually constructed by dividing the data into a number of equal sections, processing these as required, then displaying the resulting plots sequentially. With cumulative waterfalls, the data is again divided into the same equal sections, but now displaying the processed results of the sum of all previous sections. This improves visibility of weak information that may be lost if noise when splitting the data in many sections.

Here, the sixteen frequency band files are cumulatively folded and the peak surface plotted to produce Figure 11. To start cumulative folding band zero is first folded. then bands 0 and 1 are summed and the sum folded.

This process continues until all bands are summed and folded. It can be seen from Figure 11 that once 5 bands are summed and folded that the target pulsar (red line) starts to dominate.

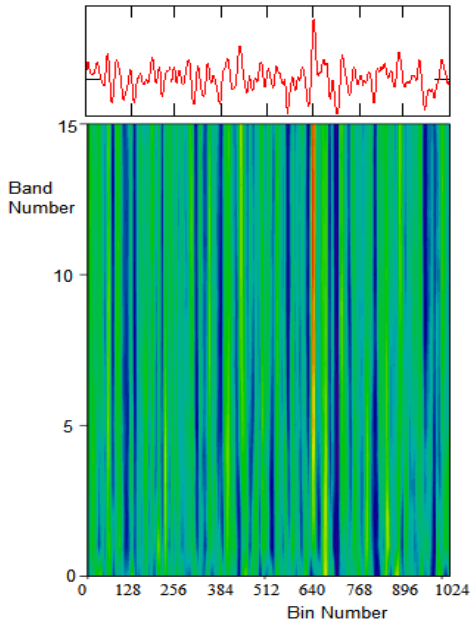

Figure 11. Frequency Waterfall (4,13)

With the conventional waterfall method, where only individual bands are folded for display which for weak pulsar signals does not give a useful presentation. This process continues until all bands are summed and folded. This plot confirms the broad band nature of the target.

Band Response Analysis

Figure 12 presentation provides more evidence of the target wide frequency coverage. The red plot indicates the peak SNR observed as the bands are cumulatively summed and folded. After folding bands 0,1, 2 and 3 which seem to track noise peaks, it is seen there is an increasing trend in the summed and folded SNR, leveling off after the folded sum up to band 10. The green dashed plots track the individual band signal + noise fold peaks, whilst the solid red plots and dashed red lines present the cumulative and individual band SNRs of the target pulsar.

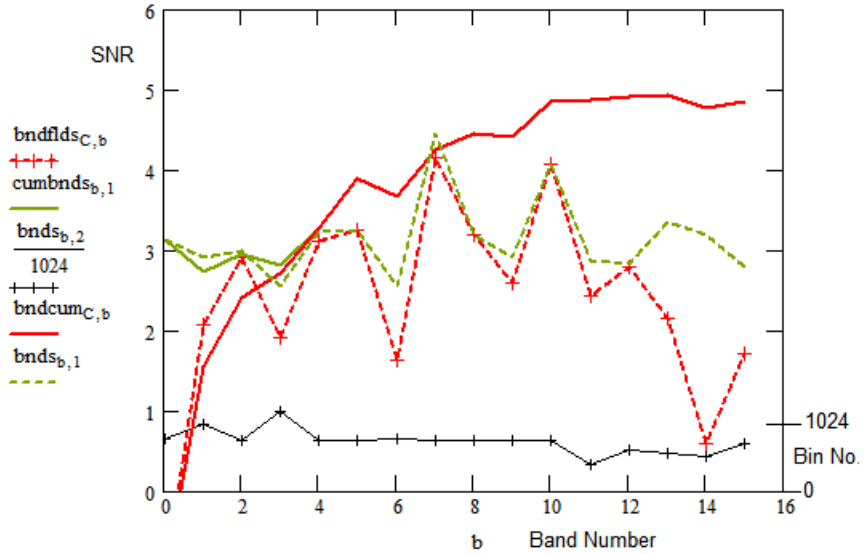

Figure 12. Cumulative Frequency Band peak SNR (red) (11,12,13,14)

Finally, the thin black crossed point line describes the individual band peak bin value (= 637, scale on right-hand axis). This shows that the target peak dominates between bands 4 and 10. With a fully integrated SNR of 5:1, it is calculated that any individual band SNR exceeding 5/√16 = 1.25:1 can contribute to the final figure - in this case, all bands except 0 and 14 contain useful components. It can be concluded that blanking bands 0 and 14 should lead to an increased final result.

The frequency band analysis clearly demonstrates that the target pulse source is broad band, the folded band peaks occur at the target pulsar characteristic bin and the varying levels in each band is a sign of the pulsar frequency scintillation property.

Cumulative *Time Waterfall*

The red line under the peak bin 637 in Figure 13 indicates that from about section 50. the integrated bin position 637 is becoming dominant resulting in the profile pattern in Figure 6.

With low SNR data, the cumulative waterfall representation is clearer than the conventional section SNR form, where the section pulse SNR is prone to drop below noise by the factor √(128).

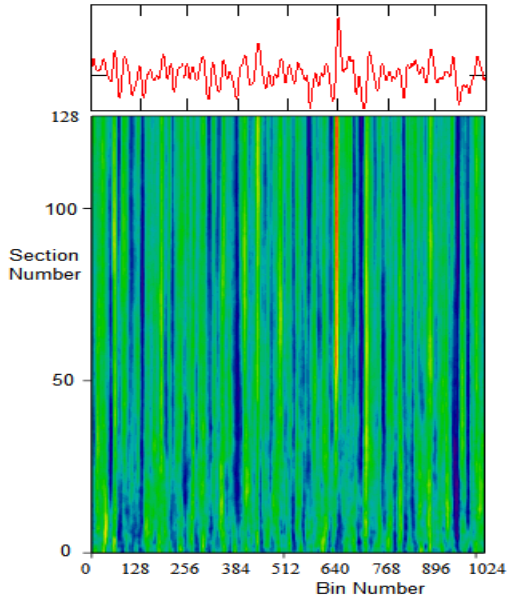

Figure 13. Time/Section Cumulative Waterfall (4,18)

The vertical green noise streaks appear typical of persistent natural folded noise peaks that once established seem to maintain a fairly flat profile.

Both waterfall results confirm the presence of a regular pulse train.

Cumulative SNR

To produce the cumulative SNR plot, the combined de-dispersed file is split into 128 sections, each section is folded and added to all previous sections. The accumulating summed folds are then checked for a maximum and this is plotted against section number in Figure 14 to produce the green curve (peak of noise or target pulse). Also plotted in red is the target pulsar at bin 637. This shows that the candidate takes over the integrated peak by about section number 50. Studying the candidate curve, there are several regions of sharp rises which can be attributed to strong scintillation. There are some negative sloping regions where the target signal is weak or subsumed in background noise. The rises are associated with 'strong' section SNRs and the falls associated with

weak or negative section SNRs. The green crosses line represents the characteristic bin number of the accumulated peak and again shows the target bin number remains constant at 637 (the target pulsar bin peak) from about section 48.

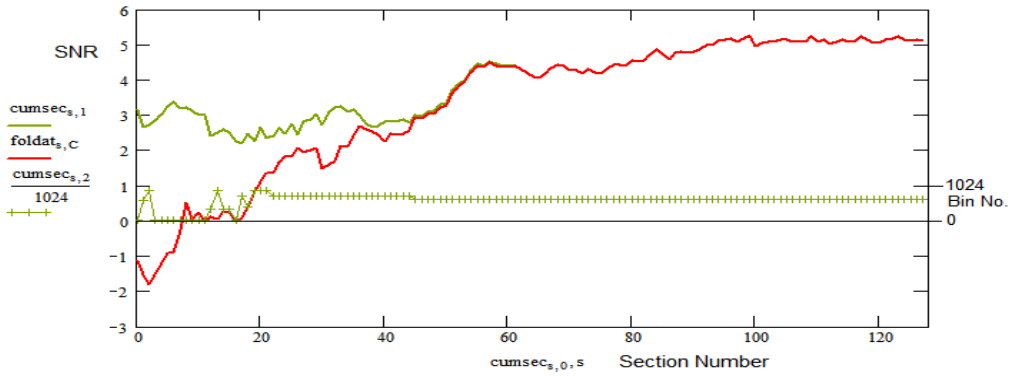

Figure 14. Cumulative SNR - noise ,green; bin 637,red (17,18)

To clarify the characteristics of the background noise, Figure 15 plots the apparent SNR of all noise components with the target pulsar bin region blanked. From this it appears that the accumulated response remains noise-like and does not exhibit the growing trend of a true semi-persistent pulse train. (bins 0 to 630, blue; 643 to 1023, green)

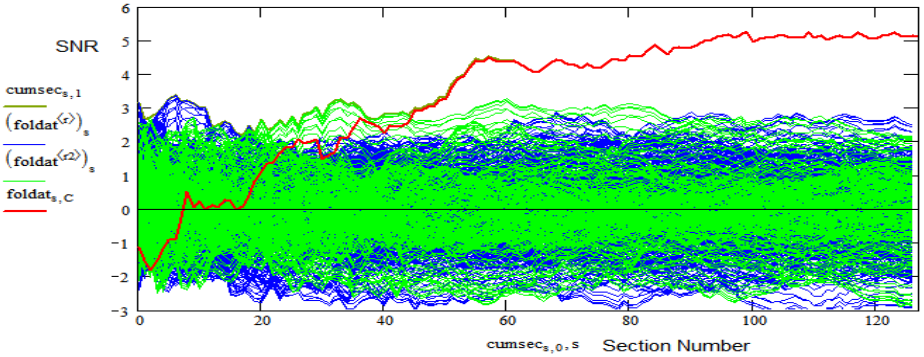

Figure 15. Cumulative SNR Plot for Target/Noise Comparison (17,18)

Scintillation

A particular problem in intercepting Pulsar B0329 is its feature of short and long-term scintillation caused by non-linearities and temporal changes in the interstellar medium.

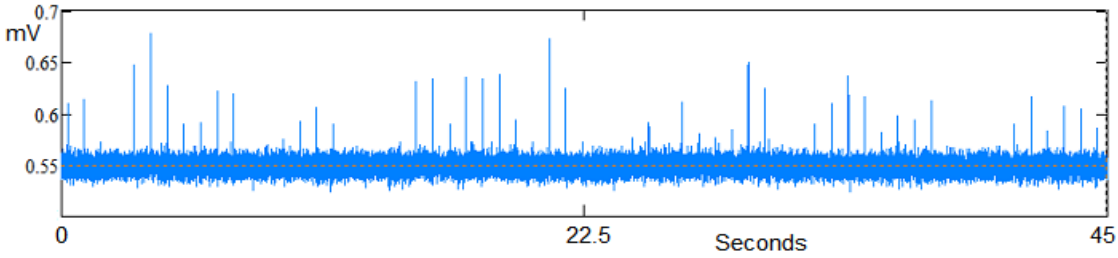

Figure 16a. Pulse-by Pulse B0329 Recording - 46m antenna

This causes long and short timescale variations in amplitude and is also variable in frequency. The blue plot in Figure 16a is a 45 second pulse-by-pulse recording taken with the 46 m dish at the Stanford Research Institute (by R. Ferranti) and clearly shows the short-term pulse-by-pulse scintillation.

Figure 16b plot is the present 1.6 m^2 aperture recording and represents the full compressed 4.67 hour, 128 section recording. Each section comprises 183 synchronously folded pulsar periods; even so, no integrated pulses are visible.

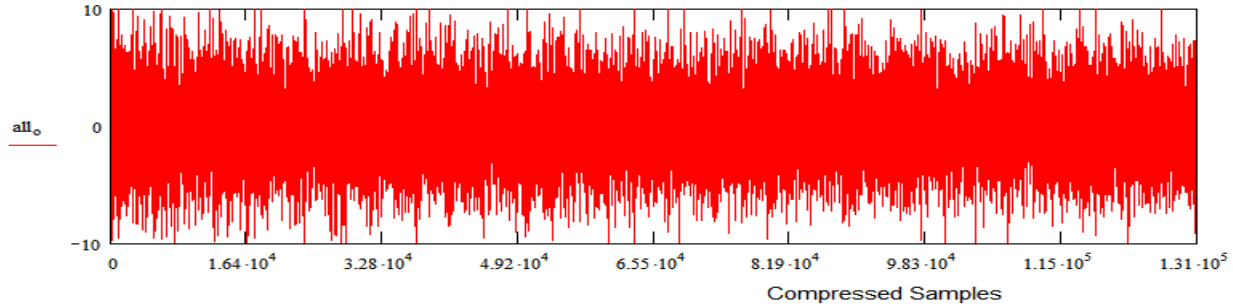

Figure 16b. Compressed Video Record - 1.5 m^2 antenna (3)

However, since the analysis has identified the bin number corresponding to the target pulsar relative position, the pulsar bin 637 contents can be selected for display as shown in Figure 16c.

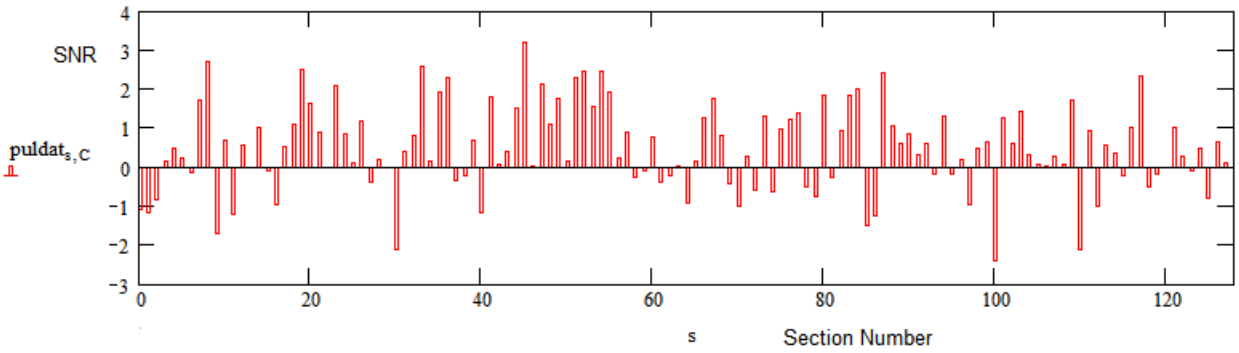

Figure 16c. 1.5 m^2 antenna Extracted Target Bin (3)

This shows that although the pulse amplitude is comparable to the noise level, there is a majority of positive, variable amplitude indications and groupings indicating both scintillation and confirming the pulsar signal presence. Caution is needed when interpreting individual responses due to the ambient noise level which is only suppressed by averaging in folding.

Data Searching

Another method of demonstrating the presence of scintillation is by constructing a rolling-block average along the data record. In Figure 17a, the red curve is again the cumulative sum of previous section folds. The blue curve is now the rolling average of 14 section folds of the target; the value displayed at the average mid-point.

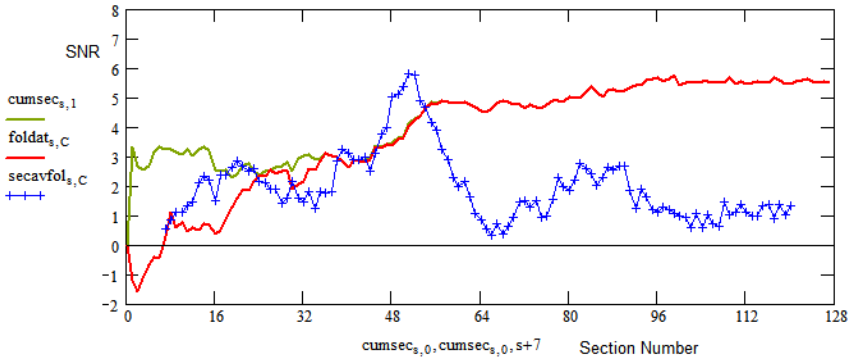

Figure 17a. 14-section Rolling Average Indicating Scintillation (17,18,20)

This rolling average technique is sufficient to better indicate the data section regions where major contributions to the final folded result reside. In Figure 17a, the dominant region appears around section 48, coinciding with the sharp slope increase of the cumulative sum. There are also strong regions in sections before and after section 48 - another indication of scintillation. Another point to note is that around section 50, the integrated SNR from the 14 sections averaged is greater than the final full data integrated fold. 14 sections corresponds to just 31 minutes of observation time demonstrating how positive scintillation can help as well as often hindering successful observations.

As well as indicating scintillation, strong points the general amplitude trend can reflect the antenna beam shape when observations are carried out in the drift scan mode. The beam shape is evident for this example when increasing the rolling block average to 32 sections as shown in Figure 17b. What is interesting is that the peak SNR indicated by this 32-section rolling average significantly exceeds the full data final SNR result and accounts for the superior SNR witnessed in the original profile of Figure 6.

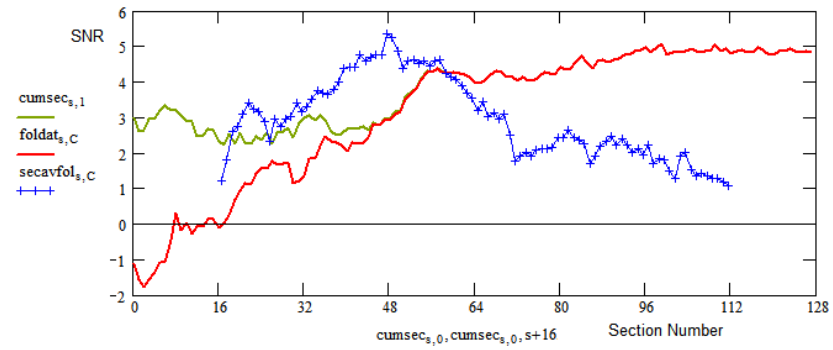

Figure 17b. 32-section Rolling Average Indicating Antenna Beamshape (17,18,20)

Another interesting comparison is offered in Figure 18. Here, the red curve is the section peak SNR (signal+noise) with an 8-section rolling average compared to the blue curve which plots the target pulsar 8-section rolling average SNR. Around section 50 the target pulsar response predominates, whereas the noise peak SNR dominates over most of the range fluctuating around 3:1 SNR level.

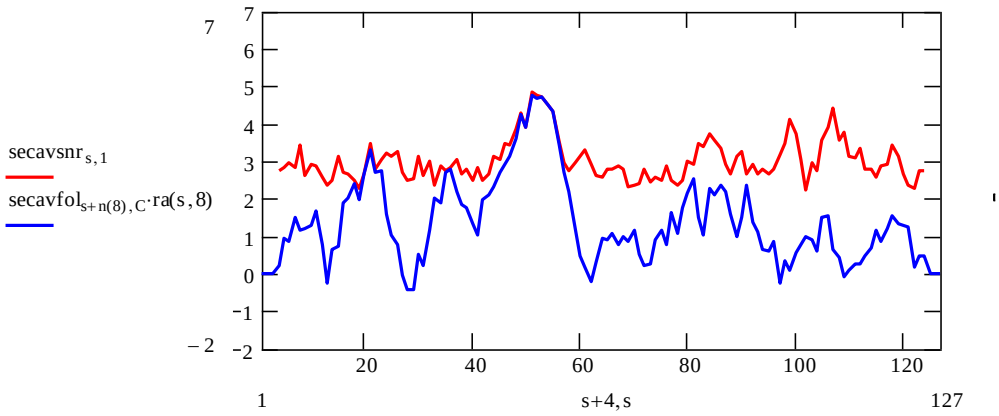

Figure 18. 8-section Rolling Average Pulsar/Noise Comparison (19,20)

Best Folding Range

A comparison of these rolling average plots hints that there is an optimum folding data range that ensures the best fold result. The red curve in Figure 19 plots the peak folded result as a function of the number of sections averaged as the whole data is scanned rolling from a single section to all sections averaged. In this example, it is noted that the curve peaks at *N* = 96 sections averaged but that over most section values the result is fairly high above 80 section rolling average but that it trails off above 120 sections averaged.

The blue curve is the *N* = 96 rolling average section scan showing that optimum scan center is at section 51. Note the rolling average scan range of 96 sections is only possible centered on bins 48 to bin 79.
The output files 20 and 21 compute the data for these plots.

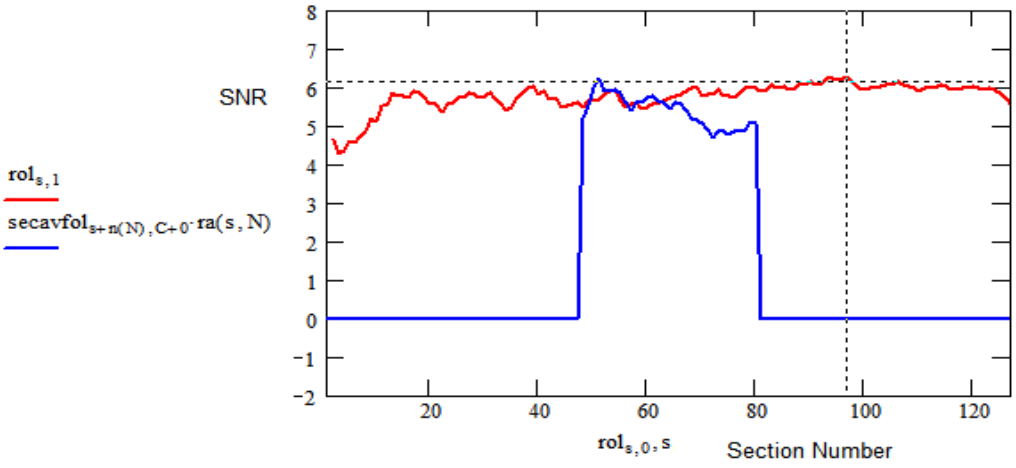

Figure 19 Rolling Average Optimum Range Selection (20,21)

It is interesting to note, that while folding the raw data at the correct topocentric period checked at the period/P-dot test phase was measured as 4.85:1, after optimum de-dispersing, this rose to 5.11:1, this best rolling average adjustment increased the measured value to 6.25:1. Further improvements could be obtained by blanking low SNR bands 0 and 14 (see Figure 12). In addition blanking sections 30,100 and 112, the three largest target negative SNR sections (see Figure 16c), raises the final SNR to 7.02:1 (Figure 20).

Blanking all negative SNR sections (see Figure 16c) appears even more beneficial, but without inspecting the data directly, because of contributions being comparable to the pulse level, this less easy to justify.

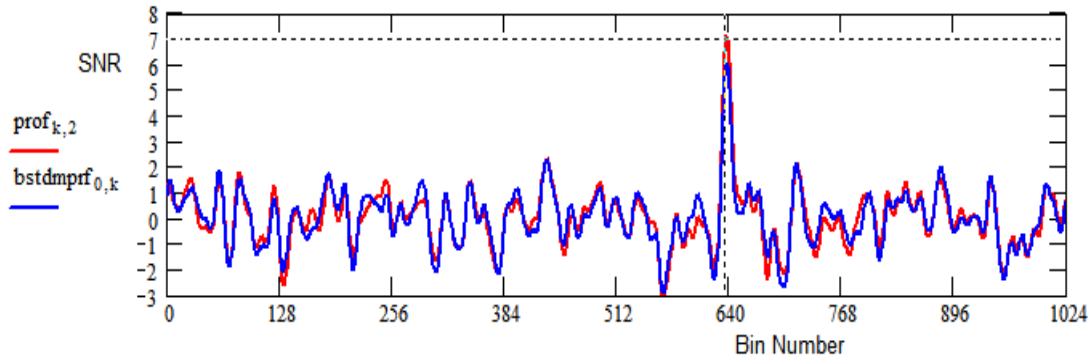

Figure 20. Improved SNR with Bands 0,14 and Sections 30,100 and 114 Blanked and Optimum Rolling Average

Conclusions

An alternative software solution for low signal-to-noise ratio pulsar data analysis, compatible with GNU Radio controlled SDR data collection and pre-processing has been described. The post-processing technique involves data compression for fast analysis of long observations whilst maintaining accurate timing. The software produces a large number of folded data files describing a wide variety of information needed for accurate measurement and validation of the various pulsar identifying parameters - some in detail not previously recognized. The advantages of the data compression method include minimal information loss together with a significant reduction in computing time. In the example described, 16800 seconds of recording time in 10MHz RF bandwidth was post-processed, producing 21 folding analysis files in 25 seconds, highlighting different pulsar validation properties. MathCad was used to plot the data files, but most are compatible with Excel. A Python GUI is to be investigated.

The cumulative SNR and rolling section averaging approaches applied to both synchronized compressed sections and frequency bands has proved very fast and useful for identifying very weak pulsar pulse trains in recorded data. The Appendix contains MathCad plots of the relevant data file information supporting pulsar validation.

References

[1] PRESTO Home, https://www.cv.nrao.edu/~sransom/presto/

[2] SM Ransom. Searching for Pulsars with PRESTO https://www.cv.nrao.edu/~sransom/PRESTO_search_tutorial.pdf

[3] G Dell'Immagine, A Dell'Immagine. Linux pulsar software for recording and analysis. https://github.com/gio54321/pulsar-distro-guide

[4] M Leech. https://www.ccera.ca/papers/memo-12-a-pulsar-observing-capability-at-ccera/

[5] M Klaassen. http://parac.eu/projectmk17b.htm

[6] V Morello, et al. Optimal periodicity searching: Revisiting the Fast Folding Algorithm for large-scale pulsar surveys. arXiv:2004.03701v2 [astro-ph.IM], 3 Aug 2020.

[7] PW East. An Analytical Method of Recognizing Pulsars at Moderate SNR., Journal of the Society of Amateur Radio Astronomers. November-December 2018.

[8] PW. East, Getting the Best from the Pulsar Folding Algorithm., Journal of the Society of Amateur Radio Astronomers. May-June 2021.

PW East April 2022

Peter East, *pe@y1pwe.co.uk* is retired from a Defense Electronics career in radar and electronic warfare system design. He has authored a book on Microwave System Design Tools, is a member of the British Astronomical Association since the early '70s and joined SARA in 2013. He has had a lifelong interest in radio astronomy; presently active in amateur detection of pulsars using SDRs, and researching low SNR pulsar recognition and analysis. He has recently written another book, 'Galactic Hydrogen and Pulsars - an Amateurs Radio Astronomy' describing his work in Radio Astronomy.
He maintains an active RA website at *http://www.y1pwe.co.uk*

Appendix. MathCad Plots

pulsaranalysis.mcd - March 2022 pwe - Accepts text files from syn_compress.exe and plots folding analysis files for pulsar recognition

Mode = 0 Period Range Divisor = 2
Pulsar Period = 714.492092 msData clock= 2.00 ms
Pulsar Pulse Width = 6.50 ms
Pulsar Dispersion Measure = 26.70
Rolling Average Number = 8
Input file bytes =537600000
RF Centre = 611.0 MHz, RF Bandwidth = 10.0 MHz
DM Band Delay = 9.716ms Delay bins = 13.924ms
Blanked Bands: 0
Blanked Sections:
No. Data Samples = 134400000
No: FFTs = 16
Input Data per FFT channel = 8400000
No. of Output fold blocks 128 ; bins = 1024
No. of Output samples = 131072
Working file duration = 16800 secs
Number of pulsar periods = 23513
ppm adjustment = 0.00
Max Pulse ppm drift = 0.00 ms
Compression Ratio = 183.70
Period Search Range = -12.50 ppm to 12.50 ppm
P-dot Search Range = -10.63 pp10e10 to 10.63 pp10e10

Best Profile

$k := 0 .. 1047$

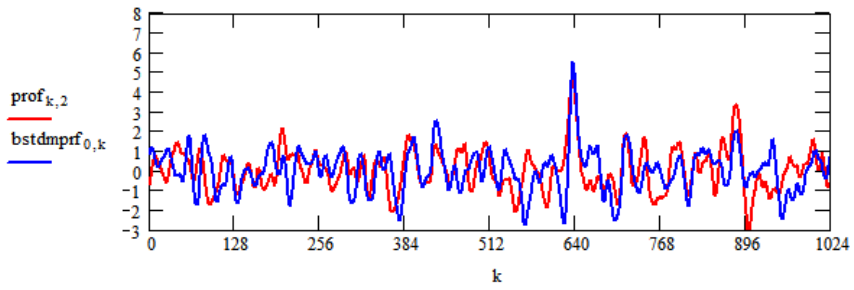

Period/P-dot Search

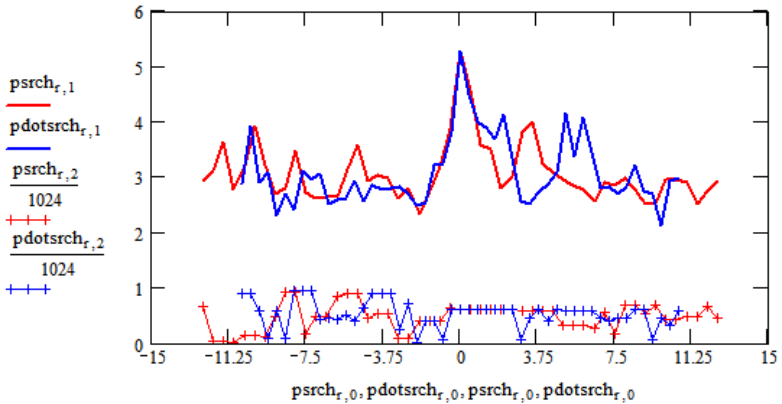

prof := READPRN("profile.txt") bnds := READPRN("bandS.txt") blnks := READPRN("Blanks.txt")

psrch := READPRN("periodS.txt") dmsearch := READPRN("dmSearch.txt") blnkf := READPRN("Blankf.txt")

pdotsrch := READPRN("pdotS.txt") cumbnds := READPRN("cumbands.txt")

bndflds := READPRN("bandat.txt") puldat := READPRN("puldat.txt") rawdat := READPRN("rawdat.txt")

cumsec := READPRN("cumsec.txt") dmsrchns := READPRN("dmSrchns.txt")

s := 0 .. 127 Target Bin No. C := 637 r := 0 .. 59 b := 0 .. 15

Band Properties

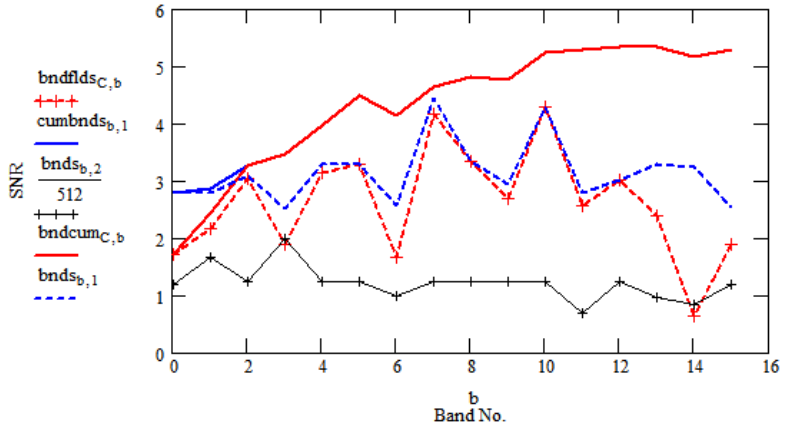

DM Search

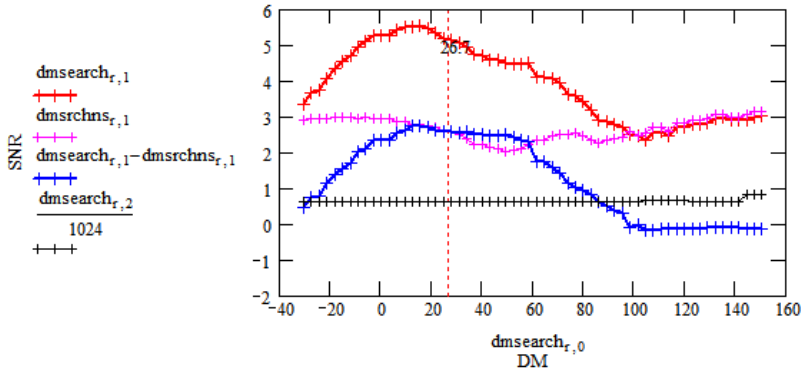

Cumulative Section SNR

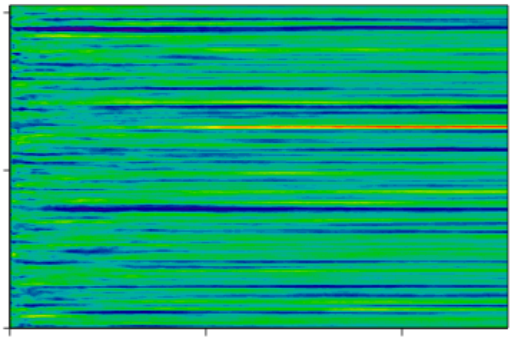

foldat

Cumulative Band SNR

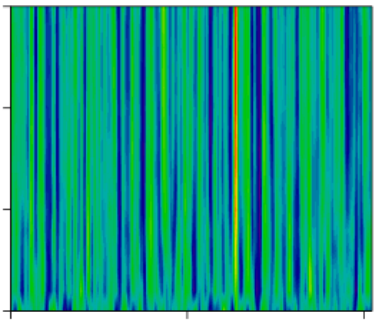

bndcum

secsnr:= READPRN ("secsnr.txt") secavsnr:= READPRN ("secavsnr.txt")

allbands:= READPRN ("allbands.txt") bstdmprf := READPRN ("dmprf.txt")

foldat := READPRN ("foldat.txt") bndcum:= READPRN ("bandcum.txt")

ppd2d := READPRN ("ppd2d.txt") rol := READPRN ("secavrol.txt")

Out := READPRN ("outdat.txt") secavfol:= READPRN ("secavfol.txt")

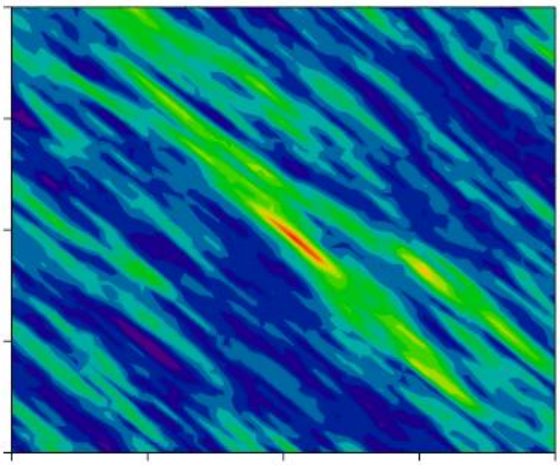

2-D Period/P-dot

ppd2d

Cumulative Peak/Target SNR

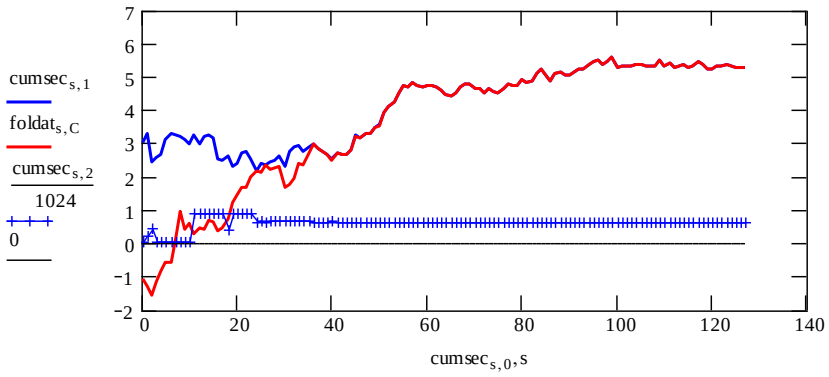

r := 00 , 1 .. C – 20 r2 := C + 20 .. 900

Cumulative Target and Noise

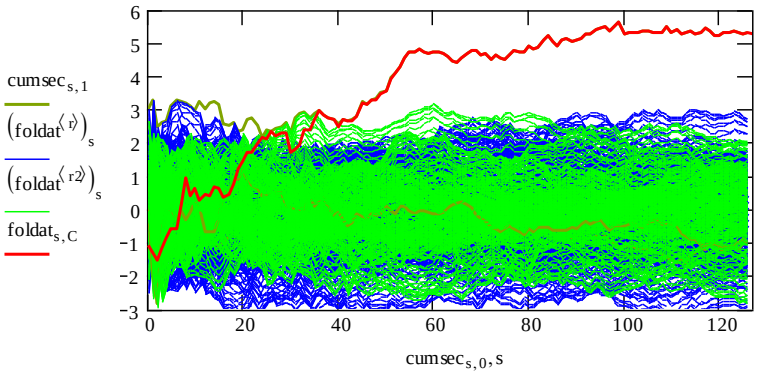

$$n(p) := -\text{floor}\left[\left(\sum_{x=1}^{p-1} x - \frac{p}{2}\right) + 1\right] + 128\cdot(p-1) \qquad ra(s,p) := \text{if}\left[\left[\left(128 - \frac{p}{2}\right) + 1 > s > \frac{p}{2} - 1\right], 1, 0\right]$$

Rolling Average (RA) Search - SNR RA peak,red; section peak, green; target 8sec RA, blue

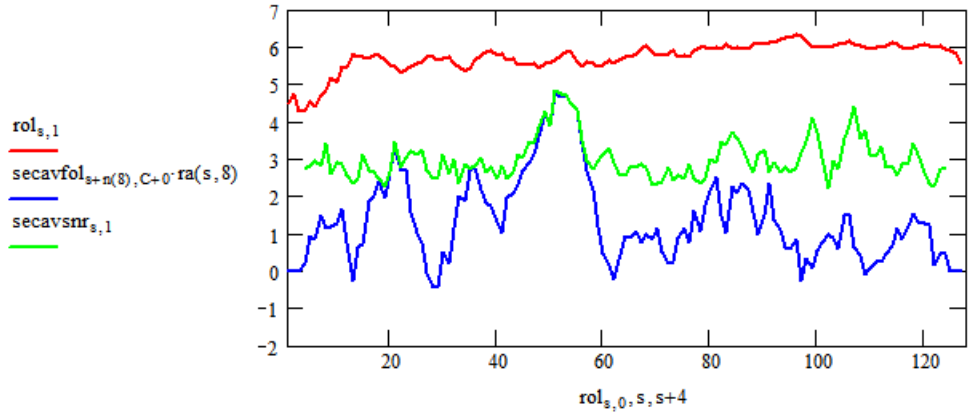

Target Section SNR

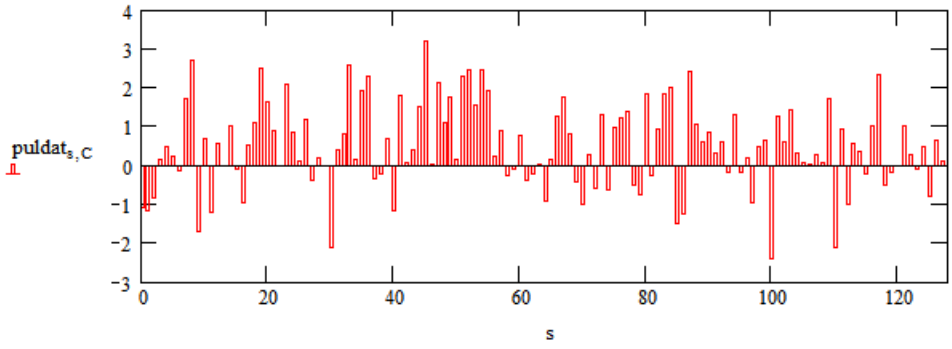

Rolling Average Responses - 4,red; 32,blue; 64,green; 96 (optimum),magenta.

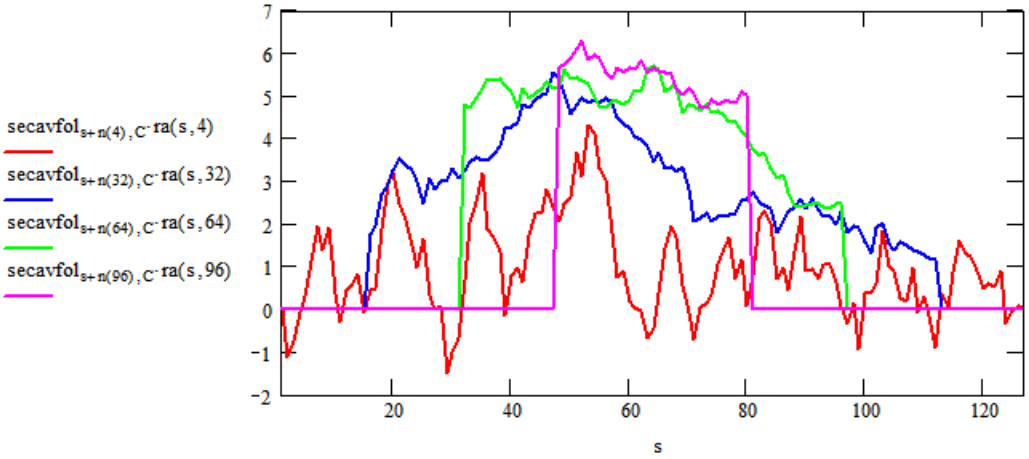

Editor Note: Fun Article

The Supernatural Gap in Radio Astronomy,

by Julian Jove, April 1, 2022

Major media newscasts are celebrations of ignorance and stupidity, so we must turn to the supernatural for real answers. It has long been known that, just like astrology, the supernatural is an important part of radio astronomy. It is only natural that we take this route. Artists, scientists, bricklayers, journalists and other ne'er-do-wells and charlatans have attempted to prove the simple hypothesis of how the infinitesimal *gap* between space and time or between light and shadow is managed by the laws of physics.

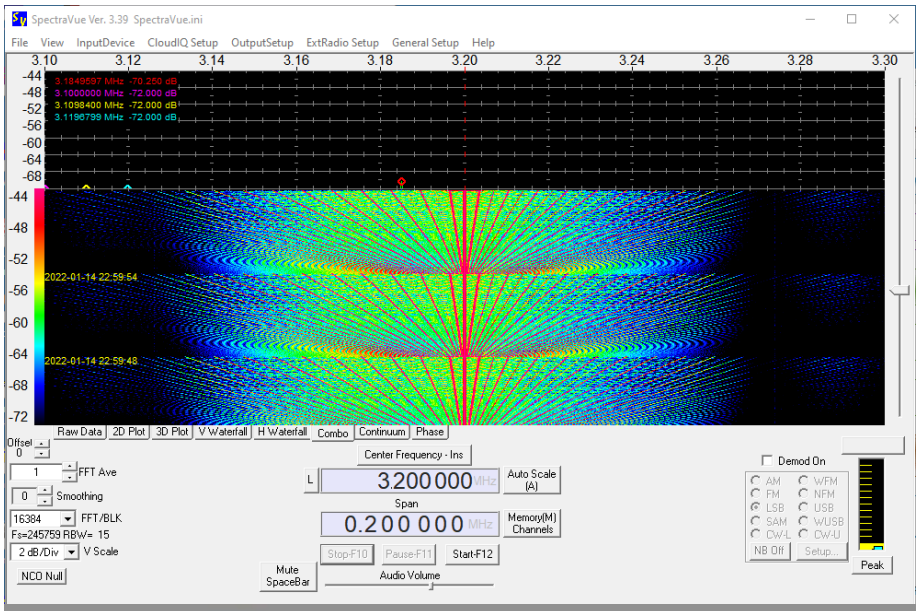

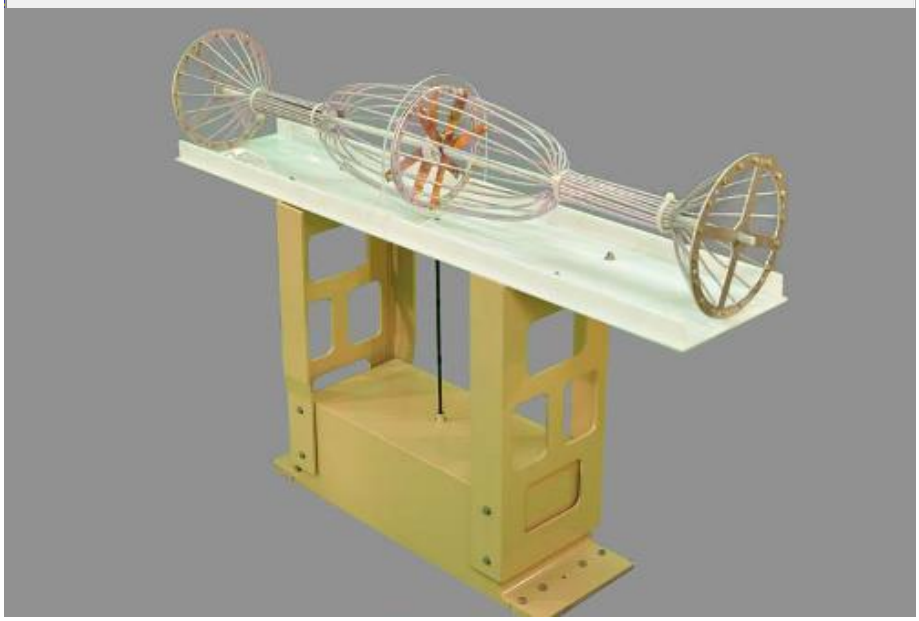

I have applied rational thought to this problem and herewith prove beyond any shadow of doubt the incontrovertible and immutable truths of the *gap* as a real supernatural phenomenon. The experiments started on January 14 and ran through April 1, 2022 and produced the inarguable spectra shown left. Nothing but a supernatural *gap* can explain the effects seen there.

The spectra were obtained while riding the Sun's gray line at the equator with the "Ultimate HF Antenna" shown left and its companion subheterodyne receiver the "Ulitmator" (in box below antenna). Only third-order tensor analysis of depth nine was needed and thus employed.

At Earth's equator, the gray line moves at approximately 15 femtoparsecs per sidereal second. Any elementary school student knows that this movement produces a Doppler frequency shift of precisely 4% per half-frequency at 3.2 MHz. To see what I am talking about, one must hold the spectra image at arm's length with eyes focused on infinity while looking at the center portion. After a moment, the gap will pop out of the image. Be careful, this is startling, and one may find oneself trapped between the real and unreal, between space and time, between light and shadow. Questions/comments never appreciated: juljove@gmail.com.

Observation Reports

Special Note:

These observation reports are from SARA members and have not been verified by peer review.

These observations are included in the journal to allow for discussion on improving the SARA member's observation system.

Some observations may be **false positives**, therefore the SARA staff requests that recommendations to improve the observation be addressed directly to the author.

Solar Radio Bursts and Gravity Waves Observed at HAARP, Gakona, Alaska USA

Whitham D. Reeve and Christian Monstein

Observations: Solar flares and coronal mass ejections (CME) were produced by the Sun on 30 and 31 March 2022 and their associated radio emissions were detected by the Callisto installation at the HAARP facility in Gakona, Alaska. The first image (figure 1) shows a Type II slow-sweep solar radio burst associated with a coronal mass ejection (CME). The radio sweep starts about 1735 UTC with a fundamental frequency of 60 MHz and then sweeps down to just below 20 MHz, the ionosphere's cutoff frequency at the time. Band-splitting is visible in the fundamental. A 2nd harmonic is seen in the spectrogram at 80 MHz about 1 minute after the fundamental. Band-splitting also appears to have taken place in the 2nd harmonic. A 3rd harmonic is visible at the top of the plot at approximately 1739. The irregular traces below 20 MHz are broadcast stations and other HF traffic that is seen every day in the Callisto spectrograms.

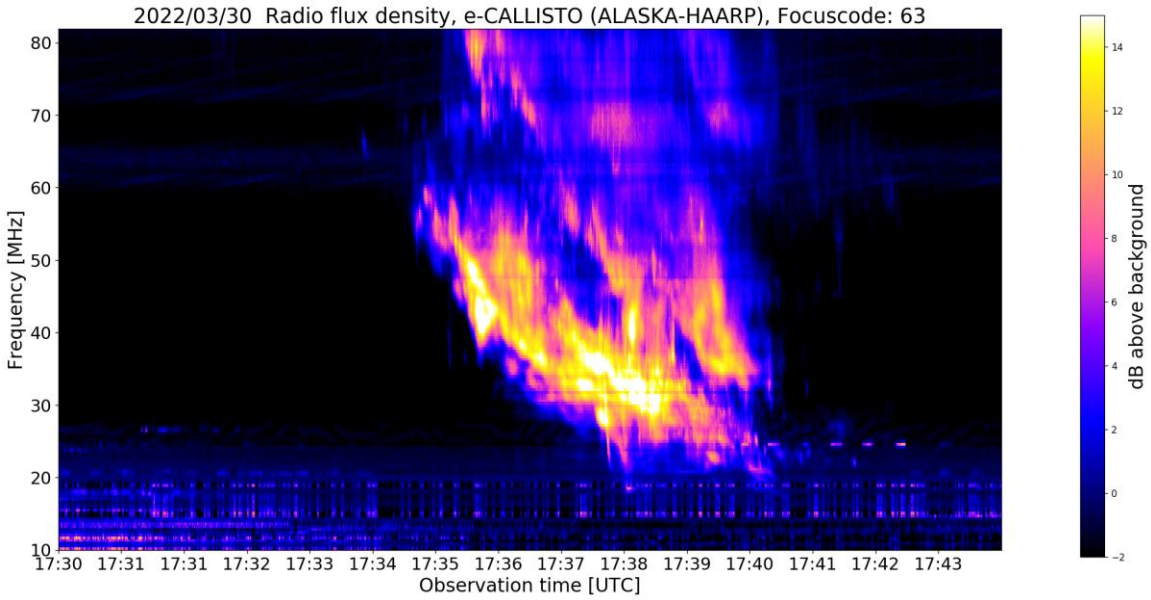

Figure 1 ~ Type II solar radio sweep with 2nd and 3rd harmonics and band-splitting observed on 30 March 2022. Credit: FHNW Brugg/Windisch and IRSOL Locarno, Switzerland, {Callisto}

The next image (figure 2) shows another Type II slow sweep but this one was accompanied by a Type IV noise storm; these occurred almost exactly 24 hours later on 31 March. The Type II burst is much weaker than the day before, starting at about 1835 and 50 MHz. The Type IV noise storm is visible from about 1838 to 1841 and covers the frequency range from slightly under 25 MHz to the upper limit of the spectrogram at 80 MHz. Vestiges of the storm again appear in the spectrogram at 1844 at lower frequencies.

The two images discussed so far show only one polarization of the dual polarized Callisto system. Type II radio sweeps normally are unpolarized, and the HAARP Callisto data show this to be the case. On the other hand, Type IV noise storms can be strongly polarized (up to 100%), but the radio flux densities observed by the system showed the emissions were unpolarized (or very weakly polarized) in the 1830 to 1845 plots. Readers interested in solar radio emissions, may refer to a tabular summary of their characteristics at {Solar}. Also, a discussion of the source and effects of Type II bursts may be found at {Reeve18}.

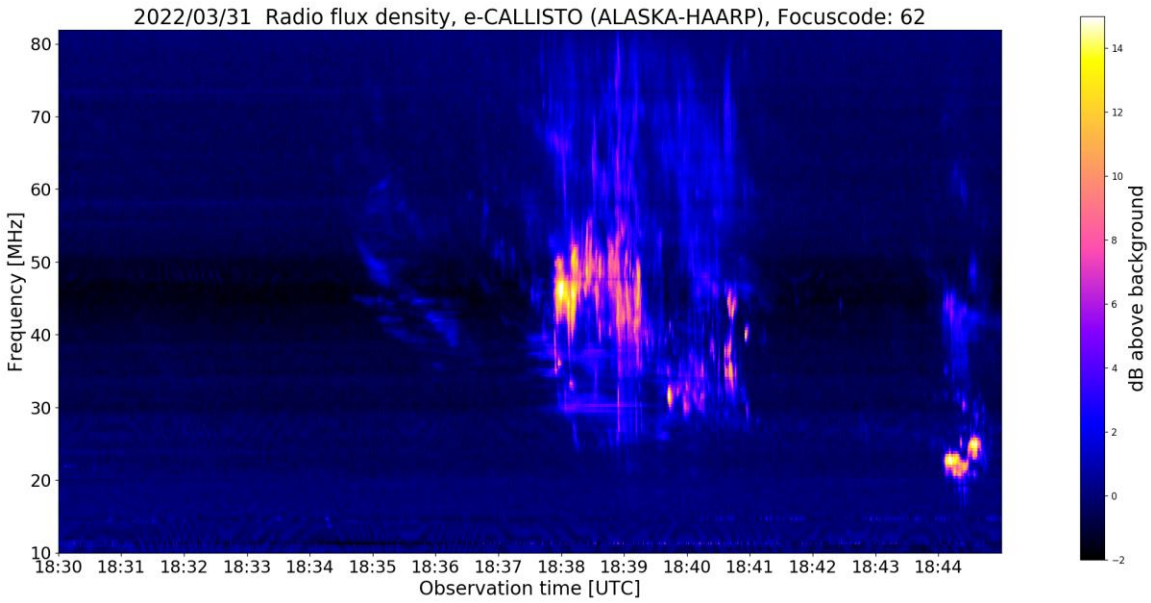

Figure 2 ~ Type II solar radio sweep accompanied by a Type IV noise storm observed on 31 March 2022. Credit: FHNW Brugg/Windisch and IRSOL Locarno, Switzerland, {Callisto}

The last two images (figure 3) show weak atmospheric gravity waves (AGW) that manifest as slightly lighter blue, quasi-periodic bands sweeping gracefully from the lower-left to upper-right. The phenomena persisted for about 30 minutes, from 1900 to 1930 on 31 March. The gravity waves may have been caused by a traveling ionospheric disturbance (TID) that focused as spectral caustics the solar radio emissions from the Type IV noise storm discussed above. The noise storm persisted for several hours but mostly was too weak to be seen without the focusing effects. However, the storm can be seen between 20 and 50 MHz at about 1926. The plots below are for right-hand circular polarization. The plots for left-hand circular polarization show much weaker gravity waves, possibly indicating some level of polarization in the underlying radio emissions.

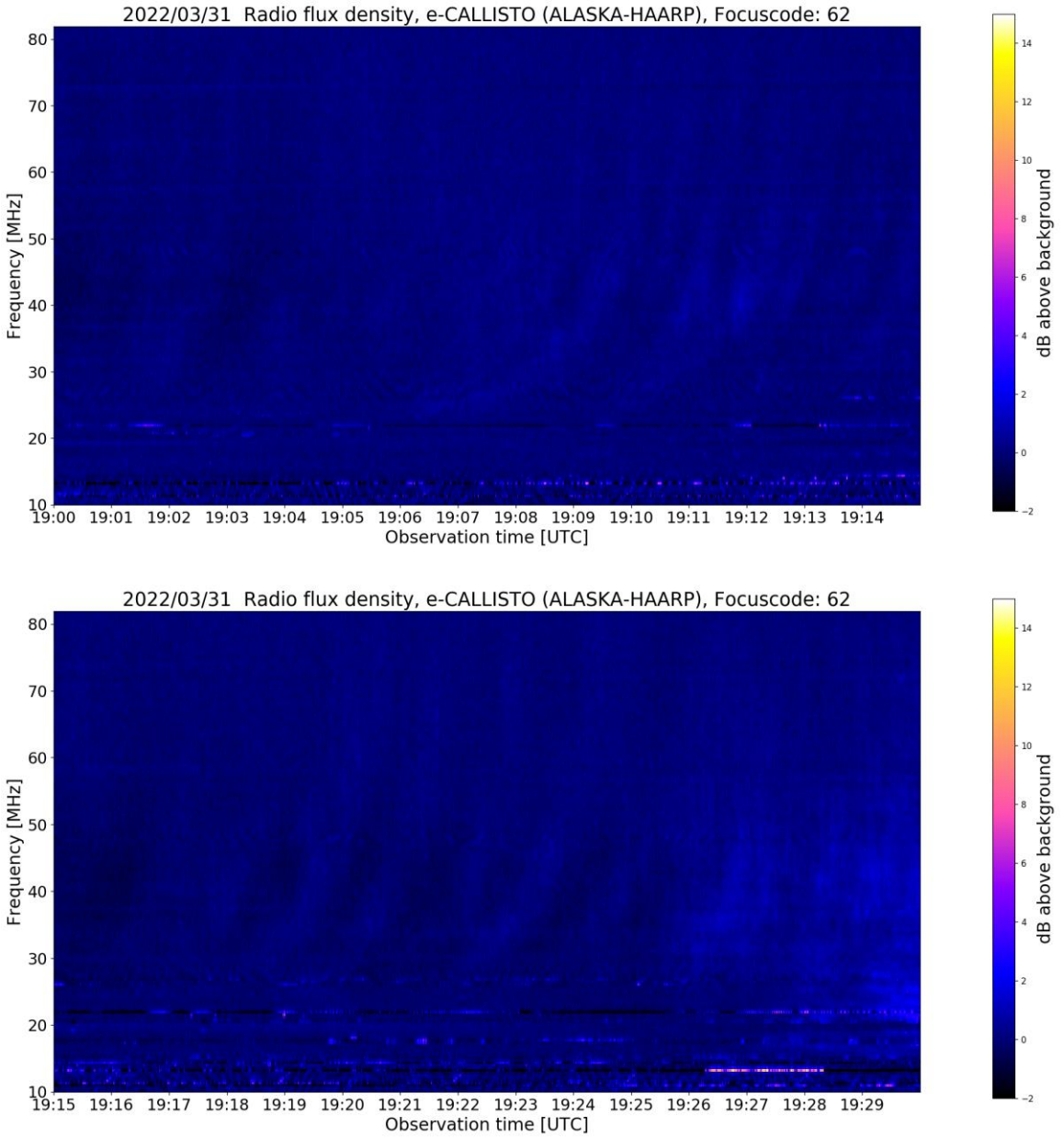

Figure 3 ~ Gravity waves observed on 31 March 2022 from 1900 to 1915 (upper) and 1915 to 1930 (lower). Weak evidence of the Type IV noise storm is seen between 1926 and 1930 UTC from below 20 to over 50 MHz. Credit: FHNW Brugg/Windisch and IRSOL Locarno, Switzerland, {Callisto}

The source of the atmospheric gravity waves and traveling ionospheric disturbance may have been related to the geomagnetic storm conditions earlier in the day from 0600 to 1500 UTC. More complete information on the AGW and TID phenomena may be found at [Hunsucker].

Instrumentation: Active crossed-dipole (LWA Antenna) connected through an LWAPC-Q power coupler (with quadrature coupler) to a UPC-590L-M dual up-converter (5 to 85 MHz RF, 200 MHz IF) and dual Callisto instruments controlled by a PC running Callisto software. FITS data files produced by the system are automatically uploaded to FHNW in Switzerland {Callisto}.

References:
[Hunsucker] Hunsucker, R., Atmospheric Gravity Waves Generated in the High-Latitude Ionosphere: A Review, Reviews of Geophysics and Space Physics, Vol. 20, No. 3, May 1982
{Callisto} http://soleil.i4ds.ch/solarradio/callistoQuicklooks/
{Reeve18} Reeve, W., Analysis of a Type II Solar Radio Burst Observed on 20 October 2017, 2018, available at: https://www.reeve.com/Documents/CALLISTO/Reeve_TypeII-Burst.pdf
{Solar} https://www.reeve.com/Solar/Solar.htm

Sudden Frequency Deviations Caused by Coronal Mass Ejections

Whitham D. Reeve

Observations: A sudden frequency deviation (SFD) usually occurs in real-time when Earth's ionosphere rapidly responds to a solar flare; however, in this case, the disturbance was caused by a pair of coronal mass ejections (CME) that left the Sun three days before. The narrowband horizontal waterfall (below) represents the demodulated signals from three HF receivers in response to the CMEs' impact with Earth's magnetosphere on 31 March 2022. A radio blackout at 25 MHz occurred almost immediately, while reception at 15 and 20 MHz continued for quite some time afterwards. The peak-to-peak frequency deviation was about 30 Hz at 20 MHz and less so, but still significant, at 15 and 25 MHz. Prior to impact all traces were straight and steady.

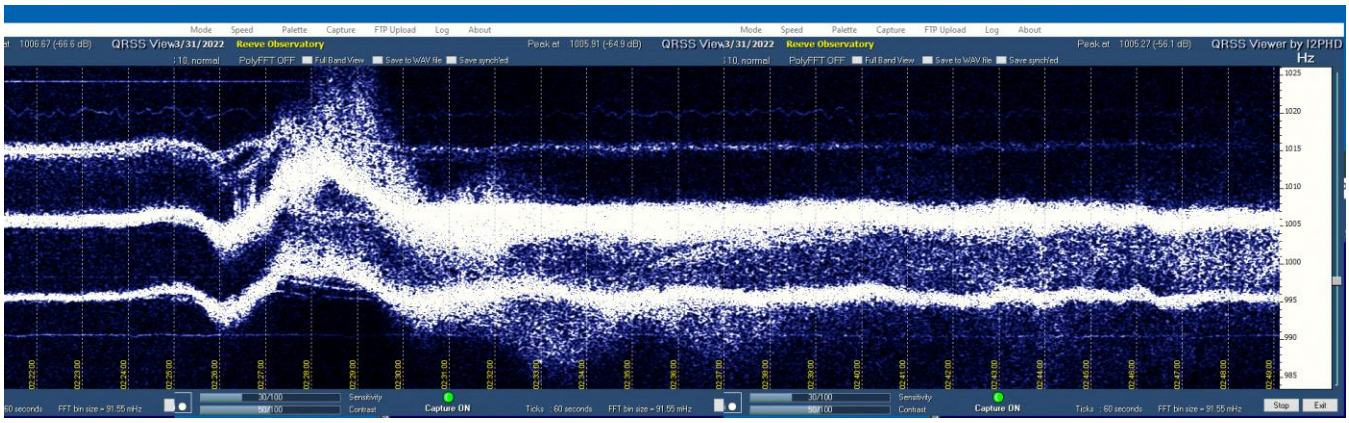

The waterfall plot consists of spliced spectra images with a total length of 27 min. Time is shown on the lower horizontal scale and runs left-to-right from 0222 to 0249 UTC with 1 min tick marks. The frequency scale is on the right and runs bottom-to-top from 984 to 1026 Hz. The receivers were set to lower sideband (LSB) mode and tuned 995, 1005 and 1015 Hz above the respective carrier frequencies of 15, 20 and 25 MHz. Therefore, the demodulated signals are shown by the lower trace at 995 Hz for 15 MHz, middle trace at 1005 Hz for 20 MHz, and upper trace at 1015 Hz for 25 MHz. The transmitting stations were WWV (15, 20 and 25 MHz) near Fort Collins, Colorado and WWVH (15 and 20 MHz) near Kekaha, Kauai, Hawaii.

The traces indicate a slight frequency rise starting at 0224, the time when the ionosphere along the propagation path was initially disturbed by rapid compression of the geomagnetosphere by the CMEs. Among other effects, this changed the ionosphere's height and the carrier frequency's wave number along the propagation path. The initial slight rise was followed by a dip in the received frequency, which is characteristic of SFDs, and then a higher rise in frequency peaking at about 0228. At this point, the 25 MHz carrier was blacked out and the 15 and 20 MHz carriers were strongly disturbed, indicated by the diffuse nature of the traces resulting from mutual interference of the many propagation paths that were produced. The blackout indicated that ionospheric absorption had

increased at 25 MHz. The ionospheric disturbance continued for approximately 1.5 hours. See {Reeve15} for additional information on the concepts behind sudden frequency deviations.

Instrumentation: Three Icom R-8600 wideband receivers connected through a multicoupler to a steerable HF log periodic dipole array antenna 13.8 m above ground level. Argo software produced the spectra images from a PC soundcard connected to the receivers through an 8-port analog audio mixer.

Geomagnetic: Although geomagnetic effects are not part of this observation report, the CME impact produced a sudden storm commencement (SSC) at 0224 on the Anchorage SAM-III magnetometer, signifying CME impact. Geomagnetic storm conditions persisted for several days afterwards.

References:

{Reeve15} Reeve, W., Sudden Frequency Deviations Caused by Solar Flares, Part 1, Concepts, 2015, available at: https://www.reeve.com/Documents/Articles%20Papers/Propagation%20Anomalies/Reeve_SuddenFreqDevConcepts_P1.pdf

Membership

New Members

Please welcome our new or returning SARA members who have joined since the last journal. If your name is missing or misspelled, please send an email to treas@radio-astronomy.org. We will make sure it appears correctly in the next Journal issue.

First name	Last name	City	State	Country	Call Sign
Douglas	Hemme	Surprise	AZ	USA	N7APS
Evan	Digby	Maple Ridge	British Columbia	Canada	
Blake	Sabo	Du Quoin	IL	USA	
JR	Subramanian	Madurai	Tamil Nadu	India	
David	Williams	Bethesda	MD	USA	W3DKL
Phillip	Weber	Hellerton	PA	USA	KH2EI
Monte	Hill	Southside	AL	USA	W4MJH
Prabaker	Balasubramanium	Richmond	CA	USA	
Stanley	Kroll	Orlando	FL	USA	AC4KM
Giselle	Koo	Boulder	CO	USA	
Gabriel	Altman	Westminster	CO	USA	
Jasleen	Batra	Broomfield	CO	USA	
Phaedra	Curlin	Boulder	CO	USA	
Lemay	Gerald	Drummondville	QC	Canada	VA2GJ
Douglas	Hemme	Surprise	AZ	USA	N7APS
Barry	Ptak	Moorhead	MN	USA	KC0LMX

Membership dues are $20.00 US per year and all dues expire in June. Student memberships are $5.00 US per year. Memberships must be renewed in June of each year. Or pay once and never worry about missing your dues again with the SARA Life Membership. SARA Life Memberships are now offered for a one-time payment of twenty times the basic annual membership fee (currently $400 US).

Journal Archives & Other Promotions

The rich and diverse legacy of member contributed content is available in the SARA Journal Archives. Table of contents for journals is available online at radio-astronomy.org/store.

The entire set of The Journal of The Society of Amateur Radio Astronomers is available on USB drive. It goes from the beginning of 1981 to the end of 2017 (over 6000 pages of SARA history!) Or you can choose one of the following USB drive's or DVD:* (Prices are US dollars and include postage.)

All SARA journals and conference proceedings are available through the previous calendar year.

Prices, US dollars, including postage

Members	
Each USB drive	$15.00
USB drive + 1-year membership extension	$30.00
Non-members	
Each USB drive	$25.00
USB drive + 1-year membership	$30.00
Non-USA members	
Each USB drive	$20.00 (airmail)
USB drive+ 1-year members extension	$35.00

*Already a member and want any or all these USB drives or DVD's? Buy any one for $15.00 or get any three for $35.00.

SARA Store (radio-astronomy.org/store.)

SARA offers the above USB drives, DVDs, printed Proceedings and Proceedings on USB drive and other items at the SARA Store: http://www.radio-astronomy.org/e-store. Proceeds from sales go to support the student grant program. Members receive an additional 10% discount on orders over $50 US. Payments can be made by sending payment by PayPal to treas@radio-astronomy.org or by mailing a check or money order to SARA, c/o Brian O'Rourke, 337 Meadow Ridge Rd, Troy, VA 22974-3256

SARA Online Discussion Group
SARA members participate in the online forum at http://groups.google.com/group/sara-list. This is an invaluable resource for any amateur radio astronomer.

SARA Conferences
SARA organizes multiple conferences each year. Participants give talks, share ideas, attend seminars, and get hands-on experience. For more information, visit http://www.radio-astronomy.org/meetings.

Facebook
Like SARA on Facebook
http://www.facebook.com/pages/Society-of-Amateur-Radio-Astronomers/128085007262843

Twitter
Follow SARA on Twitter@RadioAstronomy1

What is Radio Astronomy?

This link is for a booklet explaining the basics of radio astronomy.
http://www.radio-astronomy.org/pdf/sara-beginner-booklet.pdf

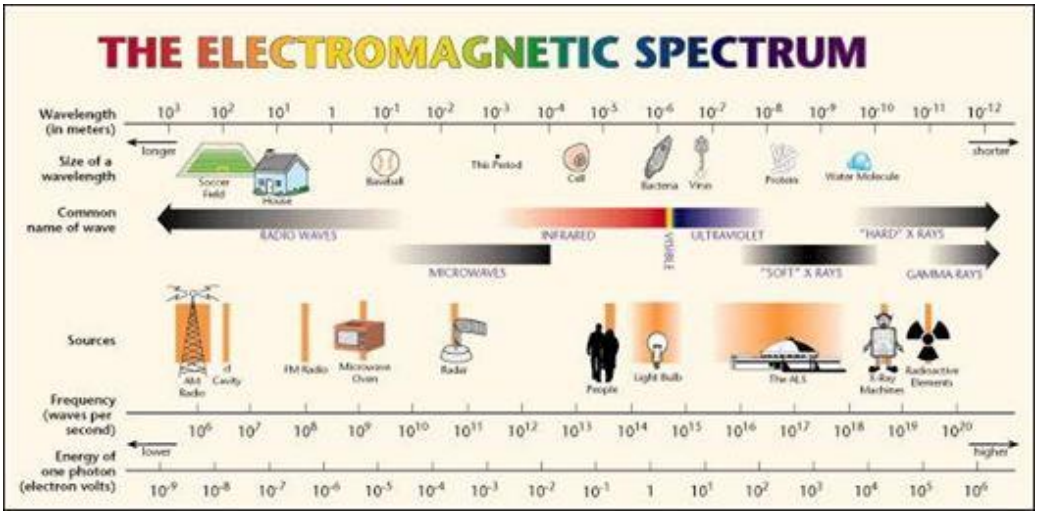

Administrative

Officers, directors, and additional SARA contacts

The Society of Amateur Radio Astronomers is an all-volunteer organization. The best way to reach people on this page is by email with SARA in the subject line SARA Officers.

President: Dennis Farr, WB4RJK, https://www.radio-astronomy.org/contact/President +1 813 833-3918
Vice President: Dr. Rich Russel, AC0UB https://www.radio-astronomy.org/contact/Vicepresident
Secretary: Bruce Randall, NT4RT, https://www.radio-astronomy.org/contact/Secretary +1 803-327-3325
Treasurer: Brian O'Rourke, K4UL, https://www.radio-astronomy.org/contact/Treasurer
Past President: Ken Redcap, tbd@radio-astronomy.org +1 319-591-1131
Founder Emeritus and Director: Jeffrey M. Lichtman, KI4GIY, jeff@radioastronomysupplies.com +1 954-554-3739

Board of Directors

Name	Term expires	Email
Ed Harfmann	2022	edharfmann@comcast.net
Dr. Wolfgang Herrmann	2023	messbetrieb@astropeiler.de
Tom Jacobs	2023	tdj0@bellsouth.net
Charles Osborne	2023	k4cso@twc.com
Keith Payea	2022	kbpayea@bryantlabs.net
Steve Tzikas	2022	Tzikas@alum.rpi.edu
Jon Wallace	2023	wallacefj@comcast.net
David Westman	2022	david.westman@engineeringretirees.org

Other SARA Contacts

All Officers	http://www.radio-astronomy.org/contact-sara	
All Directors and Officers	http://www.radio-astronomy.org/contact/All-Directors-and-Officers	
Eastern Conference Coordinator	http://www.radio-astronomy.org/contact/Annual-Meeting	
All Radio Astronomy Editors	http://www.radio-astronomy.org/contact/Newsletter-Editor	
Radio Astronomy Editor	Dr. Richard A. Russel	drrichrussel@netscape.net
Contributing Editor	Whitham D. Reeve	whitreeve@gmail.com
Educational Outreach	http://www.radio-astronomy.org/contact/Educational-Outreach	
Grant Committee	Tom Crowley	grants@radio-astronomy.org
Membership Chair	http://www.radio-astronomy.org/contact/Membership-Chair	
Technical Queries (David Westman)	http://www.radio-astronomy.org/contact/Technical-Queries	
Webmaster	Ciprian (Chip) Sufitchi, N2YO	webmaster@radio-astronomy.org

Resources

Great Projects to Get Started in Radio Astronomy

Radio Observing Program

The Astronomical League (AL) is starting a radio astronomy observing program. If you observe one category, you get a Bronze certificate. Silver pin is two categories with one being personally built. Gold pin level is at least four categories. (Silver and Gold level require AL membership which many clubs have membership. For the bronze level, you need not be a member of AL.)

Categories include
1) SID
2) Sun (aka IBT)
3) Jupiter (aka Radio Jove)
4) Meteor back-scatter
5) Galactic radio sources

This program is a collaboration between NRAO and AL. Steve Boerner is the Lead Coordinator and a SARA member.

For more information:
Steve Boerner
2017 Lake Clay Drive
Chesterfield, MO 63017
Email: sboerner@charter.net
Phone: 636-537-2495
http://www.astroleague.org/programs/radio-astronomy-observing-program

Radio Jove

The Radio Jove Project monitors the storms of Jupiter, solar activity and the galactic background. The radio telescope can be purchased as a kit or you can order it assembled. They have a terrific user group you can join.
http://radiojove.gsfc.nasa.gov/

INSPIRE Program

The INSPIRE program uses build-it-yourself radio telescope kits to measure and record VLF emissions such as tweeks, whistlers, sferics, and chorus along with man-made emissions. This is a very portable unit that can be easily transported to remote sites for observations.
http://theinspireproject.org/default.asp?contentID=27

SARA/Stanford SuperSID

Stanford Solar Center and the Society of Amateur Radio Astronomers have teamed up to produce and distribute the SuperSID (Sudden Ionospheric Disturbance) monitor. The monitor utilizes a simple pre-amp to magnify the VLF radio signals which are then fed into a high definition sound card. This design allows the user to monitor and record multiple frequencies simultaneously. The unit uses a compact 1-meter loop antenna that can be used indoors or outside. This is an ideal project for the radio astronomer that has limited space. To request a unit, send an e-mail to supersid@radio-astronomy.org

Radio Astronomy Online Resources

AJ4CO Observatory – Radio Astronomy Website: http://www.aj4co.org/	National Radio Astronomy Observatory http://www.nrao.edu
Radio Astronomy calculators https://www.aj4co.org/Calculators/Calculators.html	NRAO Essential Radio Astronomy Course http://www.cv.nrao.edu/course/astr534/ERA.shtml
Introduction to Amateur Radio Astronomy (presentation) http://www.aj4co.org/Publications/Intro%20to%20Amateur%20Radio%20Astronomy,%20Typinski%20(AAC,%202016)%20v2.pdf	Exotic Ions and Molecules in Interstellar Space -- ORION 2020 10 21. Dr. Bob Compton https://www.youtube.com/watch?v=r6cKhp23SUo&t=5s
RF Associates Richard Flagg, rf@hawaii.rr.com 1721-1 Young Street, Honolulu, HI 96826	The Radio JOVE Project & NASA Citizen Science – ORION 2020.6.17. Dr. Chuck Higgins https://www.youtube.com/watch?v=s6eWAxJywp8&t=5s
RFSpace, Inc. http://www.rfspace.com	UK Radio Astronomy Association http://www.ukraa.com/
CALLISTO Receiver & e-CALLISTO http://www.reeve.com/Solar/e-CALLISTO/e-callisto.htm	CALLISTO software and data archive: www.e-callisto.org
Deep Space Exploration Society http://DSES.science	Radio Astronomy Supplies http://www.radioastronomysupplies.com
Deep Space Object Astrophotography Part 1 -- ORION 2021 02 17. George Sradnov https://www.youtube.com/watch?v=Pm_Rs17KIyQ	Radio Jove Spectrograph Users Group http://www.radiojove.org/SUG/
European Radio Astronomy Club http://www.eracnet.org	Radio Sky Publishing http://radiosky.com
British Astronomical Association – Radio Astronomy Group http://www.britastro.org/baa/	The Arecibo Radio Telescope; It's History, Collapse, and Future - ORION 2020.12.16. Dr. Stan Kurtz, Dr. David Fields https://www.youtube.com/watch?v=rBZlPOLNX9E
Forum and Discussion Group http://groups.google.com/group/sara-list	Shirleys Bay Radio Astronomy Consortium marcus@propulsionpolymers.com
GNU Radio https://www.gnuradio.org/	SARA Twitter feed https://twitter.com/RadioAstronomy1
SETI League http://www.setileague.org	SARA Web Site http://radio-astronomy.org
NRAO Essential Radio Astronomy Course http://www.cv.nrao.edu/course/astr534/ERA.shtml	SARA Facebook page https://www.facebook.com/pages/Society-of-Amateur-Radio-Astronomers/128085007262843
NASA Radio JOVE Project http://radiojove.gsfc.nasa.gov Archive: http://radiojove.org/archive.html https://groups.io/g/radio-jove	Simple Aurora Monitor: Magnetometer http://www.reeve.com/SAMDescription.htm
National Radio Astronomy Observatory http://www.nrao.edu	Stanford Solar Center http://solar-center.stanford.edu/SID/
A New Radio Telescope for Mexico - ORION 2021 01 20. Dr. Stan Kurtz https://www.youtube.com/watch?v=Q9aBWr1aBVc	

For Sale, Trade and Wanted

At the SARA online store: radio-astronomy.org/store.

SARA Polo Shirts

New SARA shirts have arrived.

We now have a good selection of X, XX, and XXX shirts available in all colors including white!

Shirts are $20 at the conference and $25 shipped.

Contact the treasurer at treas@radio-astronomy.org for availability and shipping.

Scope in a Box $295

radio-astronomy.org/store.

Kit of parts and software to build a working Radio Telescope to detect Hydrogen Line emissions. Available to USA addresses only at this time.

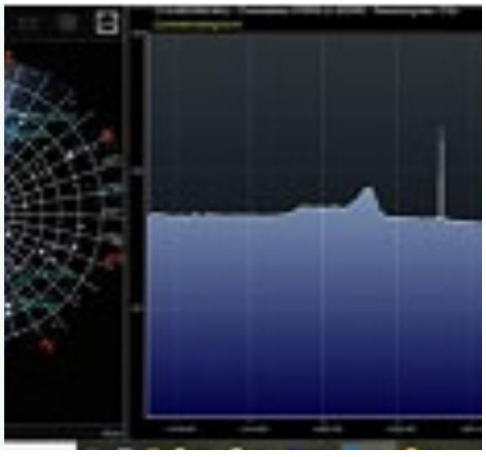

SuperSID Complete Kit ($112-$160 depending on options)
radio-astronomy.org/store.

SARA Publication, Journals and Conference Proceedings (various prices)
radio-astronomy.org/store.

SARA Journal USB Drive ($15-$35 depending on shipping option)
radio-astronomy.org/store.

The USB drive covers the society journal "Radio Astronomy" from the founding of the organization in 1981 thru 2020. Articles cover a wide range of topics including: cosmic radiation, pulsars, quasars, meteor detection, solar observing, Jupiter, Radio Jove, gamma ray bursts, the Itty Bitty Telescope (IBT), dark matter, black holes, the Jansky antenna, methanol masers, mapping at 408 MHz and more. This CD contains all of the above and more with over 4800 pages of articles on radio astronomy. Also included is a copy of Grote Reber's handwritten, 34 page document "Carriage and Mirror Detail" of his historic antenna now on display at the National Radio Astronomy Observatory (NRAO) in Greenbank, WV. You also get an electronic copy of the 109 page "Basics of Radio Astronomy" from JPL Goldstone-Apple Valley Radio Telescope. Also included is the NRAO 40-foot radio telescope "Operators Manual", which by the way, you get to operate if you attend the Eastern SARA conference in July.

SARA Advertisements

There is no charge to place an ad in Radio Astronomy; but you must be a current SARA member. Ads must be pertinent to radio astronomy and are subject to the editor's approval and alteration for brevity. Please send your "For Sale," "Trade," or "Wanted" ads to edit@radio-astronomy.org. Please include email and/or telephone contact information. Please keep your ad text to a reasonable length. Ads run for one bimonthly issue unless you request otherwise.

Radio-Astro-Machine, zzblac@gmail.com
Elevation rotation adapter plate for Scope in a Box and custom machining. For further information visit https://radio-astro-machine.wixsite.com/my-site or send an email.

Typinski Radio Astronomy, Inc., info@typinski.com
Antenna systems and feed line components for HF radio astronomy

Jeff Kruth, WA3ZKR, kmec@aol.com
RF components from HF to MMW, various types including mixers, RF switches, amplifiers, oscillators, coaxial components, waveguide components, etc. I have a very large collection of stuff and the facilities to test and provide data. Please email with your needs and I will see if I have something for you. Have fun!

Stuart and Lorraine Rumley, sales@valontechnology.com
The Valon Technology 2100 Downconverter, when combined with our 5009 frequency synthesizer module, provides a high-performance, compact receiver downconverter system. Applications include hydrogen line studies at 1420MHz and radio astronomy in the protected 30MHz segment of the 21 cm band. For more information visit http://www.valontechnology.com/2100downconverter.html or send an email.

Radio2Space, filippo.bradaschia@primalucelab.com
SPIDER radio telescopes and turn-key-systems designed specifically for education.
https://www.radio2space.com
We developed our SPIDER radio telescopes as turn-key-system just to avoid the problem you perfectly highlighted in your website: "Purchasing a radio telescope isn't like buying an optical telescope. They are harder to find, and usually require assembly and software troubleshooting. In some cases, a radio telescope must be built from components." Our SPIDER radio telescopes are not designed for amateurs that prefer to build a radio telescope but to schools, universities, museums, and other science institutes that needs for a complete and ready-to-use system, just like the optical telescopes they can normally buy!

Radio Astronomy Supplies
http://www.radioastronomysupplies.com
jeff@radioastronomysupplies.com
Research and Educational Radio Telescopes and all associated equipment since 1994

Membership Information

Annual SARA dues Individual $20, Classroom $20, Student $5 (US funds) anywhere in the world. Membership includes a subscription to Radio Astronomy, the bimonthly Journal of The Society of Amateur Radio Astronomers, delivered electronically (via a secure web link, emailed to you as each new issue is posted). We regret that printing and postage costs prevent SARA from providing hardcopy subscriptions to our Journal.

We would appreciate the following information included with your check or money order, made payable to SARA:

Name: _____

Email Address : _____
(required for electronic Journal delivery)

Ham call sign: _____ (if applicable)

Address: _____

City: _____

State: _____

Zip: _____

Country: _____

Phone: _____

Please include a note of your interests. Send your application for membership, along with your remittance, to our Treasurer.

For further information, see our website at:
http://radio-astronomy.org/membership

How to get started?

SARA has a made a kit of software and parts to detect the Hydrogen line signal from space. This is an excellent method to get started in radio astronomy. It teaches the principles of antenna design, signal detection, and signal processing. Read more about this and other projects on our web site.

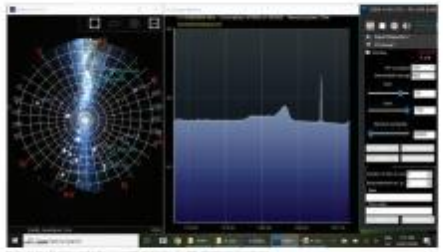

Society of Amateur Radio Astronomers, Inc.
Founded 1981

Membership supported, nonprofit [501(c) (3)]
Educational and Radio Astronomy Organization

Knowledge through Common Research, Education and Mentoring

SARA members have been privileged to use this forty foot diameter drift-scan hydrogen line radio telescope every year at their annual meeting in Green Bank.

http://radio-astronomy.org

Why Radio Astronomy?

Because about sixty five percent of our current knowledge of the universe has stemmed from radio astronomy alone. The discovery of quasars, pulsars, black holes, the 3K background from the "Big Bang" and the discovery of biochemical hydrogen/carbon molecules are all the result of professional radio astronomy.

The Society of Amateur Radio Astronomers

SARA was founded in 1981, with the purpose of educating those interested in pursuing amateur radio astronomy.

The society is open to all, wishing to participate with others, worldwide.

SARA members have many interests, some are as follows:

SARA Areas of Study and Research:

- Solar Radio Astronomy
- Galactic Radio Astronomy
- Meteor Detection
- Jupiter
- SETI
- Gamma Ray/High Energy Pulse
- Detection
- Antennas
- Design of Hardware / Software

The members of the society offer a friendly mentor atmosphere. All questions and inquiries are answered in a constructive manner. No question is silly!

SARA offers its members an electronic bi-monthly journal entitled Radio Astronomy. Within the journal, members report on their research and observations. In addition, members receive updates on the professional radio astronomy community and, society news.

Once a year SARA meets for a three-day conference at the Green Bank Observatory in Green Bank West Va.

There is also a spring conference held at various cities in the Western USA. Previous meeting have been at the VLA in Socorro, NM and at Stanford University.

How do I get started?

Just as a long journey begins with the first step, the project you elect must start with a clear idea of your objectives. Do you wish to study the sun? Jupiter? Make meteor counts? Do you wish to engage in imaging radio astronomy? What you decide will not only determine the type of equipment you will need, but also the local radio spectrum.

How do amateurs do radio astronomy?

Radio astronomy by amateurs is conducted using antennas of various shapes and sizes, from smaller parabolic dishes to simple wire antennas. These antennas are connected to receivers and most of these receivers are software defined radios these days. Data from the receivers are collected by computers, and the received signals will be displayed as charts, graphs or maybe even sky maps. As diverse as the observed objects, so is are the instruments and tools used. SARA members will always be supportive to find good solutions for what one wishes to observe.

Is amateur radio astronomy instrumentation expensive?

Technical information freely circulated in our monthly journal helps amateurs to obtain good low noise equipment from off the shelf assemblies, or to build their own units. The actual cash investment in radio astronomy equipment need not exceed that of any other hobby.

What are amateurs actually looking for in the received data?

The aim of the radio amateur is to find something new and unusual. Just as an amateur optical observer hopes to notice a supernova or a new comet, so does an amateur radio observer hope to notice a new radio source, or one whose radiation has changed appreciably.

The Reber Telescope at NRAO. Constructed by Grote Reber in 1937 in his back yard in Wheaton, Illinois

SARA Members discussing the IBT (Itty Bitty Telescope)